

INTEGRATION OF SPV BASED SYSTEMS INTO DISTRIBUTION GRID WITH POWER QUALITY ANALYSIS

A Thesis Submitted to the
Delhi Technological University
For the Award of Doctor of Philosophy
In
Electrical Engineering

Submitted By:
PRIYANKA CHAUDHARY
(2K14/PhD/EE/06)



Under the Supervision of:
Dr. M. Rizwan
Associate Professor

DEPARTMENT OF ELECTRICAL ENGINEERING
DELHI TECHNOLOGICAL UNIVERSITY
(Formerly Delhi College of Engineering)
DELHI-110042, INDIA

2018

© DELHI TECHNOLOGICAL UNIVERSITY, DELHI, 2018, ALL RIGHTS RESERVED

DECLARATION

I Priyanka Chaudhary a student of Ph.D. hereby declare that the thesis titled **“Integration of SPV Based Systems into Distribution Grid with Power Quality Analysis”** which is submitted by me to the Department of Electrical Engineering, Delhi Technological University, Delhi in partial fulfillment of the requirement for the award of the degree of Doctor of Philosophy has not previously formed the basis for the award of any Degree, Diploma Associate ship, fellowship or other similar title or recognition.

Place: New Delhi

Date: 22-10-2018

Priyanka Chaudhary

(PRIYANKA CHAUDHARY)

CERTIFICATE

On the basis of declaration submitted by Ms. Priyanka Chaudhary, student of Ph.D., I hereby certify that the thesis titled “**Integration of SPV Based Systems into Distribution Grid with Power Quality Analysis**” which is submitted to the Department of Electrical Engineering, Delhi Technological University, Delhi in partial fulfillment of the requirement for the award of the degree of Doctor of Philosophy, is an original contribution with existing knowledge and faithful record of research carried out by her under my guidance and supervision.

To the best of my knowledge this work has not been submitted in part or full for any Degree or Diploma to this University or elsewhere.

Place: New Delhi

Date: 22-10-2018



(Dr. M. Rizwan)

Supervisor

Associate Professor

Department of Electrical Engineering
Delhi Technological University, Delhi

ACKNOWLEDGEMENT

First and foremost, I sincerely acknowledge my most sincere gratitude to my supervisor Dr. M. Rizwan for his valuable guidance, support and motivation throughout this research work. He is an outstanding mentor and working with him has been a remarkable experience. The valuable hours of discussion that I had with him undoubtedly helped in supplementing my thoughts in the right direction for attaining the desired objectives. I consider it my proud privilege to have worked with him and above all a very pleasant and kind person, ever ready to lend a helping hand. I am forever thankful to him for all his wise words and inspiring thoughts.

I wish to express gratefulness to Prof. Madhusudan Singh, Head, Department of Electrical Engineering, Delhi Technological University, Delhi, for all the help and enlightened me during my research.

I am also thankful to all faculty members of the Department of Electrical Engineering, Delhi Technological University, Delhi, for their encouragement and moral support for the completion of this thesis.

I would like to extend my special thanks to SRC members mainly Prof. T. S. Bhatti, Professor, Centre for Energy Studies, IIT Delhi who have given me valuable guidance and advice to improve quality of my research work.

I extend my personal thanks to my friends and colleagues specially, Md. Tausif Ahmad, Imran Ahmad Quadri, Ritika Gour, Astitva Kumar, Ayushi Chugh, Masood Anzar, Priyanka Anand, Arshad Hussain Quadri, Jagriti Surubhi, Nikita Gupta for their valuable support and reminding me to complete my work at the earliest.

The assistance of the valuable staffs in Electrical Energy Utilization Laboratory of Delhi Technological University is gratefully acknowledged. I am especially thankful to Mr. Vickey Kumar Prasad and Mr. TPS Rana for their substantial technical assistance and companionship during development and tests of prototype system.


I want to take this opportunity to thank my parents, from the bottom of my heart for everything that they have done and continue to do for me. They never lost their faith in me and sacrificed a great lot in their lives to help me come this far. Every bit of mine would always remain indebted to my loving parents whose blessings have been and will always be an inseparable part of every stride of my life. I also want to thank my brother, Prashant and my sister, Tapasya for being a constant source of motivation.

This acknowledgement would not be complete without mentioning my husband. He is my core support system and words cannot articulate my admiration for him. He gave his unconditional support and continued to be a source of inspiration during my research.

I am wholly indebted to ALMIGHTY who is omnipotent and superpower of the universe.

Place: New Delhi

Date: 22.10.2018


(Priyanka Chaudhary)

ABSTRACT

The integration of solar photovoltaic (SPV) with grid as distributed generation (DG) are able to solve the demand and generation mismatch issues especially in developing countries. Integration of SPV systems at medium voltage (MV)/ low voltage (LV) grid level poses some negative impacts such as voltage limit violation at the point of common coupling (PCC), frequency variations, grid stability issues, etc.

The large scale penetration of PV power into electric distribution system possesses a great threat to grid stability and reliability. Therefore, the utilities are developing the smart grid approach across the world and PV power forecasting is the one of the key tool for this new paradigm. An intelligent approach based on wavelet transform and generalized neural network (GNN) is proposed for very short term PV power forecasting. Further, an energy management system supporting high penetration of solar photovoltaic generation for smart grid using solar forecasts and energy storage system has been also developed and presented in this thesis.

Voltage source converter (VSC) is the key component which is used to supply AC loads and integrate with the grid. The control of VSC plays very important role to synchronize the PV plant with the utility grid. The performance of control techniques mainly depends on the algorithm used to calculate the reference grid currents and use to give the switching signal patterns for insulated- gate bipolar transistor (IGBT) switches. Hence, integration of solar PV as a DG must have efficient and coordinated control measures for the proper synchronization.

Intelligent and adaptive control techniques for three phase grid connected SPV system are developed in this work. These proposed algorithms provides reactive power, harmonic compensation and help system to transmit active power to the grid and loads effectively. The performance of the proposed algorithms has been validated through simulations carried out in MATLAB/Simulink platform and also implemented on hardware prototype.

CONTENTS

Declaration	i
Certificate	ii
Acknowledgement	iii
Abstract	v
Contents	vii
List of Figures	xii
List of Tables	xix
List of Symbols, abbreviations and nomenclature	xx
CHAPTER 1 INTRODUCTION	
1.1 General	1
1.2 Current status of RES in India	4
1.3 Renewable energy initiatives in India	7
1.4 Distributed power generation	8
1.5 Integration of solar PV systems and grid management	9
1.5.1 Necessity, issues and challenges	9
1.5.2 Power quality analysis	10
1.6 Problem formulation	11
1.7 Organization of the thesis	12
CHAPTER 2 LITERATURE REVIEW	
2.1 Introduction	15
2.2 Mathematical modeling of RES based components	15
2.3 Short term solar energy forecasting	19
2.4 Impacts of high PV penetration in distribution system and energy management	23
2.5 Control algorithms for grid integration of solar PV systems	33
2.6 Power quality analysis	38

2.7	Knowledge gap analysis	39
CHAPTER 3 MODELING OF RENEWABLE ENERGY BASED COMPONENTS		
3.1	Introduction	42
3.2	Solar PV plant modelling	42
3.2.1	Mathematical description of solar PV array	43
3.2.2	DC bus voltage selection	44
3.2.3	DC/DC converter	45
3.2.4	DC bus capacitance	46
3.2.5	Voltage source converter	46
3.2.6	Interfacing inductor	47
3.2.7	Ripple filter	47
3.3	Mathematical modelling of fuel cell	47
3.4	Pump hydro storage model	49
3.5	Hardware components	52
3.5.1	d-SPACE 1104	53
3.5.2	Sensing and conditioning circuit	54
3.5.3	Gate isolation and amplifier circuit	57
3.5.4	Passive ripple filter	58
3.6	Conclusion	58
CHAPTER 4 SHORT TERM SOLAR ENERGY FORECASTING		
4.1	Introduction	59
4.2	Solar energy forecasting and its necessity	59
4.3	Intelligent approach for STSEF	60
4.3.1	Generalized neural network	60
4.3.2	Wavelet theory	64
4.4	Short term solar energy forecasting using wavelet-GNN hybrid model	66
4.4.1	Data collection	67
4.4.2	Day and weather type classifications	68
4.4.3	Correlation analysis of PV power with meteorological parameters	69

4.4.4	Statistical error indices	69
4.4.5	Hybrid model for short term solar energy forecasting	70
4.5	Results and discussion	71
4.6	Validation of proposed with existing solar PV generation forecasting models	75
4.7	Conclusions	78
CHAPTER 5 ENERGY MANAGEMENT SUPPORTING HIGH PV PENETRATION FOR SMART GRID ENVIRONMENT		
5.1	Introduction	79
5.2	Smart energy management	79
5.3	Application of solar power generation forecasting model in smart grid environment	81
5.3.1	Data collection	83
5.3.2	Day and weather type classifications	83
5.3.3	Correlation of PV power with meteorological parameters	83
5.4	Demand response modelling	84
5.4.1	Electricity pricing	85
5.4.2	Load modelling	86
5.4.3	Demand response case studies	87
5.5	Algorithm for proposed energy management system	90
5.6	Results and discussions	92
5.7	Conclusions	100
CHAPTER 6 DEVELOPMENT OF CONTROL ALGORITHMS FOR GRID INTEGRATION OF SPV SYSTEM		
6.1	Introduction	102
6.2	System description	103
6.3	Control algorithms for grid integration of SPV system	104
6.4	GDBP NN based $I \cos\phi$ control	105

6.4.1	Control algorithm	106
6.4.2	Results and discussion	113
6.5	QNBP NN I $\cos\phi$ control of grid integrated PV system	120
6.5.1	Control algorithm	120
6.5.2	Results and discussion	127
6.6	GNN – EKF control	134
6.6.1	Control algorithm	134
6.6.2	Results and discussion	144
6.7	NLMS and PLMS based control	156
6.7.1	Control algorithm	156
6.7.2	Results and discussion	159
6.8	Predictive current control approach	165
6.8.1	Control algorithm	165
6.8.2	Results and discussion	168
6.9	Adaptive notch filter and ANFIS based DC link voltage controller for PV system	171
6.9.1	Control algorithm	171
6.9.2	Results and discussion	174
6.10	Conclusions	175

CHAPTER 7 CONTROL AND STABILITY STUDIES OF GRID TIED SPV SYSTEM

7.1	Introduction	177
7.2	System description	178
7.3	SPV system modelling	179
7.3.1	State space modelling	180
7.3.2	SPV plant modelling considering uncertainty	182
7.4	Development of control algorithm	185
7.4.1	MPPT control	185
7.4.2	Controller design	186

7.5	Result and discussion	191
7.6	Conclusions	196
CHAPTER 8 CONCLUSIONS AND FUTURE SCOPE		
8.1	Conclusions of proposed work	197
8.2	Recommendations for future work	200
	REFERENCES	201
	APPENDIX - A	220
	APPENDIX - B	221
	LIST OF PUBLICATIONS	223

LIST OF FIGURES

Figure 1.1	Global PV capacity in GW between years 2005-2017	2
Figure 1.2	Growth of RES year wise	4
Figure 1.3	Installed capacity of Indian power sector source wise	5
Figure 1.4	India's RES installed capacity	5
Figure 2.1	A simple network structure	24
Figure 2.2	High voltage (HV) transmission system voltage drop characteristics	24
Figure 2.3	Low voltage (LV) distribution system voltage drop characteristics	24
Figure 2.4	IEEE 15 bus radial system	26
Figure 2.5	Typical solar irradiance profile for a day	26
Figure 2.6	Voltage profiles during a day simulation without deploying voltage control	27
Figure 2.7	Voltage profiles during a day simulation with deploying voltage control	27
Figure 3.1	Single diode model of PV cell	43
Figure 3.2	DC/DC boost converter	45
Figure 3.3	Equivalent circuit of a solid oxide fuel cell (SOFC)	48
Figure 3.4	Block diagram of the turbine mode of the system	51
Figure 3.5	Block diagram of the pump mode of the system	52
Figure 3.6	Block diagram of developed hardware prototype	53
Figure 3.7	Developed experimental prototype setup	53
Figure 3.8	Schematic representation of voltage sensing circuit for grid side voltage	55
Figure 3.9	Voltage sensing circuit for the proposed experimental setup	55
Figure 3.10	Schematic diagram of current sensing circuit for source side	56
Figure 3.11	Current sensing circuit for the proposed experimental setup	56
Figure 3.12	Circuit diagram of gate trigger circuit	57
Figure 3.13	Gate trigger circuit for the developed prototype	57
Figure 3.14	Passive ripple filters	58

Figure 4.1	Generalized neural network model	61
Figure 4.2	Block diagram of model development using ANN	63
Figure 4.3	Decomposition and reconstruction in wavelet	66
Figure 4.4	Hybrid forecasting model for SPV generation forecast	67
Figure 4.5	Short term PV power forecasting for cloudy day	71
Figure 4.6	Short term PV power forecasting for cloudier day	72
Figure 4.7	Short term PV power forecasting for mostly sunny day	72
Figure 4.8	15 minutes ahead PV power forecasting for sunny day	72
Figure 4.9	Training results for short term PV power forecasting for winter season	73
Figure 4.10	Test results for short term PV power forecasting for winter season	73
Figure 4.11	Training results for short term PV power forecasting for summer season	74
Figure 4.12	Test results for short term PV power forecasting for summer season	74
Figure 4.13	Training results for short term PV power forecasting for rainy season	74
Figure 4.14	Test results for short term PV power forecasting for rainy season	75
Figure 4.15	Testing performance of ANN and GNN model for the month of winter season	76
Figure 4.16	Testing performance of ANN and GNN model for the month of summer season	77
Figure 4.17	Testing performance of ANN and GNN model for the month of rainy season	77
Figure 5.1	P-V and I-V characteristics of 5 kW _p SPV system at different solar irradiances	81
Figure 5.2	Hybrid forecasting model for SPV generation forecast	82
Figure 5.3	Flowchart for demand response algorithm	87

Figure 5.4	EENS as a function of consumer flexibility for different DR cases	89
Figure 5.5	Peak reduction (kW) as a function of consumer flexibility for different DR cases	89
Figure 5.6	Schematic representation of proposed system	91
Figure 5.7	Flowchart of proposed algorithm	91
Figure 5.8	15 minutes ahead PV power forecasting for cloudy day	93
Figure 5.9	15 minutes ahead PV power forecasting for cloudier day	93
Figure 5.10	15 minutes ahead PV power forecasting for mostly sunny day	93
Figure 5.11	15 minutes ahead PV power forecasting for sunny day	94
Figure 5.12	15 minutes ahead PV power forecasting for winter season	94
Figure 5.13	15 minutes ahead PV power forecasting for summer season	95
Figure 5.14	15 minutes ahead PV power forecasting for rainy season	95
Figure 5.15	Solar power generation forecasting, operational storage and no DR program for a typical day	97
Figure 5.16	Solar power generation forecasting, operational storage and DR program for a typical day	98
Figure 5.17	Solar power generation forecasting, operational storage and No DR program summer season (Ideal case)	98
Figure 5.18	Solar power generation forecasting, operational storage and with DR program summer season	99
Figure 5.19	Solar power generation forecasting, operational storage and with DR program winter season	99
Figure 5.20	Solar power generation forecasting, operational storage and with DR program rainy season	100
Figure 6.1	Schematic diagram of test system under study	105
Figure 6.2	Detailed description of the proposed VSC control algorithm	106
Figure 6.3	Proposed GDBP NN structure for calculating weighted fundamental active current components	107
Figure 6.4	Proposed GDBP NN structure for calculating weighted fundamental reactive current components	107

Figure 6.5	(a) Performance parameters (b) Waveforms of phase ‘a’ of source voltage and source current	114
Figure 6.6	(a) Performance parameters (b) Waveforms of phase ‘a’ of source voltage and source current	115
Figure 6.7	(a) Performance indices (b) Waveforms of phase ‘a’ of source voltage and source current	116
Figure 6.8	THD for (a) load current of phase ‘a’ (b) grid current	117
Figure 6.9	Performance parameters under non-linear load conditions for variable solar irradiance	118
Figure 6.10	Comparison of V_{dc} for nonlinear load (a) balanced conditions (b) unbalanced conditions	119
Figure 6.11	Proposed VSC control algorithm	121
Figure 6.12	QNBP NN structure for calculating weighted fundamental active current components	123
Figure 6.13	QNBP NN structure for calculating weighted fundamental reactive current components	125
Figure 6.14	Performance parameters for dynamic linear load in ZVR mode	128
Figure 6.15	Performance indices under dynamic nonlinear load, PFC mode	129
Figure 6.16	Performance parameters under non-linear load conditions for variable solar irradiance	130
Figure 6.17	Performance parameters under linear load	131
Figure 6.18	(a) Grid voltage and current of phase ‘a’, (b) Grid voltage and current of phase ‘a’ for PFC mode	132
Figure 6.19	Performance parameters under non-linear load conditions	132
Figure 6.20	(a) Non-linear current, (b) THD	132
Figure 6.21	Improved THD for grid current under non-linear load	133
Figure 6.22	Performance parameters under dynamic non-linear load	133
Figure 6.23	Performance under non-linear load conditions for variable solar irradiance	133

Figure 6.24	(a) Summation type GNN model, (b) A summation type GNN structure to determine fundamental active element of load current	135
Figure 6.25	(a) Performance parameters (b) estimated weights for under steady state linear load conditions in PFC mode	145
Figure 6.26	(a) Performance parameters (b) estimated weights under dynamic linear load conditions for ZVR	147
Figure 6.27	(a) Performance indices (b) weights with training parameters for phase 'a' with steady state loading in PFC mode	148
Figure 6.28	THD for (a) load current of phase 'a' (b) grid current and (c) grid voltage in ZVR mode	149
Figure 6.29	Performance parameters under non-linear load conditions for variable solar irradiance	150
Figure 6.30	Performance parameters under linear load for EKF GNN	152
Figure 6.31	Grid voltage and current of phase 'a' for PFC mode	153
Figure 6.32	Performance parameters under non-linear load conditions for EKF GNN	153
Figure 6.33	(a) Non-linear current, (b) Current and voltage of Phase 'a'	153
Figure 6.34	(a) THD spectrum of Non-Linear Load (b) Improved THD for grid current under non-linear load	154
Figure 6.35	Performance parameters under dynamic non-linear load for GNN EKF	154
Figure 6.36	Performance of intermediate weight signals under dynamic non-linear load for GNN EKF	155
Figure 6.37	Performance parameters under non-linear load with solar PV ON for GNN EKF	155
Figure 6.38	Performance parameters under variable solar irradiance for GNN EKF	156
Figure 6.39	Performance under linear dynamic load PNLMS	160
Figure 6.40	Performance parameters under dynamic non-linear load for PNLMS	161

Figure 6.41	Performance under variable solar irradiance for PNLMS	161
Figure 6.42	THD spectrum for load current and grid current for PNLMS	162
Figure 6.43	Performance of developed controller under non-linear load conditions	163
Figure 6.44	(a) Voltage and non-linear load current of Phase 'a', (b) THD of load current	163
Figure 6.45	Improved THD for grid current under non-linear load for PNLMS	164
Figure 6.46	Performance of developed controller under dynamic non-linear load for PNLMS	164
Figure 6.47	Internal weight signals under dynamic non-linear load	165
Figure 6.48	Intermediate signals for dynamic non-linear load	165
Figure 6.49	Performance under steady state linear load conditions in PFC mode for predictive current control	169
Figure 6.50	Performance under dynamic linear load conditions for predictive current control	170
Figure 6.51	Performance under dynamic non-linear load conditions in ZVR mode for predictive current control	170
Figure 6.52	Performance under variable solar irradiance for predictive current control	171
Figure 6.53	THD spectrum of load and grid current for predictive current control	171
Figure 6.54	Calculation of reference current	173
Figure 6.55	Schematic of VSC control	173
Figure 6.56	Performance of proposed algorithm for Non-linear load with variable solar irradiance	175
Figure 7.1	Proposed System for stability studies	178
Figure 7.2	Phase locked loop (PLL) for proposed controller	182
Figure 7.3	Block diagram of proposed controller	186
Figure 7.4	Performance of controller under STC	192
Figure 7.5	DC link voltage V_{dc} (V) for various irradiances	193

Figure 7.6	Performance at changing atmospheric conditions in terms of grid current compared with performance of PI controller	193
Figure 7.7	PV array voltage for MPPT, PV array (P_{PV}) and grid power (P_g), reactive power supplied by inverter (Q_g)	194
Figure 7.8	Performance under LG fault	194
Figure 7.9	Corresponding positive sequence active and reactive currents	195
Figure 7.10	Performance analysis for three phase short circuit fault	195
Figure B.1	5 kW _p PV system installed at roof top of EEU laboratory, DTU	221
Figure B.2	5 kW _p PV system output and grid connection	221
Figure B.3	Grid connected inverter in laboratory	222

LIST OF TABLES

Table 1.1	Estimated and Cumulative achievement of grid interactive RES	6
Table 1.2	Off grid and captive power renewable energy system	7
Table 1.3	IEEE standards for different renewable energy sources	11
Table 4.1	Day type classifications	68
Table 4.2	Comparison of testing performance for GNN and GNN-W short term solar PV generation forecasting model	76
Table 4.3	Comparison of testing performances using GNN-W and ANN	78
Table 5.1	Different DR cases according to the payback	88
Table 5.2	Comparison of testing performance for GNN-W based short-term solar irradiance forecasting model	96
Table 6.1	Performance parameters of the proposed system	118
Table 6.2	Comparative analysis of proposed GNN controller with existing ANN based controllers	119
Table 6.3	Performance parameters of the proposed system	131
Table 6.4	Performance parameters of the proposed system for EKF GNN	151
Table 6.5	Comparative analysis with other existing algorithms	151
Table A.1	The developed system design specifications.	220

LIST OF SYMBOLS, ABBREVIATIONS AND NOMENCLATURE

A	Diode ideality factor
A_1 - A_2	Coefficient approximate vectors for wavelet transform
$c_{j0,k}$	Scaling function of detail coefficients
C	DC link capacitor (μF)
$(\text{COE})_{\text{op}}$	Cost of energy at off-peak
$(\text{COE})_{\text{p}}$	Cost of energy at peak
C_r	Filter capacitance (μF)
D	Duty cycle
D_1 - D_2	Coefficient detail vectors for wavelet transform
E_1	Error between the actual DC link voltage and the reference DC link voltage
E_2	Error between the actual q-axis inverter current and the q-axis inverter current
e_i	Rotor voltage for imaginary component of synchronous reference frame
E_{fc}	Reversible open circuit voltage (Volts)
E^0	Standard reversible cell voltage (Volts)
E_i	Error in between GNN output and desired output
e_r	Rotor voltage for real component of synchronous reference frame
E_{MP}	Charging energy from hydrokinetic system to pump (Watts)
E_{op}	Energy required during off-peak period
E_{p}	Sum squared error
E_{peak}	Energy required during peak period
E_{pvop}	PV energy output during off-peak period

E_{pvpeak}	PV energy output during peak period
f_{max}	Maximum switching frequency (kHz)
f_{sw}	Switching frequency (kHz)
F_1	Sigmoidal characteristic function
F_2	Gaussian characteristic function
G	Gravitational acceleration constant (9.8 m/s ²)
G_d and G_q	Two control inputs to the controller
h	Current ripple
H	Net head pumping (Meter)
i_a, i_b and i_c	Inverter's output currents for phase A, B and C respectively (Ampere)
I_d	d-axis inverter current
i_i	Rotor current for imaginary component of synchronous reference frame
i_{cr-pp}	Current ripple
i_{fc}	Output current of fuel cell (Ampere)
I_i	Stator current for imaginary component of synchronous reference frame
I_{in}	Input current (Ampere)
I_{inv}	Inverter Current (Ampere)
i_{La}, i_{Lb}, i_{Lc}	Load currents of phase 'a', 'b' and 'c' respectively (Ampere)
I_{Lp}	Fundamental active current component
I_{Lq}	Fundamental reactive current component
I_m	Maximum current of SPV system at maximum power point (Ampere)
I_{MPP}	PV current at maximum power point (Ampere)

I_o	Module saturation current (Ampere)
i_{psa}	Active reference component of grid current
I_{pV}	SPV output current (Ampere)
i_{qsa}	Reactive reference component of grid current
I_q	q-axis inverter current
i_r	Rotor current for real component of synchronous reference frame
I_R	Stator current for real component of synchronous reference frame
I_{rs}	Reverse saturation current of diode (Ampere)
i_{sa}, i_{sb}, i_{sc}	Grid currents of phase 'a', 'b' and 'c' respectively (Ampere)
$i_{sa}^*, i_{sb}^*, i_{sc}^*$	Reference currents of phase 'a', 'b' and 'c' respectively (Ampere)
I_{sc}	Photocurrent (Ampere)
J	Dilation index
k	Boltzmann constant ($1.38 \times 10^{-23} \text{ JK}^{-1}$)
K	Scaling index
k_i	Short circuit current/temperature coefficient
K_i	Integral gain of PI controller
K_p	Proportional gain of PI controller
L	Actual solar irradiance
L_b	Input inductor of boost converter (mH)
L_f	Interfacing inductor (mH)
L_s	Scaled solar irradiance
L_{max}	Maximum value of solar irradiance in a particular column
L_{min}	Minimum value of solar irradiance in a particular column
N	Number of cells in stack

N_p	Number of cells connected in parallel in SPV module
N_s	Number of cells connected in series in SPV module
N_{OCT}	A constant term
O_i	Final output of generalized neuron
O_Σ	Output of Σ_A part network
O_Π	Output of Π part network
P_i	Mole fraction of species
P_m	Maximum power output of SPV system (Watts)
P_{pv}	Active power output of SPV system (Watts)
q	Electric charge (1.602×10^{-19} C)
Q	Electric charge (1.602×10^{-19} C)
Q_{GT}	Water volumetric flow rate from upper reservoir to lower through the turbine (m^3/s)
Q_{MP}	Water flow rate from the pump (m^3/s)
R	Universal gas constant (JK/Kmol)
R_{dt}	Ratio between the daily measured and theoretical clear sky insolation
R_{fc}	Equivalent resistance of fuel cell (Ohms)
R_p	Shunt resistance (Ω)
R_r	Filter resistance (Ω)
R_s	Series resistance (Ω)
S	Solar irradiance (W/m^2)
T	Cell temperature (Kelvin)
T_k	Actual temperature (Kelvin)
T_{ref}	Reference temperature (Kelvin)
T_s	Switching time (ms)

u_{pa}, u_{pb}, u_{pc}	In phase unit templates of phase voltages
u_{qa}, u_{qb}, u_{qc}	Quadrature unit templates of phase voltages
V_a, V_b, V_c	Phase voltage of utility grid (Volts)
V_{ab}, V_{bc}, V_{ca}	Line voltage of utility grid (Volts)
V_{act}	Activation overvoltage (Volts)
V_{con}	Concentration overvoltage (Volts)
V_{dc}	DC link voltage (Volts)
V_{dc}^*	Reference DC link voltage (Volts)
V_{fc}	Output voltage of fuel cell (Volts)
V_{fca}, V_{fcb} and V_{fcc}	Voltage across ripple filter capacitors (Volts)
V_i	Stator voltage for imaginary component of synchronous reference frame
V_m	Maximum voltage of SPV system at maximum power point (Volts)
V_{ohm}	Ohm voltage (Volts)
V_{PV}	SPV output voltage (Volts)
V_r	Stator voltage for real component of synchronous reference frame
V_t	Voltage at point of common coupling (Volts)
V_t^*	Reference voltage at point of common coupling (Volts)
V_{te}	Error between sensed and reference voltage at point of common coupling (Volts)
W	Weights of GNN
W_{pdc}	Active current component
W_{qt}	Function of reactive loss current component
W_{pv}	Feed forward weight function of solar power
W_{ap}, W_{bp}, W_{cp}	Updated weights for hidden layer of active components
W_{aq}, W_{bq}, W_{cq}	Updated weights for hidden layer of reactive components
W_{Lp}	Mean active component of load current
W_{Lq}	Mean reactive component of load current
W_{Σ}	Weights of summation part of GNN

ΔW	Change in weights of GNN
X_{obs}	Actual value of quantity
X_{pred}	Forecasted value of quantity
X_i	Input to GNN model
$X_{\text{o}\Sigma}$	Output of summation part of GNN
$X_{\text{o}\Pi}$	Output of product part of GNN
Y_{max}	Normalization upper range (0.9)
Y_{min}	Normalization lower range (0.1)

Greek Symbols

ω_b	Base angular frequency (pu)
ω_m	Angular mechanical speed of rotor (pu)
Ψ	Mother wavelet function
Ψ_i	Stator flux linkage for imaginary component of synchronous reference frame
Ψ_r	Stator flux linkage for real component of synchronous reference frame
λ_1 and λ_2	Control parameters of SMC
λ_i	Rotor flux linkage for imaginary component of synchronous reference frame
λ_p	Gain scale factor of Π
λ_r	Rotor flux linkage for real component of synchronous reference frame
λ_s	Gain scale factor of Σ_A
η_{MP}	Pumping efficiency
η_{GT}	Efficiency of turbine generator set
Γ	Temperature parameter at maximum power point
Σ_A	Aggregation function used with sigmoidal characteristic function
Π	Aggregation function used with Gaussian characteristic function

α_1 and α_2	Control parameters of SMC
α	Momentum factor for better convergence
η	Learning rate
$\phi_{j0, k}$	Scaling function of coarse scale coefficients
$\omega_{j, k}$	Scaling function of detail coefficients
μ	Micro
Ω	Ohm
ϕ	Phase
γ	Temperature parameter at maximum power point
σ_1 and σ_2	Siding variables
σ_x	Standard deviations of the variables x
σ_y	Standard deviations of the variables y

Nomenclature

ACR	Avoided cost rate
ADC	Analog to digital converter
ANN	Artificial neural network
ANFIS	Artificial neural fuzzy inference system
AR	Autoregressive
ARMA	Autoregressive moving average
DAC	Digital to analog converter
CWT	Continuous wavelets transform
CPP	Critical pricing program
DWT	Discrete wavelet transforms
DFIM	Doubly fed induction machine
DFSOGI	Double frequency second order generalized integrator
DG	Distributed generators
DISCOMS	Distribution companies
DR	Demand response

EENS	Expected energy not supplied
EKF	Extended kalman filter
EES	Electrical energy storage
EPLL	Enhanced phase locked loop
EMS	Energy management system
ESS	Energy storage system
FC	Fuel cell
FLC	Fuzzy logic controller
FISPWM	Frequency inverted sin pulse with modulation
GA	Genetic algorithm
GBI	Generation-based incentives
GDBP	Gradient descent back propagation
GNN	Generalized neural network
HV	High voltage
IGBT	Insulated-gate bipolar transistor
INC	Incremental conductance
ISSBC	Interleaved soft switching boost converter
JNSM	Jawaharlal Nehru National Solar Mission
LF	Low frequency
LMS	Least mean square
LV	Low voltage
MAE	Mean absolute error
MNRE	Ministry of New and Renewable Energy
MPP	Maximum power point
MPPT	Maximum power point tracking
MV	Medium voltage
NISE	National institute of solar energy
NLMS	Normalized least mean square
NSM	National Solar Mission

NWP	Numerical weather forecasting
NWS	National weather service
PCC	Point of common coupling
PCU	Power conditioning unit
PFC	Power factor correction
PHS	Pumped hydro storage
PI	Proportional Integral
PNLMS	Proportionate normalized least mean square
PPMC	Pearson product-moment correlation coefficient
P&O	Perturb and observe
PQ	Power quality
PQR	Power quality and reliability
PSO	Particle swarm optimization
PV	Photovoltaic
QNBP	Quasi newton back propagation
PWM	Pulse width modulation
RBF	Radial basis function
RES	Renewable energy sources
RMSE	Root mean square error
RTP	Real-time pricing
SERCs	State electricity regulatory commissions
SMC	Sliding mode controllers
SOFC	Solid oxide fuel cell
SPV	Solar photovoltaic
SRF	Synchronous Reference Frame
SSEZ	Small scale energy zone
STATCOM	Static synchronous compensator
STSEF	Short term solar energy forecasting
SVC	Static VAR compensator

SVM	Support vector machines
SVR	Support vector regression
THD	Total harmonic distortion
TOD	Time of day
TOU	Time of use
UPF	Unity power factor
VSC	Voltage source converter
VSI	Voltage source inverter

CHAPTER 1

INTRODUCTION

1.1 GENERAL

The demand of electrical energy is increasing drastically because of urbanization, growth in population and industrialization etc. The renewable energy sources (RES) are being utilized globally to meet the energy demand due to various advantages. These advantages includes sustainability, increased economic growth, new employment opportunities, intensify human welfare as well as contribution towards climate safe future etc. The power generation from renewable energy resources was 26.5 % as on December 2017. However it is expected to increase exponentially to fulfill the demand in the near future. Solar photovoltaic systems are gaining attention and wide spread acceptance as distributed generators (DG) because of large availability of its resources with quite visible positive impacts on the environment. Further, the advancement in the solar photovoltaic technology including enhanced efficiency of solar cells because of mass production of high-quality wafers, thin wafers handling capability, high minority carriers lifetime maintenance, optical losses minimization and reduction in the cost of energy generation over the last several decades also attracts the use of solar photovoltaic technology for power generation. In addition, the leading forces behind the increased deployment of SPV (solar photovoltaic) technology are declining cost of solar PV systems and incentives provided by the governments of various countries. The global capacity of PV during 2005 to 2017 is presented in Fig. 1.1 [1]. In India most of the land area receives solar energy of about 5 kWh/m² every day for an estimated 300 or more clear days of the year. If 1 % of such land area is

utilized for generating electricity through the use of SPV at an overall efficiency of 10%, then 429×10^9 kWh of electrical energy can be generated every year.

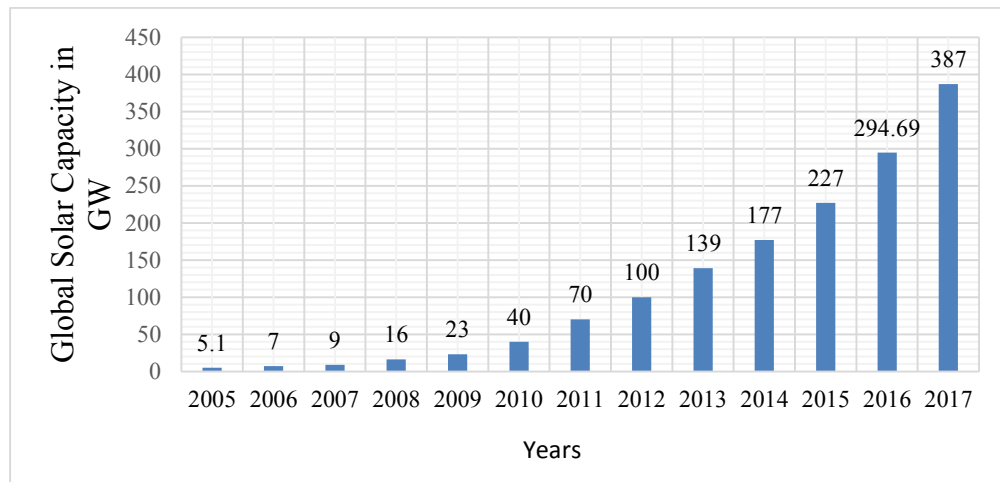


Fig. 1.1 Global PV capacity in GW between years 2005-2017

The integration of SPV into electric power system is increasing drastically. This provides more power from renewable energy sources but cause adverse effects as well in the distribution grid like voltage limit violation at point of common coupling, poor power quality, frequency disturbances, grid stability issues etc. Accordingly, grid codes and regulations has been modified by the authorities to accommodate the grid connected PV systems [2].

Voltage fluctuations are major concern for grid connected SPV systems which may lead to voltage limit violations. Overvoltage or voltage rise occurs when the PV penetration increases and cause reverse power flow which may cause unstable operation of grid [3]. A typical low voltage (LV) system is usually designed in such a manner that the power will flow from a high voltage (HV) substation to the low voltage consumer loads. With the massive utilization of solar photovoltaic energy generation as a distribution generation, it becomes mandatory to deploy efficient and coordinated control measures for the integration and measurement related issues [4]. These control

approaches are helpful in accommodating and facilitating the integration of SPV systems into distribution grid with benefits.

The energy storage system (ESS) used to store the excess power generation from solar PV systems in order to control the active or real power flow between the utility and the SPV power generation system. There are various types of storage systems available for grid connected SPV systems. Different type of energy storage and their use in grid connected SPV system for distribution voltage regulation are provided in further sections with detail insight. Active power curtailment is another method to provide voltage regulation support in distribution systems. An inverter can be used to curtail the active power from PV system [5]. Other methods for active power control are also available in previous works which are also being discussed in this thesis. To maintain the voltage within limits at point of common coupling (PCC) one can provide reactive power support. This can also be done by using PV inverters and other technologies also. FACTS devices can also be used as voltage fluctuations mitigation devices as they can provide better voltage control functionality. Devices like static synchronous compensator (STATCOM), static VAR compensator (SVC) and shunt capacitor banks devices gives better voltage control and fast response in case of sudden voltage rise.

Variability of output power from a solar photovoltaic generation plant can lead to the unstable operation of the power system. These fluctuating output power problems lead to the issues in its use and at the same time generates the market needs for electrical energy storage (EES). The proper amount of power must be provided by the utilities to meet the varying consumer demands. An imbalance between demand and supply may cause the damage in the stability of utility grid as well as the power quality. The issues like unbalancing can be reduced via implementation of resource forecasting, EES and

demand-side management. With the help of these three aspects, power management for the improved dispatch of utility-scale PV plants can be assured [6]. The SPV output power forecasting helps in controlling of variables and optimize the capacity of energy storage system. Hence in this thesis, control approaches for solar PV grid integration, short term solar energy forecasting and energy management for smart grid environment are discussed.

1.2 CURRENT STATUS OF RES IN INDIA

Continuous growth in energy demand, depleting fossil fuels and emerging economy makes mandatory to enhance the existing potential of renewable energy for Indian power sector [7]. Considering this fact, India has set up a separate ministry for renewable energy development in early 1980s i.e. Ministry of New and Renewable Energy (MNRE). Last three and half years shows a large capacity addition of 27.07 GW from renewable energy under grid connected mode, which has 12.87 GW from Solar Power, 11.70 GW from Wind Power, 0.59 from Small Hydro Power and 0.79 from Bio-power [8].

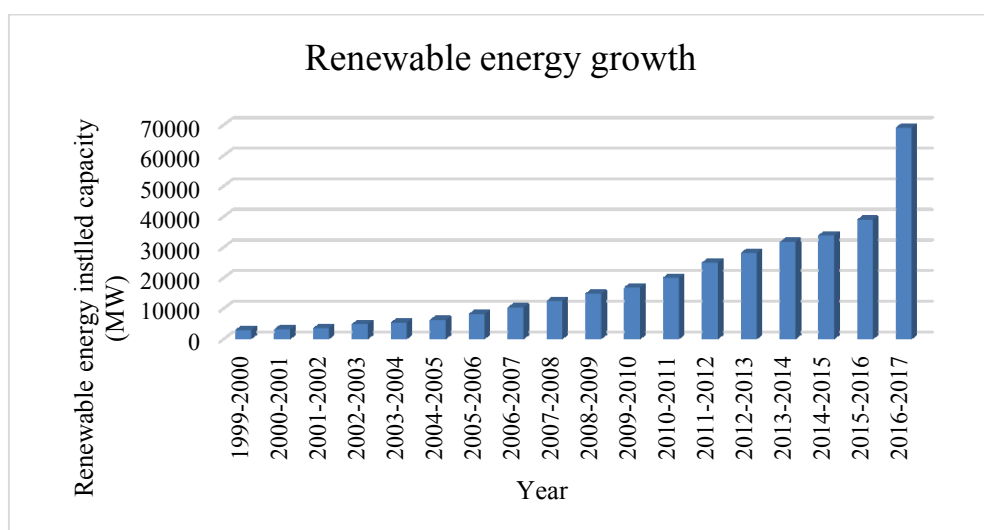


Fig. 1.2 Growth of RES year wise

As on 30.06.2018, total installed capacity of Indian power sector is 346202 MW approximately, in which contribution from different sources are: thermal 64.32%, hydro 13.11 %, nuclear 1.96 % and RES 20.6 % [9]. RES includes solar, wind, small hydro and biomass etc. Fig. 1.3 shows installed capacity of Indian power sector source wise.

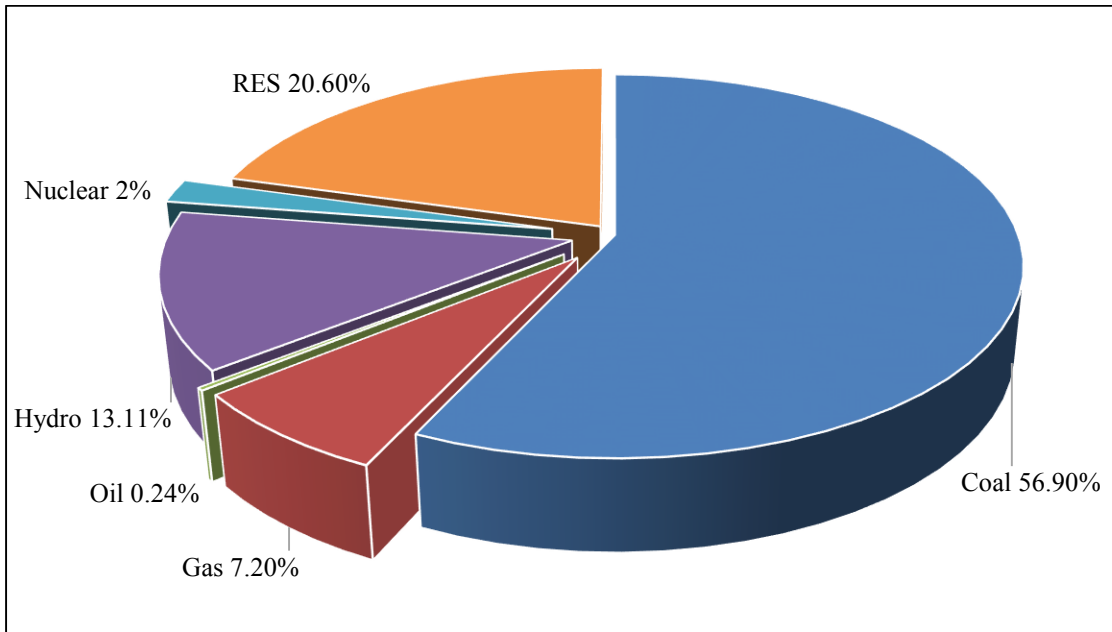


Fig. 1.3 Installed capacity of Indian power sector source wise

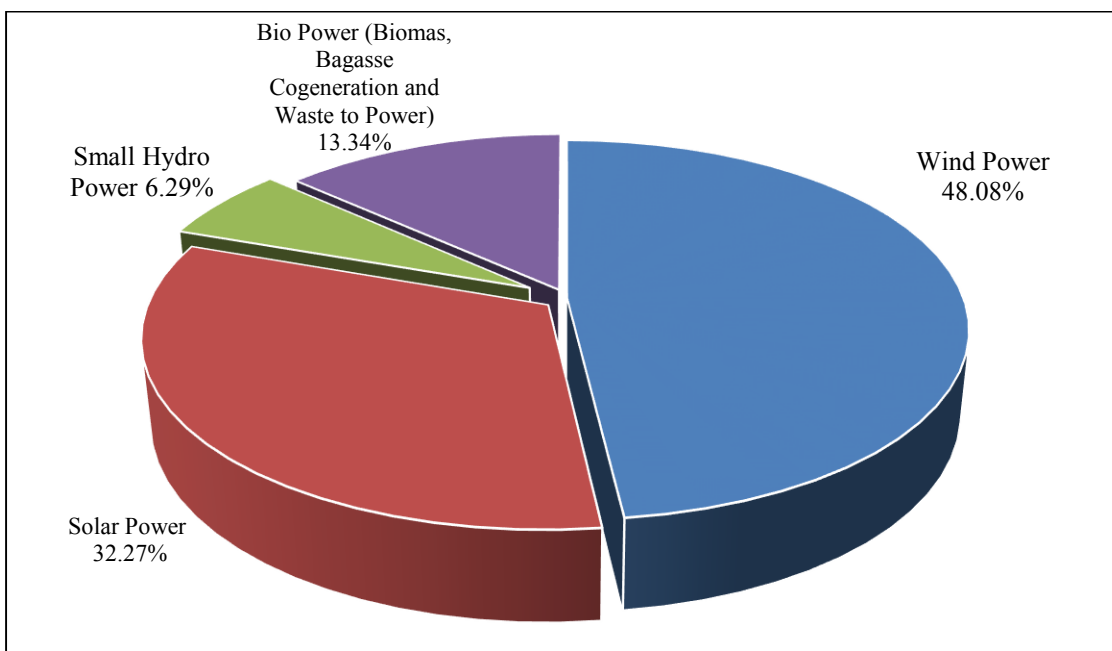


Fig. 1.4 India's RES installed capacity

Installed capacity from various renewable energy sources as on 30.06.2018 is shown in Fig. 1.4. Total grid-connected capacity of 71325.42 MW has been achieved in India through renewable energy generation till 30.06.2018. It consists of wind power capacity of 34293.48 MW, solar power generation 23022.83 MW, biomass power generation of 9515.91 MW and small hydropower capacity with 4493.20 MW.

RE sector capacity acceleration keeps going on this way, it will cross 175000 MW mark by 2022. Cumulative achievement in year 2018-2019 is presented in Table 1.1.

Table 1.1 Estimated and cumulative achievement of grid interactive RES

Sector	FY- 2018-19		Cumulative Achievements (as on 30.06.2018) (MW)
	Target (MW)	Achievement (April-June 2018)	
Wind Power	4000.00	148.48	34293.48
Solar Power	11000.00	1371.14	23022.83
Small Hydro Power	250.00	7.40	4493.20
Bio Power (Biomass, Bagasse Cogeneration and Waste to Power)	352.00	14.00	9515.91
Total	15602.00	1541.22	71325.42

Renewable energy resources are being utilized by many to generate their own power in their backyards. Table 1.2 shows off-grid/ distributed RE systems source wise.

Table 1.2 Off Grid and Captive Power Renewable Energy System

Sector	FY- 2018-19		Cumulative Achievements (as on 30.06.2018) (MW)
	Target (MW)	Achievement (April-June 2018)	
Waste to Energy	18.00	0.00	172.15
Biomass Gasifiers	1.00	0.00	163.37
SPV Systems	200.00	66.44	737.85
Total	219.00	66.44	1073.37

1.3 RENEWABLE ENERGY INITIATIVES IN INDIA

The Indian government is playing very important role in promoting the adoption of RES by providing attractive schemes, incentives, such as generation-based incentives (GBIs), viability gap funding, concessional finance, capital interest subsidies and fiscal incentives etc [10-12]. Further, the National Solar Mission (NSM) was launched to promote use of energy from sun for electricity generation and other uses. The NSM aims to reduce the fossil fuel based generation and make solar as one of the prominent source in the country. Also government target is to reduce the capital cost on solar power generation.

To achieve the renewable energy target of 175 GW by the year 2022, major initiatives are taken such as solar park, solar roof top projects, solar defence scheme, solar PV power plants on canal bank and canal tops, solar pump, solar rooftop etc. Moreover, Indian government has also taken drives to promote RES electricity generation. One such scheme is the Electricity Act 2003 [13] in which the requirement

of license for stand-alone generation and distribution systems in rural areas has been removed. Further, National Rural Electrification Policy, 2005 and National Rural Electrification Policy, 2006 are brought up for speed up the rural electrification. The New Tariff Policy (2006) makes it mandate to purchase a minimum percentage of energy from such sources [14-18]. A project launched on 11th January, 2010 by the Prime Minister, which is known as Jawaharlal Nehru National Solar Mission (JLNSM) set a huge target from grid connected solar power [19]. This mission is also secure the reduction of overall cost of power generation with solar energy.

1.4 DISTRIBUTED POWER GENERATION

A Distributed Generation (DG) is defined as a relatively very small power generation system operating in isolation from the central generating station and located in close proximity of load center. The generation capacity of a DG generally ranges from a few kW to thousands of kW includes small conventional energy sources like small gas engines, diesel generators and RES such as solar photovoltaic, wind, bio gas, etc. The power output of DG is used with the existing distribution system, but the size of DG system is very small compared to the conventional system [20]. As the integration RES based DG in the distribution grid poses significant impacts like voltage limit violation at point of common coupling, poor power quality, frequency disturbances, grid stability issues. Therefore, generation close to load end increases the power quality and reliability (PQR) of supplied electricity to sensitive demands. DGs can significantly reduce requirement to expand the existing traditional system, on the other hand controlling the large numbers of DGs in the network pose several challenges from security and operation point of view [21]. SPV technologies are more prominent and promising among DG sources as energy from sun is the most abundant form of renewable energy. Power electronic converters has played a major role in making the

use of solar PV more convenient with the time. Power Electronic interface helps in converting the DC output of solar PV in AC power and as well as reduces the intermittency of the output power. Further, solar PV can be added or installed as per the size and pattern of loads [22]. The distributed solar power generation system does not require complex planning and pre approvals.

Distributed generation can be either grid integrated or isolated to feed nearby load. Distributed generation may also be referred as dispersed generation if the size is range about one to hundred kilowatts, particularly used to fulfill the household requirements. DG system offers attractive solution to today's energy deficit issues especially rural users, while a large amount of investment is needed to connect to the main grid. DG installations provides several benefits such as modularity, load management, reliability, efficiency, no emission and improved security.

1.5 INTEGRATION OF SPV BASED SYSTEMS INTO DISTRIBUTION GRID

1.5.1 Necessity, Issues and challenges

The integration of solar PV with grid as DG is able to solve the demand and generation mismatch issues especially in developing countries. As the integration of solar PV systems at medium voltage (MV)/low voltage (LV) grid level poses some negative impacts such as voltage limit violation at the point of common coupling (PCC), frequency variations, grid stability issues, etc. Therefore, the grid-integrated solar PV system must follow the codes and regulations defined by the authorities such as IEEE 1547, IEC 61727 and VDE-AR-N4105. Further, the control of voltage source converter (VSC) plays very important role to synchronize the plant with the utility grid. The performance of controller is mainly depends on the algorithm used to calculate the reference grid currents and to give the switching signal patterns for insulated-gate

bipolar transistor (IGBT) switches. Hence, integration of solar PV as a DG must have efficient and coordinated control measures for the proper synchronization. Two types of topologies are mainly adopted by researchers for grid integration of solar PV systems: single stage and two stage system topologies.

1.5.2 Power quality analysis

Integration of solar PV systems to the grid causing positive benefits with more power generation as well as adverse effects like degradation of power quality, because of intermittent nature of solar PV systems. Also, the power quality problems in the distribution systems are arise due to different types of nonlinear loads and expansion of the distribution system in not well planned manner [23-24]. Power quality is quantified in terms of voltage limit violation at point of common coupling, frequency disturbances, grid stability issues etc. and cause failure or mal-operation of customer's equipment. The poor power quality leads to overheating of transformers, poor power factor and low efficiency of connected equipment etc. As the integration of RES based DG system requires large power electronics interface, which again degrade the power quality [25]. Massive utilization of solar photovoltaic systems as a distribution generation makes mandatory to deploy efficient and coordinated control measures for the integration and measurement issues. These control techniques are helpful in accommodating and facilitating the integration of SPV systems into distribution grid with benefits. Filters such as passive, active, hybrid in series, shunt and combination of both are used to mitigate the power quality issues [26]. Grid codes and regulations has been defined by the authorities to accommodate the grid connected PV systems. IEEE 1547, IEC 61727 and VDE-AR-N4105 are major standards for SPV integration as a distribution generator (DG) in low voltage distribution systems. These standards are used to maintain the stability and power quality specified by grid codes for SPV integration.

These standards define and used to maintain the stability and power quality specified by grid codes for SPV interconnections. A Comparison based on power and voltage levels of various standards is provided in Table 1.3.

Table 1.3 IEEE standards for different renewable energy sources

S. No.	Standard	System type	Voltage level	Power
1	IEEE1547	All RES	Primary/Secondary Distribution Voltages	≤ 10 MVA
2	VDE-AR-N4105	All RES	Voltages less than and equals to 1 kV	≤ 100 kVA
3	IEC 61727	Solar PV	Low voltages	≤ 10 kVA

1.6 PROBLEM FORMULATION

The large scale penetration of PV power into electric distribution system possesses a great threat to grid stability and reliability. Therefore, the utilities are developing the smart grid approach across the world and PV power forecasting is the one of the key tool for this new paradigm. An intelligent approach based on wavelet transform and generalized neural network (GNN) is proposed for very short term PV power forecasting.

Further, an energy management system supporting high penetration of solar photovoltaic generation for smart grid using solar forecasts and energy storage system has been also developed and presented in this thesis.

Voltage source converter (VSC) is the key component which is used to supply AC loads and integrate with the grid. The control of VSC plays very important role to synchronize the PV plant with the utility grid. The performance of control techniques mainly depends on the algorithm used to calculate the reference grid currents and to give the switching signal patterns for insulated- gate bipolar transistor (IGBT) switches.

Hence, integration of solar PV as a DG must have efficient and coordinated control measures for the proper synchronization.

Intelligent and adaptive control techniques for three phase grid connected SPV system are developed in this work. These proposed algorithms provides reactive power, harmonic compensation and helps the system to transmit active power to the grid and loads effectively. The performance of the proposed algorithms has been validated through simulations carried out in MATLAB/Simulink platform and also implemented on hardware prototype.

1.7 ORGANIZATION OF THE THESIS

This thesis consists of eight chapters including: Introduction, literature review, modeling of RES based components, short term solar energy forecasting, energy management supporting high PV penetration for smart grid, development of control algorithms for grid integration of SPV system, control and stability studies of grid tied solar PV system, conclusions and future scope followed by references.

Chapter-1: This chapter provides brief introduction about the current state of RES in India, Initiatives taken by government, distributed generation, integration of solar PV system into grid and power quality issues and its mitigation.

Chapter-2: The brief literature review on mathematical modelling of solar PV system, control algorithms for grid integration of solar PV systems, impacts of high PV penetration in distribution system and power quality analysis is given in this chapter. Further, a comprehensive literature review of existing short term solar energy forecasting and energy management supporting high PV penetration for smart grid is

also presented. Based on the exhaustive literature review, knowledge gap analysis is presented in the last section of chapter.

Chapter-3: This chapter presents the design and development of various components of SPV plant. Mathematical modelling and selection of various components such as DC bus capacitance, DC bus voltage, interfacing inductors, voltage source converter, and ripple filter are given in detail. Further the development of sensing and measurement circuit, gate isolation driver circuits, interfacing inductors etc. are also presented.

Chapter-4: This chapter presents an intelligent model for 15 minutes ahead short term solar energy forecasting. An intelligent approach based on wavelet transform and generalized neural network (GNN) is developed and applied for the short term solar energy forecasting problem, keeping in view of the requirement of distribution companies (DISCOMS)/utility. The proposed approach is also applied to choose the appropriate energy storage system.

Chapter-5: This chapter is focused on the development of energy management system supporting high penetration of solar photovoltaic generation for smart grid using solar forecasts and storage system.

Chapter-6: This chapter deals with the development of control techniques for integration of solar PV system into grid. Mathematical modelling, MATLAB model development and real time implementation of the proposed algorithms are discussed in detail. Further the simulation and hardware results are also presented under different load and irradiance conditions.

Chapter-7: This chapter deals with the robust controller development for the solar PV system considering nonlinearity and uncertainties. Solar PV system is also modelled considering uncertainties. Robust control law is developed considering the internal plant dynamics and stable operation range for parameters.

Chapter-8: This chapter presents a summary of conclusions drawn from the above chapters. Some suggestions for future work are also provided in the thesis.

CHAPTER 2

LITERATURE REVIEW

2.1 INTRODUCTION

This chapter contains a brief review of the previous work done on the topics dealt in this thesis. The topics includes: Mathematical modeling of RES based components, short term solar energy forecasting, impacts of high PV penetration in distribution system, energy management system for accommodating high PV penetration, control algorithms for grid integration of solar PV systems and power quality analysis.

Based on the literature survey, it is tried to find some research gap and accordingly problems are formulated.

2.2 MATHEMATICAL MODELING OF RES BASED COMPONENTS

Integration of a solar PV array with the grid requires various power electronic based components. These components includes, DC/DC converter and inverter. A DC/DC converter used to implement maximum power point tracking (MPPT) controller to track the maximum power of SPV array. Inverter provides conditioning in the SPV output and make this able to match the grid requirements. This section presents a brief literature survey mathematical modelling of various component such as solar PV array, power electronics converters required for grid integration, fuel cell and pumped hydro storage etc.

This chapter is partially based on the following published papers

1. **Priyanka Chaudhary** and M. Rizwan, "Voltage regulation mitigation techniques in distribution system with high PV penetration: A review" *Renewable and Sustainable Energy Reviews (Elsevier)*, Volume 82, No. 3, 3279-3287, 2018. ISSN: 1364-0321, **Impact Factor: 8.05.**

Output parameters of solar PV array depends upon various meteorological parameters like solar irradiance, temperature, wind direction, humidity etc [27-28]. Natrajan Pandiarajan et.al [29] presented circuit model of photovoltaic module for a common use of material scientists and power electronic circuit designers for developing the better PV power plans. The authors presented the detailed modeling procedure for the circuit model with equations using simpower sytem block of MATLAB/Simulink. This paper also presented the MPPT control with DC/DC boost converter with appropriate simulation results.

Samer Said et.al [30] considers the PV cell as the main building block for simulation and monitoring the performance of PV array. The proposed model simulated for various temperature & isolation values and P-V, I-V characteristics obtained for different parameters. The authors also studied different patterns of partial shading on PV arrays. This paper describes a model of PV array which is suitable to simulate the dynamic performance of PV base power generating systems. By-pass diode significantly affects the output characteristics of PV array in case of shading. Authors simulate the presented model for comparing the shaded and unshaded PV array characteristics. This study consists of two major sections; one is under uniform insolation and another is under partial shaded conditions. Presented results conclude that presence of multiple peaks (local peaks) reduces the MPPT efficiency because it fails to observe the global peak.

Kashif Ishaque et.al [31] presented a two diode model of PV cell. The proposed model gives better accuracy at low values of solar irradiance and allows predicting solar PV system performance more accurately. Authors estimate the values of R_p and R_s so that the input parameter can be reduced to four and hence computational time can be reduced. A standard PV module datasheet is used as information to PV simulator. Large

array simulation is supported by the simulator and that can be interface with different power converter & MPPT algorithms. Model accuracy verified by using five different modules from various manufacturers.

However, there are various topologies of DC-DC converter including buck, boost, push pull, half bridge, full bridge, flyback, buck-boost etc. The choice of topology depends on system requirements and its applications.

Ahmed H. El Khateb et. al [32] presented a combination of cuk and buck DC-DC converter for a standalone PV system. A MPPT control technique is implemented with the converter to provide a constant voltage/current to battery even under the changing atmospheric conditions. The proposed system has been tested under different operating conditions.

Amudhavalli D. et.al [33] proposed a new topology of DC-DC boost converter for solar photovoltaic power generation system. This topology comprises a interleaved soft switching boost converter (ISSBC) with maximum power point tracking control. Proposed converter minimizes the switching losses by adopting a resonant soft switching method. Advanced P&O MPPT technique has been used in this work to increase the efficiency of the system. The model has been simulated on MATLAB/Simulink platform as well as hardware implementation also done by using this boost converter topology authors are able to reduce input current ripple and output voltage ripple.

Yungtaek Jang et.al [34] developed a new two inductor, two switch boost converter topology. Proposed converter gives a wide range of output voltage regulation with a variable load and input voltage. An auxiliary transformer is also incorporated with this converter to couple the current paths of the two boost inductors. Authors

verified the performance of proposed two inductor boost converter with a 1KW prototype circuit designed for 40-70V battery voltage input and deliver upto 2.9 A at 380V output.

Moreover, fuel cells are being utilized for power generation for domestic and industry level applications. PV power generation combines with FC provides an attractive and efficient solution for increasing power generation. A typical fuel cell power generating system includes fuel cell stacks, a fuel processor, power conditioning unit (PCU) etc. FCs are high current and low voltage devices, so AC application of FC needs voltage boost before conversion to 220 V, 50 Hz AC.

Samaiah et al. [35] investigated and compared the mitigation of low frequency (LF) current ripples by using cascaded converter with conventional push-pull converters for FC applications. A single stage, single phase FC for grid connected as well as standalone mode is proposed based on boost inverter by Jang et al. [36]. Bensmail et al. [37] presented modelling of a hybrid PV/FC system, which utilized a power conditioning unit (PCU) for effective management. Akin et al. [38] proposed a soft-switched space vector PWM controlled parallel resonant DC link based inverter for fuel cell applications. Further, authors used the proposed converter with an induction motor to evaluate the results of a controller.

Seyezhai et al. [39] investigated the use of single phase hybrid cascaded multilevel inverter (HCMLI) with a PEMFC. The proposed inverter controlled using a novel hybrid modulation technique which combines fundamental frequency switching scheme and variable frequency inverted sin pulse with modulation (FISPWM) technique.

Energy storage systems play a key role to maintain the power quality and reliability in today's scenario of distributed generation. Pumped hydro storage (PHS) is a mechanical based energy storage system. A PHS plant consists of two water reservoirs, placed at different levels. During off-peak period, water is pumped from the lower reservoir to the upper reservoir. The stored water is fed back from the upper reservoir to lower with the help of turbine during peak period. S. Ekoh et al. [40] presented an optimal sizing method for a standalone hybrid wind- PV and PHS to evaluate performance with reliability and cost analysis. PHS is becoming the most encouraging technology to support the high level of renewable energy penetration in modern power systems [41-42].

2.3 SHORT TERM SOLAR ENERGY FORECASTING

The variability and uncertainty associated with the solar energy becomes significant challenges for successful and economically efficient integration of solar power generating plants into utility grid [43]. The availability of solar energy measuring stations is scarce even throughout the world because of high instrumental cost. In India, the data of solar irradiance is available for limited stations. Hence, the forecasting of solar energy will play a significant role for sustainable power generation.

PV power forecasting approaches can be broadly classified into two categories- physical model based methods and statistical model based methods. Physical methods utilize performance model of the particular PV system in deterministic manner, whereas in statistical methods available historic datasets are used to train the forecasting model with ignoring reliance on PV models [44].

Statistical method such as autoregressive (AR) and artificial neural network (ANN) model used a past set of measurements as training dataset and perform

numerical analyses to develop forecasting models which can forecast the PV output based on numerical weather forecasting (NWP) data [45].

Hybrid forecasting methods are reported and developed utilizing both physical and statistical model based approaches. Hybrid models utilized two or more separate forecasting methods to improve the accuracy of forecasting. The statistical models includes multiple linear regression, stochastic time series, autoregressive integrated moving average with exogenous variables (ARIMAX) and general exponential smoothing, state space model, and support vector regression (SVR) [46].

Statistical methods such as machine learning and time-series methods are very popular and most widely used by researchers, in recent years. The forecasting accuracy of machine learning methods increases with the as the size of training datasets. Various machine learning based forecasting models are reported in literature for irradiance and consequent PV power forecasting on the basis of short to midterm after in depth study it is found that the artificial neural network (ANN) based techniques are mostly adopted in recent research works. ANN is a set of large number of highly interconnected processing neurons working in unison to solve specific problems and it can learn from the examples. ANN can be configured for a specific application through a machine learning process. Many researchers have developed applications of ANN for solar radiation and other weather data forecasting and these can improve typical statistical approaches [47].

A large number of machine learning methods are applied in [48] by authors on historical National Weather Service (NWS) weather forecasts with a correlation to generation data from solar modules. Presented model are developed using linear least square regression along with support vector machines (SVM) and authors made a

conclusion that the models derived with SVM's with Radial basis function (RBF) kernels provides a very promising way to improvise accuracy in solar power forecasting.

Six meteorological parameters namely temperature, dew point, wind velocity, sky cover, precipitation, humidity are used to predict short-term solar power. Four types of NN methods for 24 hour ahead solar forecasting for a 20 kW system are presented in [49]. Besides machine learning methods, time series based forecasting models to deal with stochastic properties of the irradiance or Solar PV generation data had also been developed and investigate by other researchers.

R. Huang et al. [50] mentioned that an ARMA (autoregressive moving average) model is preferable over Persistence model for short and medium-term forecasting for a micro-grid level.

The hybrid approach presented by AU Haque et al. [51] combines a data filtering technique based on wavelet transform and a soft computing model based on fuzzy adaptive resonance theory mapping network and optimized using a technique based on firefly algorithm. The authors mentioned that model provides superior performances compared to other individual and hybrid ANN based techniques.

To improve real-time control performance and reduce possible negative impacts of PV systems a weather-based hybrid method for 1-day ahead hourly forecasting of PV power output is presented in [52] and results shows that the proposed approach provides better forecasting accuracy than the simple SVR and traditional ANN techniques. The proposed solar power forecasting approach comprises classification, training, and forecasting stages and in the classification stage, the self-organizing map

and learning vector quantization networks are used to classify the collected historical data of PV power output and to a practical solar PV power generation system.

Chen C. et al. in [53] presented an advanced statistical method for solar output power forecasting based on artificial intelligence techniques which used past power measurements and meteorological forecasts of solar irradiance, relative humidity and temperature as input. The developed method is helpful in operational planning for transmission system operator and for PV power system operators trading in electricity markets.

A novel photovoltaic power forecasting model considering aerosol index data as an additional input and weather classification using back propagation ANN approach is presented in [54] to improve the forecasting accuracy of conventional methods using ANN.

In [55] Yang C. et al. proposed a spatio-temporal solar forecast model based on AR model with exogenous inputs and applied for both hour-ahead and day-ahead timescales. Exogenous inputs are historical values of irradiance from five different locations in Colorado and cloud cover percentage from neighboring sites.

Chow et al. [56] presented ANN based short-term forecast of energy generated by a 40 kWp building integrated PV system. A number of mathematical models for solar irradiance forecasting under cloudless skies are available in the literature. The forecasted outputs obtained using statistical models were satisfactory with the constraint of clear sky weather condition.

Due to high uncertainty in weather conditions, fuzzy logic, neural network based models are proposed by researchers to estimate the solar irradiance at a certain

location using different meteorological parameters. Short term solar energy forecasting models such as hourly, weekly are available in literature but 15 minutes ahead solar energy forecasting less reported in the literature using hybrid methods. ANN has some inherent limitations and drawbacks such as difficulty in deciding the structure of ANN, neuron type selection, needs large training time etc.

These drawbacks can be overcome by using a Generalized Neural Network (GNN) and has been proposed in the past. However, load forecasting models based on GNN and other applications using GNN are widely available [57-74] but do not have much applications in short term resource forecasting.

Chaturvedi D.K. et al. [75] presented a method that integrates wavelet transform, adaptive genetic algorithm and fuzzy system with GNN for short term electrical load forecasting problem. Performance of the developed approach is compared with other GNN variants on the basis of forecasting error.

In paper [76] the global solar irradiance forecasting is done on hourly basis with generalized neural network model (GNN).

2.4 IMPACTS OF HIGH PV PENETRATION IN DISTRIBUTION SYSTEM AND ENERGY MANAGEMENT

High PV penetration in distribution networks may lead to various technical impacts on the system. Voltage rise issue is one of the most likely negative effect of the high PV penetration. This problem is actually lead to reverse power flow in the network which violate the distribution network standards. To control the voltage of LV distribution system is very critical issue in the presence of large PV penetrations as the resistivity of LV grids make voltage control different from transmission system. A simple network structure is shown in Fig. 2.1.

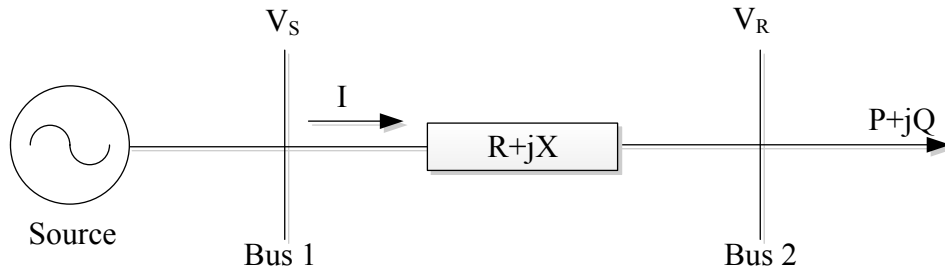


Fig. 2.1 A simple network structure

According to the Fig. 2.1 voltage drop across the line can be written as:

$$\begin{aligned} \Delta V &= I(R + jX) = \frac{(P+jQ)^*}{V_R} (R + jX) \\ &= \frac{PR+QX}{V_R} + j \frac{PX-QR}{V_R} \end{aligned} \quad (2.1)$$

The phasor diagrams for HV and LV networks are shown in Fig. 2.2 and 2.3 respectively to represent the voltage drop characteristics. Accordingly, the expression for voltage drop across the line is determined. If the effect of charging in HV transmission system is neglected, the magnitude of resistance is very small in comparison with the reactance because of high X/R ratios.

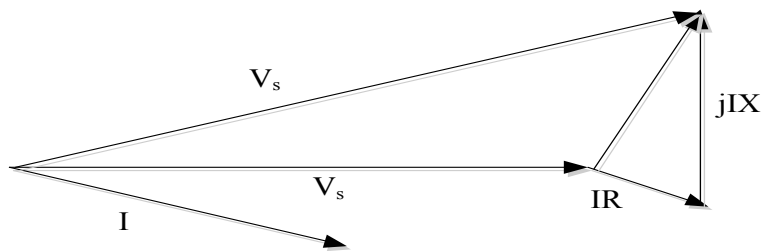


Fig. 2.2 High voltage (HV) transmission system voltage drop characteristics

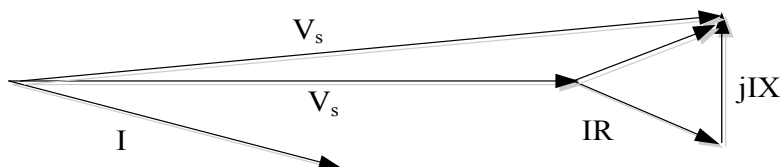


Fig. 2.3 Low voltage (LV) distribution system voltage drop characteristics

For HV transmission system X/R ratio is high, resistance effect can be neglected in equation 2.1.

$$\Delta V = \frac{QX}{V_R} + j \frac{PX}{V_R}$$

$$|\Delta V| \cong \frac{QX}{V_R} \quad (2.2)$$

For LV systems X/R ratio is low, hence resistive effect can no longer be ignored, in this case. Hence by ignoring the imaginary part equation can be rewritten as:

$$|\Delta V| = \frac{PR+QX}{V_R} \quad (2.3)$$

Derivative of equation 2.3 with respect to the power transfer is

$$|\Delta V| = \frac{\partial |\Delta V|}{\partial P} dP + \frac{\partial |\Delta V|}{\partial Q} dQ = \frac{R}{V_R} dP + \frac{X}{V_R} dQ \quad (2.4)$$

Equation 2.4 clearly shows that with increase in active power transmission, voltage difference will automatically increase. Whereas by applying negative reactive power increment, voltage difference magnitude can be reduced. Above given discussion clearly give an insight issues concern with the high PV penetration in the LV distribution networks.

As we know in traditional radial distribution network uses on load tap changing transformers at substations line regulators on distribution feeder with shunt capacitors for voltage regulations. Direction of power flow at the point where regulators are placed, decide the voltage regulation action required. In case of PV integration voltage profile changes along a feeder due to changing direction and magnitude of real and reactive power flows with high PV penetrations. The PV penetration depends upon solar radiation which varies daily, hourly and over a shorter period of time (minutes to seconds). An IEEE 15 bus system shown in Fig. 2.4 has been used here to show the different voltage profiles throughout the day with or without voltage control techniques

with insertion of PV systems at different buses (Bus 5, 7, 8, 13, 14). Fig. 2.5 shows a typical solar irradiance profile throughout a day.

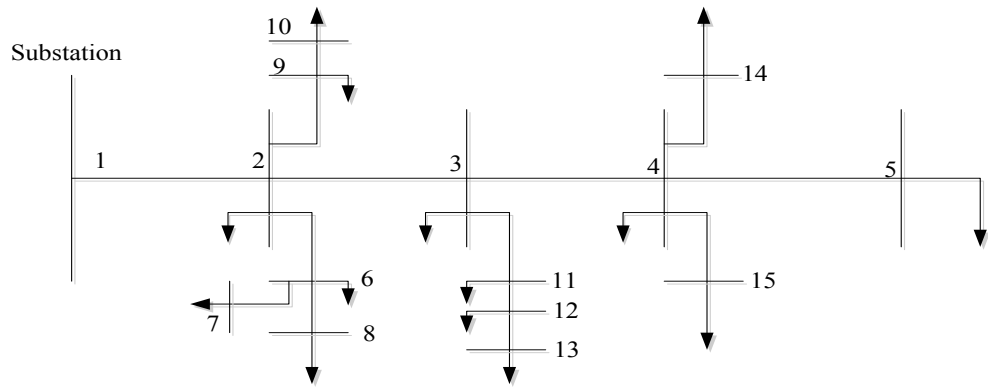


Fig. 2.4 IEEE 15 bus radial system

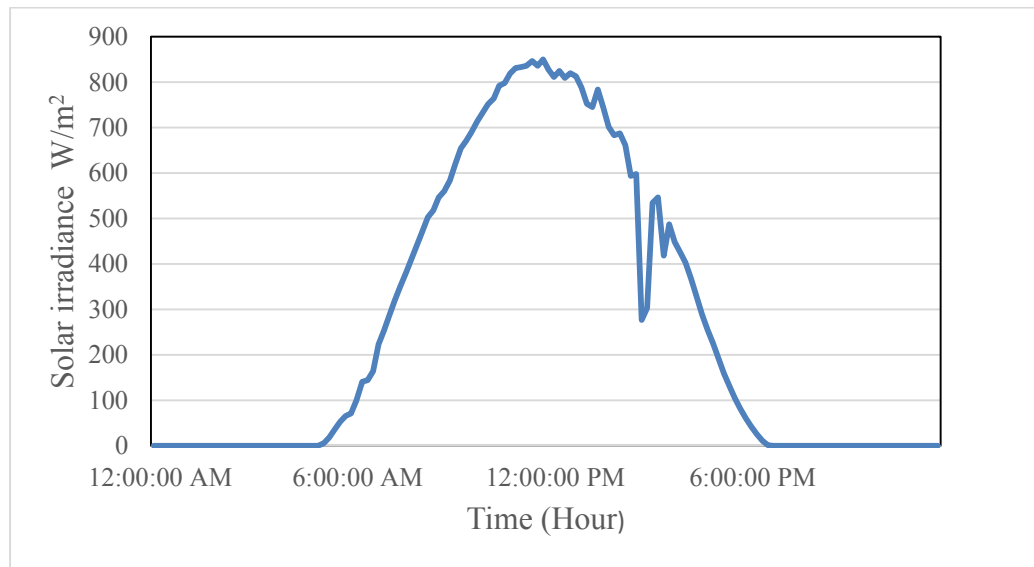


Fig. 2.5 Typical Solar irradiance profile for a day

Without any voltage control, as shown in Fig. 2.6, the distribution grid experienced voltage rise around noon time because during high irradiance period PV will generate more power. Fig. 2.7 presents voltage profiles during a day simulation with deploying voltage control.

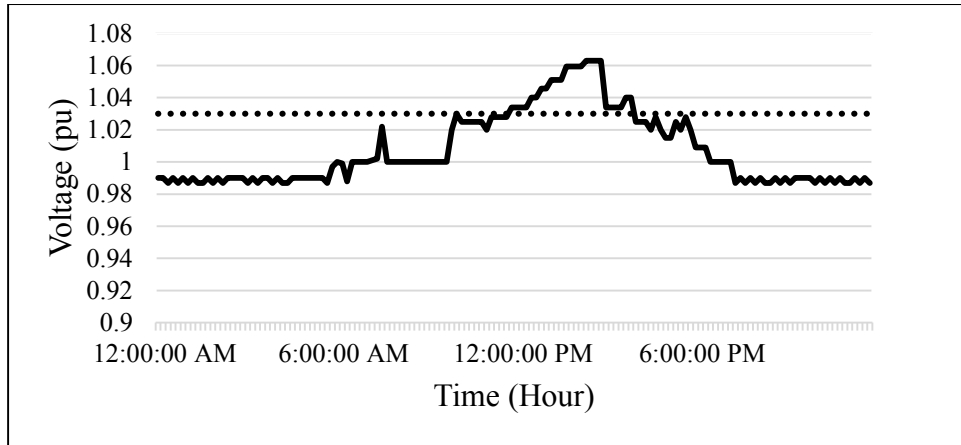


Fig. 2.6 Voltage profiles during a day simulation without deploying voltage control

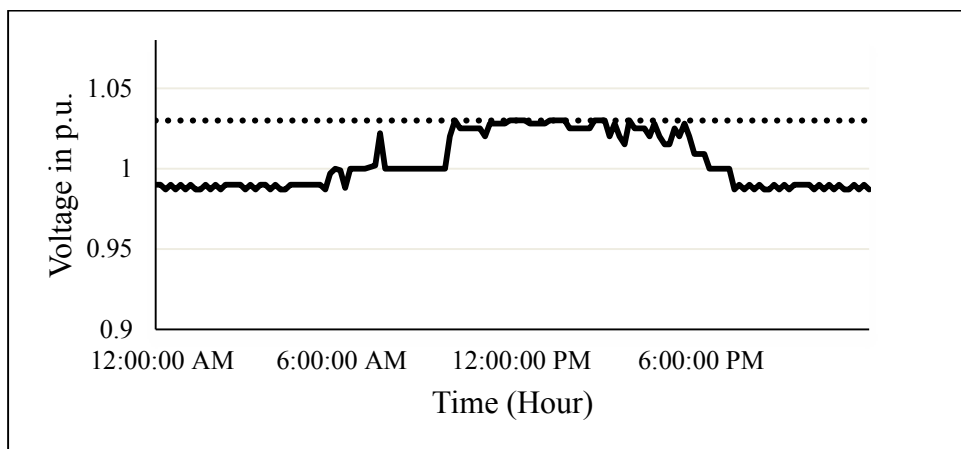


Fig. 2.7 Voltage profiles during a day simulation with deploying voltage control

Shivashankar et. al [77] mentioned about the need of analysis of behavior of the distribution system in case of PV integration. Authors also came up with a comprehensive tool to investigate the day long changes in the network's performance due to PV integration. They have used this developed tool to investigate the single phase PV impacts on a three phase distribution network.

Operation and protection problems on distribution network with high PV penetration has been investigated by M Haque Mejbaul et. al [78]. Simulations on a prototype test system has been performed. Conclusion made by authors show that both system protection on voltage profile have significant impacts on system's performance.

Issues related to the reverse power flow and voltage rise and voltage limit violation defined by various standards due to high PV penetrations are mentioned by MJE Alam et. al [79]. Authors also describe that the severity of voltage problem depends on the relative size and location of distribution generator (DG) and loads, distribution topology and method of voltage regulation. Researchers also discussed about the voltage performance of the feeder and flow of active and reactive power with various loadings with various PV input assumptions.

M.E. Baran et. al [80] presented about the interaction between multiple PV inverter and grid can cause the stability violation of LV distribution network. Authors overviewed the bilateral impacts of DG or distribution networks first and later on added the recent advance done to provide voltage support functionality in case of high PV penetration.

E. Demiork et. al [81] carried out a work to observe the capability of power transformer to facilitate the power flow requirements with the anticipated high penetrations of small scale embedded generation within small scale energy zone. Further they have described about considered small scale energy zone (SSEZ), as a section of low voltage network with a high PV penetration of embedded generator along with the controllable loads and energy storage units. With varying level of SSEZ, simulation has been carried out by authors on an approved UK generic PSCAD/EMTDC electrical network model.

PC Chen et. al [82] evaluated the impact of different levels of PV penetration in a distribution feeder connected to utility grid. Authors concluded that the distributed PVs in a wide geographical area with different weather conditions have less impact on the frequency and voltage of the distribution network.

M. Zillamann et. al in [83] presented that the battery energy storage (BES) can help in buffering wind and SPV generation, by taking extra energy generated by the system and to return it back to network when it is required. Authors also investigated the use of battery in distribution network voltage regulation with different control strategies.

Y. Yang et. al [84] proposed an effective battery sizing technique is proposed for distributed battery energy storage system for mitigation of voltage rise issues in distribution system for high PV penetration. A cost benefit analysis is also presented by authors considering load shifting and peak power generation etc.

F. Marra et. al [85] proposed different concepts of energy storage to maintain the voltage limits in distribution systems with high PV penetrations. They have proposed a storage based reactive power control approach and grid reinforcement and active power curtailment can be avoided. The proposed algorithm can be summaries as:

- worst case of load and generation with the LV grid model under study has been considered, then a load flow algorithm made to run, identification of critical nodes on which voltage is above the maximum limit. Further in this algorithm combined storage is added with the feeder. Then the minimum power is calculated which can keep critical voltage V_{\max} .

S. Ghosh et. al [86] came up with the importance of active and reactive power control in mitigation of voltage rise issue for distribution system in case of high PV penetration. The authors enhance the droop based reactive power control by active power curtailment algorithm.

G. Mokhtari et. al [87] proposed a robust and efficient algorithm to coordinate customer's resources and control voltage rise in LV distribution network with local and distributed control strategies.

HT Yang et. al [88] proposed the use of droop base active power curtailment strategy for voltage rise prevention in LV radial type feeders caused by high PV penetration.

A combined approach using real power curtailment and reactive power compensation of SPV system has been proposed by TT Ku et. al [89] to prevent overvoltage problems when load transfer between distribution systems executed.

S. Ghosh et. al [90] presented a local voltage regulation technique for distribution networks with high PV penetration. This technique utilizes a very short term solar generation forecast and active power curtailment and average smart PV inverter. The effectiveness of the proposed methodology has been demonstrated by authors on a standard test feeder with real time load and PV generation data.

SJ Lewis et. al [91] authors proposed a method to provide information to electricity utilities with an information how PV system affect the system and solutions to mitigate the negative impacts. In this work effective management of SPV system is done in order to utilize the benefits and reduced risks.

T. Stetz et. al [92] presented an encompassing cost benefits analysis for different voltage control techniques. The result shows that the local reactive power control methods and PV active power output curtailment methods are capable of reducing the necessity of a voltage driven grid reinforcement.

S. Hashemi et al. [93] developed a strategy in order to examine the effect of reactive power absorption by SPV inverter and using electrical energy storage system as a solution for increasing the PV hosting capacity in LV networks.

Importance to carryout voltage stability analysis of electric distribution system has been mentioned by the R. Yan et al. [94]. In this paper authors modified an IEEE 13 bus network in order to conduct network stability analysis in case of variable PV penetration. Authors have demonstrated that voltage instability issues of distribution system in case of PV integration can be efficiently solved by support of inverter reactive power.

The growing penetration level of solar photovoltaic technology is becoming a challenging task in the smart energy management systems. The power generated from the solar photovoltaic systems is intermittent. Therefore, it is imperative to best predict the incoming solar energy and estimate the power generated from SPV systems [95-100].

P. Tian et al. [101] present a two-level hierarchical optimization method for microgrid community energy management system for smart grid applications. The control executed consequently from lower level to upper level to minimize the operational cost.

A supervisory power management system (PMS) for a grid-tied microgrid and energy storage systems with fewer numbers of required sensors is developed [102]. The proposed system incorporates the renewable energy variations, grid availability and price of electricity with changes in local area loads. Utility grid's frequency and voltage of the local bus under integration of RES should be within prescribed limits. ESS becomes important to meet up these challenges.

Storage and microgrid are scheduled to operate in utility supportive mode [103-105]. Being subjected to high operational cost in the islanded mode of operation, ESS coordination, incentive and price-based demand response (DR) makes the significant impact on the economy of microgrids [106]. An online smart, dynamic energy management system is proposed using evolutionary adaptive dynamic programming and reinforcement learning framework [107].

From the consumer point of view, ESS can lower the electricity cost because it stores electricity purchased at a low price during off-peak periods and it can be used during peak times instead of using expensive power, and one can also get the benefit to sell the surplus amount to utility or other consumers during peak loads. The relationship between ESS and electrical power system considering distributed generators are invested and widely available in the literature [108-112]. Problems like optimization of energy storage capacity and energy management with peak load shaving at fixed storage capacity are typically associated with ESS. Optimization of energy storage capacity is essential for a reliable operation of distributed generators (DG) like solar PV, wind farm, etc. Forecasting power output and also demand management play significant roles in optimizing the size of the ESS capacity. According to the form of energy stored ESS can be classified into various types such as mechanical energy storage; electrochemical energy storage; electrical and magnetic field energy storage; thermal energy storage. Pumped hydro storage (PHS) a type of mechanical energy storage is the oldest and largest of all commercially available technologies. Most of the world's energy storage capacity is in the form of pumped hydro storage due to low cost, high life cycle and large storage capacity often able to store hundreds to thousands of megawatts per installation.

These advantages make pumped hydro storage an ideal technology for leveling and peak shaving of loads. Another important aspect of smart grid management is to analyze the behavior of user such as load shifts can be referred as demand-side management [113-117].

Time-varying electricity tariffs are widely applied in electricity markets to ignore peak over loading which causes reduced or rescheduled energy consumptions. A visible real-time information is essential for price-based responses to make the consumer aware about the general energy reduction and some responses such as load shifting may be controlled automatically by smart devices or controllers by the consumer needs.

A mathematical model for smart loads for demand-side management is provided [118] using neural network load estimator as a function of day time, time of use (TOU) price and ambient temperature, etc.

M. Jin et al. [119] formulated a multi-objective optimization with prevailing constraints for large-scale micro-grid, flexible loads and utility trade-off.

The demand response can be simplified as rescheduling the flexible loads for the high generation periods from low generation periods. The intelligent methods available in the literature are limited to energy management between the storage system and SPV and rarely quotes the dynamic scheduling considering the resource forecasting and grid-connected mode with demand-side management.

2.5 CONTROL ALGORITHMS FOR GRID INTEGRATION OF SOLAR PV SYSTEMS

In literature, various control techniques are widely available for effective integration of DG systems with reactive power compensation and harmonics

elimination capabilities to the distribution grid at PCC. As per available literature, broadly classified as conventional, intelligent and adaptive techniques [120-126]. Some of the conventional control techniques are Synchronous Reference Frame (SRF) theory, Enhanced phase locked loop based approaches, Instantaneous Reactive Power theory, power balance theory based approach, conductance fryze, etc. Control techniques based on conventional approaches for VSC grid synchronization are not much successful for nonlinearities associated with RES based systems as these approaches possess overshoots and long settling time in response. Intelligent and adaptive approaches are key solutions to these issues which results in better accuracy and very fast dynamic response.

Varma et. al. [127] have proposed a PV-STATCOM for improving the power transfer capabilities of the system to transmit real power to utility with existing converter system.

Hamid et. al. [128] presented a scheme based on power conditioner unit placed in parallel with the plant and works in feed-forward mode behaves to compensate the PV plant's output current distortion to reduce the current harmonics from a photovoltaic (PV) plant.

Kannan et. al. [129] proposed $I \cos \phi$ controlling algorithm for DSTATCOM which provides continuous source harmonic reduction, reactive power compensation and load compensation with performance comparison of the Fuzzy Logic Controller with the conventional Proportional Integral (PI) controller.

Arya et. al. [130] implemented DSTATCOM using a learning-based anti-Hebbian control algorithm for compensation of linear and nonlinear loads.

Mishra et. al. [131] have proposed an optimized control algorithm JAYA to optimize the coefficients of PI controller and filter parameters of PV fed DSTATCOM.

Singh et. al. [132] proposed grid interfaced SPV generating system using a neural network based control algorithm which utilizes LMS (least mean-square) and known as Adaline (adaptive linear element) to estimate reference source currents.

Moreover, Jain et al. [133] presented PV power generation system with an adjustable DC link voltage for voltage variations at PCC utilizing two-stage based circuit topology with interweaved DFSOGI (Double Frequency Second Order Generalized Integrator) based control technique to control multifunctional VSC for dynamic loads at PCC.

A large numbers of approaches based on artificial neural networks (ANN) are widely reported by many authors for DSTATCOM with dynamic loadings [134-141] but less available for PV fed DSTATCOM systems.

A hybrid control algorithm is proposed in [142] and called as gradient descent back propagation (GDBP)-based $I \cos\phi$ for a distribution static compensator (DSTATCOM) to avail harmonic mitigation, power factor correction (PFC) mode under non-linear reactive loads.

Artificial neural network based approaches are complex and needs large computational time. Further, generalized neural network (GNN) based control strategy can be used to overcome above mentioned. Applications of GNN are widely available in load forecasting, solar irradiance/energy forecasting, load frequency control in power system, power system stabilizer, electrical machines and control system related problems [142-148]. Less work is reported in literature for application of GNN as

control strategy for grid tied PV systems. GNN based models reduces training time as well as improve the performance of the system.

Further, to improve the performance of the system improved filter technologies can be adopted to predict the weights. Extended Kalman filter (EKF) [149-152] may be adopted to estimate and updating the weights of the artificial neural network models.

In order to enhance the efficiency of PV systems, the maximum power point tracking of solar PV array is significantly important. MPPT tracking is complex due to non-linear nature of SPV system and varying meteorological parameters like solar irradiance, ambient temperature, wind velocity and relative humidity etc. Large number of MPPT techniques have been developed and presented in literature and includes perturb and observe, incremental conductance, constant voltage, open circuit voltage, short circuit current, extremum seeking control and hybrid etc, techniques based on artificial neural networks, fuzzy logic, genetic algorithms [153].

Roberto Feranda et. al [154] presented a comparative study of ten most widely used maximum power point tracking algorithms using MATLAB/Simulink. Authors compared ten most common techniques namely constant voltage method, short circuit pulse method, open voltage method, perturb and observe method, temperature methods, incremental conductance method. According to the authors conclusion open voltage and short circuit pulse techniques provides low energy output in comparison with P & O and incremental conductance algorithms. Temperature methods continuously calculate and update the correct voltage reference. Authors analyzed the constant voltage technique is worst among the all ten MPPT methods.

Hairul Nissah Zainudin et. al [155] compared two MPPT techniques namely incremental conductance and P & O on the basis of simplicity, digital or analogical

implementation, number of sensors required, speed of convergence, hardware required for implementation, cost etc. Comparative analysis is carried out by keeping current and voltage as sensing element and by varying solar irradiance and temperature. MATLAB/Simulink platform have been used to carried out the results in terms of efficiency, energy yield etc. Authors analyzed the performance for three type of converters; Boost converter, buck converter and cuk converter. Paper concluded that the incremental conductance MPPT algorithm is best in all the cases.

Ragasudha C. P. et. al [156] presented design and implantation of standalone solar photovoltaic system for the purpose of battery charging with maximum power point tracking controller. Authors also developed a 600 W prototype for the same system for the performance analysis. They have chosen a buck converter to implement the incremental conductance MPPT techniques with IC MPT612. The designed system is effectively track the MPP (Maximum power point) of the PV panel and gives efficient operation.

M. Abdulkadir et. al [157] designed and simulate a system incorporated with maximum power point tracking algorithm with a high frequency boost converter. Designed controller is able to track the MPP of PV panel by the adjustment of the duty cycle of the switch used in the boost converter. MATLAB/Simulink software is used to develop the designed model. Developed model tested under the practical environmental conditions for different loading levels. Authors also modified the original incremental conductance algorithm and found new incremental conductance MPPT algorithm more efficient.

Mostafa Mosa et. al [158] proposed a modified MPPT controller using a model predictive control. Developed controller has been implemented using DC-DC

multilevel converter which is used to step up the small dc voltage. Performance of designed system has been analyzed under different solar irradiance and temperature conditions on a MATLAB/Simulink platform and obtain results are validated by using dSPACE 1103 control desk with a real time simulation.

2.6 POWER QUALITY ANALYSIS

In today's world, power quality is becoming an issue for distribution systems. Lot of research is being carried out on the improvement of power quality on different aspects such as voltage, current and frequency deviation [159-164]. Grid connected solar photovoltaic systems consists at power electronics converters in order to convert DC to AC, these converter inject harmonics into grid. PV system suffers from the output voltage fluctuations due to non-uniform irradiance conditions. These all things make PV system unstable in terms of grid connection.

S.K Khardem et.al [165] presented a technical review of power quality problems associated with the renewable energy based distributed generation system. This review paper also described the role of custom power devices like STATCOM, DVR, etc. in power quality improvement. Authors explained that output of PV panel depends on the solar intensity and atmospheric conditions and power quality issues are not only because of solar irradiance but also depend upon the inverters, filters, controlling mechanism etc. According to the authors a special attention is required to maintain the voltage profile and power flow. Custom power devices are found to be very capable for integration of renewable energy based generating plants into the grid.

Masoud Farhoodnea et.al [166] presented a dynamic PQ analysis of highly penetrated grid connected photovoltaic systems in distribution network system under varying atmospheric conditions. From the results and discussions it can be observed

that the high penetrated grid connected PV systems may become a cause of power quality problems such as voltage flicker, power factor reduction and harmonics etc.

2.7 KNOWLEDGE GAP ANALYSIS

This section summarizes the research gaps found from the literature survey discussed in the previous sections.

Short term solar energy forecasting:

The forecasted outputs obtained using statistical models were satisfactory with the constraint of clear sky weather condition. Due to high uncertainty in weather conditions, fuzzy logic, neural network based models are proposed by researchers to estimate the solar irradiance at a certain location using different meteorological parameters. Short term solar energy forecasting models such as hourly, weekly are available in literature but 15 minutes ahead solar energy forecasting less reported in the literature using hybrid methods. ANN has some inherent limitations and drawbacks such as difficulty in deciding the structure of ANN, neuron type selection, needs large training time etc. These drawbacks can be overcome by using a Generalized Neural Network (GNN) and has been proposed in the past.

Further, in the present scenario the bidding of power is done on 15 minutes basis by many distribution companies. Keeping in mind aforesaid, 15 minutes ahead short term solar energy forecasting has been done and presented. Therefore, an intelligent approach based on wavelet transform and generalized neural network (GNN) is developed and applied for the short term solar energy forecasting problem. The results obtained from the proposed model are evaluated on the basis of statistical indicators

like root mean square error (RMSE) and mean absolute error (MAE). It is concluded that the performance of the proposed model is found better as compared to GNN model.

Energy management supporting high PV penetration for smart grid:

Variability of output power from a solar photovoltaic generation plant can lead to the unstable operation of the power system. These fluctuating output power problems lead to the issues in its use and at the same time generates the market needs for EES. The proper amount of power must be provided by the utilities to meet the varying consumer demands. An imbalance between demand and supply may cause the damage in the stability of utility grid as well as the power quality. The issues like unbalancing can be reduced via implementation of resource forecasting, EES and demand-side management. With the help of these three aspects, power management for the improved dispatch of utility-scale PV plants can be assured.

In this thesis, the solar energy forecasting is performed using a hybrid model consisting of neural networks and wavelet transform. The performance of the proposed model is evaluated based on both root mean square error (RMSE) and mean absolute error (MAE). To validate the proposed method the above results are compared with other existing approaches like ANN and found better within desired limits. There is a pumped hydro storage (PHS) in the configuration under study to meet the grid requirements. In order to obtain more accurate and practical results, demand response (DR) program has been also integrated in the formulation of the problem. An adequacy analysis is also carried out under various consumer flexibility scenarios. Performance analysis of the proposed energy management system has been done using MATLAB/Simulink platform, and the same is validated on 5 kW SPV system. Further, the proposed model can be applied to large-scale systems.

Development of control algorithms for grid connected solar PV system:

Based on the exhaustive literature review on the development of control techniques for grid connected solar PV system, it has been concluded that some major problems associated need further improvisation. These include the convergence, response time, large computational time, complexity, large static error, stability under dynamic conditions. In this work these problems have been considered to develop intelligent control techniques for grid integration of solar PV system.

Control and Stability Studies of Grid Tied SPV System:

This chapter deals with the robust controller development for the solar PV system considering nonlinearity and uncertainties. Solar PV system is also modelled considering uncertainties. Robust control law is developed considering the internal plant dynamics and stable operation range for parameters.

CHAPTER 3

MODELING OF RENEWABLE ENERGY BASED COMPONENTS

3.1 INTRODUCTION

Based on literature review in previous chapter, it is found that the modelling of different components of the proposed system is needed. In this chapter, modelling and design of various components of three phase grid connected solar PV system are presented in detail. These components includes solar PV array, DC/DC converter, DC link capacitor design, voltage source converter, AC interfacing inductors, ripple filters etc. Further, modelling and design of fuel cell (FC) and pump hydro storage (PHS) are also presented in detail to implement solar PV based power generating system of smart energy management.

Further, development of an experimental prototype for grid integrated solar PV using VSC is discussed in detail with each component.

3.2 SOLAR PV PLANT MODELLING

Grid integration of a solar PV array requires a power electronic interface between the grid and the solar PV array. Power conditioning unit (PCU) comprises of DC/DC converter, MPPT controller and inverter, used to condition the SPV output and make this able to match the grid requirements. Control of voltage source converter (VSC) in a grid-tied system plays a significant role to control and synchronize the SPV system with the utility grid. Utilization of SPV based power generation systems as a DG makes mandatory to deploy efficient and coordinated control measures for the VSC. In literature, various control techniques are widely available for effective integration of SPV systems such as Synchronous Reference Frame (SRF) theory,

Enhanced Phase Locked Loop (EPLL) based approaches, Instantaneous Reactive Power theory, power balance theory-based approach, conductance fryze, etc. Intelligent, adaptive and hybrid approaches are key solutions to integrate SPV systems with the grid and results in better accuracy with a very fast dynamic response as per available literature.

3.2.1 Mathematical description of solar PV array

The solar cells are interconnected and hermetically sealed to constitute a photovoltaic module to achieve high power ratings. Further, a PV array is constituted by series-parallel combination of PV modules for higher ratings. The maximum power for SPV system is governed by the following equation:

$$P_m = (n_s * V_m)(n_p * I_m) \quad (3.1)$$

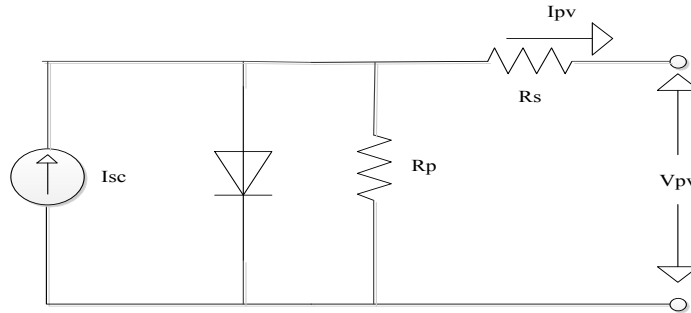


Fig. 3.1 Single diode model of PV cell

Equations for the output current using Fig. 3.1 can be obtained as follows:

$$I_{sc} - I_D - \frac{V_D}{R_p} - I_{PV} = 0 \quad (3.2)$$

Where,

$$I_D = I_{scref} \left[\exp \left(\frac{qV_{oc}}{kAT} \right) - 1 \right] \quad (3.3)$$

$$I_{sc} = [I_{scref} + K_i(T_k - T_{ref})] * S/1000 \quad (3.4)$$

I_{sc} depicts the photocurrent in amperes generated from solar incident current at the standard condition (25°C and 1000W/m²), K_i represents the short-circuit current/temperature coefficient at I_{scref} (0.00065A/K), T_k and T_{ref} are the actual and reference temperature in Kelvin, S shows the actual solar irradiance coming at the surface of device and 1000W/m² is the irradiation at standard testing conditions. Reverse saturation current I_{rs} of diode can be written as:

$$I_{rs} = I_{scref} + \left[\exp\left(\frac{qV_{oc}}{N_s k A T}\right) - 1 \right] \quad (3.5)$$

The saturation current is the function of temperature and given by;

$$I_o = I_{rs} \left[\frac{\left(\frac{T}{T_{ref}}\right)^3 e^{qCg}}{A k} * \left(\frac{1}{T_{ref}} - \frac{1}{T}\right) \right] \quad (3.6)$$

The output current equation can be written as:

$$I_{PV} = I_{sc} N_p - N_s I_o \left[\exp\left\{\frac{q(V_{PV} + I_{PV} R_s)}{N_s A k T}\right\} - 1 \right] V_{PV} + \frac{I_{PV} R_s}{R_p} \quad (3.7)$$

In equation (3.6) k is the Boltzmann constant (1.38×10^{-23} J K⁻¹), q is the electronic charge (1.602×10^{-19} C), T is the cell temperature (°C or K); A is the diode ideality factor, R_s the series resistance (Ω) and R_p is the shunt resistance (Ω). N_s is the number of cells connected in series and N_p is the number of cells connected in parallel.

A Vikram Solar ELDORA 270 of 270.66 W_p solar PV module has been used to obtain a 10 kW_p solar photovoltaic system.

3.2.2 DC bus voltage selection

The value of DC bus voltage for VSC should be greater than twice of the peak of the phase voltage of the three phase grid. The DC bus voltage is calculated as,

$$V_{dc} = 2\sqrt{2}V_{L-L}/(\sqrt{3} m) = 2\sqrt{2} \times 415/(\sqrt{3} \times 1) = 677.69 \text{ V} \quad (3.8)$$

Where V_{L-L} the AC line voltage of the VSC and m is the modulation index. Modulation index m is taken as 1, while AC line voltage of VSC is 415 V, then as per equation (3.8) V_{dc} is calculated as 677.69V. Therefore, the value of DC link voltage should be greater than the calculated value and thus selected as 700 V.

3.2.3 DC/DC converter

A DC/DC boost converter is required to boost the PV array voltage and to implement the MPPT algorithm which keeps on tracking the maximum power point of the PV array. The value of input inductor (L_b) is calculated as:

$$L_b = \frac{V_{PV} D}{\Delta i f_{sw}} \quad (3.9)$$

Where, $D = 1 - \frac{V_{PV}}{V_{DC}}$ (3.10)

DC link Capacitors (C)

$$C = \frac{I_{in} D}{\Delta v f_{sw}} \quad (3.11)$$

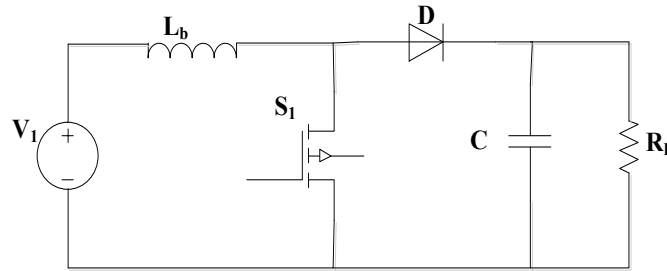


Fig. 3.2 DC/DC boost converter

A circuit of DC/DC boost converter configuration is presented in Fig. 3.2. Input ripple current ΔI_1 is considered as 6% of input current to the DC/DC boost converter and switching frequency (f_{sw}) is chosen as 10 kHz.

3.2.4 DC bus capacitance

The selection of the DC capacitor is governed by the DC bus voltage value and power requirements. By energy conservation law, the equation depicting C_{dc} can be written as:

$$\frac{1}{2}C_{dc}[V_{dc}^2 - V_{dc1}^2] = 3k_1aVIt, \quad (3.12)$$

$$C_{dc} = \frac{3k_1aVIt}{0.5[V_{dc}^2 - V_{dc1}^2]} \quad (3.13)$$

Where V_{dc} depicts the reference DC voltage and V_{dc1} is the minimum voltage level at DC bus, a denotes the over loading factor, V and I are the phase voltage phase current respectively of the VSC and t shows the time to DC bus voltage to be recovered. The reference DC bus voltage $V_{dc} = 700$ V, $V_{dc1} = 678$ V, $V = 240$ V, $I = 15$ A, $t = 30$ ms, $a = 1.2$, and $k_1 = 0.1$. Hence according to equation (3.13) the obtained C_{dc} is 1283 μ F and is chosen as 1500 μ F.

3.2.5 Voltage source converter design

The three phase voltage source converter consists of a six switching devices which converts DC voltage into AC voltage.

In the VSC, IGBT semiconductor switches are used and designed for 415 V, 25 kW at 0.8 p.f. lagging load.

The voltage rating (V_{sw}) of the IGBTs of VSC is given as:

$$V_{sw} = V_{dc} + \Delta V_{dc}, \quad (3.14)$$

In above equation ΔV_{dc} depicts the 10% overshoot in the DC link voltage under dynamic load. $\Delta V_{dc} = 0.1 \times 700 = 70$ V.

Considering safety factor of IGBTs the voltage rating is chosen as 1200 V. The current rating of the IGBT is calculated as 30 A.

3.2.6 AC interfacing inductor ratings

The design of the AC interfacing inductance (L_f) primarily depends on the current ripple, i_{cr-pp} , switching frequency f_s , and DC bus voltage (V_{dc}), and can be considered as

$$L_f = \sqrt{3}mV_{dc}/(12af_s i_{cr-pp}), \quad (3.15)$$

i_{cr-pp} is considered as 15%. $f_s = 10$ kHz, $m = 1$, $V_{dc} = 700$ V, and $a = 1.2$, and L_f is obtained as 2.8 mH. The selected value of interfacing inductor is 3 mH.

3.2.7 Ripple filter design

Series combination of R and C is connected in each phase to make low impedance path to high frequency elements and high impedance path to fundamental element.

The filter time constant should be very small compared with the fundamental time period (T). If R_r is filter resistance and C_r is filter capacitance then $R_r C_r \leq T_f$. Further considering T_s is switching time.

$$R_r C_r = T_s/10 \quad (3.16)$$

Considering switching frequency f_s is 10 kHz, the ripple filter parameters are obtained to be $R_r = 5 \Omega$ and $C_r = 10\mu F$.

3.3 MATHEMATICAL MODELLING OF FUEL CELL

A fuel cell works on the electrochemical process and converts fuel (hydrogen) energy into form of electricity. It works on principal of chemical reaction between oxidant and the fuel for producing electrical energy with heat and water byproducts. The equivalent circuit of a solid oxide fuel cell (SOFC) is shown in Fig. 3.3. Fuel cells possesses several advantages over other renewable energy resources such as high

efficiency, high power quality, less or no moving parts which results in lesser noise, low maintenance and fuel flexibility. Efficiency of fuel cells varies 40-60% and in cogeneration applications can be further improve up to 90%. Cost is also lesser now a days due to high temperature operation which removes the requirement of precious metal catalysts.

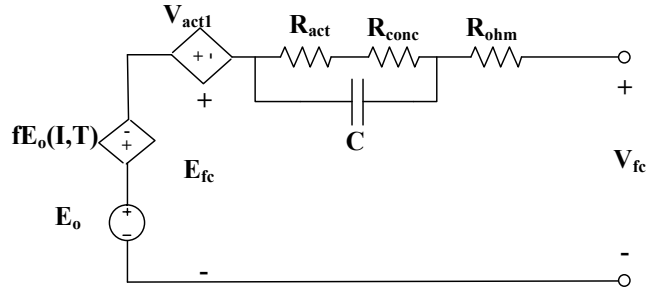


Fig. 3.3 Equivalent circuit of a solid oxide fuel cell (SOFC)

Tafel equation is used to calculate the output voltage of a fuel cell.

$$V_{fc} = E_{fc} - V_{act} - V_{con} - V_{ohm} \quad (3.17)$$

Where, E_{fc} denotes the reversible open circuit voltage, V_{act} is activation overvoltage, V_{con} shows the concentration overvoltage and V_{ohm} is the ohm voltage.

Value of the reversible open circuit voltage (E_{fc}) can be found using Nernst equation:

$$E_{fc} = N \left\{ E^0 + \frac{RT}{2F} \ln \left(\frac{P_{H_2}}{P_{H_2O}} (P_{O_2})^{0.5} \right) \right\} \quad (3.18)$$

Where, E^0 is standard reversible cell voltage, R denote universal gas constant (JK/kmol), T shows the stack temperature in Kelvin, N is the number of cells in stack and P_i (P_{H_2} , P_{H_2O} and P_{O_2}) is mole fraction of species. Ohmic voltage in equation (3.17) is because of electrical resistance of electrodes and the resistance offered due to flow of ions in the electrolyte and can be computed using Ohm's law:

$$V_{ohm} = i_{fc} * R_{fc} \quad (3.19)$$

V_{act} is the voltage due to cell current and hydrogen concentration and can be written as:

$$V_{act} = -A \ln i_{fc} \quad (3.20)$$

Constant A depends on the type of cell used, concentration voltage V_{conc} is ignored by considering the operation in linear region and hydrogen, oxygen flow constant.

3.4 PUMP HYDRO STORAGE MODELLING

A pumped hydro storage (PHS) system use electricity to pump water to the higher altitude to store it as potential energy and convert it back into electricity by releasing water passed back through a turbine to the lower reservoir. During off-peak hours or surplus SPV generation, the water is pumped to the upper reservoir. During peak hours or less PV generation water flow from the upper reservoir to lower through turbine/generator to produce electricity and supply the power to loads or grid.

The PHS system consists of a turbine/generator unit and a motor/generator unit. The various machine of fixed or variable speed can be used for pumped hydro storage such as synchronous machine, cage rotor induction machine, wound rotor induction machine and squirrel cage induction machine, etc. Each machine has various advantages and disadvantages. However, in the present system variable speed machines are being widely used because they have various advantages like lower mechanical stress, provide dynamic compensation for torque and power fluctuations and improve the overall efficiency of system and power quality. For the present work, a variable speed doubly fed induction machine (DFIM) is considered. Based on the literature review, DFIM is the best-suited machine for PHS applications because of more optimal dynamic performance for PHS and capability of adjusting power flow. Nowadays DFIM units employ VSC consisting of fully controlled power electronic switches. The dynamic performance for motoring mode can be described by following equations:

The stator voltage equations are as follows

$$V_R = \frac{d\psi_R}{dt} - I_R R_a - \psi_I \omega_b \quad (3.21)$$

$$V_I = \frac{d\psi_I}{dt} - I_I R_a + \psi_R \omega_b \quad (3.22)$$

The rotor voltage equations are as follows

$$e_R = \frac{d\lambda_R}{dt} + i_r r_a + \lambda_I (\omega_m - \omega_b) \quad (3.23)$$

$$e_I = \frac{d\lambda_I}{dt} + i_i r_a - \lambda_R (\omega_m - \omega_b) \quad (3.24)$$

Subscripts r and i shows the components of the real and imaginary axis of the synchronous reference frame (SRF). e , i and λ are rotor voltage, current, and flux linkage respectively. PHS with DFIM has two control variables: gate position control and speed control because the machine is no longer locked with system frequency. Two basic control approaches are available in literature: one is electrical power is controlled using power converter, and speed is controlled using adjustment of gate valve position known as fast power control, another one is speed controlled using power converter, and power is being controlled using turbine governor adjusting gate valve positions. The comparison is made on various research work, which shows that fast power control is superior then fast speed control approaches and has been used in this work.

Turbine mode of operation:

During peak periods or if there is any shortage in the generation, the water will flow from the upper reservoir to the lower to make turbine generator set operates. The energy generated from the turbine generator set can be written as equation 3.25.

$$E_{GT} = \rho g h Q_{GT} \eta_{GT} \quad (3.25)$$

Block diagram for turbine mode of operation is given in Fig. 3.4. The power command P_{set} is added with the reference power command, i.e., rotating speed pulling-

back control to maintain machine's speed within prescribed limits which are determined by the size of the converter.

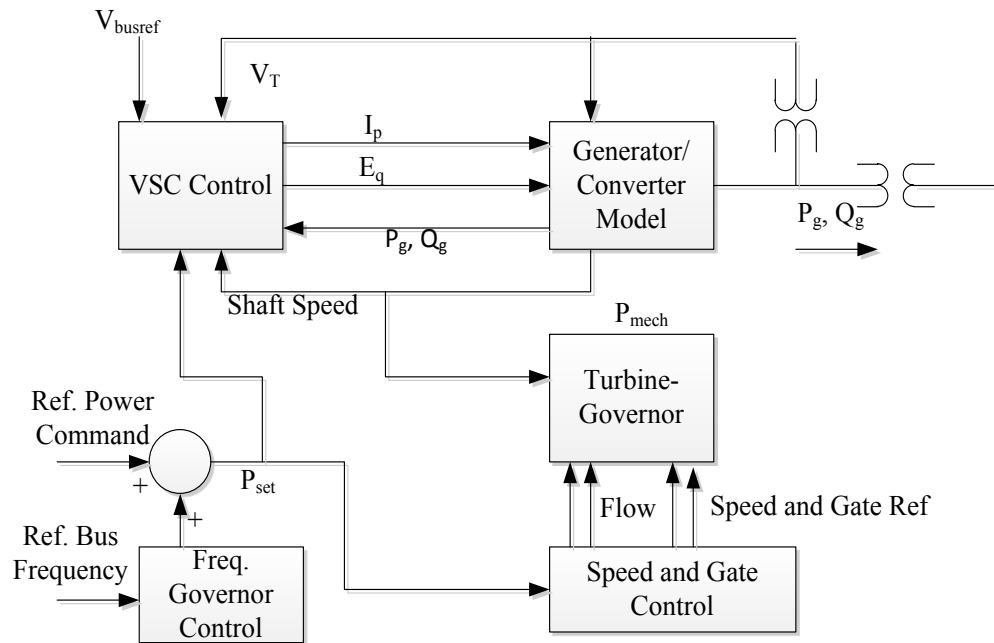


Fig. 3.4 Block diagram of the turbine mode of the system

The power error is processed with a PI controller and the active and reactive current signals through the voltage regulator is given to the VSC control. Machine shaft speed is being controlled by turbine governor control. Speed optimizer uses the P_{set} signal and with the help of speed reference provide the error in speed which is input for the hydro turbine speed governor system.

Pump mode of operation:

The energy required by the motor-pump unit to suck water from the lower reservoir to upper reservoir according to the Bernoulli's equation is given in equation 3.26.

$$E_{MP} = \frac{\rho gh Q_{MP}}{\eta_{MP}} \quad (3.26)$$

Fig. 3.5 presents the block diagram for pump mode of operation and components are identical to the turbine mode of operation explained in the above section.

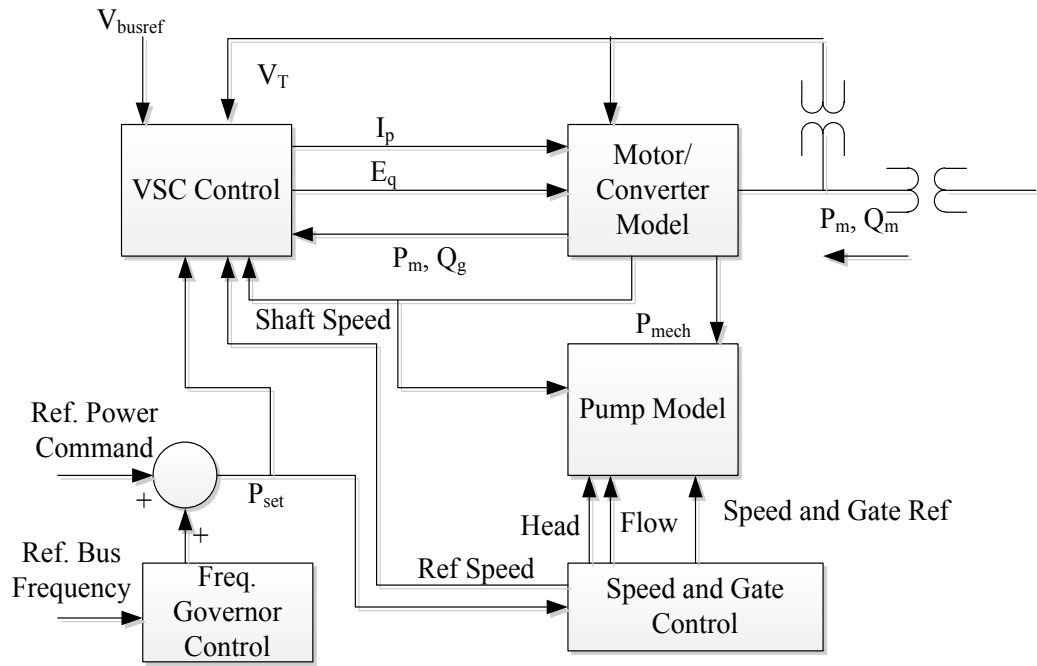


Fig. 3.5 Block diagram of the pump mode of the system

3.5 HARDWARE PROTOTYPE DEVELOPMENT

The prototype model includes various components development which are presented in detail here. AGV PVE 15 kW solar PV array simulator with $V_{ocmax} = 1500V$ and $I_{scmax} = 30 A$ is used as constant DC source to emulate the characteristics of real solar PV array. The design of VSC includes three IGBT modules with a DC voltage storage capacitor. Further, other components are sensing and signal conditioning circuits, AC interfacing inductors, ripple filter (resistance and capacitor banks), linear load and combination of resistance/diode rectifier module as nonlinear loads.

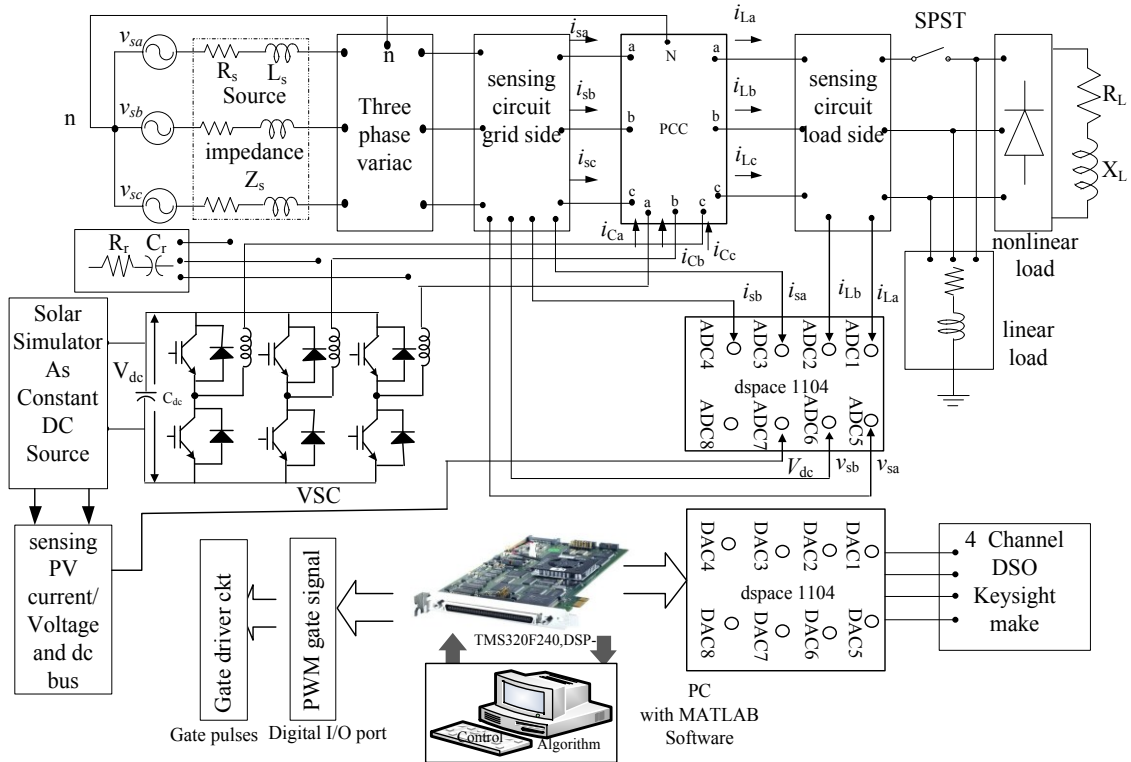


Fig. 3.6 Block diagram of developed hardware prototype

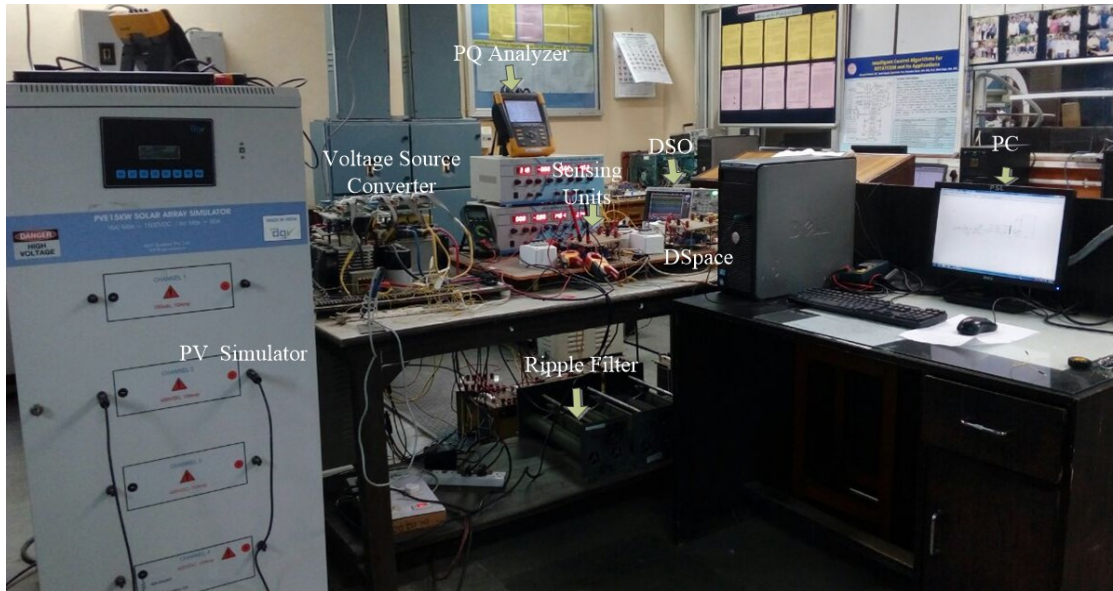


Fig. 3.7 Developed experimental prototype setup

3.5.1 d-SPACE 1104

The control operation of the grid connected solar PV system in real time is done using a DSP (dSPACE 1104 R&D controller board) with a personal computer. The

dSPACE 1104 works as a real time controller based on a Power PC 603 floating-point processor [201]. It also has a slave DSP subsystem based on the TMS320F240. The DS1104 R&D controller board is a standard board that can be plugged into a peripheral component interconnect slot of a PC. The DS1104 is specifically designed for the development of high-speed multivariable digital controllers and real-time simulations in various fields.

The dSPACE 1104 R&D controller board has various ADC, DAC and PWM (pulse width modulation) channels to make it easy to implement real time control. The voltage and current sensor outputs are given to the ADC channels of dSPACE 1104 R&D controller board. The signal from ADC channels are further scaled up in MATLAB interface to obtain the actual values of signal parameters. At second stage these signals are used as inputs to the control algorithm. The switching signals for VSC generated from control algorithm are taken out from PWM port of dSPACE and given to gate driver/isolation circuit.

3.5.2 Sensing and conditioning circuit

A sensor is a device which converts measured physical quantity into a form of signal required by the end instrument. Current and voltage of converter are measured by the current (LEM LA 25 P) and voltage (LEM LV 25 P) respectively. These currents and voltage values are input to dSPACE system. Output of these sensors are small amount of current, so a resistance is added in series to the sensor and voltage drop across it is taken as the input to dSPACE. Voltage sensor circuit and developed voltage sensor circuit in laboratory are given in Fig. 3.8 and Fig. 3.9 respectively. Further, Fig. 3.10 and 3.11 shows current sensor circuit and developed current sensor circuit respectively. These voltage sensors/current sensors operate at $\pm 15V$ DC supply and

sensed voltage signal output of sensor is given to the buffer circuitry, which consists operational amplifier (OP07) and resistive circuit.

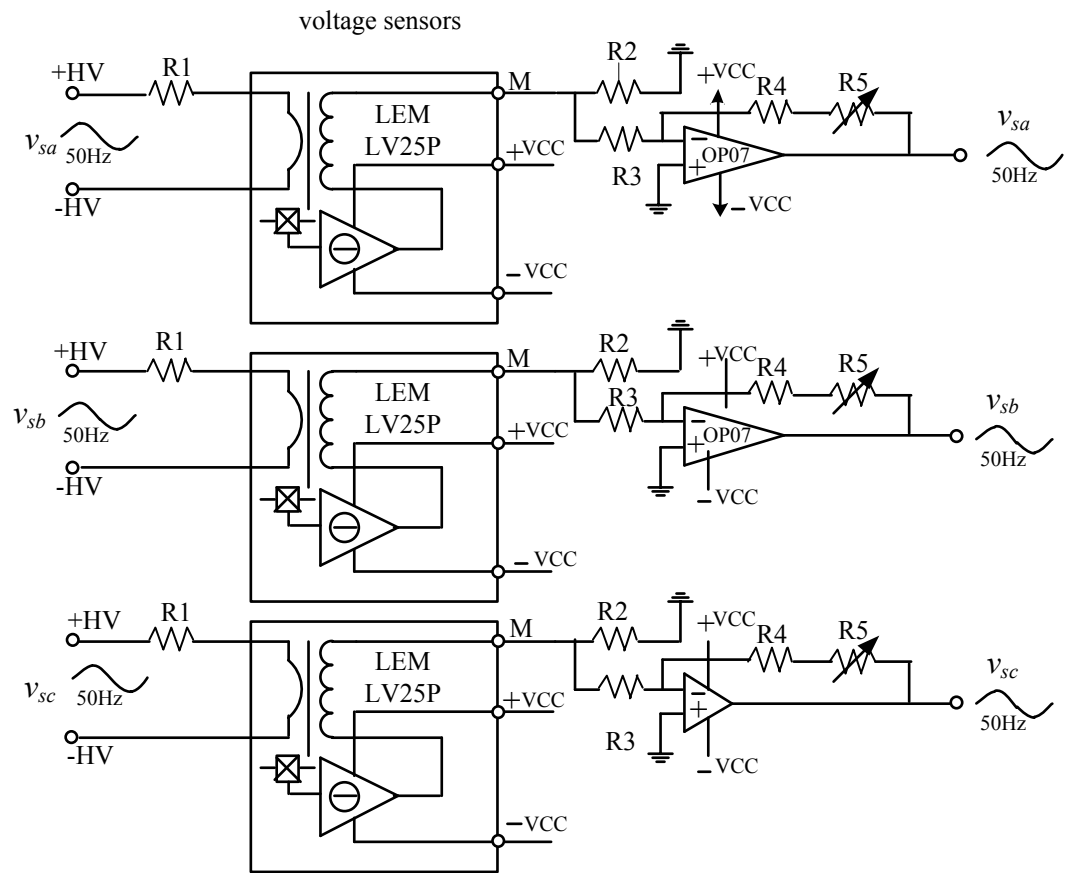


Fig. 3.8 Schematic representation of voltage sensing circuit for grid side voltage

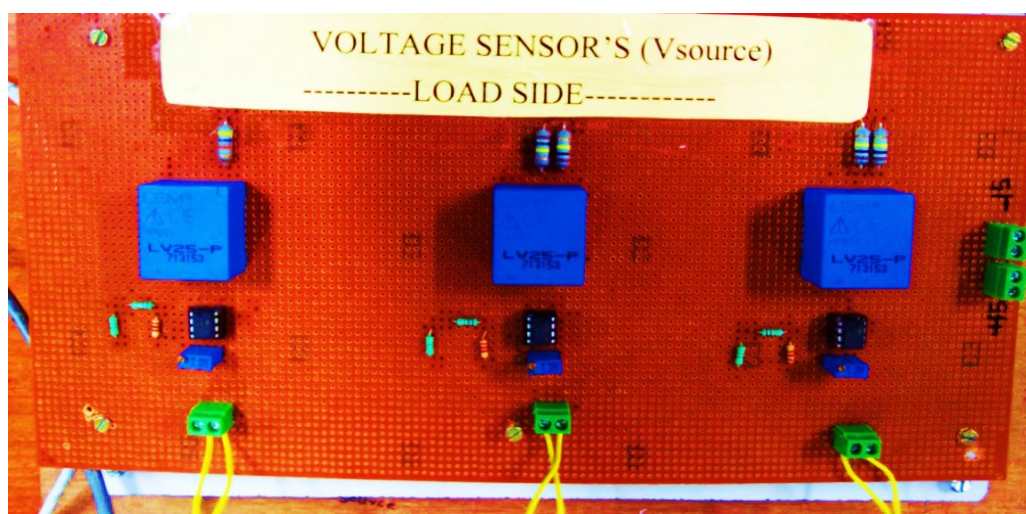


Fig. 3.9 Voltage sensing circuit for the proposed experimental setup

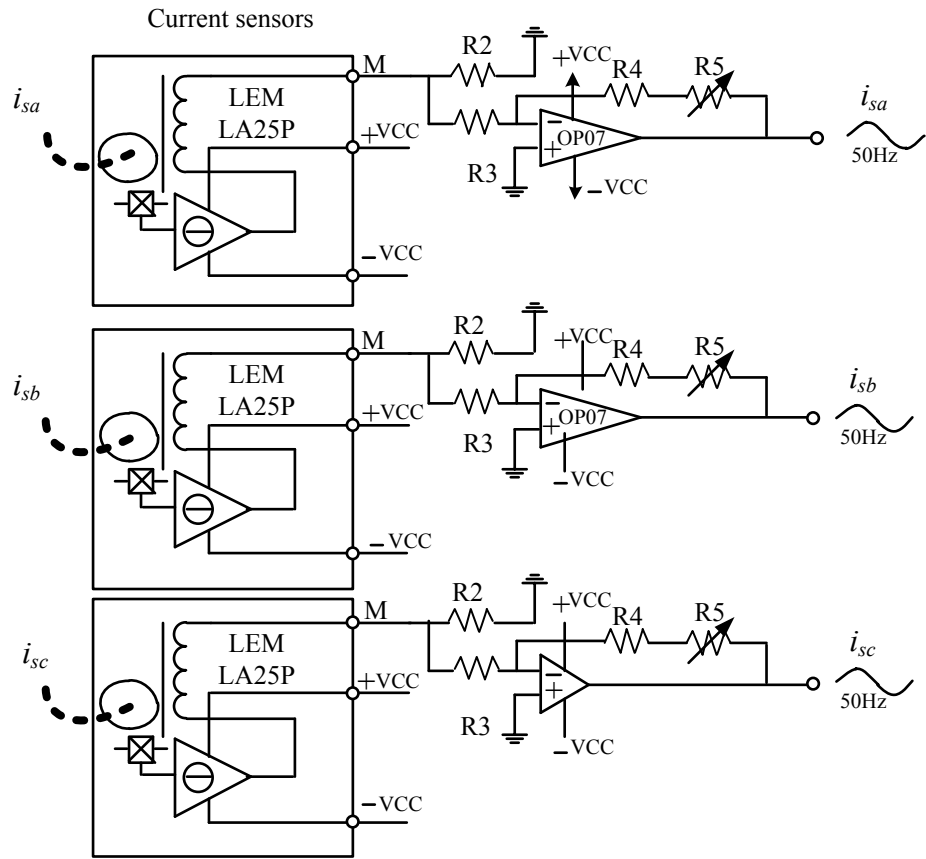


Fig. 3.10 Schematic diagram of current sensing circuit for source side

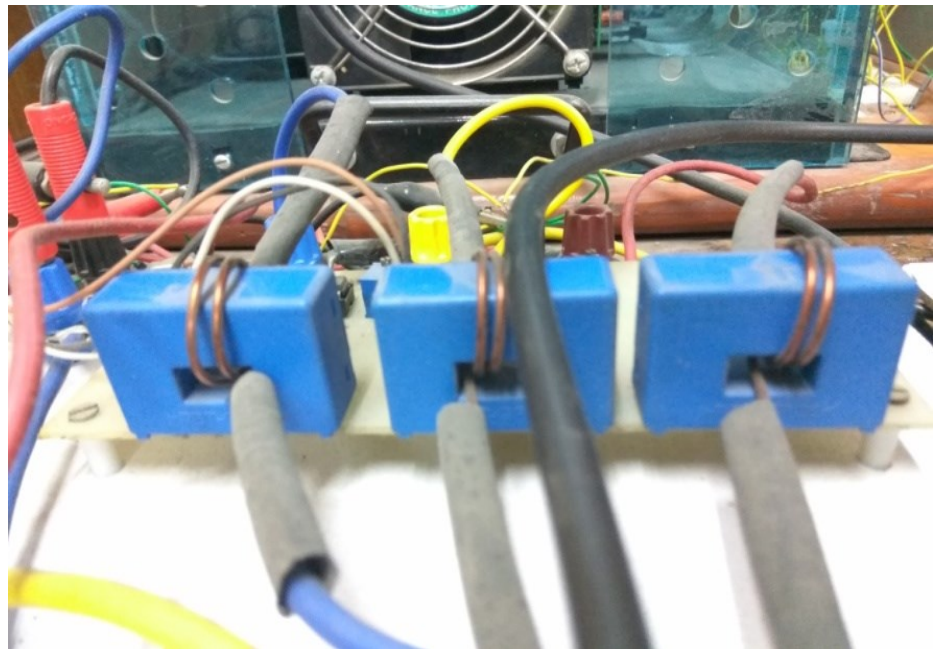


Fig. 3.11 Current sensing circuit for the proposed experimental setup

3.5.3 Gate isolation and amplifier circuit

The switching signals generated from dSPACE PWM output module are applied to the optical isolation circuit consisting of the 6N136 optocoupler and its output is amplified through 2N222A switching transistor to 15V. The optocoupler provides the optical isolation between the control circuit including dSPACE and the gate power circuit. Six similar circuits are developed to provide gating pulses to the six IGBTs of voltage source converter. Fig. 3.12 and 3.13 shows circuit diagram of gate trigger circuit and developed gate trigger circuit in laboratory respectively.

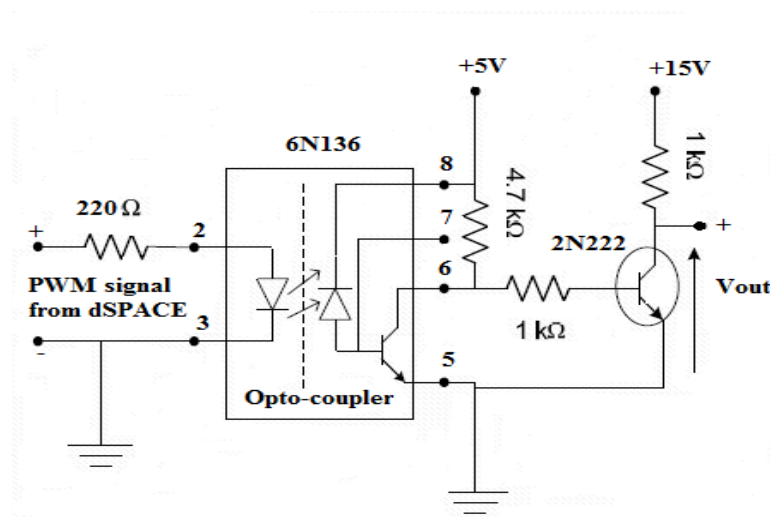


Fig. 3.12 Circuit diagram of gate trigger circuit

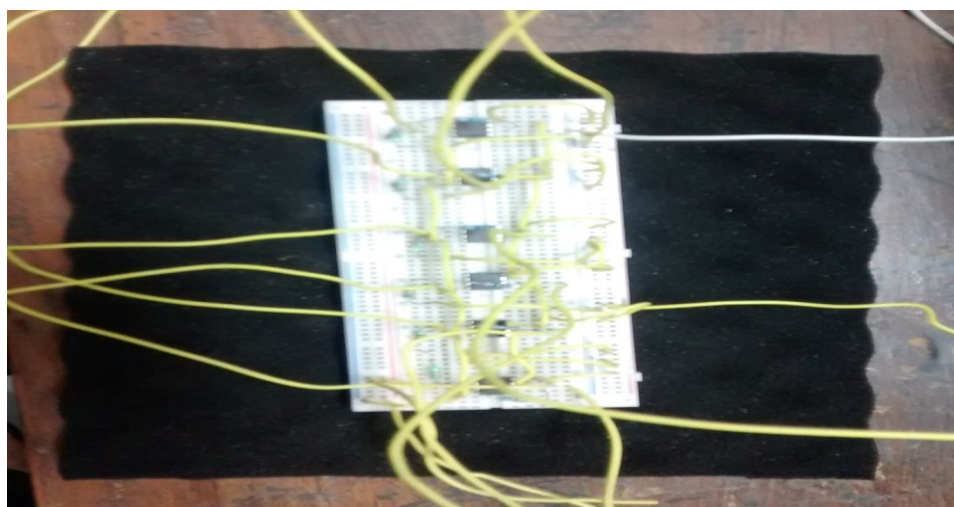


Fig. 3.13 Gate trigger circuit for the developed prototype

3.5.4 Ripple filter

The design of RC ripple filters is the same as given in section 3.2.7. The power loss in filter is negligibly small, which is approximately 3 W.



Fig. 3.14 Passive ripple filters

3.6 CONCLUSION

Mathematical modelling for various components of three phase grid connected solar PV system is discussed in detail. The developed model includes VSC, DC link capacitance, AC interfacing inductors, ripple filters, sensing and measurement circuit and gate driver circuits etc. The design and selection of ratings of various components such as IGBT switches for VSC, DC link capacitance, AC interfacing inductors and ripple filters are given in detail. Further, in next chapter simulation model of control algorithm will be implemented in real time using dSPACE DS1104 R&D controller board.

CHAPTER 4

SHORT TERM SOLAR ENERGY FORECASTING

4.1 INTRODUCTION

This chapter is focussed on short term solar energy forecasting. As the power from solar energy resource is fluctuating and nonlinear in nature, the results obtained from mathematical models are not found satisfactory. Therefore, intelligent approaches based on fuzzy logic, artificial neural network (ANN), adaptive neuro fuzzy inference system (ANFIS), genetic algorithm (GA), wavelet, generalized neural network (GNN), particle swarm optimization (PSO) etc. have been used by researchers. In this chapter, a hybrid approach based on wavelet and GNN has been used for 15 minutes ahead solar energy forecasting. Wavelet transform plays significant role in error points removing and enhancing the data stability. Using above model, fast convergence rate and stronger training and learning ability may be achieved. The proposed work would be useful for power engineers in proper operation and control of power plants.

4.2 SOLAR ENERGY FORECASTING AND ITS NECESSITY

The power generation from solar energy is gaining more attention because of advancement in the solar photovoltaic technology including enhanced efficiency of solar cells by incorporating the good materials and many other reasons. In the present scenario the bidding of power is done on 15 minutes basis by many distribution companies. Utilities has to balance the supply and demand for a reliable operation, in view of aforesaid, forecasting of solar energy becomes utmost important. Further, the uncertain and variable output of solar plants leads the inappropriate operation. Hence, this mandates short term solar energy forecasting (STSEF) for successful and

economically efficient integration of solar power generating plants into utility grid. Further, the availability of solar energy measuring stations is scarce even throughout the world because of high instrumental cost. In India, the data of solar irradiance is available for limited stations. The forecasting of solar energy will play a significant role for sustainable power generation.

4.3 INTELLIGENT APPROACH FOR STSEF

An intelligent model using wavelet transform and generalized neural network (GNN) is developed and applied for the short term solar energy forecasting.

4.3.1 Generalized neural network

Data Structure of a common neuron has summation or product as the aggregation function with linear or nonlinear threshold function. A generalized neural network acts as a multi-layer feed-forward network in which each node performs a particular function on incoming signals as well as a set of parameters pertaining to this node. The generalized neural network GNN is developed to overcome some problems associated with the performance, training and testing of artificial neural network. A GNN has number of advantages over ANN like less number of unknown weights, less training time, less number of training patterns, no hidden layer require, less complex etc.

Sigmoidal thresholding function and ordinary summation or product as aggregation functions can be used in the existing model which fails to overcome with the nonlinearities associated with real life problems. So, to deal with these problems developed model has both sigmoidal and Gaussian functions with weight sharing. The outputs of the sigmoidal and Gaussian functions are summed up and the model is known

as the summation type compensatory neuron model. Similarly, a product-type compensatory neuron models can also be developed using same approach. The developed neuron has both Σ and Π aggregation functions. The Σ_A aggregation function has been used with the sigmoidal characteristic function f_1 while the Π aggregation function has been used with the Gaussian function f_2 as a characteristic function. The output calculations can be divided into two parts: forward calculations and reverse calculations.

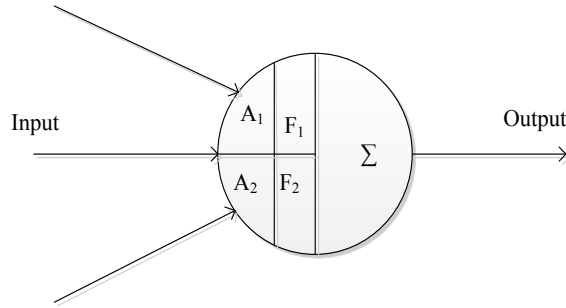


Fig. 4.1 Generalized neural network model

Learning steps of a summation type generalized neuron are given as follows:

1. Forward calculations:

i) Output of the Σ_A part with a sigmoidal characteristic function can be calculated as

$$O_{\Sigma} = \frac{1}{1 + e^{-\lambda s * s_{net}}} \quad (4.1)$$

Where,

$$s_{net} = \Sigma W_{\Sigma i} X_i + X_{o\Sigma} \text{ and } \lambda s \text{ is gain scale factor of } \Sigma_A.$$

ii) Output of the Π part with a sigmoidal characteristic function can be calculated as

$$O_{\Pi} = e^{-\lambda p * p i_{net}^2} \quad (4.2)$$

Where,

$$pi_net = \Pi W_{\Pi i} X_i * X_{o\Pi} \text{ And } \lambda p \text{ is the gain scale factor of } \Pi_A.$$

- iii) The final output of the GNN will be the function of two outputs and with the weights W and $(1-W)$ respectively, and can be written as

$$O_{pk} = O_{\Pi} * (1 - W) + O_{\Sigma} W \quad (4.3)$$

2. Reverse calculations

- iv) After the calculation of final output in forward pass, as in the feed forward neural network, the output then compared with the desired output to get the error. Back propagation training algorithm is used to train the GNN. Error of i_{th} set of input for a single GNN can be calculated by comparing the GNN output and desired output.

$$Error E_i = (Y_i - O_i) \quad (4.4)$$

- v) Sum squared error for the convergence of all the pattern is:

$$E_p = 0.5 \sum E_i^2 \quad (4.5)$$

A multiplication factor of 0.5 has been taken to simplify the calculations.

- vi) Weights associated with the Σ_A and Σ_B part of the summation type GN are:

$$W(k) = W(k - 1) + \Delta W \quad (4.6)$$

Where,

$$\Delta W = \eta \delta_k (O_{\Sigma} - O_{\Pi}) X_i + \alpha W(k - 1)$$

$$\text{And } \delta_k = \sum (Y_i - O_i)$$

- vii) Weights associated with the Σ_A part of the summation type GN are:

$$W_{\Sigma i}(k) = W_{\Sigma i}(k - 1) + \Delta W_{\Sigma i} \quad (4.7)$$

Where,

$$\Delta W_{\Sigma i} = \eta \delta_{\Sigma i} X_i + \alpha W_{\Sigma i}(k - 1)$$

$$\text{And } \delta_{\Sigma j} = \sum \delta_k W(1 - O_{\Sigma}) * O_{\Sigma}$$

α -momentum factor for better convergence and lies between 0 and 1

η -learning rate and lies between 0 and 1

viii) Weights associated with the Π part of the summation type GN are:

$$W \Pi_i(k) = W \Pi_i(k - 1) + \Delta W_{\Pi i} \quad (4.8)$$

Where,

$$\Delta W_{\Pi i} = \eta \delta_{\Pi i} X_i + \alpha W_{\Pi i}(k - 1)$$

$$\text{And } \delta_{\Pi j} = \sum \delta_k (1 - W) * (-2 * pi_net) * O_{\Pi}$$

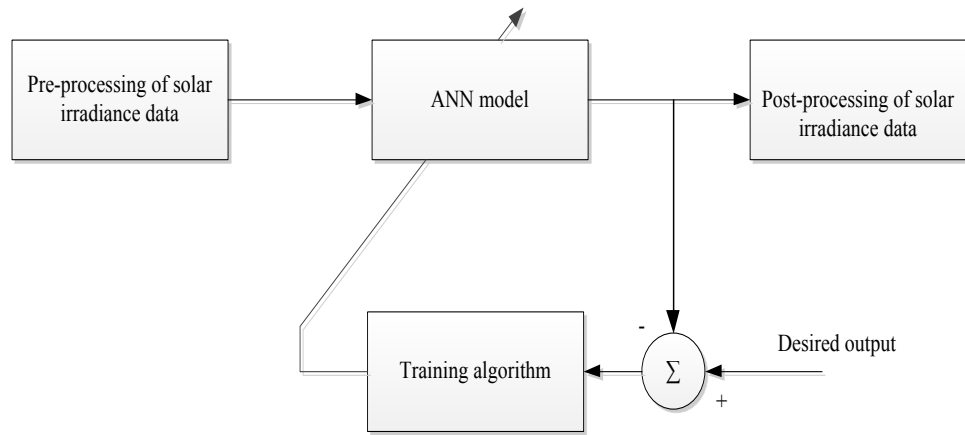


Fig. 4.2 Block diagram of model development using ANN

The generalized neuron structure consists of summation and product as aggregation functions and the aggregated outputs passes through a nonlinear thresholding function. The Σ part of the GNN structure has the summation of weighted input with sigmoidal activation function, while the Π part has the product of weighted input with gaussian activation function. The final output of the generalized neuron is a function of the weighted outputs as O_{Σ} and O_{Π} .

The output of summation part of generalized neural network can be obtained as:

$$O_{\Sigma} = f_1(\Sigma W_{\Sigma i} X_i + X_{o\Sigma}) \quad (4.9)$$

The output of product part of generalized neural network can be obtained as:

$$O_{\Pi} = f_2(\Pi W_{\Pi i} X_i + X_{o\Pi}) \quad (4.10)$$

The final output of generalized neuron will be the sum of summation part and product part and can be mathematically written as:

$$O_i = O_\Sigma * W_\Sigma + O_\Pi(1 - W_\Sigma) \quad (4.11)$$

4.3.2 Wavelet theory

There are various applications of wavelet theory available in literature such as signal processing, data compression, image de-noising, speech recognition, computer graphics, and many areas of physics and engineering. Discrete time filter banks are generally used by all practically useful discrete wavelet transforms and known as wavelet and scaling coefficients in wavelet nomenclature [167-169]. This section provides a brief summary of wavelet transform method which can be divided into two categories: continuous wavelets transform (CWT) and discrete wavelet transforms (DWT). In this research, discrete wavelet transform is used. The DWT algorithm is capable of producing coefficients of fine scales for capturing high frequency information, and coefficients of coarse scales for capturing low frequency information.

A DWT can be expressed as follows:

$$f(t) = \sum c_{j_0,k} \phi_{j_0,k}(t) + \sum_{j=j_0} \sum_k \omega_{j,k} 2^{\frac{j}{2}} \Psi(2^j t - k) \quad (4.12)$$

Where,

$f(t)$ - given signal

Ψ - mother wavelet function

J - dilation or level index

k - scaling index

$\phi_{j0, k}$ – scaling function of coarse scale coefficients

$c_{j0, k}, \omega_{j, k}$ – scaling function of detail coefficients

Wavelet processing consists of two stages: one is decomposition and another one is reconstruction. A mother wavelet based on Daubechie 8 (Db8) will be used for the filter coefficients. First the solar irradiance data is converted into low frequency and high frequency components. The decomposition process computes convolution between solar irradiance data and high pass or low pass filter. On the other hand reconstruction computes the convolution between the solar irradiance and inverse filter. Original signal has been composed into detail and approximation parameters in four levels. The reconstructed details and approximations are true parameters of original signal as follows:

$$S = A1 + D1 \quad (\text{Level 1})$$

$$= A2 + D2 + D1 \quad (\text{Level 2})$$

$$= A3 + D3 + D2 + D1 \quad (\text{Level 3})$$

$$= A4 + D4 + D3 + D2 + D1 \quad (\text{Level 4})$$

Coefficients vectors A1 and D1 are produced by down sampling and using only half length of the given original signal. These two vector coefficients cannot be combine directly to reproduce the original signal. In wavelet reconstruction process the detail and approximation components are assembled back to get the original signal back without any loss of information. The decomposing and reconstruction in wavelet is presented in Fig. 4.3.

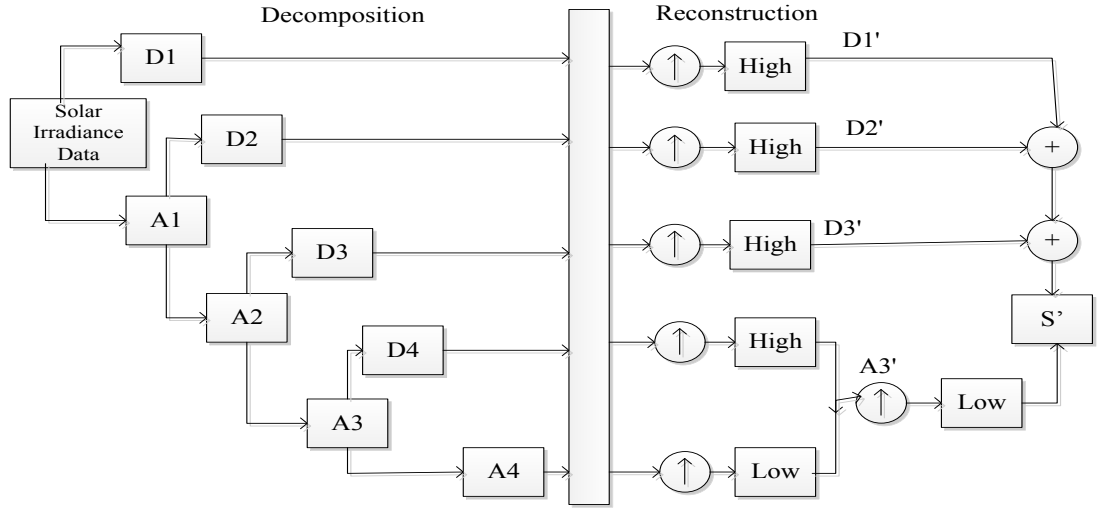


Fig. 4.3 Decomposition and reconstruction in wavelet

4.4 SHORT TERM SOLAR ENERGY FORECASTING USING WAVELET-GNN HYBRID MODEL

The input to the forecasting model is the historical dataset and past measurements of solar irradiance, temperature and PV generation for the day. The preceding block to this generation model conditions the historical dataset and classify according to day and season types. Generation output of solar PV is affected by various factors and very difficult to describe power output with a certain mathematical function [170-171]. Weather types and various meteorological parameters make significant impact on the power output of SPV systems. Output is modelled in this work with respect to the various meteorological parameters and under different day types. Solar irradiance is the factor by which the PV output power is most significantly get affected. PV power output estimation can be written as:

$$P_{PV} = \left[P_{PVSTC} * \frac{S}{1000} * [1 - \gamma * (T - 25)] \right] N_{SPV} * N_{pPV} \quad (4.13)$$

Where, T is the temperature of solar PV module in (°C) and given:

$$T = T_a + \frac{S}{1000} * (N_{OCT} - 20) \quad (4.14)$$

P_{PV} is active power output of solar PV system in watts, S is solar irradiance in W/m^2 , T_a is ambient temperature around PV panels, γ is temperature parameter at maximum power point and N_{OCT} depicts a constant term.

Further, weather conditions such as cloudy, dusts have large influence on solar irradiance reaching to the PV panels by scattering and reflecting, reduces the direct radiation to the ground. So, a good and accurate forecasting model for solar energy requires a hybrid and intelligent approach which uses historical PV power and multiple meteorological parameters. Fig. 4.4 presents the block diagram of developed hybrid approach for solar energy forecasting.

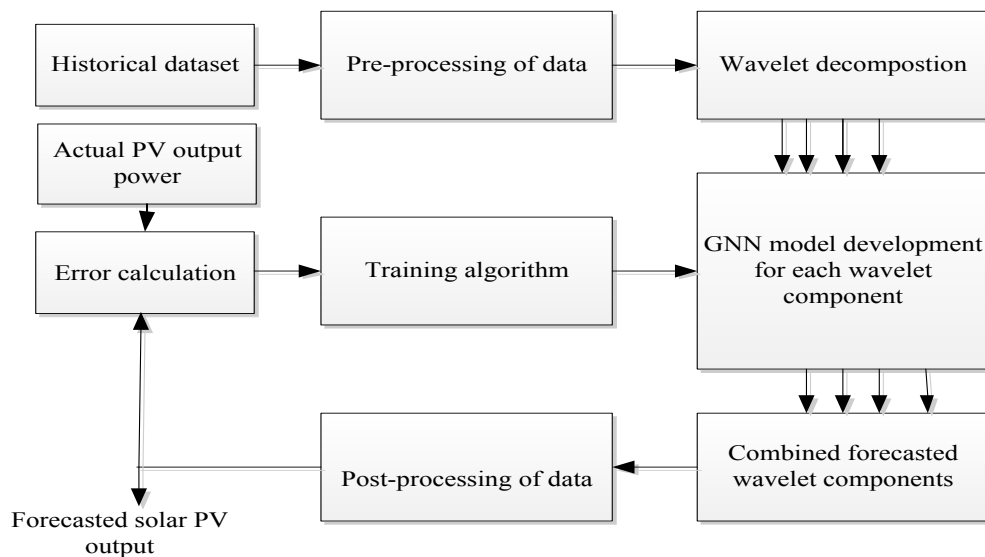


Fig. 4.4 Hybrid forecasting model for SPV generation forecast

4.4.1 Data Collection

Data for global solar irradiance, ambient temperature, average relative humidity and wind speed has been collected from Jamia Millia Islamia (JMI), National Institute of Solar Energy (NISE) and Ministry of New and Renewable Energy, Government of India for New Delhi location at 15 minutes time interval and used as input for short

term solar PV output power forecasting. Preprocessing of data is done before giving it to forecasting model because available historic dataset is generally complex in nature with different frequencies.

4.4.2 Day and weather type classifications

In this work, seasonal classification as per Indian weather condition of available solar power generation dataset has been done as summer, winter and rainy seasons. This classification will help to achieve more granularity for clustering performed on the historical dataset. Equation (4.15) is used to define the day type by using the ratio (R_{dt}) between the daily measured and theoretical clear sky insolation. Clear sky radiation model given in [172] has been used to obtain this expression.

$$R_{dt} = \frac{\text{Measured insolation for the day}}{\text{Clear sky insolation for the day}} * 100 \% \quad (4.15)$$

Five day type is categorized i.e. sunny, mostly sunny, cloudy, less cloudy, overcast and rainy/snowy. Different range of R_{dt} has been considered to decide the day type here. Table 4.1 presents the range of R_{dt} and day type classification.

Table 4.1 Day type classifications

Day type	Description	R_{dt} range
Sunny	Clear sky	$R_{dt} > 95\%$
Mostly sunny	Clear sky with very little scattered radiation	$70\% < R_{dt} \leq 95\%$
Cloudy	Partly clear sky with scattered and broken clouds	$40\% < R_{dt} \leq 70\%$
Overcast	Lower PV output with dark clouds	$25\% < R_{dt} \leq 40\%$
Rainy/snowy	Nearly zero PV power outputs	$R_{dt} \leq 25\%$

4.4.3 Correlation analysis of PV power with meteorological parameters

A Pearson product-moment correlation coefficient (PPMC) [173] has been used to perform linear regression analysis between PV power and various meteorological parameters based on historical data available. Dependency between X and Y variables can be calculated using below given formula:-

$$r_{x,y} = \frac{Cov(x,y)}{\sigma_x \sigma_y} = a_0 + \frac{\sum_{i=1}^n (x_i - \bar{x})(y_i - \bar{y})}{\sqrt{\frac{1}{n} \sum_{i=1}^n (x_i - \bar{x})^2} \sqrt{\frac{1}{n} \sum_{i=1}^n (y_i - \bar{y})^2}} \quad (4.16)$$

Where cov (x,y) is the covariance of the variables x and y, σ_x and σ_y are the standard deviations of the variables x and y.

4.4.4 Statistical error indices

In statistical error indices are used to get quantitative accuracy of forecasted outputs. Root mean square error (RMSE) and the mean absolute error (MAE) are most widely used error measure. If costs associated with a poor forecast are proportional to the forecast error MAE is appropriate for such applications having linear cost functions and while utility applications concern RMSE is more appropriate because of sensitivity to large forecast errors. The performance of the given forecasting model is evaluated on the basis of root mean square error (RMSE) and mean absolute error (MAE).

$$MAE = \frac{1}{N} \sum_{i=1}^n |x_{pred} - x_{obs}| \quad (4.17)$$

$$RMSE = \sqrt{\sum_{i=1}^n \frac{(x_{obs} - x_{pred})^2}{N}} \quad (4.18)$$

Where, x_{pred} is the forecasted value, x_{obs} is the actual value of quantity and N is the number of predicted output.

4.4.5 Hybrid model for short term solar energy forecasting

In yearly dataset has been divided for three seasons according to the Indian weather conditions i.e. summer, winter and rainy. The GNN model is trained using error back-propagation (BKP) gradient search learning algorithm and applied to the datasets. Since the obtained input and output variables from the given dataset are not of the same order of magnitude, some variables may appear to have more significance than they actually do. In keeping view aforesaid, it becomes necessary to normalize the input and output datasets in the same order of magnitude. If actual monthly data is directly used, this may cause a convergence problem during the learning process. This convergence problem can be avoided if the input and output data are scaled such that they remain within the range of (0.1–0.9). This process to scale the data within a particular range is known as normalization. The following given expression has been used to scale actual dataset for the solar energy forecasting problem

$$L_s = \frac{Y_{max}-Y_{min}}{L_{max}-L_{min}} (L - L_{min}) + Y_{min} \quad (4.19)$$

Where,

- | | |
|-----------|---|
| L | the actual solar irradiance data |
| L_s | the scaled solar irradiance data being used as input to the GNN model |
| L_{max} | maximum value of solar irradiance data in a particular column |
| L_{min} | minimum value of solar irradiance data in a particular column |
| Y_{max} | normalization upper range (0.9) |
| Y_{min} | normalization lower range (0.1) |

The results obtained during the training and testing of the GNN model are good and promising. The results further need some improvement and to achieve more accurate forecasted output wavelet integrated GNN has been used. Since the solar

irradiance data is generally complex and consists of different frequencies. Thus, for a reliable forecast wavelet decomposition method has been integrated with the GNN model in the present work. The proposed model is developed by decomposing an original irradiance data into one level, two levels, three levels and four levels of wavelet. Processed data has been used as input to the GNN model for 15 minutes ahead solar energy forecasting. In the proposed work three seasons (winter, summer and rainy) have been chosen according to the Indian weather conditions.

4.5 RESULTS AND DISCUSSION

Considering different weather conditions, various seasons are chosen accordingly for covering wider aspects of the developed model. It is clearly seen from Fig. 4.5 - Fig. 4.14 that during training, measured and trained values are closely following to measured data. Fig. 4.5 – Fig. 4.8 shows the forecasted PV power output for cloudy day, cloudy day, mostly sunny day and sunny day. It can be observed from the results that forecasted PV power output is closely following the measured values.

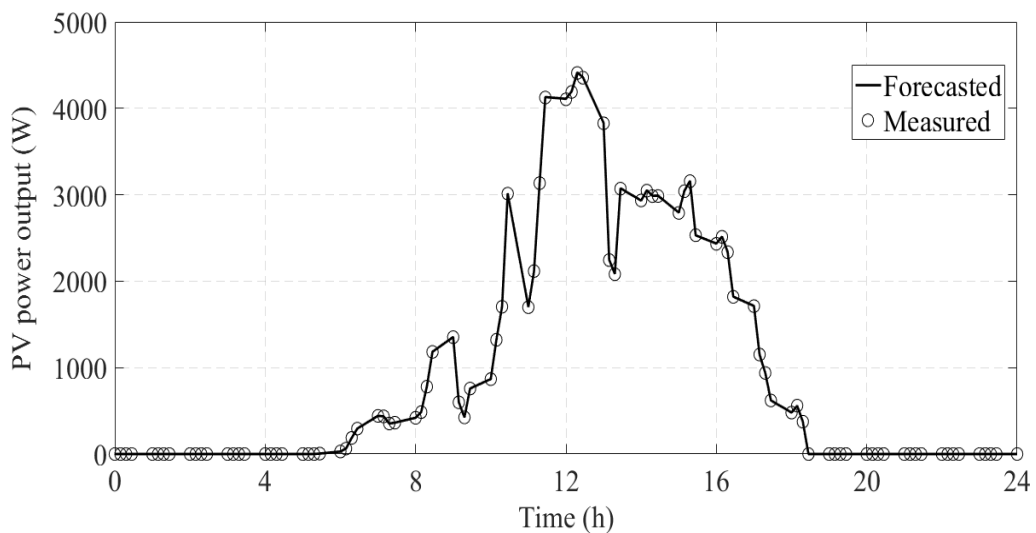


Fig. 4.5 Short term PV power forecasting for cloudy day

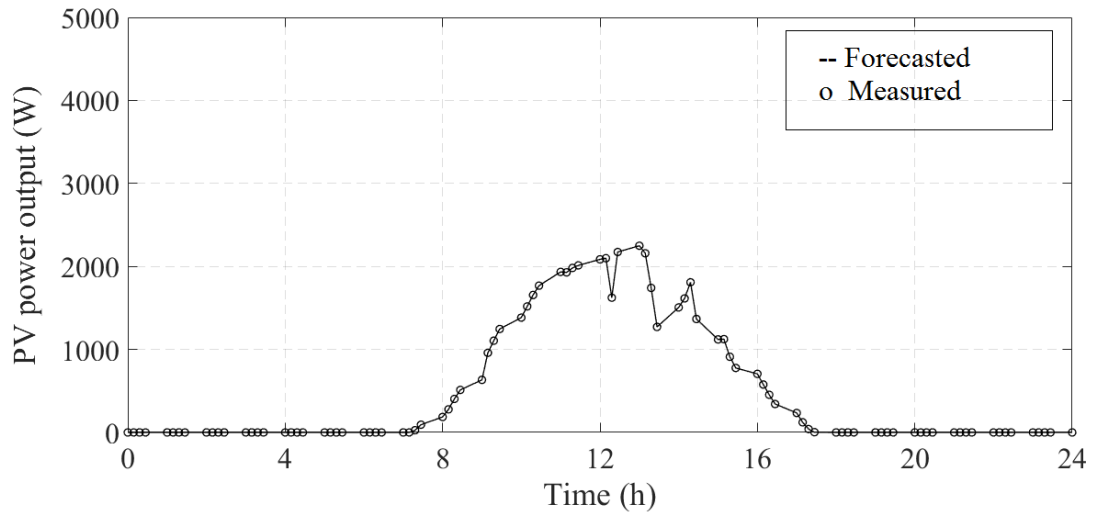


Fig. 4.6 Short term PV power forecasting for cloudier day

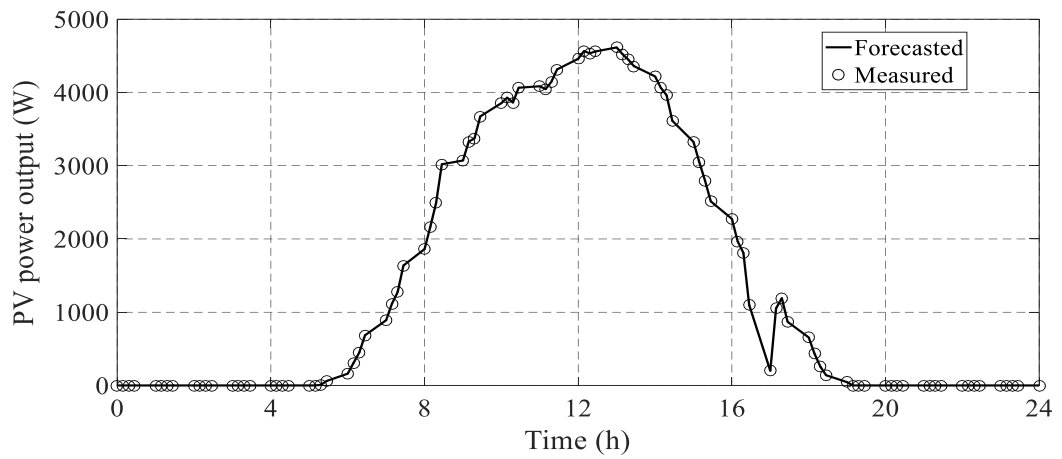


Fig. 4.7 Short term PV power forecasting for mostly sunny day

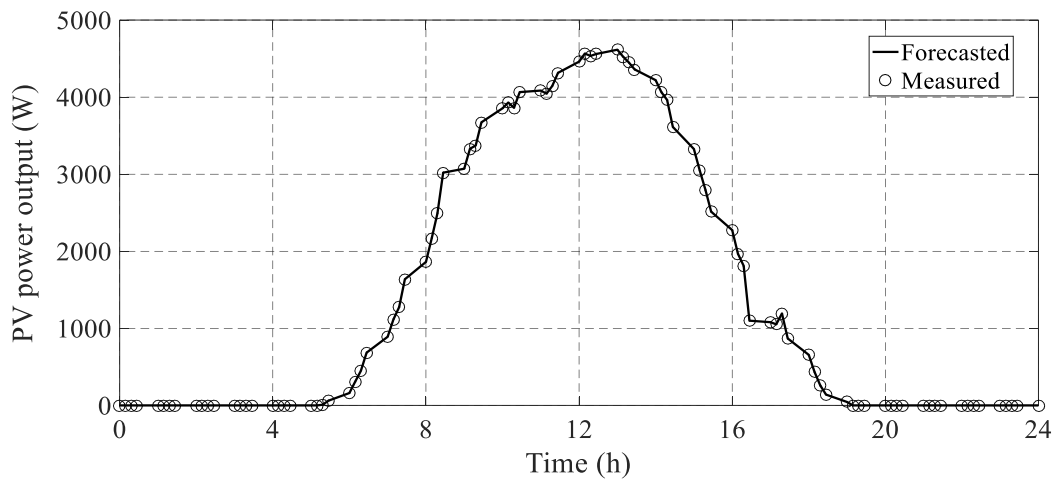


Fig. 4.8 15 minutes ahead PV power forecasting for sunny day

In yearly dataset has been divided for three seasons according to the Indian weather conditions i.e. summer, winter and rainy. Training results for winter, summer and rainy seasons are presented in Fig. 4.9, Fig. 4.10 and Fig. 4.11 respectively. Winter season data is considered for a period of five years average data for the month of January for testing the proposed approach. Similarly, for other two seasons the data of respective months has been chosen.

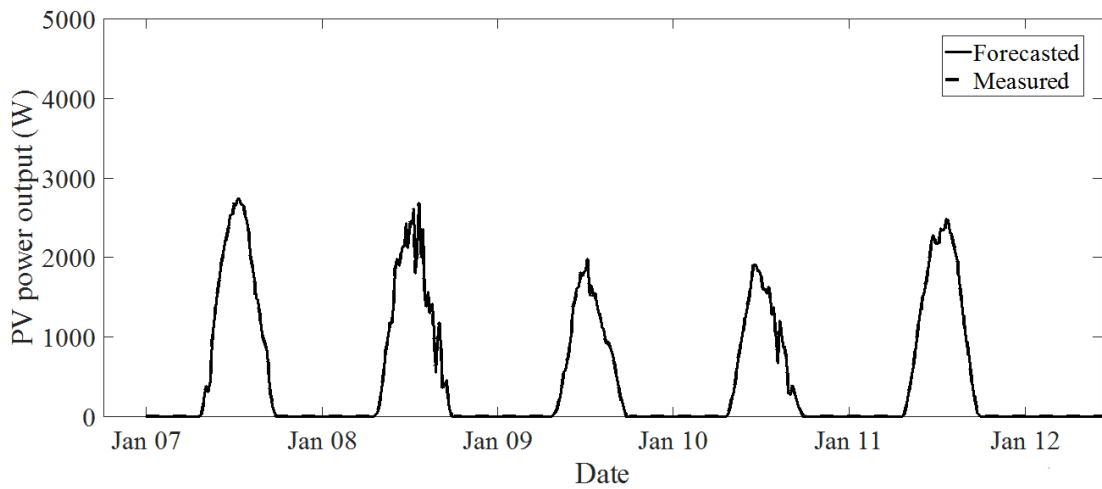


Fig. 4.9 Training results for short term PV power forecasting for winter season

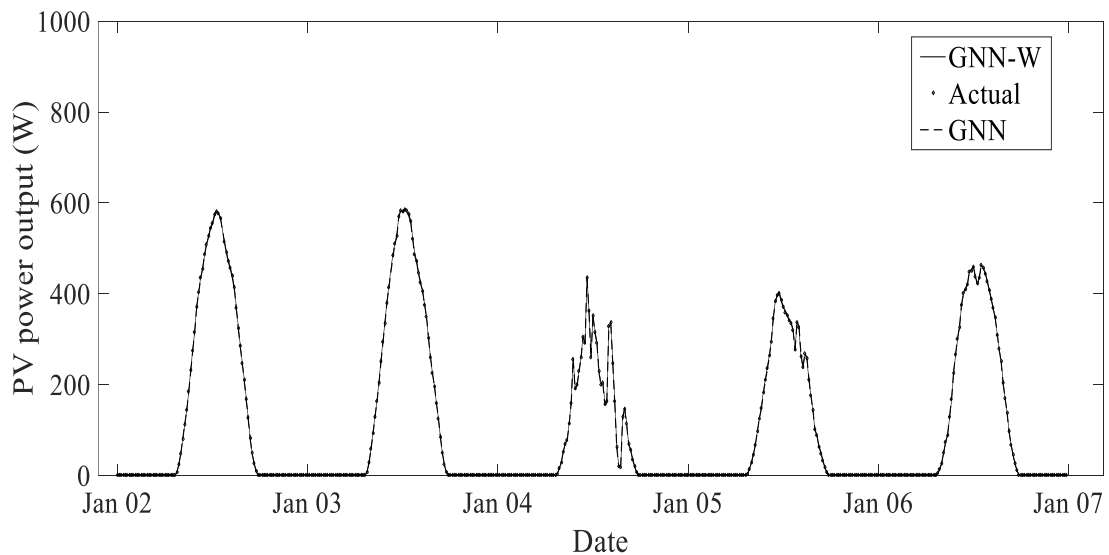


Fig. 4.10 Test results for short term PV power forecasting for winter season

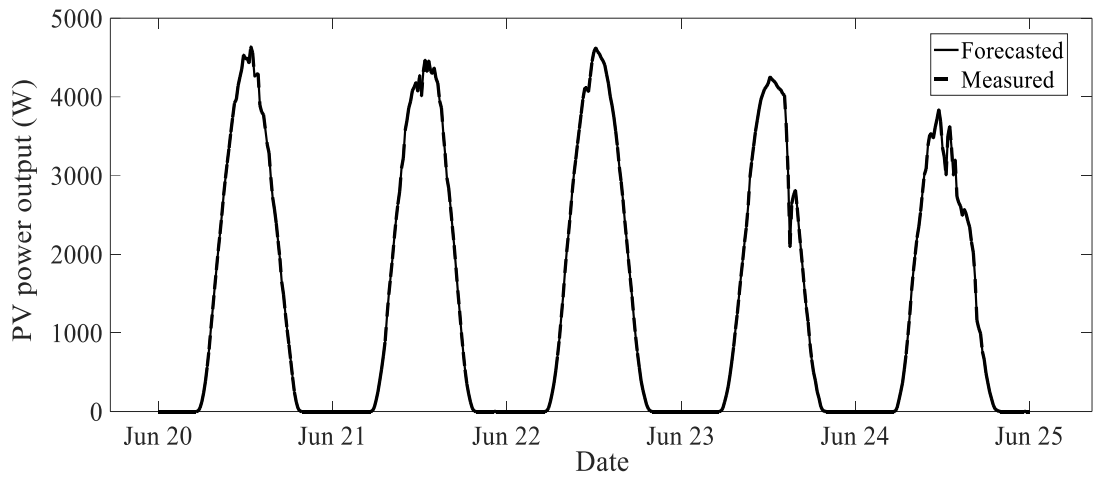


Fig. 4.11 Training results for short term PV power forecasting for summer season

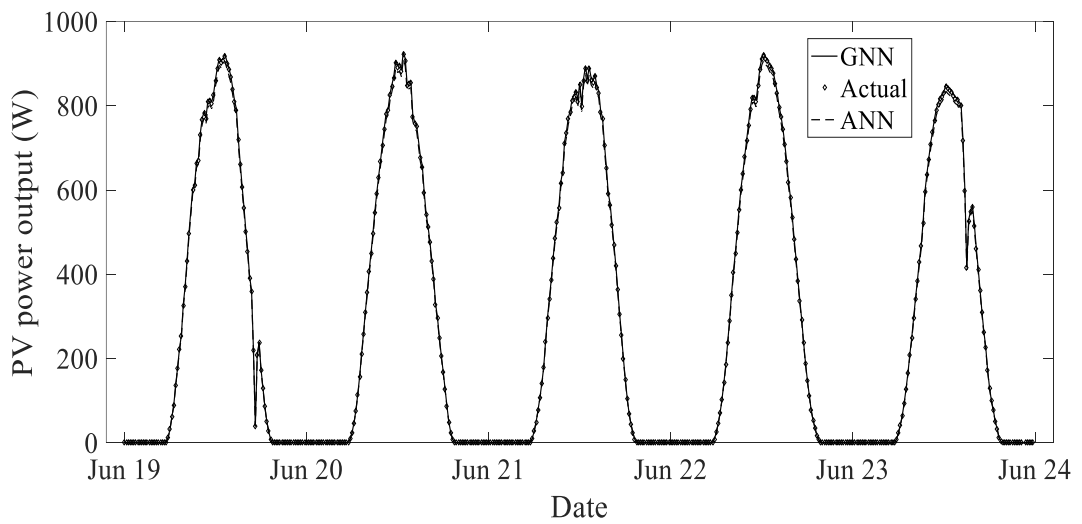


Fig. 4.12 Test results for short term PV power forecasting for summer season

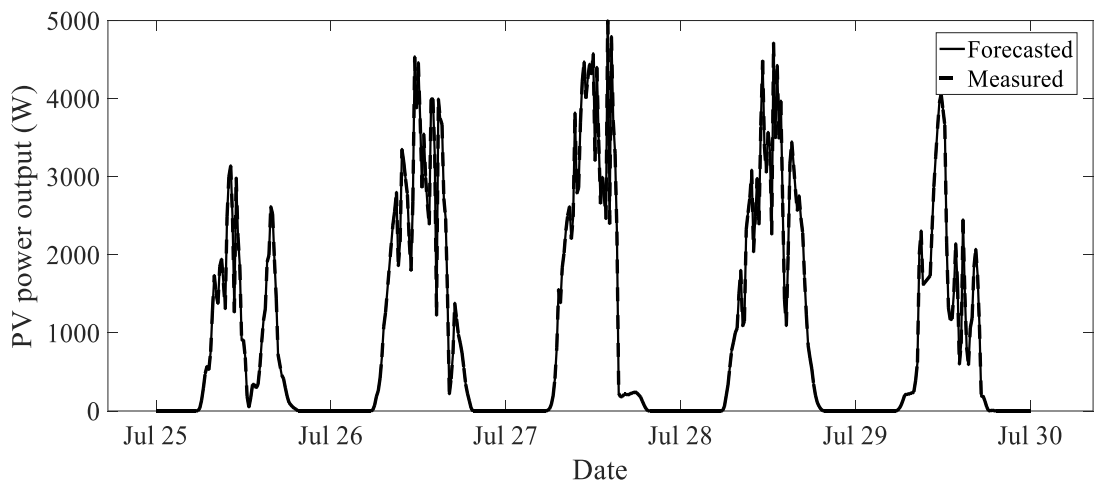


Fig. 4.13 Training results for short term PV power forecasting for rainy season

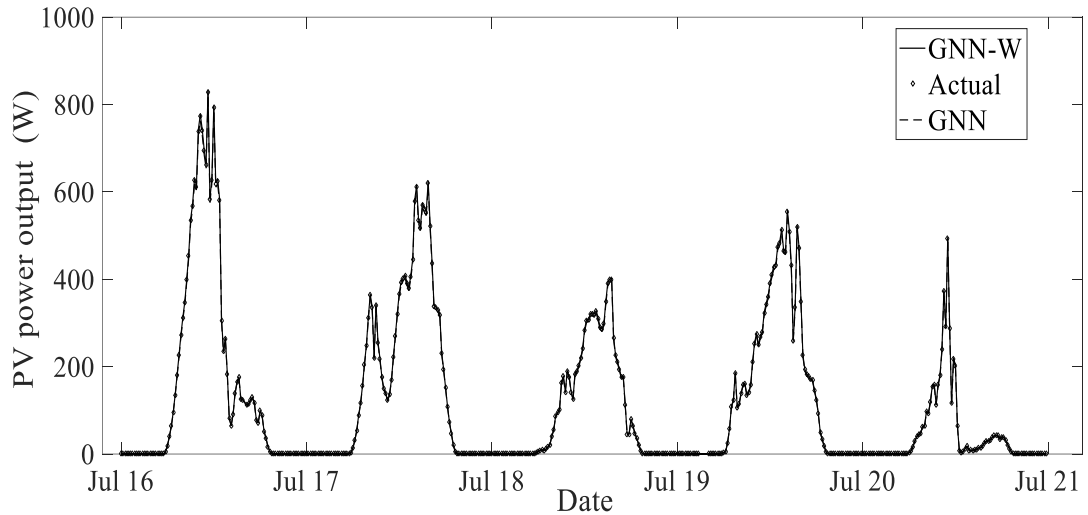


Fig. 4.14 Test results for short term PV power forecasting for rainy season

Test results for winter, summer and rainy seasons are presented in Fig. 4.12, Fig. 4.13 and Fig. 4.14 respectively. The performance of the models is evaluated on the basis of root mean square error (RMSE) and mean absolute error (MAE).

4.6 VALIDATION OF PROPOSED MODEL WITH EXISTING SOLAR PV GENERATION FORECASTING MODELS

The comparison between results of the GNN and GNN-W models has been performed and presented in Table 4.2. The values of average RMSE and MAE for other two months can also be observed from the given comparative results in Table 4.2. It is clearly seen from the results that the RMSE and MAE is less in case of GNN-W model for all the months of the year considered in this work. It can also be observed that the values of average RMSE and percentage MAE are large for rainy season because of the large uncertainties associated with the data.

Table 4.2 Comparison of testing performance for GNN and GNN-W short term solar PV generation forecasting model

Months/Seasons	Models	RMSE (W/m ²)	MAE (%)
January (Winter)	GNN	398	3.19
	GNN-W	411	3.23
May (Summer)	GNN	361	3.17
	GNN-W	370	3.08
July (Rainy)	GNN	435	3.62
	GNN-W	449	3.79

The ANN model for short-term solar PV power output forecasting is developed by using following steps: Input parameter selection; neural network architecture selection; training algorithm; training parameter selection with back propagation training algorithm for training. ANN results further comparing with developed GNN-W method (Fig. 4.15 - 4.17) to show the superiority of developed method and also shown in Table 4.3.

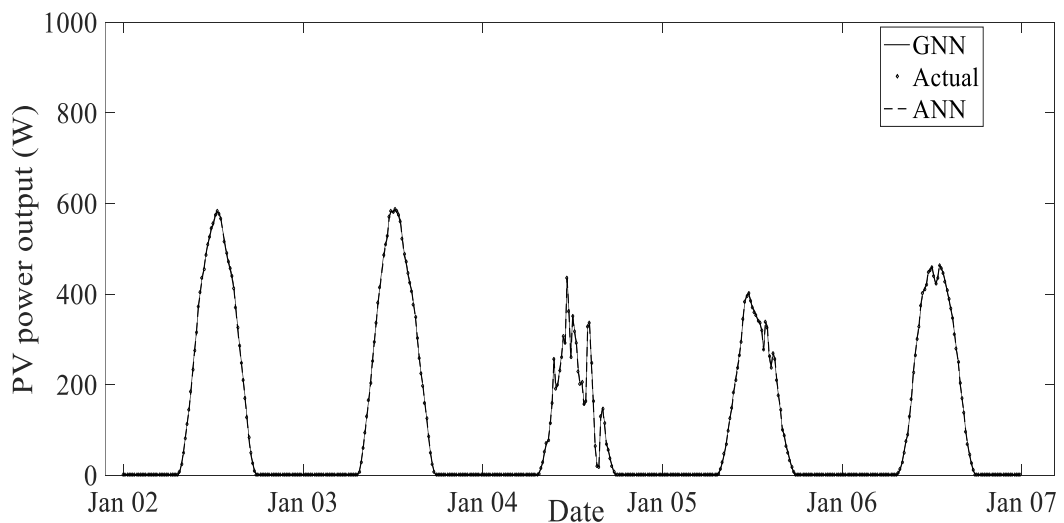


Fig. 4.15 Testing performance of ANN and GNN model for the month of winter season

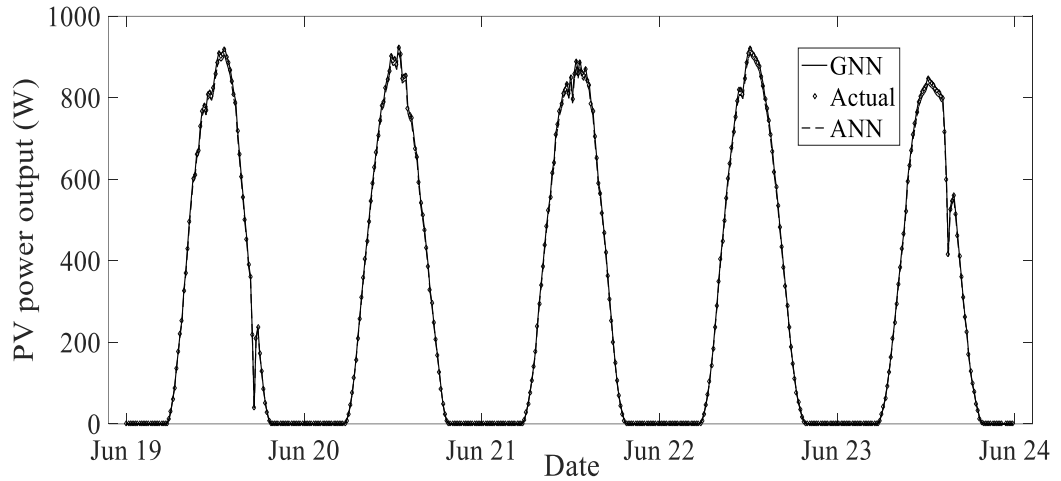


Fig. 4.16 Testing performance of ANN and GNN model for the month of summer season

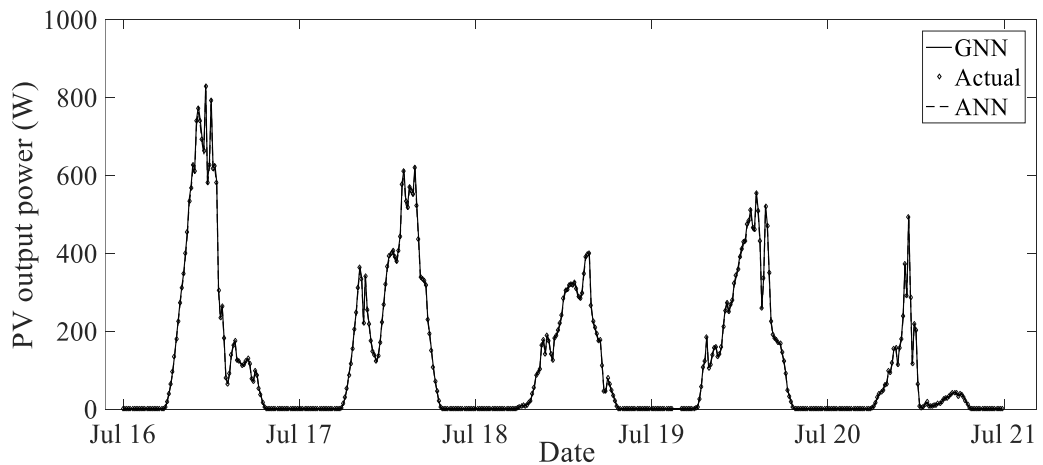


Fig. 4.17 Testing performance of ANN and GNN model for the month of rainy season

The average RMSE for winter, summer and rainy seasons for ANN are 39.4 W, 43.3 W and 51.7 W respectively in Table 4.3. The average RMSE for winter, summer and rainy seasons for GNN-W are 30 W, 34.1W and 45.2 W respectively. The percentage MAE for winter, summer and rainy seasons for ANN-based method are 3.84 %, 3.45 %, and 4.32 % respectively.

Table 4.3 Comparison of testing performances using GNN-W and ANN

Seasons	Model	RMSE(W)	MAE %
Summer	GNN-W	34.1	2.83
	ANN	43.3	3.45
Rainy	GNN-W	45.2	3.78
	ANN	51.7	4.32
Winter	GNN-W	30	2.95
	ANN	39.4	3.84

The percentage MAE for winter, summer and rainy seasons for GNN-W based method are 2.95 %, 2.83 %, and 3.78 % respectively. The same is given in Table 4.3, and it can be observed that values of average RMSE and percentage MAE for all three seasons are very low for the proposed method.

4.7 CONCLUSIONS

In this chapter, 15 minutes ahead short term solar energy forecasting models based on GNN and GNN-Wavelet have been developed and presented. The performance of the models is evaluated on the basis of statistical indicators such as MAE and RMSE. The results obtained from the GNN model are good and within the desired limits. The average RMSE for winter, summer and rainy seasons are 411, 370 and 449 Watts respectively. The percentage MAE for winter, summer and rainy seasons are 3.23 %, 3.08 %, and 3.79 % respectively. To validate the proposed method the above results are compared with other existing approaches like ANN and found better within desired limits.

CHAPTER 5

ENERGY MANAGEMENT SUPPORTING HIGH PV PENETRATION FOR SMART GRID ENVIRONMENT

5.1 INTRODUCTION

In the previous chapter, the solar energy forecasting is performed using a hybrid model consisting of generalized neural networks and wavelet transform. This chapter is focussed on developing energy management system supporting high penetration of solar photovoltaic generation for smart grid using solar forecasts and storage system. The SPV output power forecasting helps in controlling of variables and optimize the capacity of energy storage system. In this chapter, the solar energy forecasting is performed using a hybrid model consisting of GNN and wavelet transform. In this work pumped hydro storage (PHS) is used as backup to meet the grid requirements. In order to obtain more accurate and practical results, demand response (DR) program has been also integrated in the formulation of the problem. An adequacy analysis is also carried out under various consumer flexibility scenarios. Performance analysis of the proposed energy management system has been done using MATLAB/Simulink platform, and the same is validated on 5 kW SPV system.

5.2 SMART ENERGY MANAGEMENT

The growing penetration level of solar photovoltaic technology is becoming a challenging task in the smart energy management systems.

This chapter is based on the following published papers

1. **Priyanka Chaudhary** and M. Rizwan, "Energy management supporting high penetration of solar photovoltaic generation for smart grid using solar forecasts and pumped hydro storage system" *Renewable Energy (Elsevier)*, Volume 118, pp. 928-946, 2018. ISSN: 0960-1481, **Impact Factor: 4.357**.

The power generated from the solar photovoltaic (SPV) systems is intermittent. Variability of output power from a solar photovoltaic generation plant can lead to the unstable operation of the power system. These fluctuating output power problems lead to the issues in its use and at the same time generates the market needs for electrical energy storage (EES). An imbalance between demand and supply may cause the damage in the stability of utility grid as well as the power quality. The issues like unbalancing can be reduced via implementation of resource forecasting, EES and demand-side management. With the help of these three aspects, power management for the improved dispatch of utility-scale PV plants can be assured.

Grid integration of a solar PV array requires a power electronic interface between the grid and the solar PV array. Power conditioning unit (PCU) comprises of DC/DC converter, MPPT controller for SPV system and inverter, used to condition the SPV output and make this able to match the grid requirements. A control technique based on predictive current control for VSC with Perturb and Observe (P&O) maximum power point tracking (MPPT) technique is implemented in this work, details are given in Chapter 6. A Vikram Solar ELDORA 270 of 270.66 W_p solar PV module has been used to obtain a 5 kW_p solar photovoltaic system. P-V and I-V characteristics of modelled system are presented in Fig. 5.1 for different irradiances. A pumped hydro storage (PHS) system use electricity to pump water to the higher altitude, i.e., upper reservoir where it is stored as gravitational potential energy. Stored energy is converted back into electricity by releasing water passed back through a turbine to the lower reservoir. During off-peak hours or surplus SPV generation, the water is pumped to the upper reservoir. During peak hours or lower PV generation water flow from the upper reservoir to lower through turbine/generator to produce electricity and supply the power

to loads. The modelling and control of PHS are given in section 3.4 and can be referred from there.

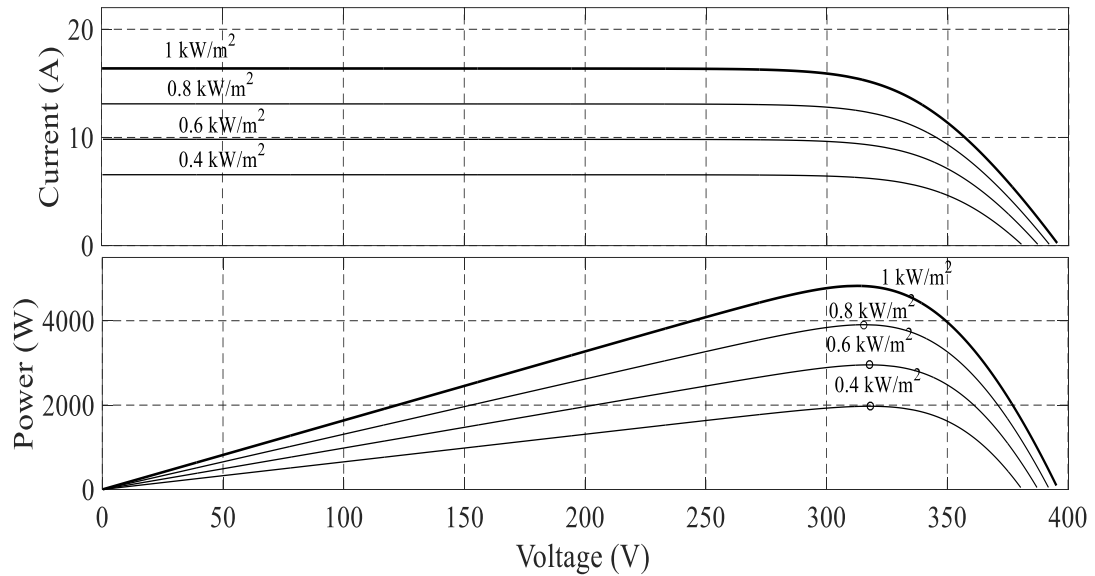


Fig. 5.1 P-V and I-V characteristics of 5 kW_p SPV system at different solar irradiances

5.3 APPLICATION OF SOLAR POWER GENERATION FORECASTING MODEL IN SMART GRID ENVIRONMENT

A hybrid forecasting model for very short-term SPV generation forecasting is proposed in this work. Since the historic data available for solar PV power output forecasting is complex and consists of different frequencies. Thus, for a reliable forecast wavelet decomposition method has been integrated with the GNN model in the present work. The proposed model is developed by decomposing an original historical data for solar PV power output and various meteorological parameters data into one level, two levels, three levels and four levels of the wavelet. Processed data has been used as input to the GNN model for 15 minutes timescale SPV power output forecasting. As seen in Fig. 5.2, the forecasting model requires a historic dataset for PV generation, the preceding block to this forecasting model is the data handling block which conditions and classifies the historical dataset according to types of days and seasons.

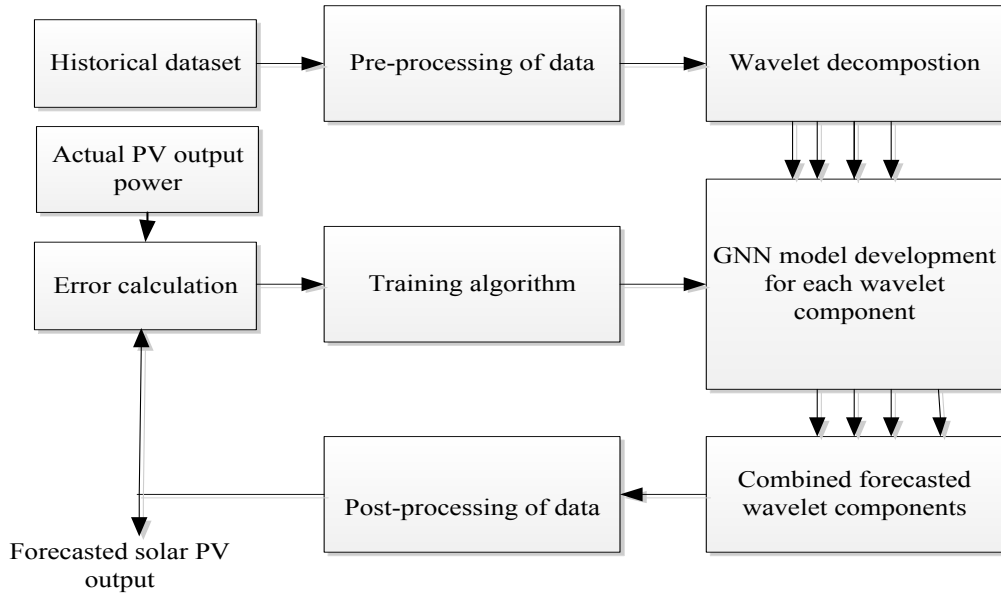


Fig. 5.2 Hybrid forecasting model for SPV generation forecast

PV power generation is affected by numerous factors, and it is very difficult to describe power output with a certain mathematical function. Weather types, different meteorological parameters make significant impact on the power output of SPV systems. Considering these points, the output is modelled in this work concerning the different meteorological parameters and under different day types like sunny, mostly sunny, cloudy, overcast and rainy/snowy. Solar irradiance is the factor by which the PV output power is affected significantly get affected. PV power output estimation can be described as following:

$$P_{PV} = \left[P_{PVSTC} * \frac{I_r}{1000} * [1 - \gamma * (T - 25)] \right] N_{SPV} * N_{pPV} \quad (5.1)$$

Where, T is the temperature of solar PV panel (°C) and given as:

$$T = T_a + \frac{I_r}{1000} * (N_{OCT} - 20) \quad (5.2)$$

Further, weather conditions such as cloudy, dust have the large influence on solar irradiance reaching to the PV panels. These factors reduce the direct irradiance to

the ground by scattering and reflecting. So, a good and accurate forecasting model for solar energy requires a hybrid and intelligent approach which uses historical PV power and multiple meteorological parameters.

5.3.1 Data collection

As the output of solar PV system is highly affected by various meteorological parameters especially solar irradiance, ambient temperature, average relative humidity and wind speed. Data for global solar irradiance, ambient temperature, average relative humidity and wind speed has been collected from Jamia Millia Islamia (JMI), National Institute of Solar Energy (NISE) and Ministry of New and Renewable Energy (MNRE), Government of India and other sources for New Delhi location at 15 minutes time interval. The collected data has been used as input for short-term solar PV output power forecasting. Historic data available is complex with different frequencies. Preprocessing of data is done before giving it to the wavelet model. Wavelet decomposition is used to decompose original historical datasets into different levels according to the frequencies.

5.3.2 Day type and weather type classifications

In this work, seasonal classification according to Indian scenario has been done such as summer, winter and rainy seasons. With the help of this classification, more granularity can be achieved to the clustering performed on the historical dataset.

5.3.3 Correlation of PV power with meteorological parameters

A Pearson product-moment correlation coefficient (PPMC) has been used to perform linear regression analysis between PV power and various meteorological

parameters based on historical data available. Dependency between X and Y variables has been calculated using formula given in (equation 4.16).

5.4 DEMAND RESPONSE MODELLING

Demand response (DR) is the reduction in load as a result of the load reductions, a certain amount of the load curtailed and to be restored. Demand response management scheme plays the significant role in a smart grid environment by improving electricity bill savings and mitigating the output fluctuations of renewable energy resources [174-175]. There are two ways in which DR program can be implemented [176]. One is utility offers consumer for reducing during specified periods and called as load response scheme. In another type of DR program customer voluntarily curtails demand in response to increasing market prices and known as price response. Direct load control programs, curtail able load program, interruptible load program and schedule load program come under the category of load response DR program. In price response DR program customer usage monitored against varying electricity rates, price response program requires high technology meters. Time of use (TOU) pricing program, critical pricing program (CPP), real-time pricing (RTP) and demand bidding, etc. are the types of pricing response DR program.

Time-varying pricing of electricity is widely applied in the electricity market due to numerous advantages as mentioned earlier. Time of use pricing has been implemented by numerous utilities all over the world which gives reduced electricity price at off-peak periods and high in case of peak demand occurs. Power generation for solar PV systems is higher during peak periods because of this integrating demand response with solar PV generation systems can be helpful in providing economic advantages. There are various types of TOU pricing has been quoted in literature. The

net metering structure is also a very important part of demand response. In TOU pricing base scheme utility meter is used to store past energy consumption data in term of quantity and function of time [177-178]. It will monitor the peak and off-peak periods for setting the price based on the peak and off peaks. In net metering structure consumer only billed for the consumption and generation differences.

In developing countries, TOU or Time of Day (TOD) pricing is now being introduced in commercial sectors earlier it was used mostly for industrial sectors [177]. Most of the State Electricity Regulatory Commissions (SERCs) in India have already implemented TOU based pricing scheme, for large industrial and commercial category customers. Some SERCs have already implemented, and others are planning to implement soon. The report includes analysis carried out by covering the various aspects such as the introduction of TOU, categorization of consumers and rate difference between peak hours, normal hours and off-peak hours. The proposed work would be useful for demand response application in developing countries also.

5.4.1 Electricity pricing

Cost of energy at peak $(COE)_p$ and Cost of energy at off-peak $(COE)_{op}$ for a certain time interval can be determined by using below-given equations. The PV energy output during peak period (E_{pvpeak}) is less than the energy required during peak period (E_{peak}) . Also, the PV energy output during off-peak period (E_{pvop}) is less than energy required during off-peak period (E_{op}) . The value of $(COE)_p$ and $(COE)_{op}$ can be calculated using below equations. Where, R_p and R_{op} are the rate of energy in \$/kWh for peak and off-peak periods respectively.

$$(COE)_p = (E_{peak} - E_{pvpeak}) \cdot R_p \quad (5.3)$$

$$(COE)_{op} = (E_{op} - E_{PVop}) \cdot R_{op} \quad (5.4)$$

For PV energy output during peak period (E_{pvpeak}) more than energy required during peak period (E_{peak}), $(COE)_p$ and $(COE)_{op}$ are given by equation 5.5 and 5.6 respectively. If the generation is more than the consumption, the consumer is rewarded with an avoided cost rate (ACR), which is typically much less than the retail rate of energy. Where $R_{ACR(P)}$ and $R_{ACR(OP)}$ are the avoided cost rate of energy in \$/kWh for peak and off-peak periods respectively.

$$(COE)_p = (E_{peak} - E_{PVpeak}) \cdot R_{ACR(P)} \quad (5.5)$$

$$(COE)_{op} = (E_{op} - E_{PVop}) \cdot R_{ACR(OP)} \quad (5.6)$$

5.4.2 Load modelling

For this work, load has been characterized into two types: static loads and flexible or time shift able load.

(a) Static loads

No flexibility is offered by the static loads and sufficient amount of generation should be present to meet the demand of such loads at each instant of time within the operating time range. Such loads can be modeled as:

$$Static\ loads\ (L_s) = \{L_s\}_{i=1}^n \quad (5.7)$$

Where i is scheduling time at which equation (5.5) must be satisfied.

(b) Flexible or time-shiftable loads

Such loads need a fixed amount of energy to be delivered within a given time interval or a deadline. In available literature, these loads are modeled as lumped models

with energy requirements modeled as different tasks. Task requirements can be described as follows:

$$\sum_{i=a_i}^{d_i} P_{ik} \Delta t = E_i; 0 \leq P_{ik} \leq m_i, \forall i \in \{a_i, \dots, d_i\} \quad (5.8)$$

Where, the quantity of energy must be delivered (E_i), maximum power transfer rate (m_i) and service time interval (a_i, \dots, d_i) are the parameters of the task, and each of them defines the flexibility of loads. Flowchart for the demand response algorithm has been implemented in the present work is shown in Fig. 5.3.

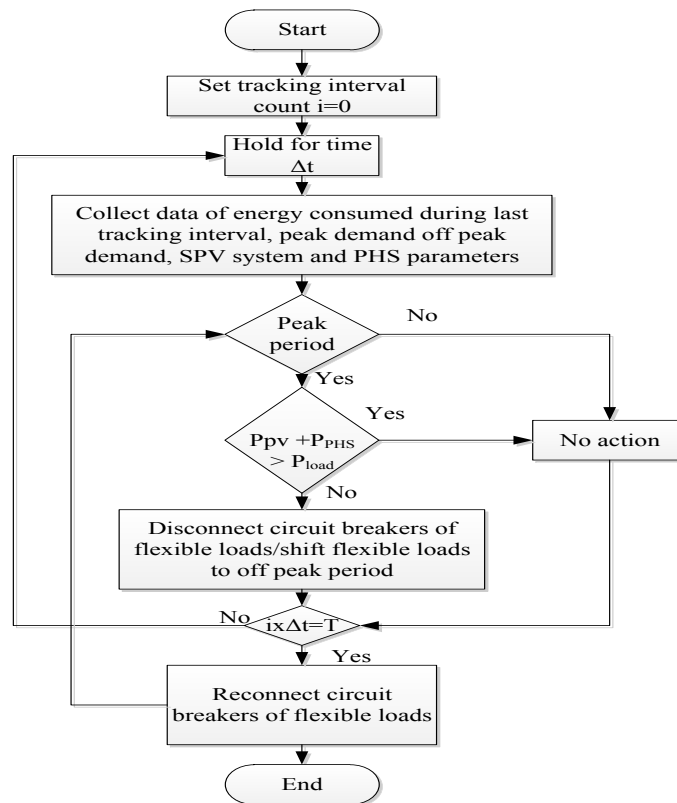


Fig. 5.3 Flowchart for demand response algorithm

5.4.3 Demand response case studies

Restoration of the reduced load is a key operational feature of demand response and referred to as payback. Four different scenarios have been considered in this work according to the payback effects to show impacts of demand response with different

levels of consumer or load flexibility. Load flexibility (f_{lt}) is being considered to vary between 5 to 40% with the steps of 5%. Table 5.1 represents different demand response cases considered in the present work.

Case 1 (DR 1): For this case, no payback is being considered, i.e., the load shedding is done by demand response program would not be restored. This is the case which shows best possible results of DR.

Case 2 (DR 2): In this case, load which is shifted from corresponding on-peak period to off-peak period is fully restored without being limited by any constraint.

Case 3 (DR3): In this case, 50% of reduced load is with constrained payback. The half load is restored with immediate action after an hour. This case has been considered to represent the practical case, the reduction in original consumption or partly service provided by the load such as maintain the room temperature with loss of some control functions.

Case 4 (DR4): In this case, 100 % of reduced load is with constrained payback. Full load is restored with immediate action after an hour. This case may use to represent the loads which need immediate start after the interruption.

Table 5.1 Different DR cases according to the payback

Case	Payback	Load Restored	Constraints
Case1 (DR1)	No	No	Not any
Case2 (DR2)	Yes	Fully	Not any
Case3 (DR3)	Yes	Half	Yes
Case4 (DR4)	Yes	Fully	Yes

In terms of reliability assessment of the developed demand response program various indices available in literature [178] has been used in this work to measure the system reliability such as Expected Energy not Supplied (EENS), reduction in peak demand etc. Fig. 5.4 shows the EENS as a function of consumer flexibility and it can be observed that for a particular demand response case EENS is small for large consumer flexibilities and provides the better adequacy and reliability.

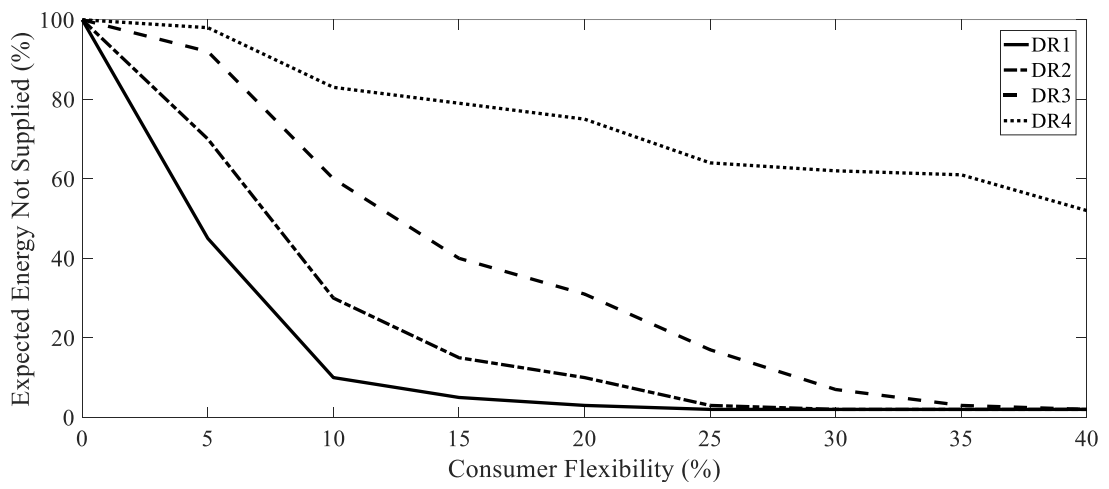


Fig. 5.4 EENS as a function of consumer flexibility for different DR cases

Fig. 5.5 shows the peak reduction as a function of consumer flexibility and it can be seen peak reduction increases with DR increases with the large consumer flexibility.

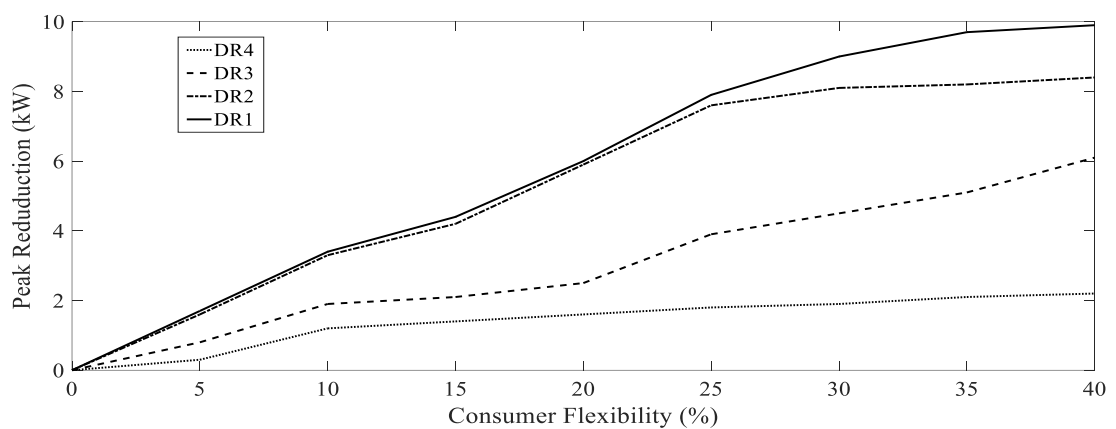


Fig. 5.5 Peak reduction (kW) as a function of consumer flexibility for different DR cases

Effect of different payback cases can also be seen from the given figures. For the same consumer flexibility, DR1 without payback is best regarding EENS and followed by DR2, DR3 and DR4. For peak reduction, considering same consumer flexibility, DR1 can result in the same approximate reduction in the peak with DR2. While the demand response in DR3, and DR4 is not able to deploy with the entire range of consumer flexibility.

5.5 ALGORITHM FOR PROPOSED ENERGY MANAGEMENT SYSTEM

This section deals with the details of the algorithm used to take decisions about the demand response, charging discharging operation of energy storage device (PHS). The developed algorithm aims to utilize the SPV generation efficiently and to minimize the cost of electricity from the utility.

Energy management system (EMS) will have to assign power from solar PV first to the non-flexible or static loads. If the output of solar PV is not sufficient to feed the load at scheduling interval, then pumped hydro storage will start operate for supplying power to the static loads. If the generation from these two is not sufficient to supply the static demand than electricity from the utility will be used. After assigning the power to static loads, the algorithm will determine the need for flexible loads. If there is extra solar power generation is available or energy storage can feed the flexible loads, then this will be given to the all active tasks at that particular scheduling interval otherwise electricity from the utility at TOU pricing is used to fulfill the demand of non-flexible loads. EMS will also decide the charging and discharging states of the pumped hydro storage. During off-peak hours or surplus solar PV generation is available water is pumped up to the upper reservoir.

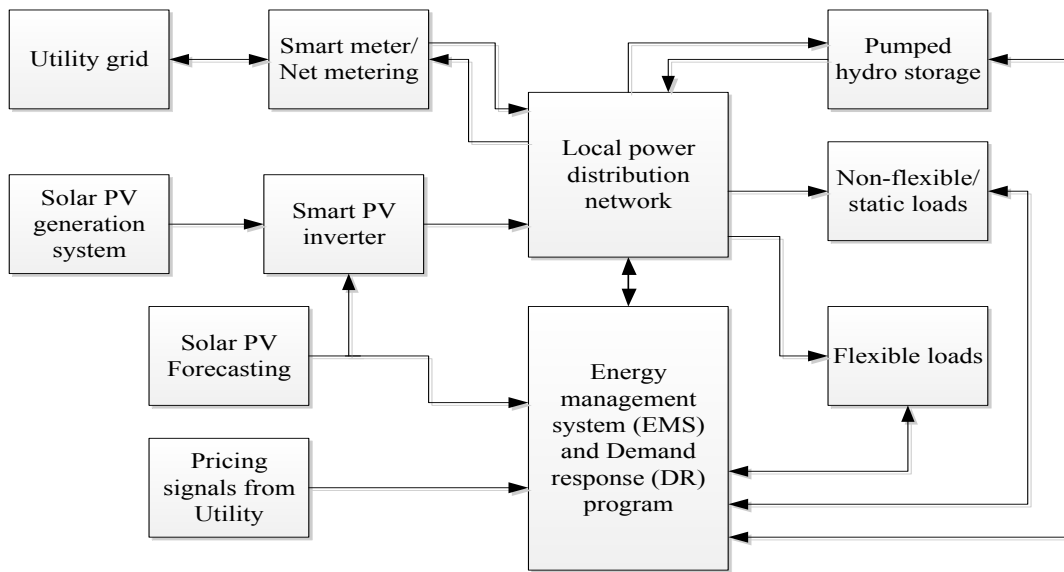


Fig. 5.6 Schematic representation of proposed system

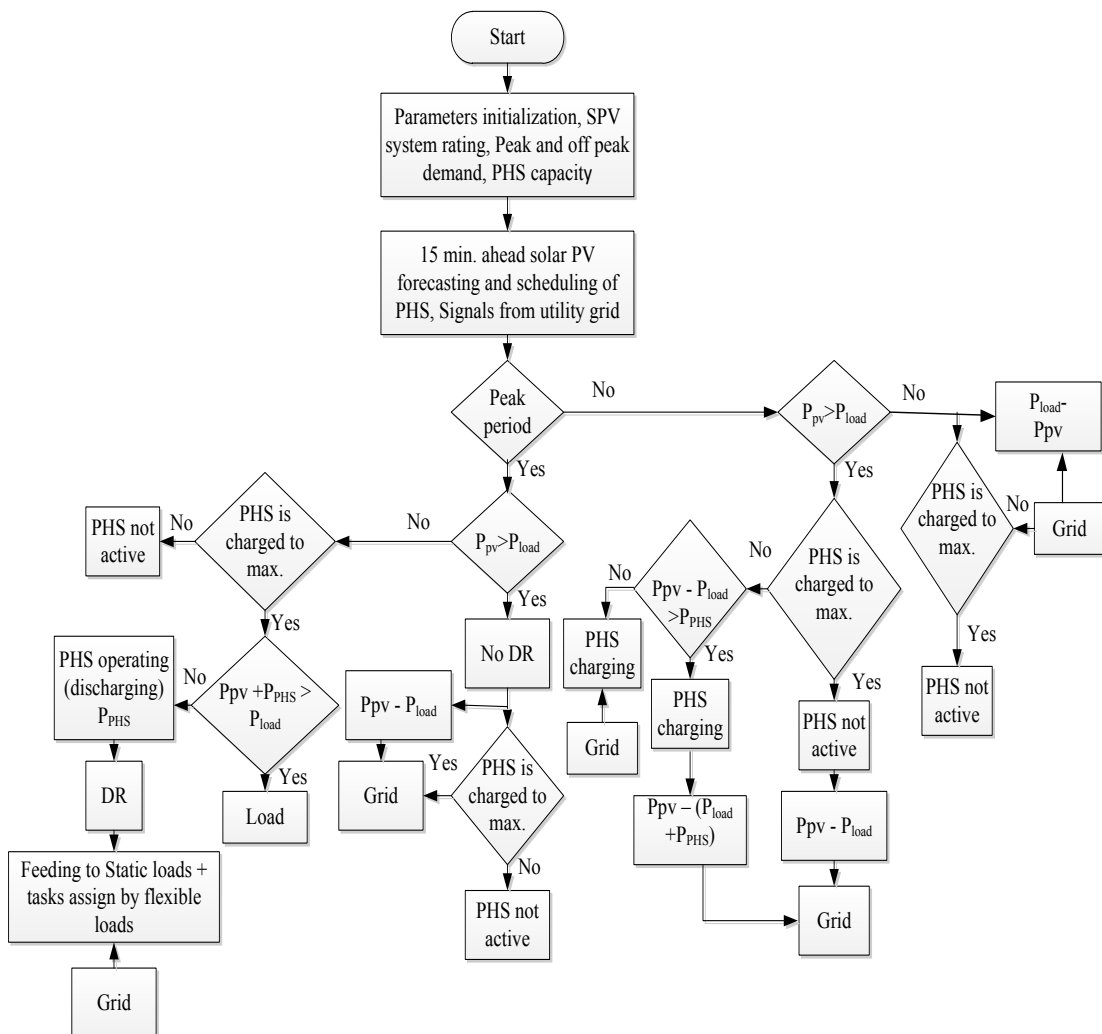


Fig. 5.7 Flowchart of proposed algorithm

During peak hours or lower PV generation water flow from the upper reservoir to lower through turbine/generator to produce electricity and supply the power to loads. Schematic representation of the proposed system is presented in Fig. 5.6. Flowchart of the overall control algorithm is shown in Fig. 5.7.

5.6 RESULTS & DISCUSSIONS

A generic load profile has been considered in this work for a residential type of distribution system. Various typical household appliances are being considered for system designing and simulation purpose in MATLAB/Simulink platform. Home appliances such as air conditioning systems, cloth washing machines, lightning loads, refrigeration loads, etc. are considered here to perform this study. Data from a residential society for a street has been considered [179]. The total installed capacity of SPV system in the micro grid is 5 kW. Also, the adequacy analysis of the developed DR algorithm has been performed in this section by peak power reduction and EENS as a function of consumer flexibility. Different consumer flexibilities have been considered parametrically varying between 5 to 40%.

(i) Solar PV power output forecasting results

The testing results for short-term solar power output forecasting of 5 kW_p SPV system using proposed GNN-W model are presented. Data has been chosen and classified according to the three season types namely: summer, winter and rainy. Moreover, for more accurate and precise forecasting results day type classification also done and used in the proposed model. Fig. 5.8 – Fig. 5.11 shows the predicted results for the cloudy day, cloudier day, mostly sunny day and sunny day. From the results, it can be seen that forecasted PV power output is closely following the measured values.

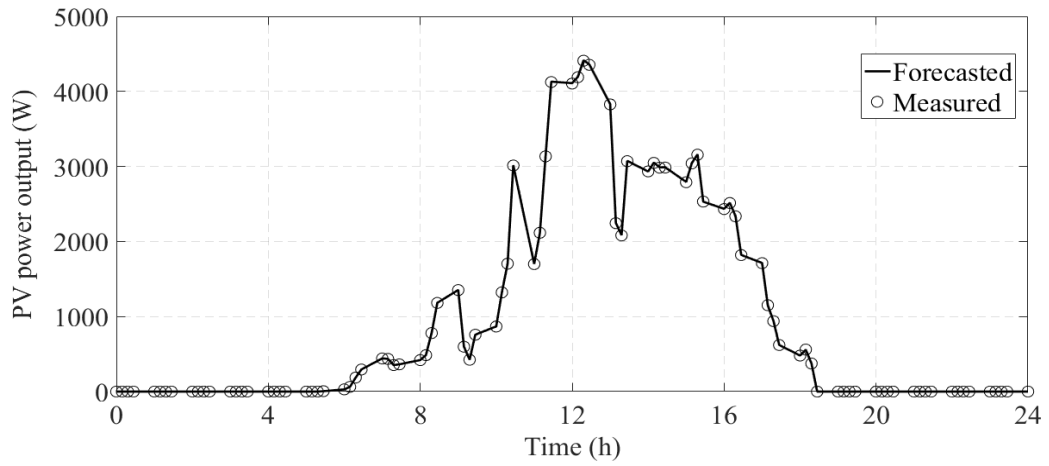


Fig. 5.8 15 minutes ahead PV power forecasting for cloudy day

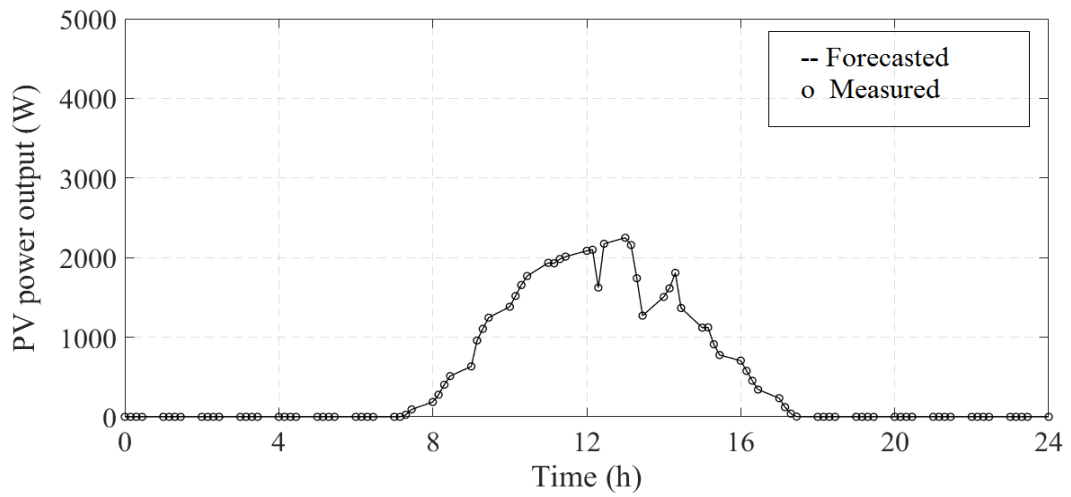


Fig. 5.9 15 minutes ahead PV power forecasting for cloudier day

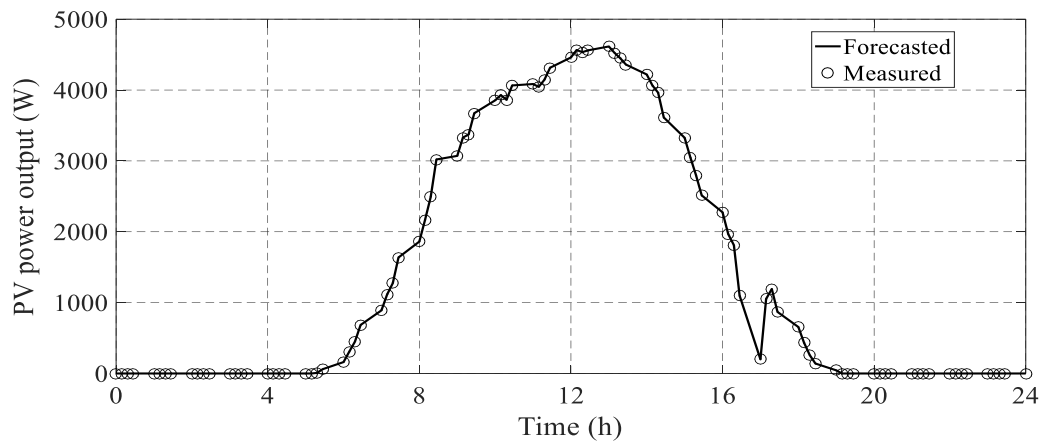


Fig. 5.10 15 minutes ahead PV power forecasting for mostly sunny day

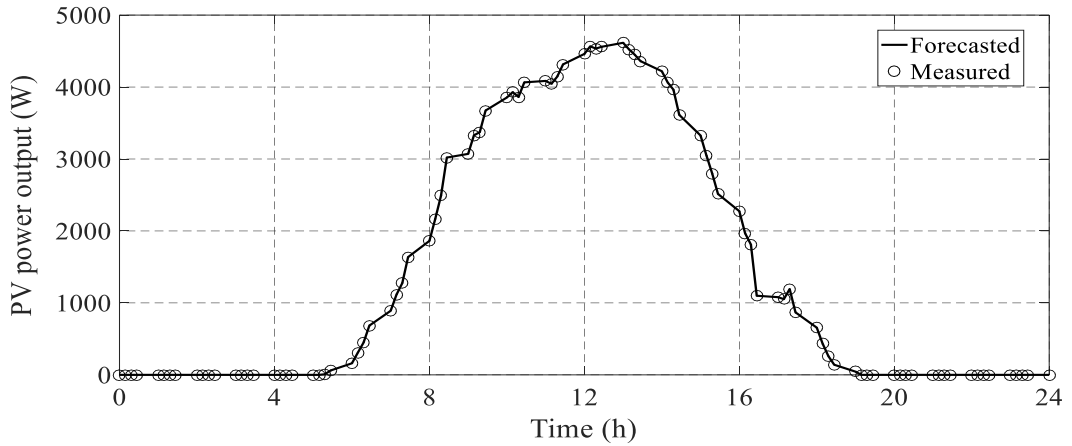


Fig. 5.11 15 minutes ahead PV power forecasting for sunny day

Results for winter, summer and rainy seasons are also presented in Fig. 5.12, Fig.5.13 and Fig. 5.14 respectively. For winter season the average data of five years for the month of January has been considered for testing the proposed approach. Similarly, for other two seasons, the data of respective months (June and July) has been considered in this work for validating the accuracy of the developed model.

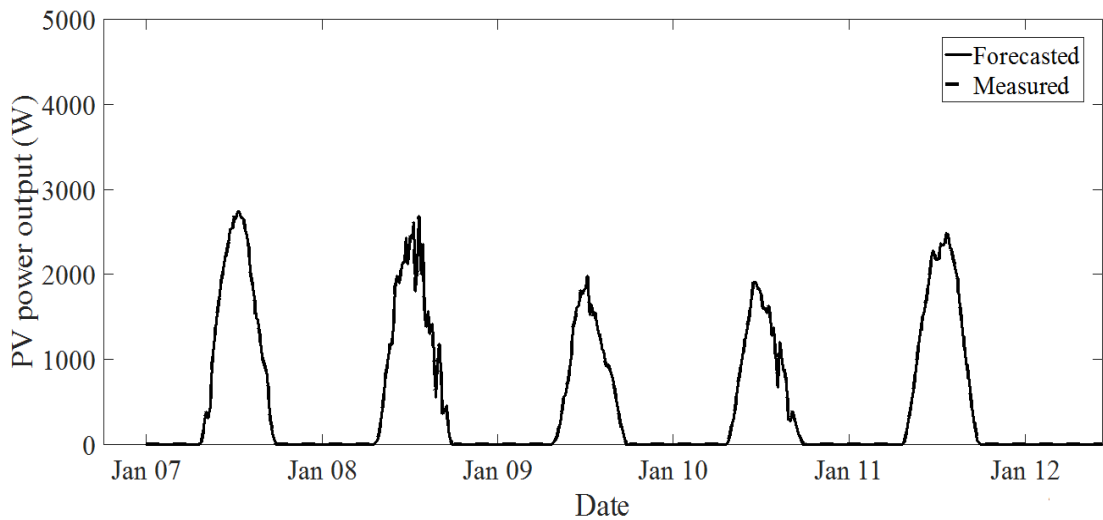


Fig. 5.12 15 minutes ahead PV power forecasting for winter season

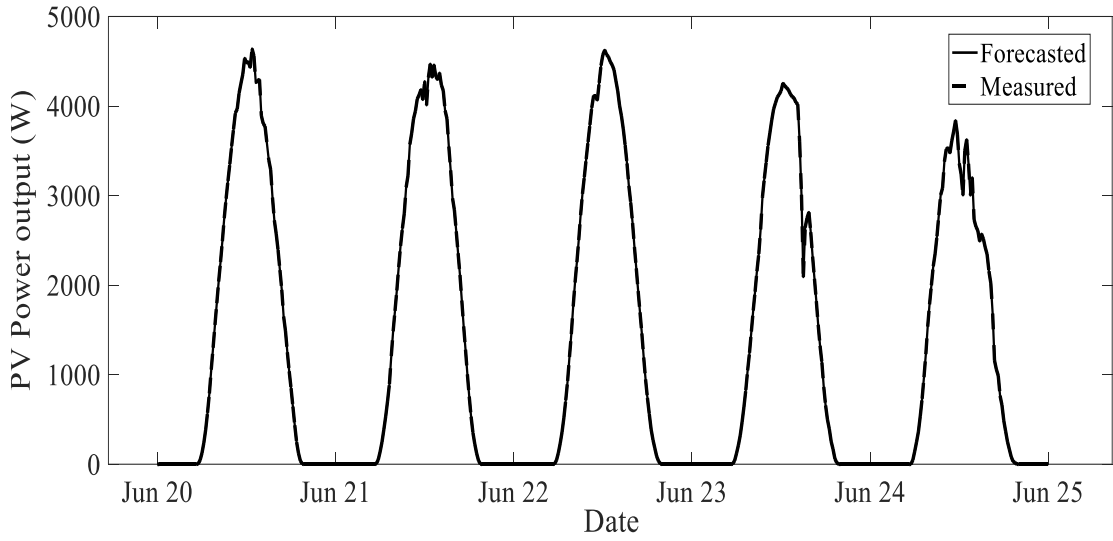


Fig. 5.13 15 minutes ahead PV power forecasting for summer season

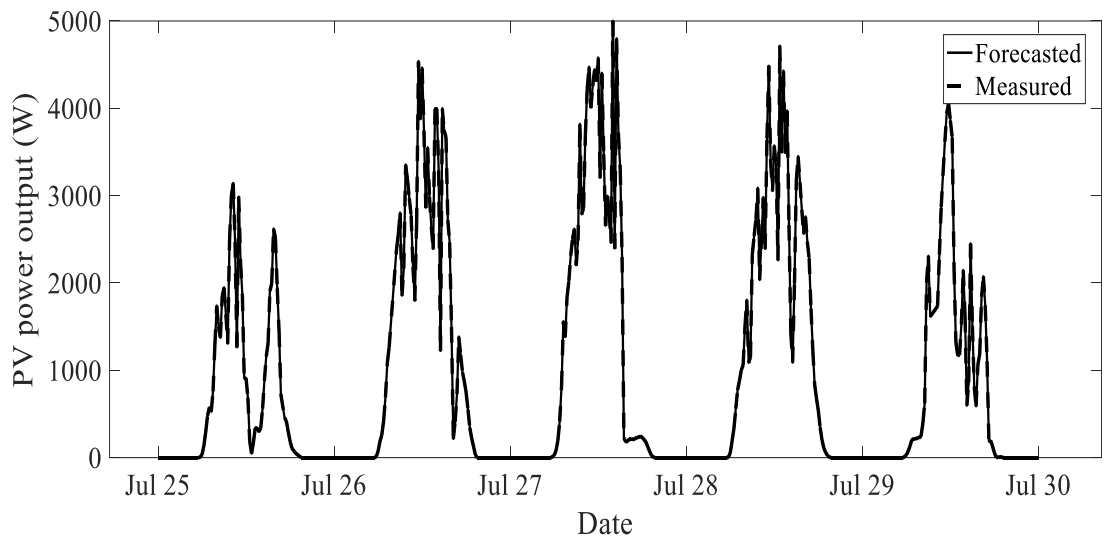


Fig. 5.14 15 minutes ahead PV power forecasting for rainy season

Cross-validation process has been done by splitting the data into two mutually exclusive categories, training data (larger one 70% of data) and test data (less data). The training data is used to build up the forecasting model, and the test data has been used to validate the developed model. Validation results are shown in the paper and train set results are not shown due to the scarcity of space. This process has been repeated with different wavelet subsets until each object of the given data has been used

as a test set once. The forecasted SPV power output in comparison with measured power is quite accurate. The maximum RMSE for winter, summer and rainy seasons are 583, 434 and 596 Watts respectively. The values of average RMSE for winter, summer and rainy seasons are 411, 370 and 449 Watts respectively. The maximum absolute error for winter, summer and rainy seasons are 7.8%, 6.9 %, and 8.1% respectively. The percentage MAE for winter, summer and rainy seasons are 3.23 %, 3.08 %, and 3.79 % respectively. The RMSE and percentage MAE for different seasons are presented in Table 5.2.

Table 5.2 Comparison of testing performance for GNN-W based short-term solar irradiance forecasting model

Seasons / Months	RMSE (Watts)	MAE (%)
Winter (January)	411	3.23
Summer (June)	370	3.08
Rainy (July)	449	3.79

From Table 5.2 it is observed that the values of average RMSE and percentage MAE is high for the month of July (rainy season) because of the large uncertainties associated with the data. It is found that GNN-W performs much better than other in term of learning time and convergence. The proposed method uses lesser number weights and training patterns in comparison to other approaches and hence reduces the complexity and the computational time. It has other advantages also such as robustness, ease in design and adaptability with the nonlinearities associated with data.

(ii) Performance of overall developed energy management system

This section deals with the analysis of the performance of overall developed energy management system. Fig. 5.15 shows a typical system for a day in which during

pump storage system is operating for peak period operation, but load demand is still not fulfilling, so rest amount of power is fed into utility grid during peak hours as solar power is not also available. Peak demand for the load curve shown is 11.5 kW which is occurring around 8:00 PM. During this time SPV power is not available, but PHS is operational and feeding the load and not sufficient to meet up the demand. This is the case when demand response algorithm is not operational.

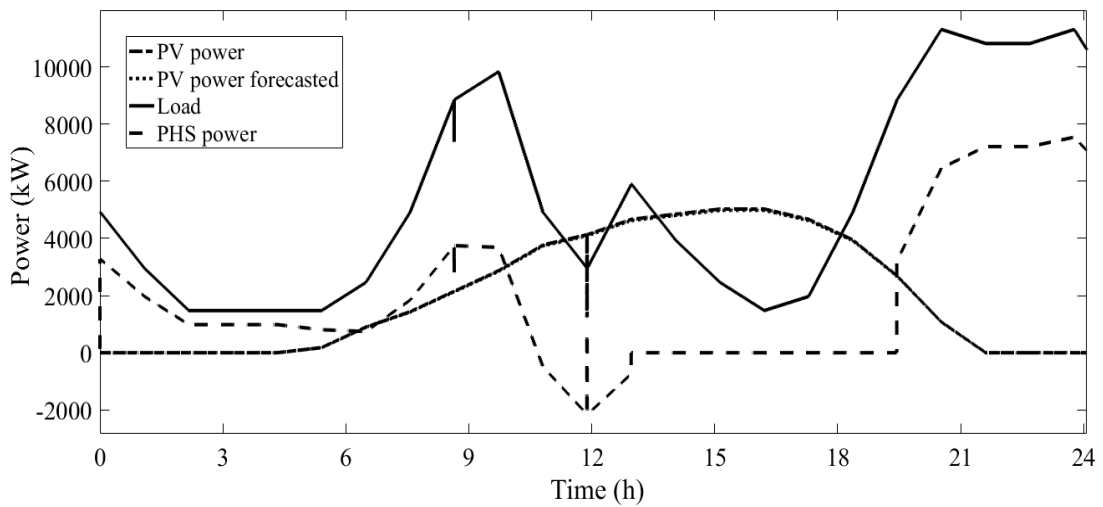


Fig. 5.15 Solar power generation forecasting, operational storage and no DR program for a typical day

Further Fig. 5.16 shows the results considering the same scenario but with demand response algorithm from which it can be seen that the flexible loads have been shifted from the peak time to the off-peak time which makes the total demand at peak time around 7.6 kW. In this case, DR algorithm is operational, and PHS can meet up the peak demand. Hence during peak time no need to take power from the grid and gives the advantage regarding saving a large amount of money.

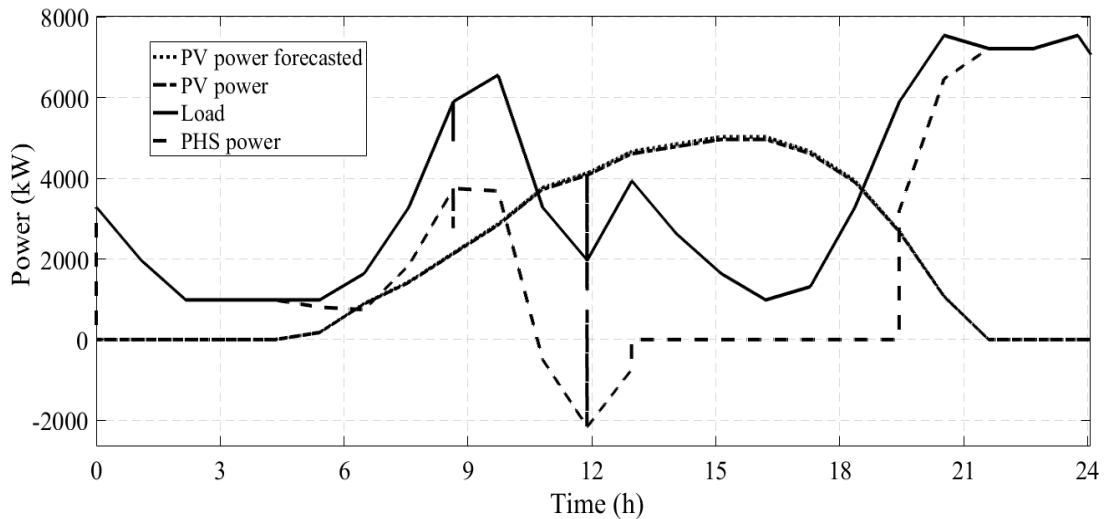


Fig. 5.16 Solar power generation forecasting, operational storage and DR program for a typical day

Fig. 5.17 shows the ideal case where the whole demand of load is being supplied by the PV and PHS system only during peak hours, while in off-peak hours it is possible to supply the load by the PV power only and PHS getting operated in pump mode of operational to refuel its upper reservoir. However, this ideal case is not the practical one. Hence for deciding the accuracy and reliability of the proposed system more practical cases are being considered for different weather types.

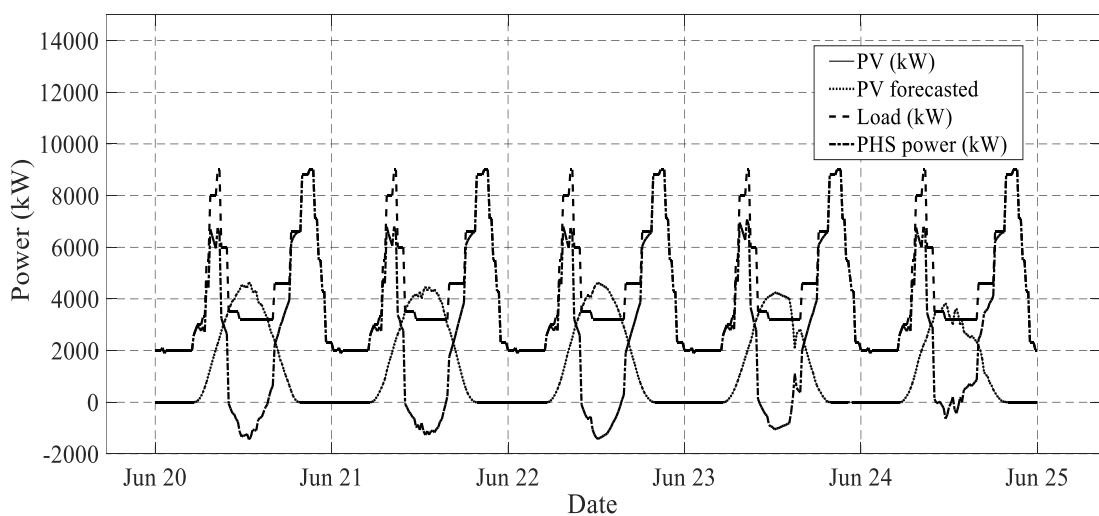


Fig. 5.17 Solar power generation forecasting, operational storage and No DR program summer season (Ideal case)

As for winter season, additional water heating loads during morning hours occurs, these practical implications are also being considered for the proposed work. During off-peak hours PHS is getting charged from the utility and supplying power to the load during off-peak hours and when PV is not available, and it is required to take very less amount of power from the utility grid. Results for summer, winter and rainy seasons are also presented in Fig. 5.18, Fig. 5.19 and Fig. 5.20 respectively.

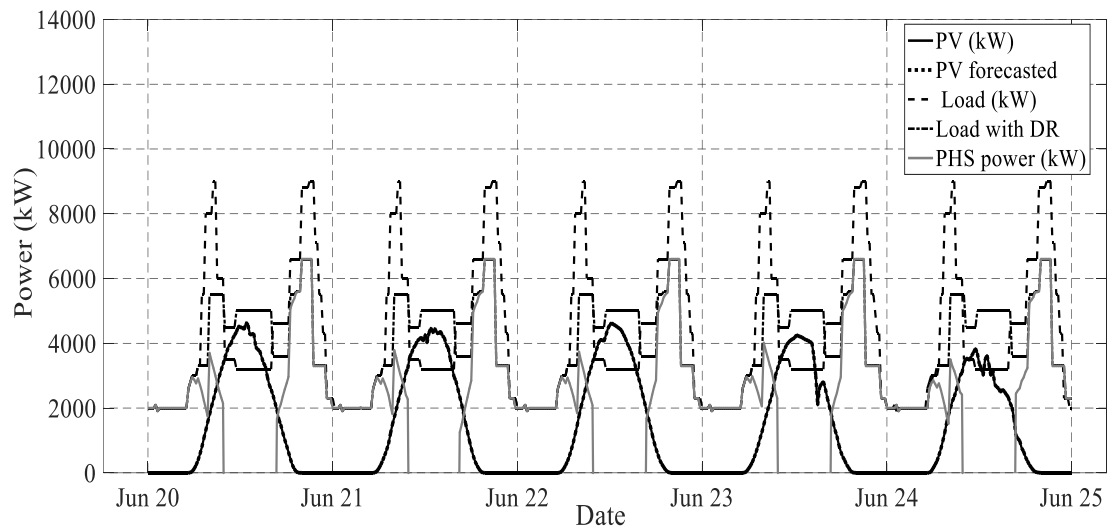


Fig. 5.18 Solar power generation forecasting, operational storage and with DR program summer season

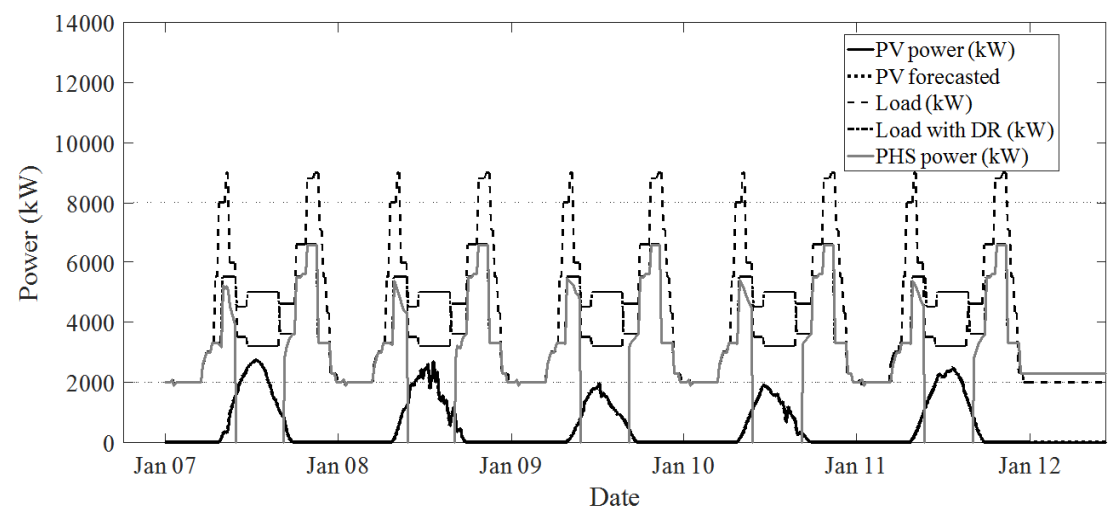


Fig. 5.19 Solar power generation forecasting, operational storage and with DR program winter season

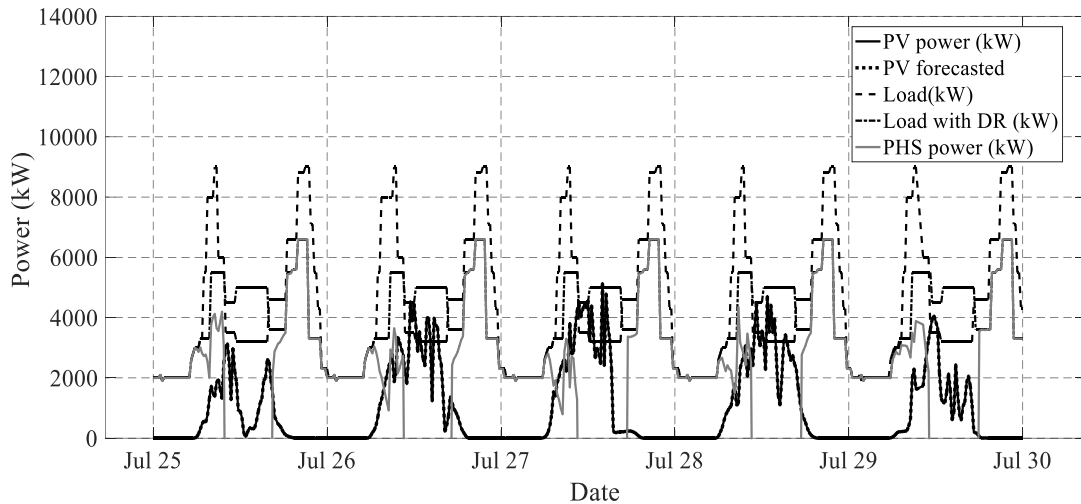


Fig. 5.20 Solar power generation forecasting, operational storage and with DR program rainy season

The results of a 24-h period have been shown and simulated with the developed EMS for different seasons and DR cases. The use time of electricity divides into the 24-h window and off-peak period has low electricity charges while peak time has high charges. During off peak periods as shown in above results power is taken from the grid to meet load demand and pump mode operation of PHS. During the peak period, excessive generation can be sold to the utility grid. These results are demonstrating that the proposed EMS enables the use of PHS and SPV power generation in the network along with DR program to reduce the cost of electricity.

5.7 CONCLUSIONS

In this chapter, a novel approach of energy management system for a smart grid environment has been developed and presented. Developed system consists of solar PV forecasting stage, PHS system and its controller and demand response algorithm. In the first stage, the PV power forecasting using hybrid GNN and wavelet approach has been done for 15 minutes ahead which is very useful to choose the appropriate back up to mitigate the power fluctuations of PV systems. The collected data has been

classified according to the three season types namely: summer, winter and rainy. Moreover, for more accurate and precise results day type classification like sunny day, partly cloudy, mostly cloudy day, overcast has been done and used in the proposed model. The validation results for short-term solar PV output forecasting using proposed GNN-W model are presented and found satisfactory. The performance analysis of the proposed forecasting model has been performed by using various error indices such as RMSE and MAE. To validate the proposed method the above results are compared with other existing approaches like ANN and found better within desired limits. Further, the power fluctuations of PV systems have been mitigated using pumped hydro storage systems instead of battery energy storage systems. Also, the demand response algorithm has been developed considering the different category of loads. Adequacy analysis of DR has been done using EENS and peak power reduction as a function of consumer flexibilities to demonstrate more practical cases. It is observed that for a particular demand response case EENS is small for large consumer flexibilities and provides the better adequacy and reliability. Overall system performance results are also presented concerning forecasted PV output, the performance of the system under DR and found satisfactorily. A possible direction for future work is to apply multi-objective optimization by considering proposed approach as a base for cost minimization and optimal operation considering resource forecasting, DR, and storage operation constraints.

CHAPTER 6

DEVELOPMENT OF CONTROL ALGORITHMS FOR GRID INTEGRATION OF SPV SYSTEM

6.1 INTRODUCTION

Solar photovoltaic systems are gaining attention and wide spread acceptance as distributed generators (DG) because of large availability of its resources with quite visible positive impacts on the environment. The integration of solar PV with grid as DG is able to solve the demand and generation mismatch issues especially in developing countries. Integration of solar PV systems at medium voltage (MV) / low voltage (LV) grid level poses some negative impacts such as voltage limit violation at the point of common coupling (PCC), frequency variations, grid stability issues, etc. Grid-integrated RES must follow the grid codes and regulations which has been defined by the authorities to accommodate the RES based generation systems. IEEE 1547, IEC 61727 and VDE-AR-N4105 are major standards for RES integration as a distribution generator (DG) in low voltage (LV) distribution system.

This chapter is based on the following published papers

- [1] Priyanka Chaudhary and M. Rizwan, "Hybrid Control Approach for SPV/FC fed Voltage Source Converter Tied to Grid" International Journal of Hydrogen Energy (Elsevier), vol. 43, no. 14, pp. 6851-6866, 2018. ISSN: 0360-3199, **Impact Factor: 3.582.**
- [2] Priyanka Chaudhary and M. Rizwan, "A Predictive Current Control for Solar PV Fed VSI in Distribution System" 17th IEEE International Conference on Environment and Electrical Engineering (IEEE EEEIC17), June 6-9, 2017, Milan, Italy.
- [3] Priyanka Chaudhary and M. Rizwan, "Grid Integration Control Algorithm for SPV Based Power System" IEECON 2018, March 7-9, 2018, Krabi, Thailand.
- [4] Priyanka Chaudhary and M. Rizwan, "A Three Phase Grid Connected SPV Power Generating System using EPLL based Control Technique" IEEE Second International Conference on Electrical, Computer and Communication Technologies (ICECCT 2017), February 22-24, 2017 Coimbatore, Tamil Nadu, India.
- [5] Priyanka Chaudhary and M. Rizwan, "Design and Development of Controller for Solar PV and Storage based Micro Grid" IEEE 41st National Systems Conference (NSC) 2017 on Super-Intelligent Machines and Man, December 1-3, 2017, Agra.
- [6] Priyanka Chaudhary and M. Rizwan, "Hybrid Control Approach using NLMS and PLMS Algorithms for Grid Connected SPV System" World Congress on Engineering 2018 (WCE 2018) 4-6 July 2018, London, UK.

DC/AC converter (Voltage source converter) is used converts the DC obtained from PV systems into AC to supply power to the AC loads and connect to the grid. VSC control is used the estimation of active, reactive current components as a basic unit of control architecture. Further, the VSC control efficient performance depends on algorithm utilized to generate the reference currents which will further use to generate the gate pulses IGBT switches. Hence, integration of solar PV as a DG must have efficient and coordinated control measures for the proper synchronization. Two types of circuit topologies are mainly adopted by researchers for grid integration of solar PV systems: single stage and two stage system topologies. This chapter focuses on development of intelligent and adaptive control techniques for grid connected solar PV system. These proposed algorithms provides reactive power, harmonic compensation and help system to transmit active power to the grid and loads effectively. The performance of the proposed techniques has been validated through simulations carried out in MATLAB/Simulink platform and also on implemented hardware prototype.

6.2 CONTROL ALGORITHMS FOR GRID INTEGRATION OF SPV SYSTEM

Various control techniques are widely reported for effective integration of SPV as DG systems with reactive power compensation and harmonics elimination capabilities to the distribution grid. The control techniques are broadly classified as conventional, intelligent and adaptive techniques. The conventional approaches for VSC grid synchronization are not much successful due to nonlinearities associated with RES based systems because of overshoots and long settling time in response. These issues may be overcome by intelligent and adaptive approaches.

Various control algorithms have been developed using intelligent approaches such as Artificial Neural Network (ANN), Generalized Neural Network (GNN), etc.

These algorithms provides reactive power, harmonic compensation and help system to transmit active power to the grid and loads effectively. In this work Gradient Descent Back Propagation (GDBP) NN based $I \cos\phi$, Quasi Newton Back Propagation (QNBP) NN based $I \cos\phi$, Extended Kalman Filter (EKF) based GNN, etc. algorithms are proposed for three phase grid connected PV system. The proposed algorithms have been developed in MATLAB/Simulink platform and also implemented on hardware prototype in laboratory. The performance analysis of these algorithms have been discussed by considering various system parameters in this thesis.

6.3 SYSTEM DESCRIPTION

The proposed system deploy a single stage circuit topology and consists of a solar PV array, voltage source converter (VSC), ripple filter to remove the excessive fluctuations from the output of VSC, loads and three phase utility grid and shown in Fig. 6.1. The developed system has been implemented with minimum number of sensors. Control of voltage source converter (VSC) in a grid integrated system plays a vital role to control and synchronize the system with the grid. VSC control is used the estimation of active, reactive current components as a basic unit of control architecture. Further, the VSC control performance depends on algorithm utilized to generate the reference currents which will further use to generate the gate pulses of IGBT switches. In this chapter, various approach has been developed and implemented to control the switching of VSC to synchronize the system with the grid and main task to separate weights of primary real and reactive parts of three phase load currents to obtain reference grid currents. The developed system design specifications is provided in appendix A.

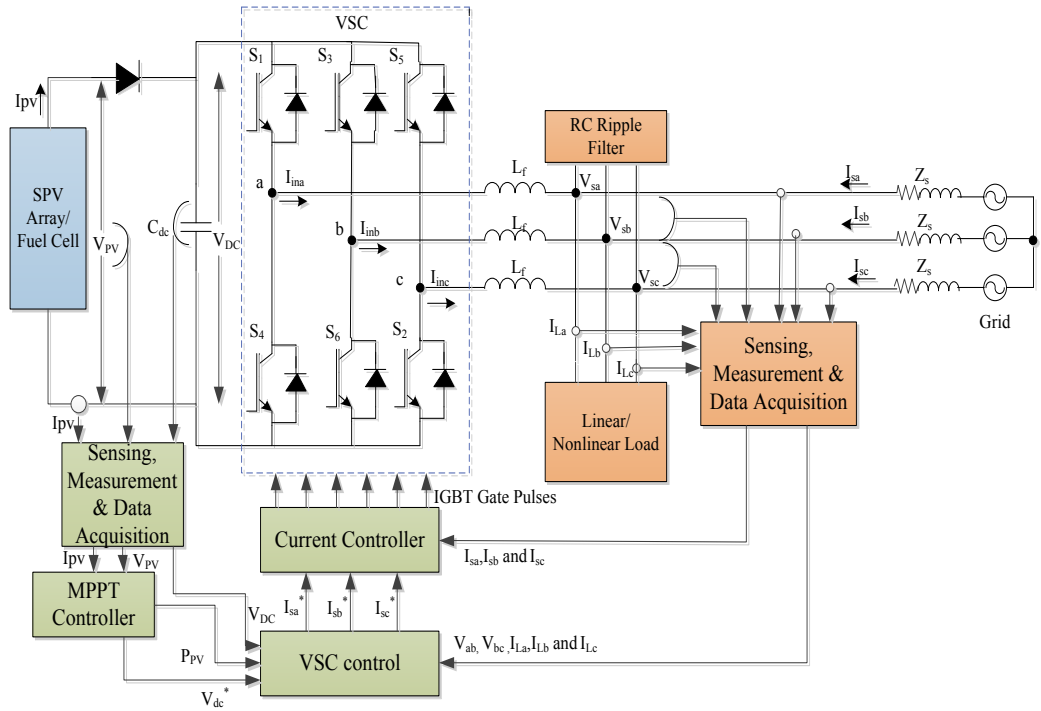


Fig. 6.1 Schematic diagram of test system under study

6.4 GDBP NN BASED $I \cos \phi$ CONTROL

A hybrid algorithm is proposed combining $I \cos \phi$ technique and gradient descent back propagation learning (GDBP) neural network for PV/FC fed VSC to provide reactive power compensation and mitigation of power quality issues. The proposed system feed active power to the connected loads, provide reactive power compensation and support the grid. The feed forward back propagation technique has been chosen to deal the complex non-linear problems associated with the proposed system. GDBP based NN is easy to implement for complex system and provides fast convergence in comparison with other algorithms. The proposed system exhibits very less static error and fast convergence, robustness, adaptive for dynamic loads, provides harmonics compensation, power factor correction, load balancing, etc. In this application, all the power quality related issues are achieved successfully by using the proposed control technique under both balanced and unbalanced, linear/non-linear loading conditions. The present section deals with the detail modeling of hybrid control

approach for VSC which combines GDBP base neural network and I cos ϕ control technique. This algorithm is very robust and provides fast response and convergence. The algorithm is used to compute weighted value of fundamental components of active currents (w_{ap} , w_{bp} and w_{cp}) and fundamental components of active currents (w_{aq} , w_{bq} and w_{cq}) from load currents. The weight training includes three stages such as input signals, error signal calculations and weights correction.

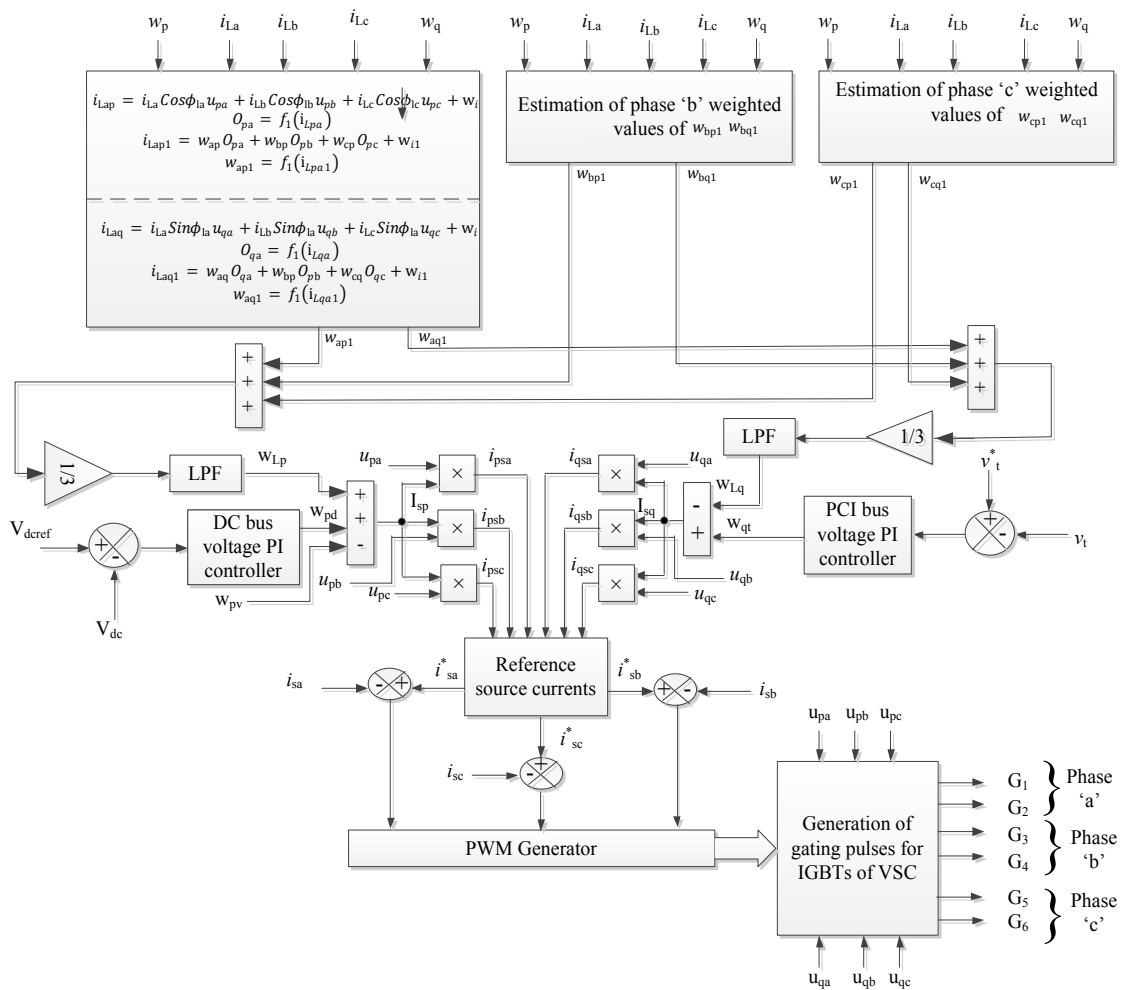


Fig. 6.2 Detailed description of the proposed VSC control algorithm

6.4.1 Control algorithm

Weights of the network is initialized for analyzing the value of corresponding neurons. The detail analysis of the proposed control technique is explained in a

systematic procedure without requirement of any particular learning process. The three layer GDBP based NN architecture for calculating weighted fundamental active and reactive current components are shown in Fig. 6.3 and Fig. 6.4 respectively.

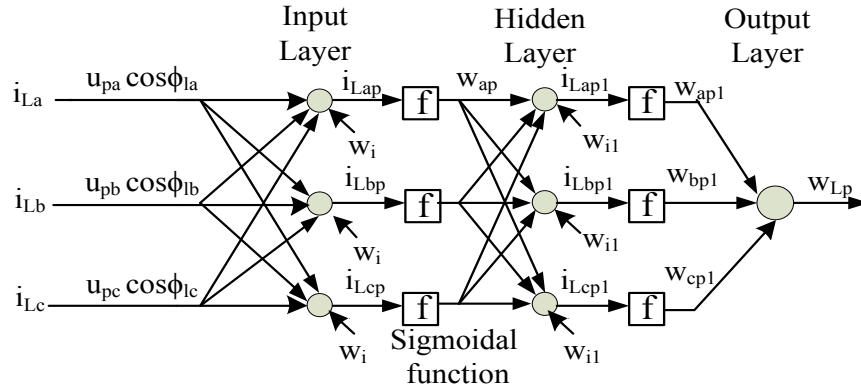


Fig. 6.3 Proposed GDBP NN structure for calculating weighted fundamental active current components

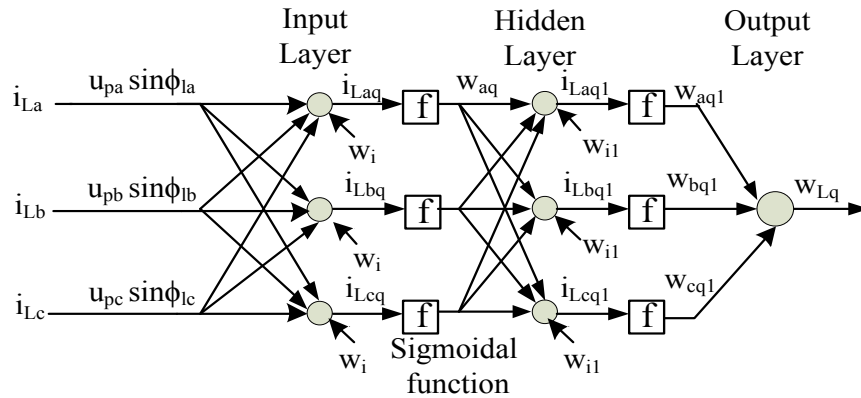


Fig. 6.4 Proposed GDBP NN structure for calculating weighted fundamental reactive current components

The detailed algorithm responsible for generation of switching signal patterns are provided in below subsection.

(a) Calculation of amplitude of terminal voltage and unit templates:

Sensed line voltages (v_{ab}, v_{bc}, v_{ca}) at PCC is used to calculate phase voltages, the amplitude of phase voltages (V_a, V_b and V_c) are calculated as equation (6.1):

$$V_a = \frac{2v_{ab}+v_{bc}}{3}, V_b = \frac{-v_{ab}+v_{bc}}{3}, V_c = \frac{-v_{ab}-2v_{bc}}{3} \quad (6.1)$$

The terminal voltage amplitude (V_t) at PCC can be computed as:

$$V_t = \sqrt{\left[\frac{2(v_a^2+v_b^2+v_c^2)}{3} \right]} \quad (6.2)$$

The in-phase unit templates of v_a , v_b and v_c are obtained as:

$$u_{pa} = \frac{v_a}{V_t}, u_{pb} = \frac{v_b}{V_t}, u_{pc} = \frac{v_c}{V_t} \quad (6.3)$$

Quadrature unit templates can be obtained from in phase unit templates as:

$$u_{qa} = \frac{u_{pc}}{\sqrt{3}} - \frac{u_{pb}}{\sqrt{3}}, u_{qb} = \frac{\sqrt{3}u_{pa}}{2} + \frac{u_{pb}-u_{pc}}{2\sqrt{3}}, u_{qc} = \frac{u_{pb}-u_{pc}}{2\sqrt{3}} - \frac{\sqrt{3}u_{pa}}{2} \quad (6.4)$$

(b) *Estimation of active and reactive loss components:*

The voltage at dc link capacitor (V_{dc}) is measured and sensed to compare it with the reference dc link voltage (V_{dc}^*) to derive the active loss component.

$$V_{dce}(k) = V_{dc}^*(k) - V_{dc}(k) \quad (6.5)$$

A PI controller is used to minimize the error (V_{dce}) of reference V_{dc}^* and sensed V_{dc} , output of which gives active current component (w_{pd}) and regulates the DC link voltage. The controller's output at k^{th} instant is computed as:

$$w_{pd}(k) = w_{pd}(k-1) + k_{pd}\{V_{dce}(k) - V_{dce}(k-1)\} + k_{id}V_{dce}(k) \quad (6.6)$$

The reactive loss component is calculated by taking error V_{te} between sensed and reference terminal voltage V_t and V_t^* respectively at PCC processed through a PI controller. Reactive loss component is responsible to maintain the constant AC terminal voltage.

$$V_{te}(k) = V_t^*(k) - V_t(k) \quad (6.7)$$

The controller output at k^{th} instant is given as:

$$w_{qt}(k) = w_{qt}(k-1) + k_{pt}\{V_{te}(k) - V_{te}(k-1)\} + k_{it}V_{te}(k) \quad (6.8)$$

In above equation w_{qt} is a function of the reactive loss current component, k_{pt} and k_{it} are proportional and integral gains respectively.

A feed forward weight can be estimated as a function of solar power (P_{PV}) and AC terminal voltage at PCC (V_t) to achieve fast dynamic response and calculated as:

$$w_{PV}(k) = \frac{2P_{PV}(k)}{3V_t} \quad (6.9)$$

(c) *Estimation of fundamental active and reactive load current:*

Fundamental active and reactive load current components extraction has been done by considering load currents (i_{La}, i_{Lb}, i_{Lc}) as inputs to the input layer and considering w_i as initial weight. The three layer GDBP based NN architectures for calculating weighted fundamental active and reactive current components are shown in Fig. 6.4. Weighted values of fundamental active current components for all phases are given by equation (6.10):

$$\left. \begin{aligned} i_{Lap} &= i_{La}\cos\phi_{1a}u_{pa} + i_{Lb}\cos\phi_{1b}u_{pb} + i_{Lc}\cos\phi_{1c}u_{pc} + w_i \\ i_{Lbp} &= i_{La}\cos\phi_{1a}u_{pa} + i_{Lb}\cos\phi_{1b}u_{pb} + i_{Lc}\cos\phi_{1c}u_{pc} + w_i \\ i_{Lcp} &= i_{La}\cos\phi_{1a}u_{pa} + i_{Lb}\cos\phi_{1b}u_{pb} + i_{Lc}\cos\phi_{1c}u_{pc} + w_i \end{aligned} \right\} \quad (6.10)$$

The above extracted components are processed through a sigmoid activation function. Output can be obtained as O_{pa}, O_{pb}, O_{pc} and calculated as:

$$\left. \begin{aligned} O_{pa} &= f_1(i_{Lpa}) = \frac{1}{1+e^{-i_{Lpa}}} \\ O_{pb} &= f_1(i_{Lpb}) = \frac{1}{1+e^{-i_{Lpb}}} \\ O_{pc} &= f_1(i_{Lpc}) = \frac{1}{1+e^{-i_{Lpc}}} \end{aligned} \right\} \quad (6.11)$$

The above output values are being input to hidden layer of the neural network considered here with initial weight of w_{i1} . Further the output of this layer can be written as fundamental component i_{Lap1} , i_{Lbp1} and i_{Lcp1} with w_{ap} , w_{bp} and w_{cp} as updated weighted of respective phase currents active components.

$$\left. \begin{aligned} i_{Lap1} &= w_{ap}O_{pa} + w_{bp}O_{pb} + w_{cp}O_{pc} + w_{i1} \\ i_{Lbp1} &= w_{ap}O_{pa} + w_{bp}O_{pb} + w_{cp}O_{pc} + w_{i1} \\ i_{Lcp1} &= w_{ap}O_{pa} + w_{bp}O_{pb} + w_{cp}O_{pc} + w_{i1} \end{aligned} \right\} \quad (6.12)$$

The updated weights for hidden layer computed as:

$$\left. \begin{aligned} w_{ap} &= w_p + \alpha\{w_p - w_{ap1}\}f'(i_{Lap1})O_{pa} \\ w_{bp} &= w_p + \alpha\{w_p - w_{bp1}\}f'(i_{Lbp1})O_{pb} \\ w_{cp} &= w_p + \alpha\{w_p - w_{cp1}\}f'(i_{Lcp1})O_{pc} \end{aligned} \right\} \quad (6.13)$$

In equation (6.13) expression w_p shows the average weighted value of active current component $f'(i_{Lap1})$ and first derivative of i_{Lap1} . α is the learning rate and used to speed up the convergence process.

$$\left. \begin{aligned} w_{ap1} &= f_1(i_{Lpa1}) = \frac{1}{1+e^{-i_{Lpa1}}} \\ w_{bp1} &= f_1(i_{Lpb1}) = \frac{1}{1+e^{-i_{Lpb1}}} \\ w_{cp1} &= f_1(i_{Lpc1}) = \frac{1}{1+e^{-i_{Lpc1}}} \end{aligned} \right\} \quad (6.14)$$

w_{ap1} , w_{bp1} and w_{cp1} as fundamental weighted values of respective phase currents active components. The mean active component of load currents (w_{Lp}) is obtained by averaging the weighted components and given as

$$w_{Lp} = \frac{(w_{ap1}+w_{bp1}+w_{cp1})}{3} \quad (6.15)$$

Further, the estimation of fundamental reactive current components for load currents have been calculated in similar way using the developed control. The sensed load currents (i_{La} , i_{Lb} , i_{Lc}).

$$\left. \begin{aligned} i_{Laq} &= i_{La}\sin\phi_{la}u_{qa} + i_{Lb}\sin\phi_{la}u_{qb} + i_{Lc}\sin\phi_{la}u_{qc} + w_i \\ i_{Lbq} &= i_{La}\sin\phi_{la}u_{qa} + i_{Lb}\sin\phi_{la}u_{qb} + i_{Lc}\sin\phi_{la}u_{qc} + w_i \\ i_{Lcq} &= i_{La}\sin\phi_{la}u_{qa} + i_{Lb}\sin\phi_{la}u_{qb} + i_{Lc}\sin\phi_{la}u_{qc} + w_i \end{aligned} \right\} \quad (6.16)$$

Similar to the active components, above extracted components are processed through a sigmoid activation function. Output can be obtained as O_{qa} , O_{qb} , O_{qc} and calculated as:

$$\left. \begin{aligned} O_{qa} &= f_1(i_{Lqa}) = \frac{1}{1+e^{-i_{Lqa}}} \\ O_{qb} &= f_1(i_{Lqb}) = \frac{1}{1+e^{-i_{Lqb}}} \\ O_{qc} &= f_1(i_{Lqc}) = \frac{1}{1+e^{-i_{Lqc}}} \end{aligned} \right\} \quad (6.17)$$

Again output values are being input to hidden layer of the neural network with initial weight of w_{i1} . Further the output of this layer can be written as fundamental component i_{Laq1} , i_{Lbq1} and i_{Lcq1} with w_{aq} , w_{bq} and w_{cq} as updated weighted of respective phase currents reactive components.

$$\left. \begin{aligned} i_{Laq1} &= w_{aq}O_{qa} + w_{bq}O_{qb} + w_{cq}O_{qc} + w_{i1} \\ i_{Lbq1} &= w_{aq}O_{qa} + w_{bq}O_{qb} + w_{cq}O_{qc} + w_{i1} \\ i_{Lcq1} &= w_{aq}O_{qa} + w_{bq}O_{qb} + w_{cq}O_{qc} + w_{i1} \end{aligned} \right\} \quad (6.18)$$

The updated weights for hidden layer computed as:

$$\left. \begin{aligned} w_{aq} &= w_q + \alpha\{w_q - w_{aq1}\}f'(i_{Laq1})O_{qa} \\ w_{bq} &= w_q + \alpha\{w_q - w_{bq1}\}f'(i_{Lbq1})O_{qb} \\ w_{cq} &= w_q + \alpha\{w_q - w_{cq1}\}f'(i_{Lcq1})O_{qc} \end{aligned} \right\} \quad (6.19)$$

In above expression w_p shows the average weighted value of reactive current component $f'(i_{Laq1})$ and first derivative of i_{Laq1} .

$$\left. \begin{aligned} w_{aq1} &= f_1(i_{Lqa1}) = \frac{1}{1+e^{-i_{Lqa1}}} \\ w_{bq1} &= f_1(i_{Lqb1}) = \frac{1}{1+e^{-i_{Lqb1}}} \\ w_{cq1} &= f_1(i_{Lqc1}) = \frac{1}{1+e^{-i_{Lqc1}}} \end{aligned} \right\} \quad (6.20)$$

w_{aq1} , w_{bq1} and w_{cq1} as fundamental weighted values of respective phase currents reactive components. The mean reactive component of load currents (w_{Lq}) is obtained by averaging the weighted components and given as:

$$w_{Lq} = \frac{(w_{aq1} + w_{bq1} + w_{cq1})}{3} \quad (6.21)$$

(d) Reference grid currents and IGBTs switching signals generation:

The total fundamental active current component of load current can be defined as:

$$I_{Lp} = w_{pd} + w_{Lp} - w_{PV} \quad (6.22)$$

The active reference components of grid currents can be obtained as:

$$i_{psa} = I_{Lp} * u_{pa}, i_{psb} = I_{Lp} * u_{pb}, i_{psc} = I_{Lp} * u_{pc} \quad (6.23)$$

Fundamental reactive current component of load current can be defined in similar manner:

$$I_{Lq} = w_{qt} + w_{Lq} \quad (6.24)$$

The reactive reference component of grid currents can be obtained as:

$$i_{qsa} = I_{Lq} * u_{qa}, i_{qsb} = I_{Lq} * u_{qb}, i_{qsc} = I_{Lq} * u_{qc} \quad (6.25)$$

Net fundamental reference grid currents (i_{sa}^* , i_{sb}^* , i_{sc}^*) can be obtained as:

$$i_{sa}^* = i_{psa} + i_{qsa}, \quad i_{sb}^* = i_{psb} + i_{qsb}, \quad i_{sc}^* = i_{psc} + i_{qsc} \quad (6.26)$$

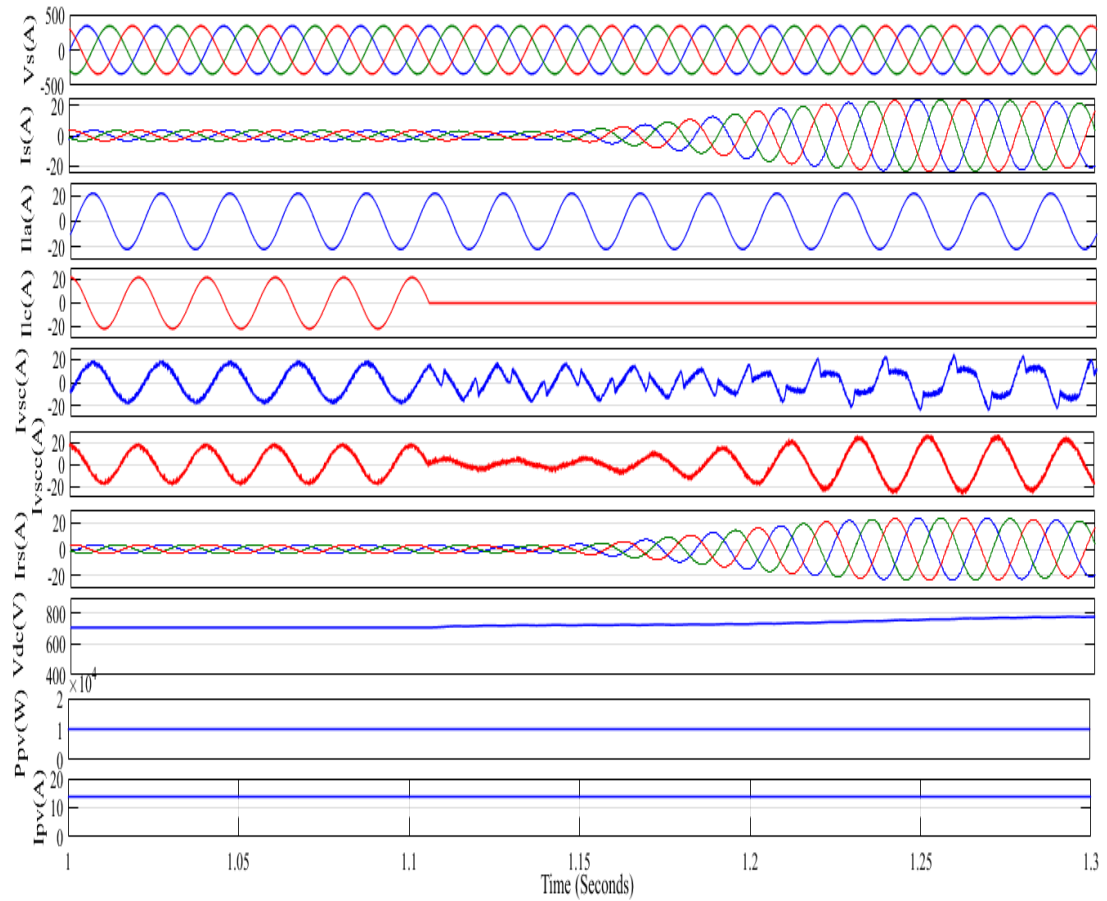
VSC switching signals has been produced by comparing reference (i_{sa}^* , i_{sb}^* , i_{sc}^*) and actual (i_{sa} , i_{sb} , i_{sc}) grid currents for individual phase and error is passed through a PI current regulator for minimization.

6.4.2 Results and discussions

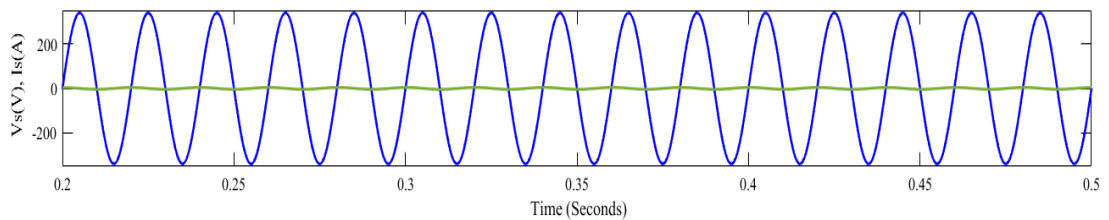
The proposed system is developed considering MPP rating of 10 kW for PV array. Validation of the proposed control technique for PV/FC fed VSC is done by simulating the developed system using MATLAB/Simulink simulation platform. Performance of the system is validated under different scenarios such as linear loads with power factor correction (PFC) mode, dynamic linear loads, nonlinear loads with PFC mode, dynamic nonlinear loads, variable solar irradiance etc.

(i) System performance under linear load for PFC

The performance of the proposed neural network based $I \cos\phi$ algorithm is evaluated for a linear load. The performance of the proposed controller is investigated on the basis of different performance indices such as grid voltage (v_s), grid current (i_s), load current (i_L), VSC current (i_{vsc}), grid real power (P_g), grid reactive power (Q_g), PCC terminal voltage (V_t), PV array power (P_{pv}), PV array current (I_{pv}) and dc-link voltage (V_{dc}) which are shown in Fig. 6.5 (a-b) under steady state linear load (at $t=0.2$ to 0.3 s) conditions. Power factor is observed to be considerably enhanced, and can be identify from the voltage and current waveforms as shown in Fig. 6.5 (b). The PV system maintains to feed maximum power to the load and grid at unity power factor (UPF) operation.



(a)



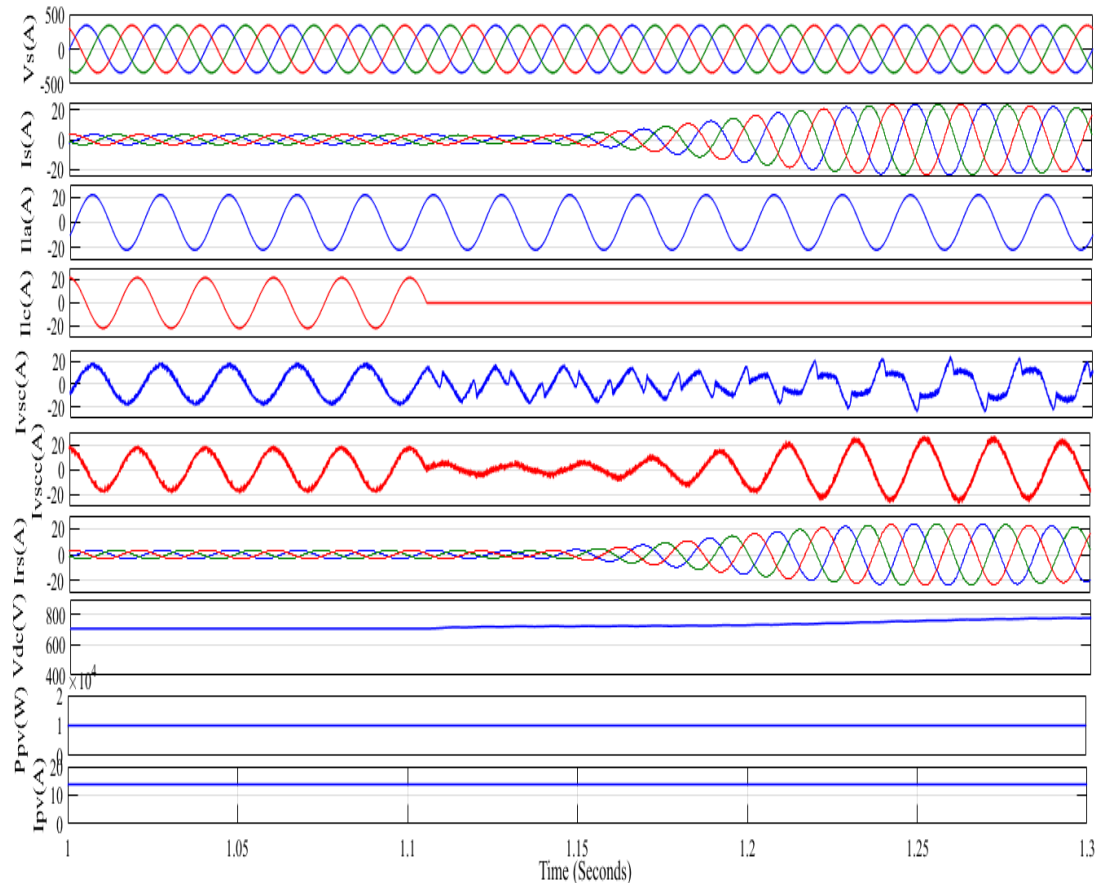
(b)

Fig. 6.5 (a) Performance parameters (b) Waveforms of phase ‘a’ of source voltage and source current

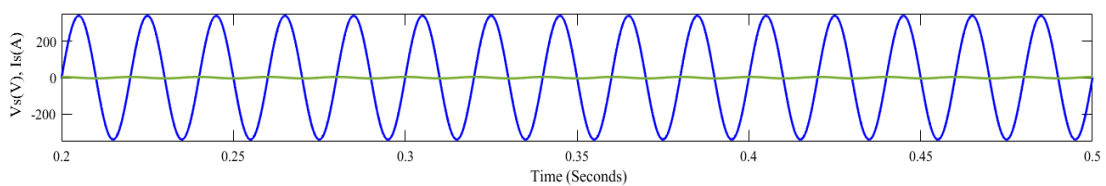
(ii) System performance analysis under dynamic linear load for zero voltage regulation (ZVR)

If load draws reactive power with unbalanced nature then this may lead changes in the terminal voltage (V_t) at PCC. Figs. 6.6 (a) shows the performance of proposed control for unbalanced linear load in zero voltage regulation (ZVR) case. Phase ‘c’ of

the given load is disconnected at 1.1 s, then also grid currents (i_s) are maintained sinusoidal with the help of VSC controller. The proposed controller takes appropriate action to incorporate the changes in the system. The PCC voltage (V_t) and DC link voltages are observed as 415 V and 700 V, respectively without significant fluctuations.



(a)



(b)

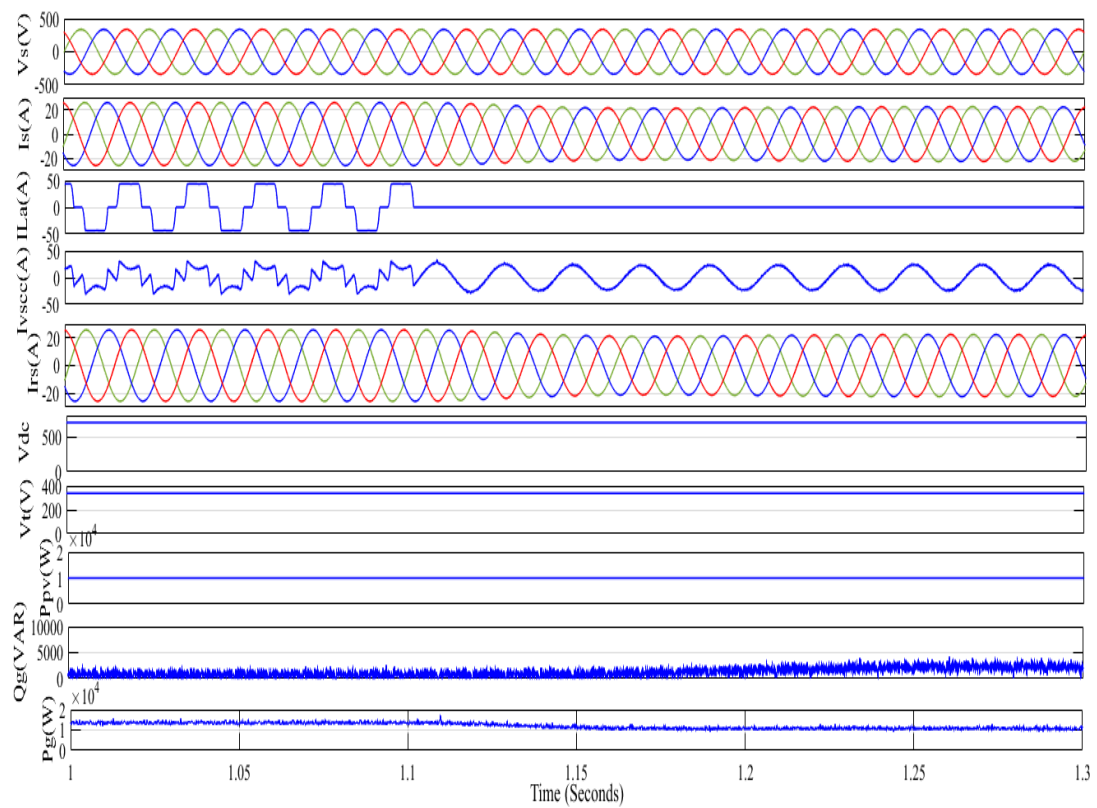
Fig. 6.6 (a) Performance parameters (b) Waveforms of phase ‘a’ of source voltage and source current

Again in this case also the improvement of power factor can be observed by analyzing the behavior of grid voltage and grid current from Fig. 6.6 (b). The reactive

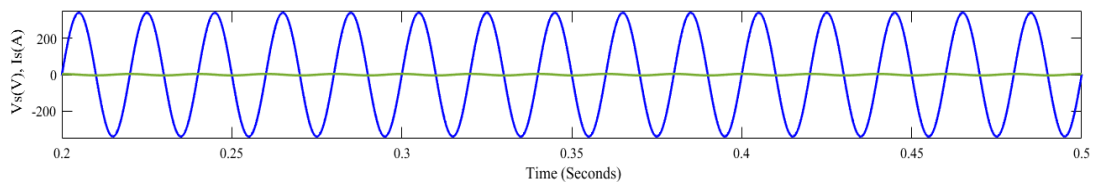
power (Q_g) feeding by grid is equal to zero, hence the compensation is also done for linear loads which are consuming reactive power.

(iii) System performance analysis under non-linear load

Dynamic behavior of proposed controller under unbalanced nonlinear load conditions is shown in Fig. 6.7 (a) show for zero voltage regulation (ZVR) mode of operation with different performance indices.



(a)



(b)

Fig. 6.7 (a) Performance indices (b) Waveforms of phase ‘a’ of source voltage and source current

Phase ‘c’ of load is disconnected at 1.1 s, grid currents (i_s) are maintained sinusoidal with the help of VSC controller at required values. The PCC voltage (V_t) and DC link voltages are also maintained constant at 415 V and 700 V, respectively. Power factor improvement can be observed from Fig. 6.7 (b).

Fig. 6.8 (a)-(b) shows the THDs at PCC for phase ‘a’ of load current, grid current respectively and obtained as 40.77%, 1.24% respectively, which is well within the limits of IEEE 519-2014 standard. Thus, the proposed algorithm effectively carries out the load balancing and harmonic compensation.

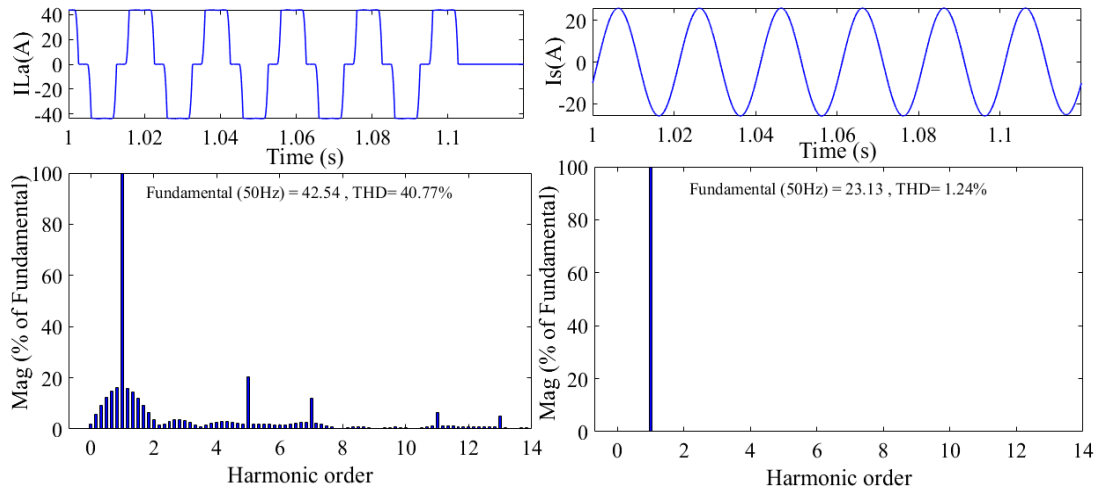


Fig. 6.8 THD for (a) load current of phase ‘a’ (b) grid current

(iv) Performance under variable solar irradiance

The solar irradiance (S) is increased to 1000 W/m² from 600 W/m² at 0.5 s as can be seen in Fig. 6.9. PV power generation system is meeting the power demand of the load and excess generation is being fed to the grid. Hence, the grid power (P_g) in Fig. 6.9 reducing after 0.5s when PV power (P_{pv}) is increasing. The system in case of variable solar irradiance keeps continue to extract maximum power from a PV system and operates at unity power factor (UPF). The source current is maintained to be sinusoidal with DC link voltage at its set reference point.

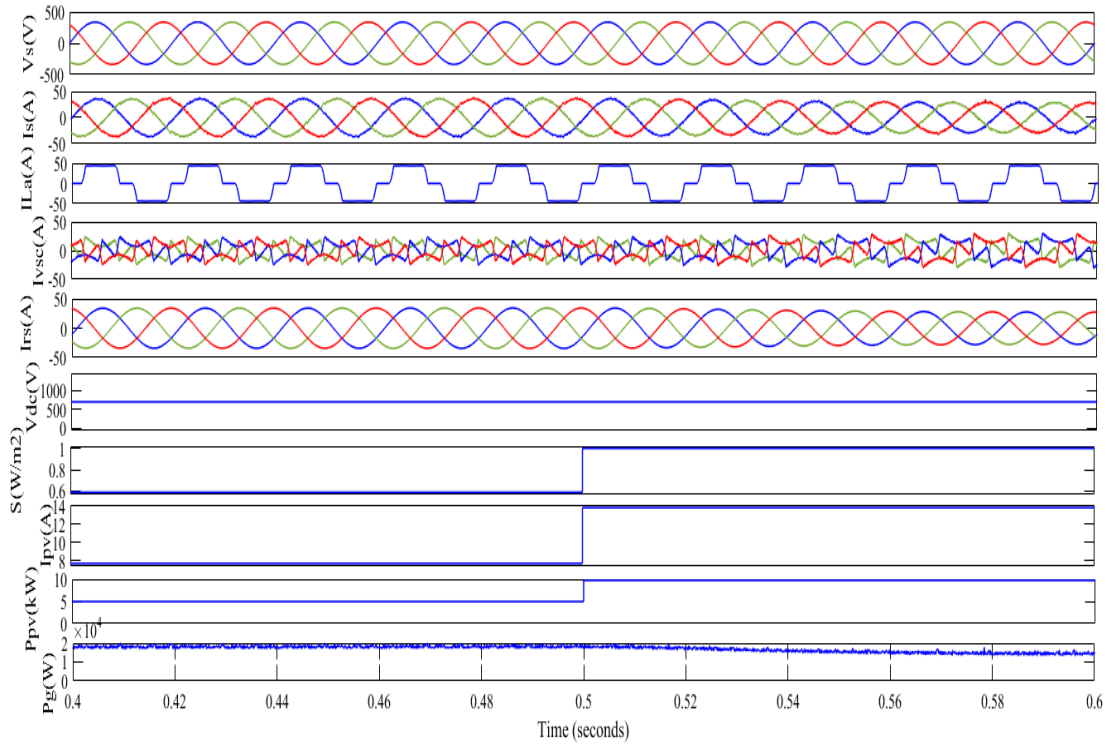


Fig. 6.9 Performance parameters under non-linear load conditions for variable solar irradiance

(v) Comparative analysis of proposed algorithm with conventional approaches

The proposed control approach based on GDBP NN $I \cos\phi$ algorithm has been analyzed and found satisfactory for each of the case discussed in the above result section. In present sub-section the THD analysis of the proposed algorithm is being compared with the conventional $I \cos\phi$ based algorithm in Table 6.1 to show the superiority of the proposed algorithm.

Table 6.1 Performance parameters of the proposed system

Operating mode	Parameters	$I \cos\phi$ based control algorithm	GDBP NN $I \cos\phi$ based control algorithm
ZVR	Grid current (A), %THD at PCC	23.27 A, 4.16 %	23.13 A, 1.24 %
	Load current (A), %THD at PCC	40.58 A, 41.62 %	42.54 A, 40.77%
	V_{dc} (V)	718 V	694V

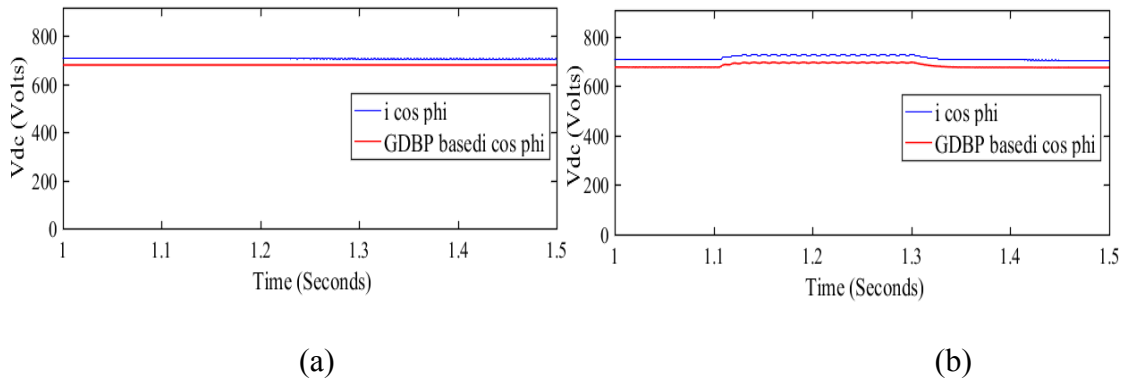


Fig. 6.10 Comparison of V_{dc} for nonlinear load (a) balanced conditions (b) unbalanced conditions

The performance of proposed GDBP-based $I \cos\phi$ control approach regarding V_{dc} is compared with $I \cos\phi$ and shown in Fig. 6.10 (a) and (b) respectively for balanced and unbalanced loading conditions. The developed GDBP NN $I \cos\phi$ based control algorithm is observed as better than other conventional, intelligent and adaptive approaches and comparison is shown in Table 6.2 for dynamic nonlinear load.

Table 6.2 Comparative analysis of proposed GNN controller with existing ANN based controllers

Algorithm	Settling Time (sec)	DC link voltage overshoot (V)	DC link voltage undershoot (V)	THD % (Grid current)
SRF	0.096	820	763	5.63
$I \cos\phi$	0.095	850	786	4.16
Conductance fryze	0.11	957	796	5.79
ANN based	0.095	815	774	3.25
ANFIS based	0.094	820	779	2.78
FLC based	0.095	815	780	2.25
Adaptive	0.095	810	770	2.18
GDBP NN $I \cos\phi$	0.093	790	775	1.24

Conventional control algorithms such as SRF, $I \cos\phi$, and conductance fryze algorithms, intelligent algorithms as ANN based algorithm, ANFIS based approaches, fuzzy logic controller (FLC) based and adaptive algorithm are compared by large

undershoot in DC link voltage, overshoot in DC link voltage, settling time and THD in grid currents, under dynamic load conditions. The proposed algorithm performs smoother and response of given algorithm found better than other approaches.

6.5 QNBP NN - $I \cos\phi$ CONTROL OF GRID INTEGRATED PV SYSTEM

6.5.1 Control algorithm

The detail control modeling of hybrid approach for SPV fed VSC which combines QNBP based NN and $I \cos\phi$ technique is presented in this section. The proposed control approach is applied in two stages. $I \cos\phi$ algorithm is used to obtain active and reactive components of given load current. Further, weights training and modifications of neural network is done using QNBP method. The developed algorithm is used to calculate weighted value of fundamental active load current component (w_{ap} , w_{bp} and w_{cp}) and fundamental reactive load current component (w_{aq} , w_{bq} and w_{cq}). Further, these components used to generate active and reactive component of reference source current in order to produce switching signals for VSC. The details of the proposed system considered in this work is presented in Fig. 6.11.

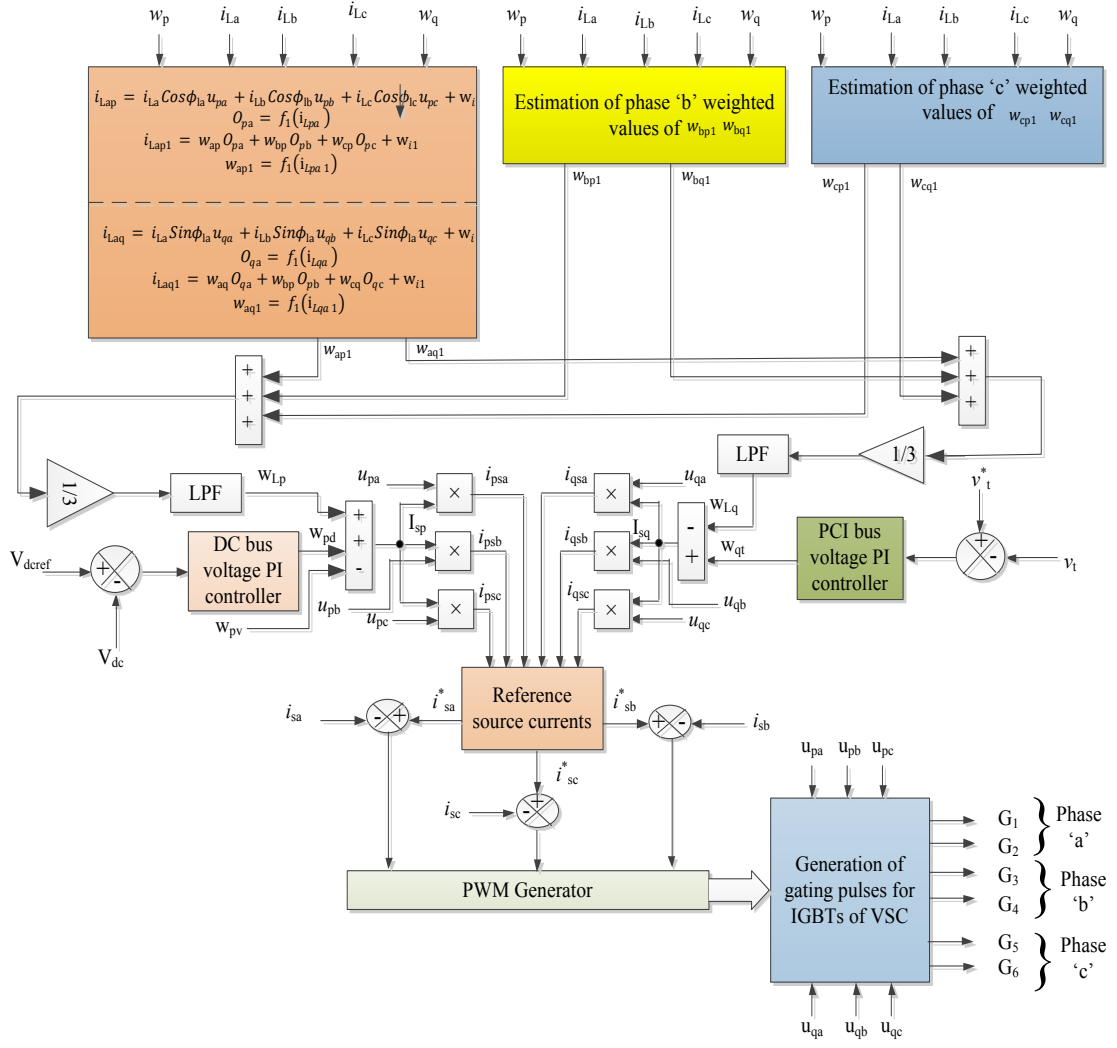


Fig. 6.11 Proposed VSC control algorithm

(a) Active and reactive loss components:

The voltage at dc link (V_{dc}) is measured and compared with the reference dc link voltage (V_{dc}^*) to get the active loss component. Further the difference between V_{dc} and V_{dc}^* is processed through a PI controller to minimize the error (E_{dc}) and regulate the dc link voltage output of PI controller gives active current component (w_{pdc}).

$$E_{dc}(k) = V_{dc}^*(k) - V_{dc}(k) \quad (6.27)$$

The controller's output at k^{th} instant is computed as:

$$w_{pdc}(k) = w_{pdc}(k-1) + k_{pd}\{E_{dc}(k) - E_{dc}(k-1)\} + k_{id}E_{dc}(k) \quad (6.28)$$

Next, the error E_{te} between sensed terminal voltage V_t and reference terminal voltage V_t^* at point of common coupling (PCC) is passed through a PI controller to get the reactive loss component which is useful to maintain the PCC terminal voltage constant.

$$E_{te}(k) = V_t^*(k) - V_t(k) \quad (6.29)$$

The controller output at k^{th} instant is given as:

$$w_{qt}(k) = w_{qt}(k-1) + k_{pt}\{V_{te}(k) - V_{te}(k-1)\} + k_{it}V_{te}(k) \quad (6.30)$$

To achieve fast dynamic response from the controller a function consisting solar power (P_{PV}) and terminal voltage at PCC (V_t) is also incorporated.

$$w_{PV}(k) = \frac{2P_{PV}(k)}{3V_t} \quad (6.31)$$

(b) Fundamental active and reactive load current estimation:

Load currents (i_{La} , i_{Lb} , i_{Lc}) are sensed and provided as inputs to the input layer of NN with w_i as initial weight to calculate fundamental active and reactive load current components. Weighted values for all phases can be calculated using basic $I \cos\phi$ algorithm as:

$$\left. \begin{aligned} i_{Lap} &= i_{La} \cos\phi_{1a} u_{pa} + i_{Lb} \cos\phi_{1b} u_{pb} + i_{Lc} \cos\phi_{1c} u_{pc} + w_i \\ i_{Lbp} &= i_{La} \cos\phi_{1a} u_{pa} + i_{Lb} \cos\phi_{1b} u_{pb} + i_{Lc} \cos\phi_{1c} u_{pc} + w_i \\ i_{Lcp} &= i_{La} \cos\phi_{1a} u_{pa} + i_{Lb} \cos\phi_{1b} u_{pb} + i_{Lc} \cos\phi_{1c} u_{pc} + w_i \end{aligned} \right\} \quad (6.32)$$

In the above equation u_{pa} , u_{pb} , u_{pc} are in-phase unit templates of phase voltages v_a , v_b and v_c . Line voltages (v_{ab} , v_{bc} , v_{ca}) at PCC are sensed to calculate phase voltages (v_a , v_b and v_c).

$$v_a = \frac{2v_{ab} + v_{bc}}{3}, v_b = \frac{-v_{ab} + v_{bc}}{3}, v_c = \frac{-v_{ab} - 2v_{bc}}{3} \quad (6.33)$$

The PCC terminal voltage amplitude (V_t) given as:

$$V_t = \sqrt{\left[\frac{2(v_a^2 + v_b^2 + v_c^2)}{3} \right]} \quad (6.34)$$

The in-phase unit templates are given as:

$$u_{pa} = \frac{v_a}{V_t}, u_{pb} = \frac{v_b}{V_t}, u_{pc} = \frac{v_c}{V_t} \quad (6.35)$$

Further in-phase templates are used to quadrature unit templates.

$$u_{qa} = \frac{u_{pc}}{\sqrt{3}} - \frac{u_{pb}}{\sqrt{3}}, u_{qb} = \frac{\sqrt{3}u_{pa}}{2} + \frac{u_{pb} - u_{pc}}{2\sqrt{3}}, u_{qc} = \frac{u_{pb} - u_{pc}}{2\sqrt{3}} - \frac{\sqrt{3}u_{pa}}{2} \quad (6.36)$$

The 3 layer QNBP NN architecture for estimating weighted fundamental active current components are given in Fig. 6.12.

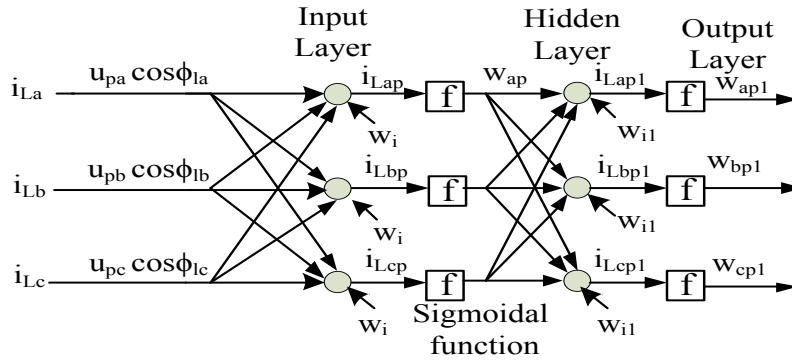


Fig. 6.12 QNBP NN structure for calculating weighted fundamental active current components

The extracted components from equation (6.36) are processed with a sigmoid activation function and gives O_{pa}, O_{pb}, O_{pc} :

$$\left. \begin{aligned} O_{pa} &= f_1(i_{Lpa}) = \frac{1}{1+e^{-i_{Lpa}}} \\ O_{pb} &= f_1(i_{Lpb}) = \frac{1}{1+e^{-i_{Lpb}}} \\ O_{pc} &= f_1(i_{Lpc}) = \frac{1}{1+e^{-i_{Lpc}}} \end{aligned} \right\} \quad (6.37)$$

The output values O_{pa}, O_{pb}, O_{pc} acts as input to hidden layer of the proposed NN with initial weight of w_{i1} . The output of hidden layer can be gives i_{Lap1}, i_{Lbp1} and i_{Lcp1} with w_{ap}, w_{bp} and w_{cp} as updated weighted values of respective active components.

$$\left. \begin{aligned} i_{Lap1} &= w_{ap}O_{pa} + w_{bp}O_{pb} + w_{cp}O_{pc} + w_{i1} \\ i_{Lbp1} &= w_{ap}O_{pa} + w_{bp}O_{pb} + w_{cp}O_{pc} + w_{i1} \\ i_{Lcp1} &= w_{ap}O_{pa} + w_{bp}O_{pb} + w_{cp}O_{pc} + w_{i1} \end{aligned} \right\} \quad (6.38)$$

The updated weights values at hidden layer by QNBP given as:

$$\begin{bmatrix} w_{ap} \\ w_{bp} \\ w_{cp} \end{bmatrix} = w_p + \frac{1}{\beta} [(w_p - w_{ap1})^{-1} (w_p - w_{bp1})^{-1} (w_p - w_{cp1})^{-1}] \begin{bmatrix} O_{pa}^{-1} \\ O_{pb}^{-1} \\ O_{pc}^{-1} \end{bmatrix} \begin{bmatrix} f'(i_{Lap1}) \\ f'(i_{Lbp1}) \\ f'(i_{Lcp1}) \end{bmatrix} \quad (6.39)$$

In above equation, w_p shows the average weighted value of active current component, $f'(i_{Lap1})$ denotes first derivative of i_{Lap1} and β is the learning rate which speed up the convergence process.

$$\left. \begin{aligned} w_{ap1} &= f_1(i_{Lpa1}) = \frac{1}{1+e^{-i_{Lpa1}}} \\ w_{bp1} &= f_1(i_{Lpb1}) = \frac{1}{1+e^{-i_{Lpb1}}} \\ w_{cp1} &= f_1(i_{Lpc1}) = \frac{1}{1+e^{-i_{Lpc1}}} \end{aligned} \right\} \quad (6.40)$$

w_{ap1}, w_{bp1} and w_{cp1} are the fundamental weighted values of respective phase currents active components and the mean active component (w_{Lp}) can be calculated as:

$$w_{Lp} = \frac{(w_{ap1} + w_{bp1} + w_{cp1})}{3} \quad (6.41)$$

Next, the calculation of fundamental reactive current components for load currents can be calculated similarly as active current components. Quadrature unit templates u_{qa}, u_{qb} and u_{qc} can be taken from equation (6.36).

$$\left. \begin{aligned} i_{Laq} &= i_{La} \sin\phi_{1a} u_{qa} + i_{Lb} \sin\phi_{1a} u_{qb} + i_{Lc} \sin\phi_{1a} u_{qc} + w_i \\ i_{Lbq} &= i_{La} \sin\phi_{1a} u_{qa} + i_{Lb} \sin\phi_{1a} u_{qb} + i_{Lc} \sin\phi_{1a} u_{qc} + w_i \\ i_{Lcq} &= i_{La} \sin\phi_{1a} u_{qa} + i_{Lb} \sin\phi_{1a} u_{qb} + i_{Lc} \sin\phi_{1a} u_{qc} + w_i \end{aligned} \right\} \quad (6.42)$$

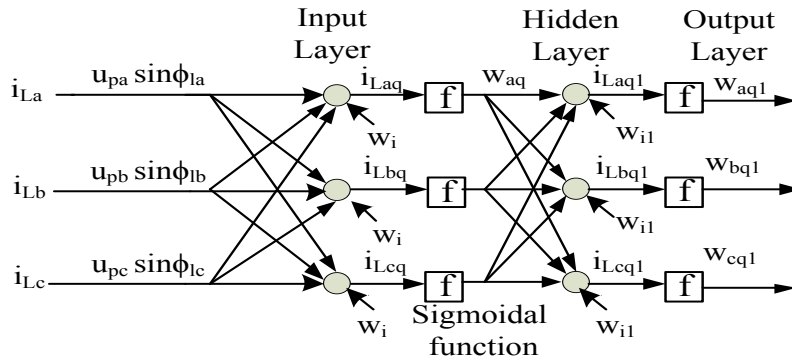


Fig. 6.13 QNBP NN structure for calculating weighted fundamental reactive current components

Further, extracted components are processed through a sigmoid activation function to obtain O_{qa}, O_{qb}, O_{qc} .

$$\left. \begin{aligned} O_{qa} &= f_1(i_{Lqa}) = \frac{1}{1+e^{-i_{Lqa}}} \\ O_{qb} &= f_1(i_{Lqb}) = \frac{1}{1+e^{-i_{Lqb}}} \\ O_{qc} &= f_1(i_{Lqc}) = \frac{1}{1+e^{-i_{Lqc}}} \end{aligned} \right\} \quad (6.43)$$

Similar to the processing of active current components these output values of sigmoid activation function are also being given to hidden layer of developed NN as input with initial weight w_{i1} . Hidden layer output given in equation (6.44) calculate fundamental component i_{Laq1}, i_{Lbq1} and i_{Lcq1} with updated weights w_{aq}, w_{bq} and w_{cq} .

$$\left. \begin{aligned} i_{Laq1} &= w_{aq}O_{qa} + w_{bq}O_{qb} + w_{cq}O_{qc} + w_{i1} \\ i_{Lbq1} &= w_{aq}O_{qa} + w_{bq}O_{qb} + w_{cq}O_{qc} + w_{i1} \\ i_{Lcq1} &= w_{aq}O_{qa} + w_{bq}O_{qb} + w_{cq}O_{qc} + w_{i1} \end{aligned} \right\} \quad (6.44)$$

The updated weights for hidden layer computed as:

$$\begin{bmatrix} w_{aq} \\ w_{bq} \\ w_{cq} \end{bmatrix} = w_q + \frac{1}{\beta} [(w_q - w_{aq1})^{-1} (w_q - w_{bq1})^{-1} (w_q - w_{cq1})^{-1}] \begin{bmatrix} O_{qa}^{-1} \\ O_{qb}^{-1} \\ O_{qc}^{-1} \end{bmatrix} \begin{bmatrix} f'(i_{Laq1}) \\ f'(i_{Lbq1}) \\ f'(i_{Lcq1}) \end{bmatrix} \quad (6.45)$$

In equation (6.46) w_q depicts the average weighted value of reactive current component and $f'(i_{Laq1})$ is the first derivative of i_{Laq1} .

$$\left. \begin{aligned} w_{aq1} &= f_1(i_{Lqa1}) = \frac{1}{1+e^{-i_{Lqa1}}} \\ w_{bq1} &= f_1(i_{Lqb1}) = \frac{1}{1+e^{-i_{Lqb1}}} \\ w_{cq1} &= f_1(i_{Lqc1}) = \frac{1}{1+e^{-i_{Lqc1}}} \end{aligned} \right\} \quad (6.46)$$

The mean reactive component of (w_{Lq}) can be calculated by averaging the weighted components of each phase.

$$w_{Lq} = \frac{(w_{aq1} + w_{bq1} + w_{cq1})}{3} \quad (6.47)$$

(c) Reference source current and VSC switching signals generation:

As per the above discussion net fundamental active current component of load current is

$$I_{Lp} = w_{pd} + w_{Lp} - w_{Pv} \quad (6.48)$$

Further, the active grid current reference component can be calculated by multiplying in-phase voltage unit templates with net fundamental active current component, which is shown as below:

$$i_{psa} = I_{Lp} * u_{pa}, i_{psb} = I_{Lp} * u_{pb}, i_{psc} = I_{Lp} * u_{pc} \quad (6.49)$$

The fundamental reactive current component of load current can also be defined in similar way as fundamental active current component:

$$I_{Lq} = w_{qt} + w_{Lq} \quad (6.50)$$

Further, the reactive grid current reference component can be calculated by multiplying quadrature voltage unit templates with net fundamental reactive current component, which is shown as below:

$$i_{qsa} = I_{Lq} * u_{qa}, i_{qsb} = I_{Lq} * u_{qb}, i_{qsc} = I_{Lq} * u_{qc} \quad (6.51)$$

Net fundamental grid reference currents (i_{sa}^* , i_{sb}^* , i_{sc}^*) given as:

$$i_{sa}^* = i_{psa} + i_{qsa}, i_{sb}^* = i_{psb} + i_{qsb}, i_{sc}^* = i_{psc} + i_{qsc} \quad (6.52)$$

Switching signals for IGBT's is generated by comparing reference grid currents (i_{sa}^* , i_{sb}^* , i_{sc}^*) and actual grid currents for each phase and the given error is minimized by using a PI current regulator.

6.5.2 Results and discussions

The proposed control technique for grid integrated solar PV system is tested using MATLAB/Simulink simulation platform. The values of different components for simulation and hardware are given in appendices. The MPP rating of solar PV array in the present work is taken as 10 kW. The studies for the proposed system has been

carried out with different scenarios like linear loads with power factor correction (PFC) mode, dynamic linear loads, nonlinear loads with power factor correction (PFC) mode, dynamic nonlinear loads and variable solar irradiance etc.

(i) Performance under linear load

Fig. 6.14 depicts the performance of the system under dynamic linear load for ZVR mode. The waveforms of all parameters are shown in the results such as grid voltage (v_s), grid current (i_{abc}), load currents for phase ‘a’ (i_{la}) and phase ‘c’ (i_{lc}), inverter current (i_c), terminal voltage (V_t), dc-link voltage (V_{dc}), PV power (P_{pv}), PV current (I_{pv}). If reactive power is drawn by load from the grid, which will further lead changes in the PCC terminal voltage (V_t).

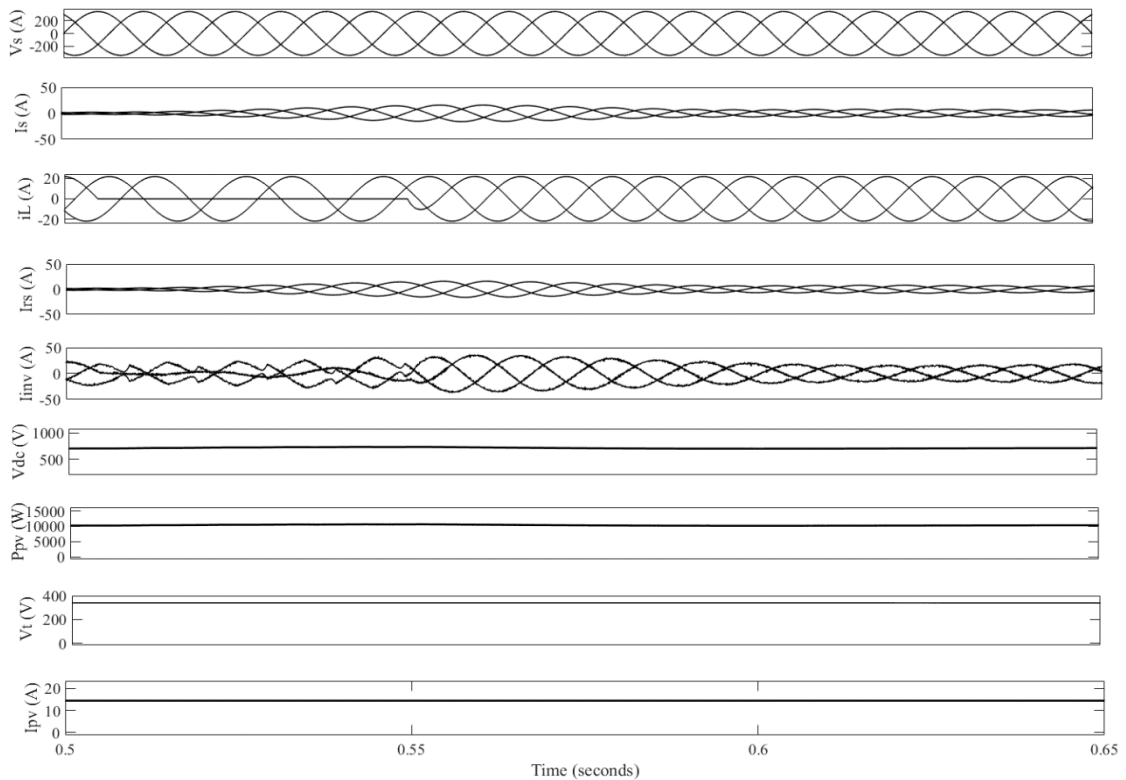


Fig. 6.14 Performance parameters for dynamic linear load in ZVR mode

At 0.51 s, phase 'c' of the given load is disconnected, in this case also the grid currents (i_{abc}) are maintained sinusoidal. The terminal voltage (V_t) and DC link voltages are also at respective reference values without significant fluctuations. The improvement of power factor can be seen by observing the behavior of grid voltage and current.

(ii) System performance analysis under non-linear load

Dynamic behavior of nonlinear load is considered in this case to investigate the performance of the proposed controller and shown in Fig. 6.15. In this case also load of phase 'c' is disconnected at 0.5 s and controller is able to maintain the grid currents (i_{abc}) sinusoidal.

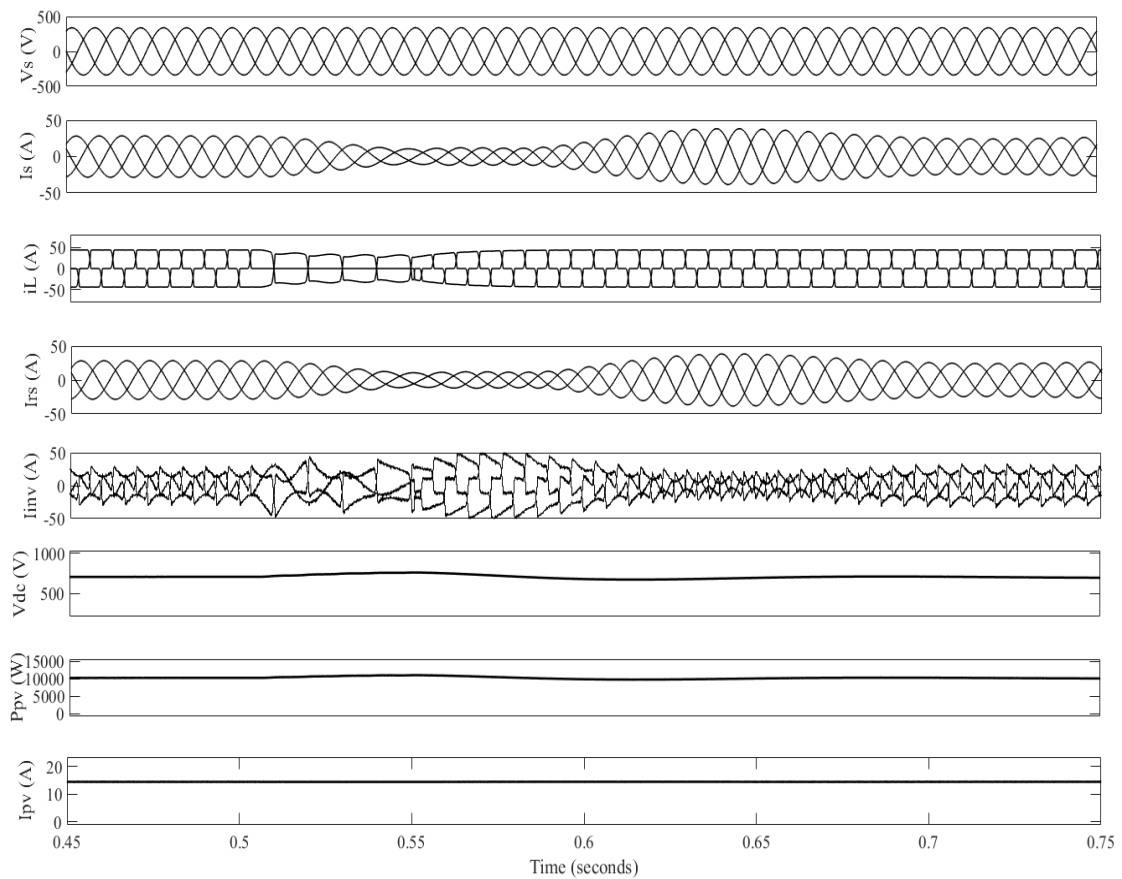


Fig. 6.15 Performance indices under dynamic nonlinear load, PFC mode

Again in this case also terminal voltage (V_t) and DC link (V_{dc}) voltages are also maintained at respective set values. The proposed controller also reduces the harmonics in grid current within the limits of IEEE 519-2014 standard. The proposed algorithm efficiently done the load balancing and harmonic compensation.

(iii) Performance under variable solar irradiance

The performance analysis for the proposed controller has been also carried out under variable solar irradiance conditions and shown in Fig 6.16. At 0.3 s the solar irradiance (S) increased to 1000 W/m² from 500 W/m². The grid power (P_g) is decreasing after 0.3s when PV power (P_{pv}) is increased by raising the solar irradiance. At varying solar irradiance also the system keeps maintaining the MPP operation and operates at unity power factor (UPF).

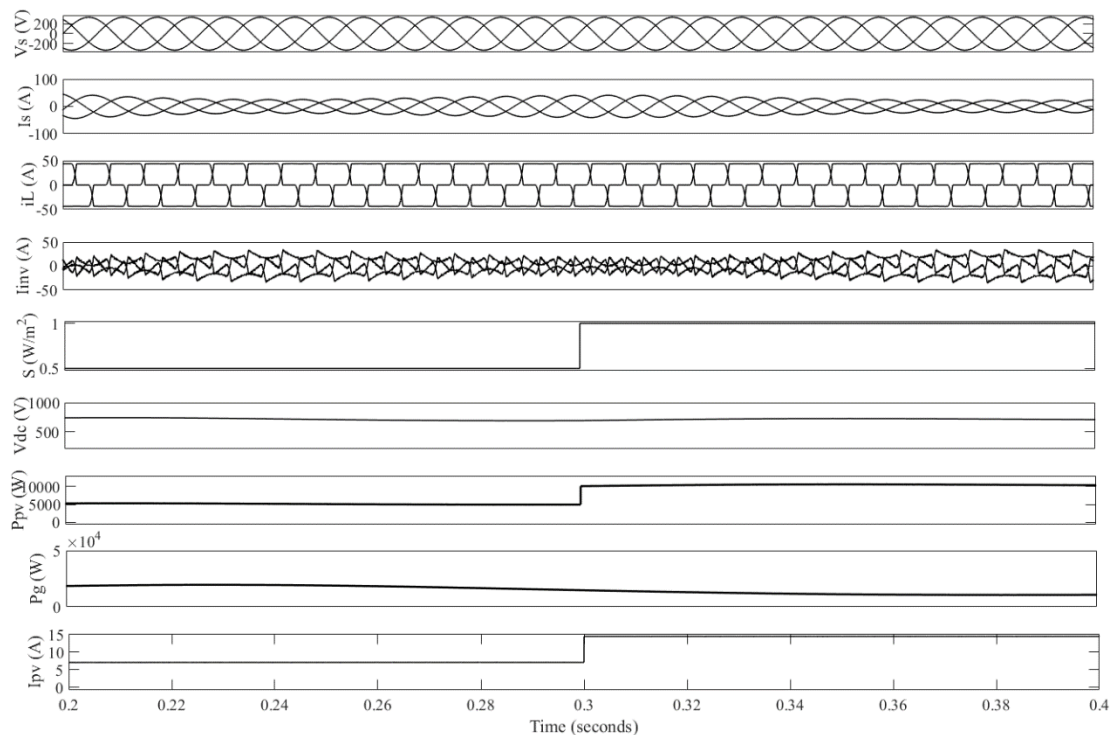


Fig. 6.16 Performance parameters under non-linear load conditions for variable solar irradiance

(iv) Comparative analysis of proposed algorithm with conventional approaches

Table 6.3 Performance parameters of the proposed system

Operating mode	Parameters	I cos ϕ based control algorithm	QNBP NN I cos ϕ based control algorithm
ZVR	Grid current (A), %THD at PCC	24.27 A, 4.16 %	24.13 A, 1.20 %
	Load current (A), %THD at PCC	41 A, 42 %	41.64 A, 41.87%
	V _{dc} (V)	717 V	698V

The proposed QNBP NN I cos ϕ based control algorithm is observed better than other conventional, intelligent and adaptive approaches under dynamic nonlinear load. The given algorithm performs smoother and response found better than other approaches.

The experimental performance of the proposed system in PFC mode under linear load is given in Fig 6.17. It shows VSC current (I_{vsc}), load current (I_{La}), grid current (I_g) and dc link voltage (V_{dc}). Fig. 6.18 (a) shows grid current and grid voltage of phase ‘a’, (b) shows the performance of controller for PFC mode.

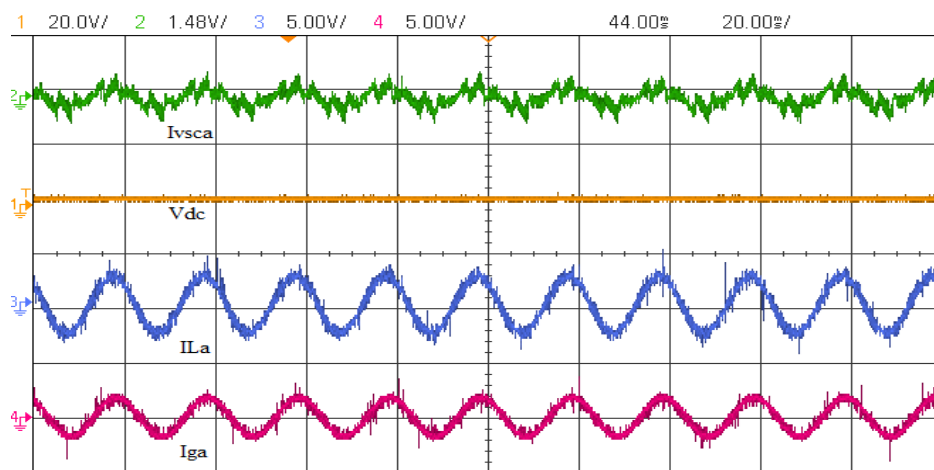
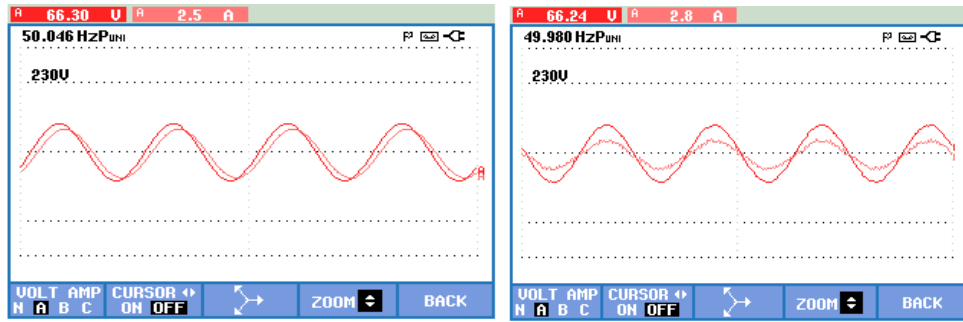


Fig. 6.17 Performance parameters under linear load



(a)

(b)

Fig. 6.18 (a) Grid voltage and current of phase ‘a’, (b) Grid voltage and current of phase ‘a’ for PFC mode

The performance of the proposed system under nonlinear load is shown in Fig. 6.18 (a) shows load current and (b) shows THD in load current which is 25.2 %. Improved THD of source current after VSC being switched on is given in Fig. 6.19 which is improved to 1.

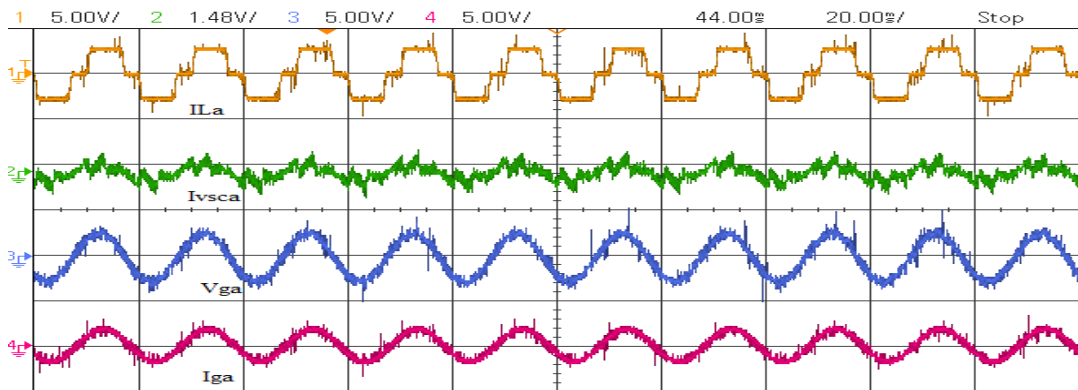
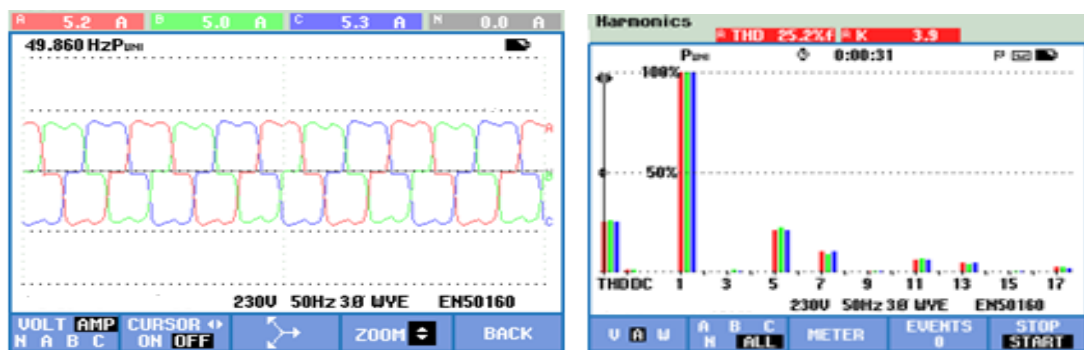


Fig. 6.19 Performance parameters under non-linear load conditions



(a)

(b)

Fig. 6.20 (a) Non-linear current, (b) THD analysis

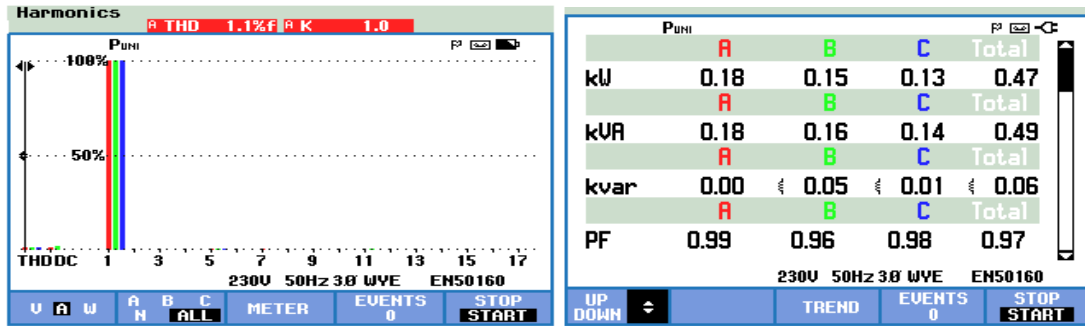


Fig. 6.21 Improved THD for grid current under non-linear load

The performance of the proposed system under nonlinear dynamic load is shown in Fig 6.22. From the results it can be observed that if the load is removed suddenly, the controller responds fast and helps in achieving steady state.

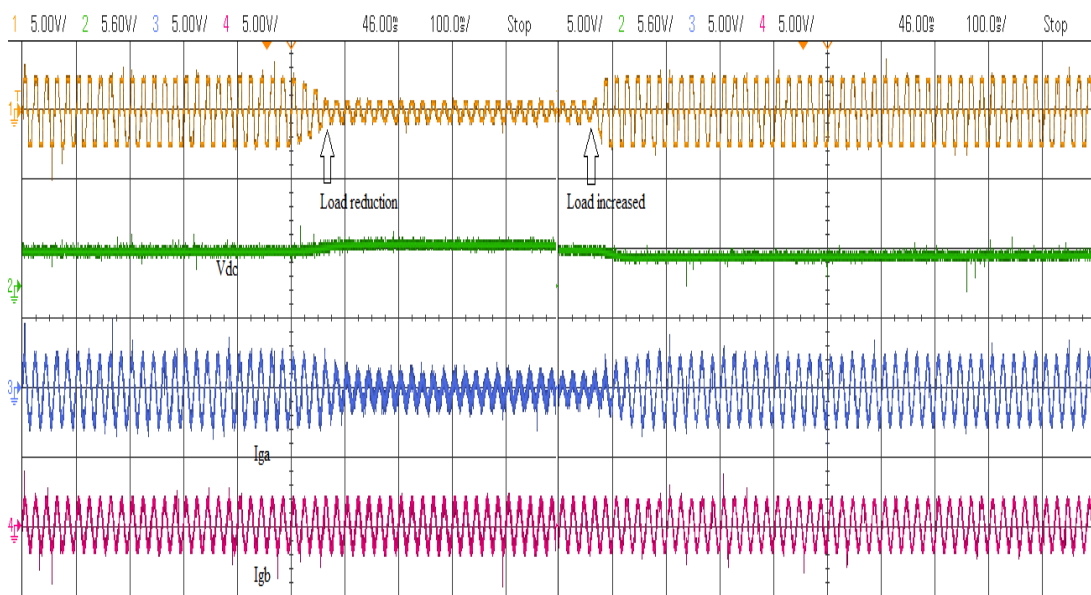


Fig. 6.22 Performance parameters under dynamic non-linear load

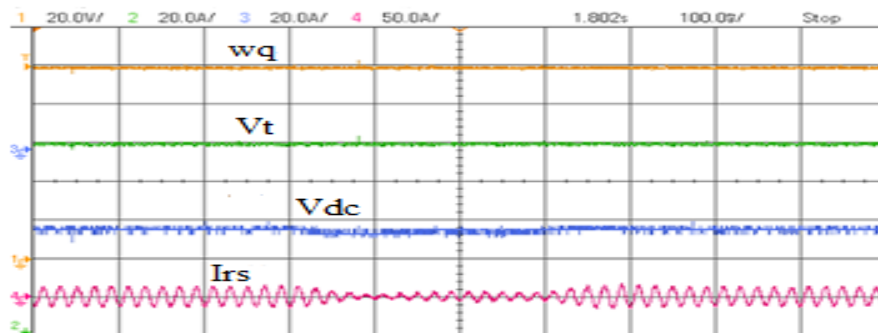


Fig. 6.23 Performance under non-linear load conditions for variable solar irradiance

6.6 GNN – EKF CONTROL

GNN based models reduces training time as well as improve the performance of the system. Considering the same a GNN based control strategy has been developed for PV DSTATCOM system in the present work. A generalized neural network acts as a multi-layer feed-forward network in which each node performs a particular function on incoming signals as well as a set of parameters pertaining to this node. To improve the performance of the system more an extended Kalman filter (EKF) based method is adopted to estimate and updating the weights of the GNN model. The main contributions of this work are: active power feeding to the connected loads and grid with mitigation of PQ issues. A GNN based approach plays role of primary control strategy and decides the switching pattern of the voltage source converter (VSC). Further, performance of the proposed algorithm has been improved with the help of EKF for GNN weight estimations. Fundamental load current components are extracted using developed GNN based control approach. Maximum power is extracted using variable step size P & O MPPT method with variations in solar irradianations. A summation type structure of GNN model is shown in Fig. 6.24 which has Σ and Π both aggregation functions and Σ_A aggregation function has been used with the sigmoidal characteristic function f_1 while the Π aggregation function has been used with the Gaussian function f_2 as a characteristic function.

6.6.1 Control algorithm

Fundamental active and reactive load current components extraction has been done by considering load currents (i_{La}, i_{Lb}, i_{Lc}) as inputs to the summation (Σ_A) and product (Π) neurons consisting unspecified weights ($W_{\Sigma i}$) and ($W_{\Pi i}$) respectively.

(a) Calculation of amplitude of terminal voltage and unit templates:

In-phase and quadrature unit templates can be calculate in similar manner as equation (6.33) – equation (6.36).

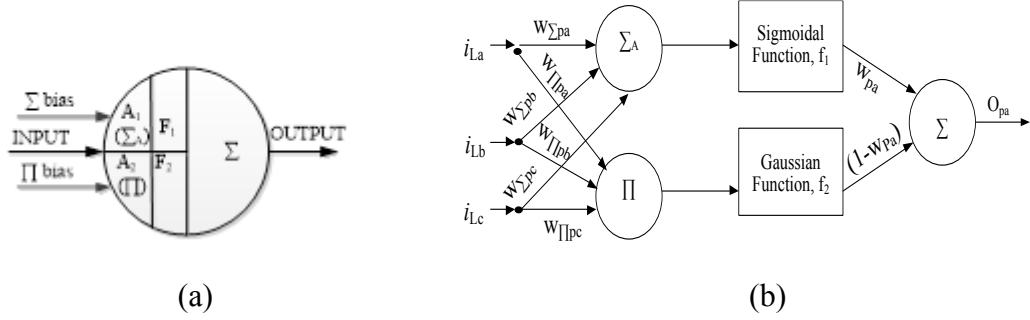


Fig. 6.24 (a) Summation type GNN model, (b) A summation type GNN structure to determine fundamental active element of load current

(b) Estimation of active and reactive loss components:

The DC link voltage (V_{dc}) is sensed and compared with the reference dc link voltage (V_{dc}^*) in order to determine the active loss component.

$$V_{dce}(k) = V_{dc}^*(k) - V_{dc}(k) \quad (6.53)$$

Further error (V_{dce}) of reference V_{dc}^* and sensed V_{dc} is processed through a PI controller, output of which active current component (w_{pd}), used to regulate the DC link. Controller output at k^{th} iteration is estimated as

$$w_{pd}(k) = w_{pd}(k-1) + k_{pd}\{V_{dce}(k) - V_{dce}(k-1)\} + k_{id}V_{dce}(k) \quad (6.54)$$

During no sunshine conditions ($P_{PV} = 0$), the set point DC link voltage is set to reference DC link voltage of DSTATCOM so that the system operates in power quality improvement mode (as a DSTATCOM).

The reactive loss component is calculated by considering error V_{te} between actual and set terminal voltage V_t and V_t^* at point of common coupling at processed it

through a PI controller. Reactive loss component maintains the constant AC terminal voltage.

$$V_{te}(k) = V_t^*(k) - V_t(k) \quad (6.55)$$

The controller output at k^{th} instant is

$$w_{qt}(k) = w_{qt}(k-1) + k_{pt}\{V_{te}(k) - V_{te}(k-1)\} + k_{it}V_{te}(k) \quad (6.56)$$

Where w_{qt} is a part of the reactive loss current component, k_{pt} and k_{it} are proportional and integral gains respectively.

A feed forward weight is estimated in order to get fast dynamic response and defined as

$$w_{PV}(k) = \frac{2P_{PV}(k)}{3V_t} \quad (6.57)$$

Where, P_{PV} is solar power.

(c) Fundamental active and reactive component of load current:

Generalized neural network (GNN) of summation type network is used in present work for estimation of fundamental active and reactive components of load current. Output calculations can be divided into two parts: forward calculations and reverse calculations. The output of summation part of generalized neural network can be obtained as:

$$O_{\Sigma} = f_1(\Sigma W_{\Sigma i} X_i + X_{o\Sigma}) \quad (6.58)$$

The output of product part of generalized neural network can be obtained as:

$$O_{\Pi} = f_2(\Pi W_{\Pi i} X_i + X_{o\Pi}) \quad (6.59)$$

The final output of generalized neuron will be the sum of summation part and product part and can be mathematically written as:

$$O_i = O_\Sigma * W_\Sigma + O_\Pi(1 - W_\Sigma) \quad (6.60)$$

Where, O_Σ is output of the summation part of the neuron, O_Π is output of the product part of the neuron and W denotes weights. The proposed control strategy using GNN utilizes GNN model is to determine the fundamental active current components of the sensed load currents (i_{La}, i_{Lb}, i_{Lc}). Sensed load currents are the input to the proposed model which further get multiplied with weights ($w_{\Sigma pa}, w_{\Sigma pb}, w_{\Sigma pc}$) and ($w_{\Pi pa}, w_{\Pi pb}, w_{\Pi pc}$) at summation (Σ_A) and product (Π) neurons respectively. At initial level these weights are referred as unknown weights and calculated by considering in-phase unit templates (u_{pa}, u_{pb}, u_{pc}) as the reference weights. A summation type GNN structure for calculation of fundamental active current component of a phase is given in Fig. 6.24 (b).

Output calculations can be divided into two parts: forward calculations and reverse calculations. The aggregation function of Σ_A and Π of the forward mode calculations for phase 'a' is shown in equation 6.61 and 6.62 respectively. Similarly, aggregation function of Σ_A and Π of the forward mode calculations of another two phases 'b' and 'c' can be calculated.

$$\Sigma_{A_{pa}} = i_{La}w_{\Sigma pa} + i_{Lb}w_{\Sigma pb} + i_{Lc}w_{\Sigma pc} + \Sigma_{bias} \quad (6.61)$$

$$\Pi_{pa} = i_{La}w_{\Pi pa} * i_{Lb}w_{\Pi pb} * i_{Lc}w_{\Pi pc} * \Pi_{bias} \quad (6.62)$$

Where Σ_{bias} and Π_{bias} denotes the initial bias of Σ_A and Π part of the structure respectively. The developed neuron has both Σ and Π aggregation functions. The Σ_A aggregation function has been used with the sigmoidal characteristic function f_1 while

the Π aggregation function has been used with the Gaussian function f_2 as a characteristic function. Output of the Σ_A part with a sigmoidal characteristic transfer function after threshold can be calculated as

$$O_{\Sigma_{Apa}} = f_1(\Sigma_{Apa}) = \frac{1}{1+e^{-\lambda_{\Sigma p} * \Sigma_{Apa}}} \quad (6.63)$$

Output of the Π part is threshold by using Gaussian transfer function and can be written as

$$O_{\Pi pa} = f_2(\Pi_{pa}) = e^{-\lambda_{\Pi p} * \Pi_{pa}^2} \quad (6.64)$$

Where $\lambda_{\Sigma p}$ and $\lambda_{\Pi p}$ are gain scaling parameters of Σ_A and Π part of network respectively and considered as unity here to avoid the complexity. Similarly, output of Σ_A and Π part of the forward mode calculations of another phases ‘b’ and ‘c’ are calculated as

$$O_{\Sigma_{Apb}} = f_1(\Sigma_{Apb}) = \frac{1}{1+e^{-\lambda_{\Sigma p} * \Sigma_{Apb}}} \quad (6.65)$$

$$O_{\Pi pb} = f_2(\Pi_{pb}) = e^{-\lambda_{\Pi p} * \Pi_{pb}^2} \quad (6.66)$$

$$O_{\Sigma_{Apc}} = f_1(\Sigma_{Apc}) = \frac{1}{1+e^{-\lambda_{\Sigma p} * \Sigma_{Apc}}} \quad (6.67)$$

$$O_{\Pi pc} = f_2(\Pi_{pc}) = e^{-\lambda_{\Pi p} * \Pi_{pc}^2} \quad (6.68)$$

The final output of the GNN will be the function of two outputs and related with the weights W and $(1-W)$ respectively through linear transfer function which can be written as

$$O_{pa} = O_{\Pi pa}(1 - W_a) + O_{\Sigma_{Apa}} W_a \quad (6.69)$$

$$O_{pb} = O_{\Pi pb}(1 - W_b) + O_{\Sigma_{Apb}} W_b \quad (6.70)$$

$$O_{pc} = O_{\Pi pc}(1 - W_c) + O_{\Sigma_A pc} W_c \quad (6.71)$$

Where W_a, W_b, W_c are weights associated with the phase 'a', 'b' and 'c' respectively. The mean active component of load currents (w_{Lp}) is obtained by averaging the final output of the GNN for each phase and given as

$$w_{Lp} = \frac{(O_{pa} + O_{pb} + O_{pc})}{3}. \quad (6.72)$$

Moreover, the estimation of fundamental reactive current components for load currents have been obtained similarly using the developed GNN model. The sensed load currents (i_{La}, i_{Lb}, i_{Lc}) with their unknown weights ($w_{Aqa}, w_{Aqb}, w_{Aqc}$) and ($w_{\Pi qa}, w_{\Pi qb}, w_{\Pi qc}$) are processed as inputs to Σ_A and Π neurons. The aggregation function of Σ_A and Π of the forward mode calculations for phase 'a' is given in equation 23 and 24 respectively. Similarly, aggregation function of Σ_A and Π of the forward mode calculations of another remaining phases 'b' and 'c' are calculated.

$$\Sigma_{Aqa} = i_{La} w_{\Sigma qa} + i_{Lb} w_{\Sigma qb} + i_{Lc} w_{\Sigma qc} + \Sigma_{bias} \quad (6.73)$$

$$\Pi_{qa} = i_{La} w_{\Pi qa} * i_{Lb} w_{\Pi qb} * i_{Lc} w_{\Pi qc} * \Pi_{bias} \quad (6.74)$$

Where Σ_{bias} and Π_{bias} denotes the initial bias of Σ_A and Π part of the network respectively. Similarly as explained above while calculating the fundamental active load current component here also Σ_A aggregation function has been used with the sigmoidal characteristic function f_1 while the Π aggregation function has been used with the Gaussian function f_2 as a characteristic function. Output of the Σ_A part with a sigmoidal characteristic transfer function after threshold can be calculated as

$$O_{\Sigma_{Aqa}} = f_1(\Sigma_{Aqa}) = \frac{1}{1 + e^{-\lambda_{\Sigma q} * \Sigma_{Aqa}}} \quad (6.75)$$

Output of the Π part is being threshold by using Gaussian transfer function and can be written as given:

$$O_{\Pi qa} = f_2(\Pi_{qa}) = e^{-\lambda_{\Pi q} * \Pi_{qa}^2} \quad (6.76)$$

Where $\lambda_{\Sigma q}$ and $\lambda_{\Pi q}$ are gain scaling parameters of Σ_A and Π part network respectively and considered as unity here to avoid the complexity. Similarly, output of Σ_A and Π part of the forward mode calculations of another two phases 'b' and 'c' are calculated as

$$O_{\Sigma Aqb} = f_1(\Sigma_{Aqb}) = \frac{1}{1 + e^{-\lambda_{\Sigma q} * \Sigma_{Aqb}}} \quad (6.77)$$

$$O_{\Pi qb} = f_2(\Pi_{qb}) = e^{-\lambda_{\Pi q} * \Pi_{qb}^2} \quad (6.78)$$

$$O_{\Sigma Aqc} = f_1(\Sigma_{Aqc}) = \frac{1}{1 + e^{-\lambda_{\Sigma q} * \Sigma_{Aqc}}} \quad (6.79)$$

$$O_{\Pi qc} = f_2(\Pi_{qc}) = e^{-\lambda_{\Pi q} * \Pi_{qc}^2} \quad (6.80)$$

The output of the GNN model as a function of weights W and $(1-W)$ through can be written as

$$O_{qa} = O_{\Pi qa}(1 - W_{a1}) + O_{\Sigma Aqa}W_{a1} \quad (6.81)$$

$$O_{qb} = O_{\Pi qb}(1 - W_{b1}) + O_{\Sigma Aqb}W_{b1} \quad (6.82)$$

$$O_{qc} = O_{\Pi qc}(1 - W_{c1}) + O_{\Sigma Aqc}W_{c1} \quad (6.83)$$

Where W_{a1} , W_{b1} and W_{c1} are the weights associated with Σ_A and Π part of the developed GNN model for fundamental reactive load current components estimation. Fundamental reactive current component of load current (w_{Lq}) is determined by taking

average of output of GNN model for reactive current component of load currents and given as

$$w_{Lq} = \frac{(O_{qa}+O_{qb}+O_{qc})}{3}. \quad (6.84)$$

(d) *GNN weight forecasting and updating using Extended Kalman Filter (EKF):*

Kalman Filter (KF) is a recursive algorithm used for estimating state of a dynamic system in the case of less availability of data which is because of presence of noise etc. KF algorithm utilize the prior knowledge to predict the past, present and as well as future state of the given system. The main advantage of KF based approach is less memory space requirement because data is updated in each and every iteration. The basic KF theory is based upon the probability of the hypothesis of predicted state of the system under consideration by hypothesis of prior state and then using the available data from measurement sensors to correct the hypothesis to get the best estimation for each iteration. Two basic assumptions are made to derive the basic equations for KF to be optimal in the sense of mean square error, which are system should be described by a model of linear state space and the noises are white and Gaussian with zero mean, uncorrelated with each other.

$$x_{k+1} = F_{k+1, k} x_k + q_k \quad (6.85)$$

$$y_{k+1} = H_{k+1} x_{k+1} + r_{k+1} \quad (6.86)$$

Equation 6.86 is known as process equation, x_k is system state vector a minimal set of data that uniquely defines behavior of system and k depicts discrete time. Where $F_{k+1, k}$ is the transition matrix to take the state x_k from time k to $k+1$ and q_k additive process noise, white and Gaussian with a zero mean and possess a covariance matrix Q_k . Measurement step is shown in equation (6.89), where H_{k+1} is the

measurement matrix, y_{k+1} is observable at time $k+1$ and r_{k+1} additive process noise, white and Gaussian with a zero mean and possess a covariance matrix R_k . The both noises are uncorrelated with each other. KF algorithm works in two repeated functional steps:

1. Forecasting step (Time update): This step is to compute the estimation of state and error covariance.

$$\hat{x}_{k+1}^- = F_{k+1, k} \hat{x}_k \quad (6.87)$$

$$P_{k+1} = F_{k+1, k} P_k F_{k+1, k}^T + Q_k \quad (6.88)$$

Where P_k error covariance matrix.

2. Correction step (Measurement update): This step is to correct the estimated state according to previous step with the help of y_{k+1} .

$$K_{k+1} = P_{k+1}^- H_{k+1}^T [H_{k+1} P_{k+1}^- H_{k+1}^T + R_{k+1}]^{-1} \quad (6.89)$$

$$\hat{x}_{k+1} = \hat{x}_{k+1}^- + K_{k+1} (y_{k+1} - H_{k+1} \hat{x}_{k+1}^-) \quad (6.90)$$

$$P_{k+1} = (I - K_{k+1} H_{k+1}) P_{k+1}^- \quad (6.91)$$

Where K_{k+1} is Kalman gain matrix.

GNN model is a nonlinear system, so basic KF approach should be extend by using linearization process and known as extended Kalman Filter (EKF). The basic difference between KF and EKF is that in EKF linearization of non-linear system function done by using Jacobian matrix and then rest of the KF steps can be applied further. Nonlinear dynamic system can be define by using following equations:

$$x_{k+1} = x_k + q_k \quad (6.92)$$

$$y_{k+1} = h(x_{k+1}, u_{k+1}) + r_{k+1} \quad (6.93)$$

Equation (6.93) depicts state of a stationary process corrupted with process noise q_k and state x_k consists of network weights. x_{k+1} is weight vector matrix and input vector depicted by u_{k+1} . The noise covariance matrix can be written as: $R_{k+1} = E[r_{k+1}r_{k+1}^T]$ and $Q_{k+1} = E[q_{k+1}q_{k+1}^T]$

In EKF linearization of measurement equation is carried out at each time step around newest state estimation by using first order Taylor approximation. GNN training problem has been considered as a problem of finding the state estimate x_{k+1} that minimizes the least squares error by using previous measurements. K_{k+1} Kalman gain can be written as:

$$K_{k+1} = P_{k+1}H_{k+1}^T [H_{k+1}P_{k+1}H_{k+1}^T + R_{k+1}]^{-1} \quad (6.94)$$

$$\hat{x}_{k+1} = \hat{x}_{k+1} + K_{k+1}[y_{k+1} - h(\hat{x}_{k+1} + u_{k+1})] \quad (6.95)$$

$$P_{k+1} = P_k - K_k H_k P_k + Q_k \quad (6.96)$$

(e) *Reference source current and VSC switching signals generation:*

The fundamental real power current component of load current can be obtained as:

$$I_{Lp} = w_{pd} + w_{Lp} - w_{PV} \quad (6.97)$$

The reference active components of grid currents can be written as:

$$i_{psa} = I_{Lp} * u_{pa}, i_{psb} = I_{Lp} * u_{pb}, i_{psc} = I_{Lp} * u_{pc} \quad (6.98)$$

Similarly fundamental reactive current component of load current can also be obtained as:

$$I_{Lq} = w_{qt} + w_{Lq} \quad (6.99)$$

The active reference components of grid currents can be written as:

$$i_{qsa} = I_{Lq} * u_{qa}, i_{qsb} = I_{Lq} * u_{qb}, i_{qsc} = I_{Lq} * u_{qc} \quad (6.100)$$

Net fundamental reference grid currents ($i_{sa}^*, i_{sb}^*, i_{sc}^*$) can be obtained as:

$$i_{sa}^* = i_{psa} + i_{qsa}, i_{sb}^* = i_{psb} + i_{qsb}, i_{sc}^* = i_{psc} + i_{qsc} \quad (6.101)$$

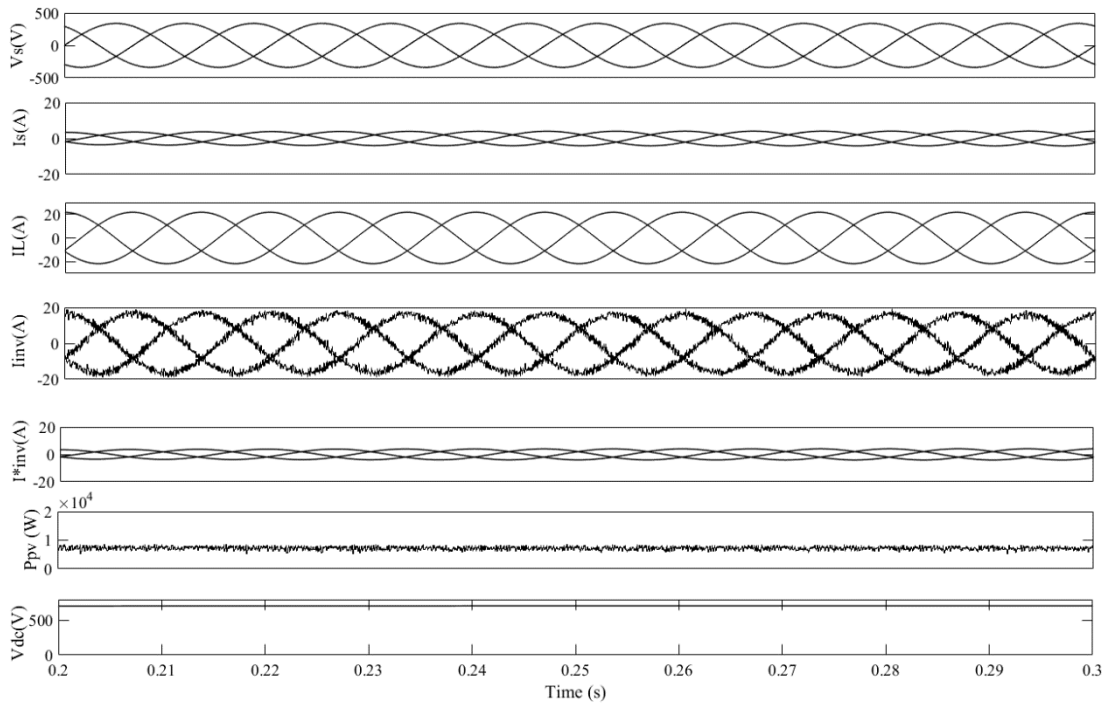
VSC gating signals has been generated by comparing reference ($i_{sa}^*, i_{sb}^*, i_{sc}^*$) and actual (i_{sa}, i_{sb}, i_{sc}) grid currents for individual phase and error is processed through PI current regulator. Hysteresis current regulator is used for indirect current control.

6.6.2 Results and Discussions

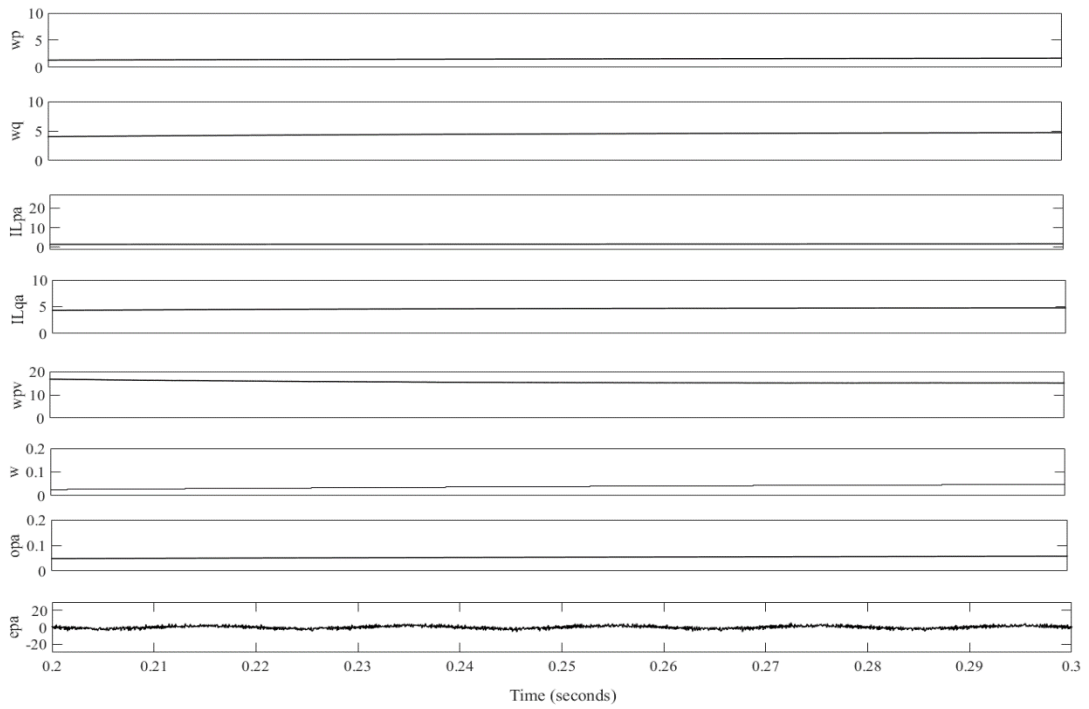
The Solar PV array is designed for maximum power rating of 10 kW and given system is designed, developed and simulated using MATLAB/Simulink platform. Evaluation of performance for the proposed system is done under linear, nonlinear load with dynamic changes and changing solar irradiance scenario.

(i) Performance under linear load for PFC:

The performance of the proposed EKF based GNN controller is evaluated with combined structure of summation and product neurons collectively in single layer. In the proposed GNN network each processed neuron consists of different weights with the inputs as measured load currents (i_{La}, i_{Lb}, i_{Lc}) with the help of this, summation weights ($w_{\Sigma pa}, w_{\Sigma pb}, w_{\Sigma pc}$) and product weights ($w_{\Pi pa}, w_{\Pi pb}, w_{\Pi pc}$) are estimated. The proposed GNN is trained to calculate the unspecified weights and EKF filter is used to predict and update the weights of GNN network.



(a)



(b)

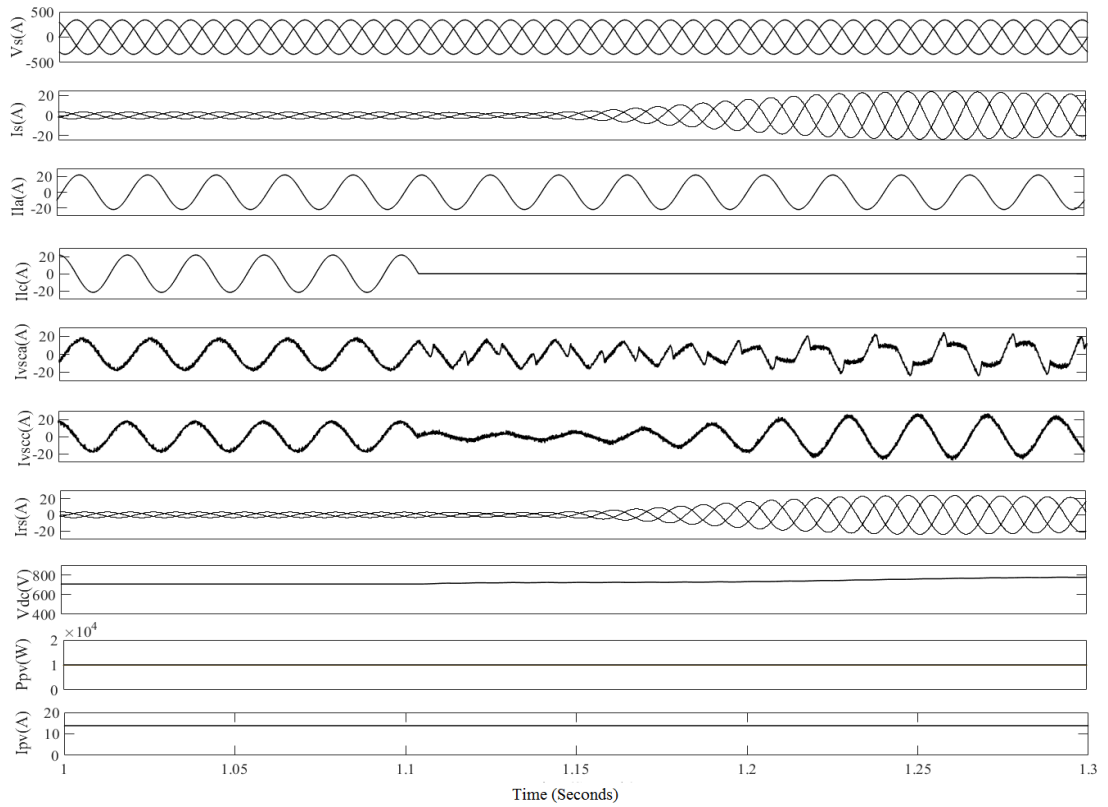
Fig 6.25 (a) Performance parameters (b) estimated weights for under steady state linear load conditions in PFC mode

The performance of the developed system is observed on the basis of various performance parameters such as grid voltage (v_s), grid current (i_s), load current (i_L),

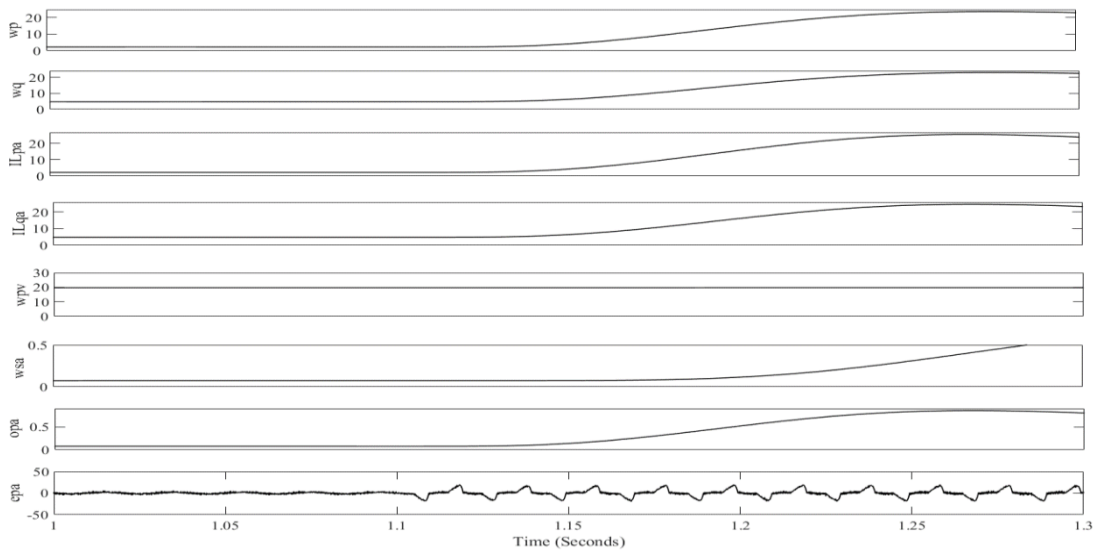
VSC current (i_{vsc}), grid real power (P_g), grid reactive power (Q_g), PCC terminal voltage (V_t), SPV array power (P_{pv}), SPV array current (I_{pv}) and voltage at DC link (V_{dc}) shown in Fig. 6.25 (a-b) under steady state linear load (at $t = 0.2$ to 0.3 s) conditions. Intermediate signals are given in Fig. 6.25 (b), depicting performance parameters and corresponding weights with a variation in error between active fundamental components of load currents. The solar PV system remains in operation to feed maximum amount of power to the load and grid at unity power factor (UPF).

(ii) Performance under dynamic linear load for zero voltage regulation (ZVR):

Load linear in nature consume real and reactive power as well, if load is drawing reactive power with unbalanced behavior then change in the terminal voltage (V_t) occurs at point of common coupling. Fig. 6.26 (a-b) showing behavior of given system for dynamic linear loading conditions under zero voltage regulation (ZVR) mode. It can be observe from results after phase 'c' of load is taken out from supply at 1.1 s, grid currents (i_s) are maintained sinusoidal with the help of voltage source converter. The PCC voltage (V_t) and voltage at DC junction are maintained at set values which are 415 V and 700 V, respectively without any fluctuations. Intermediate signals are provided in Fig. 6.26 (b), showing performance parameters and corresponding weights with a variation in error between active fundamental components of load currents. The reactive power (Q_g) taken from the utility grid is approximately equal to zero, so the compensation is also done for linear loads consuming reactive power.



(a)

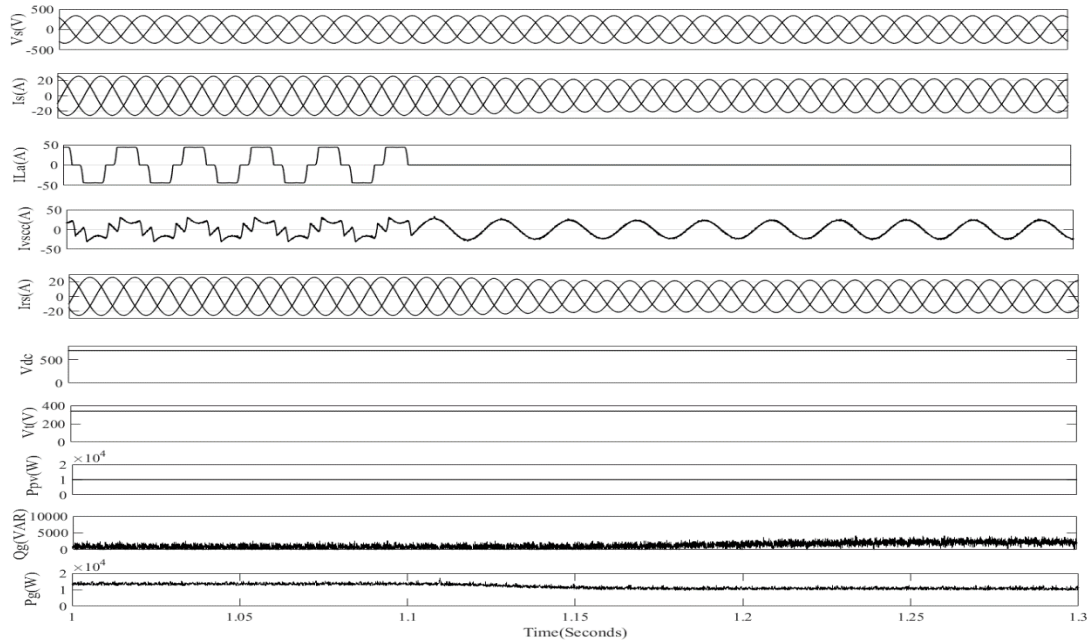


(b)

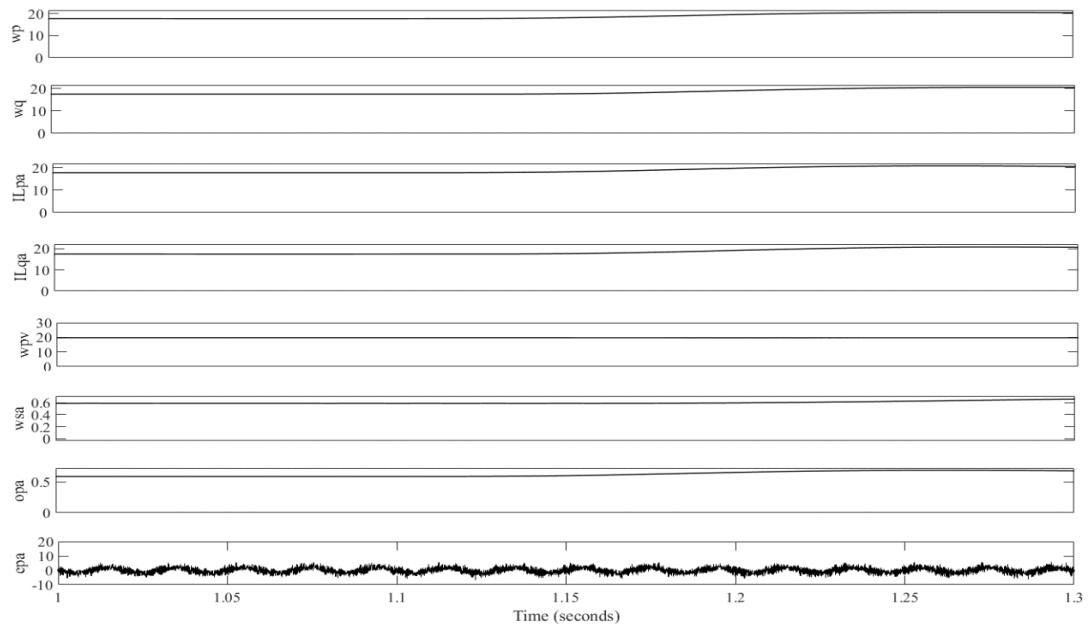
Fig. 6.26 (a) Performance parameters (b) estimated weights under dynamic linear load conditions for ZVR

(iii) Performance under non-linear load:

Fig. 6.27 (a-b) shows behavior of developed system for nonlinear loads dynamic in nature, for zero voltage regulation (ZVR) mode.



(a)



(b)

Fig. 6.27 (a) Performance indices (b) weights with training parameters for phase ‘a’ with steady state loading in PFC mode

When phase ‘c’ of load is taken out at 1.1 s, grid currents (i_s) are maintained sinusoidal with the help of proposed control. The voltage (V_t) and voltage at DC link are also maintained at respective set values. Intermediate signals are given in Fig. 6.27 (b) for corresponding weight signals with a variation in error between active fundamental components of load currents. Fig. 6.28 (a)-(c) shows the total harmonic distortion (THD) at point of common coupling for phase ‘a’ of load current, grid current and grid voltage respectively and obtained as 37.48%, 1.04% and 1.07% respectively.

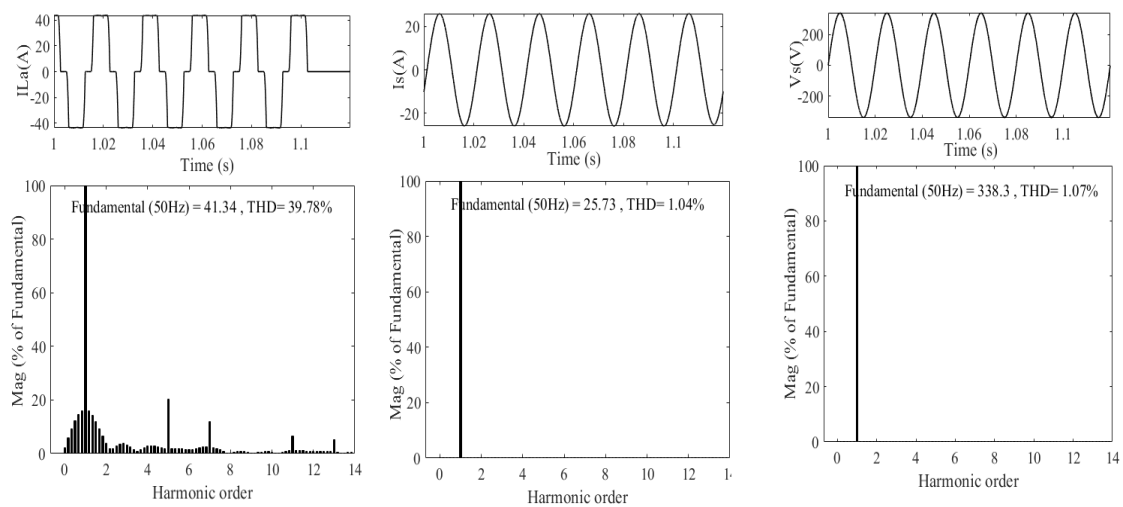


Fig. 6.28 THD for (a) load current of phase ‘a’ (b) grid current and (c) grid voltage in ZVR mode

(iv) Performance under variable solar irradiance

Dynamic behaviour of developed system is also observed under varying solar irradiance condition. The solar irradiance (S) is raised to 1000 W/m² from 600 W/m² at 0.5 s. SPV system is feeding the load and excess generation is being supplied to the utility grid. In Fig. 6.29, the grid power (P_g) decreases after 0.5s when SPV power (P_{pv}) increases. The proposed system under variable solar irradiance remains to operate at maximum power point of SPV array and work at unity power factor. Grid side current is maintained to be sinusoidal and the voltage at DC link is also maintained at set point.

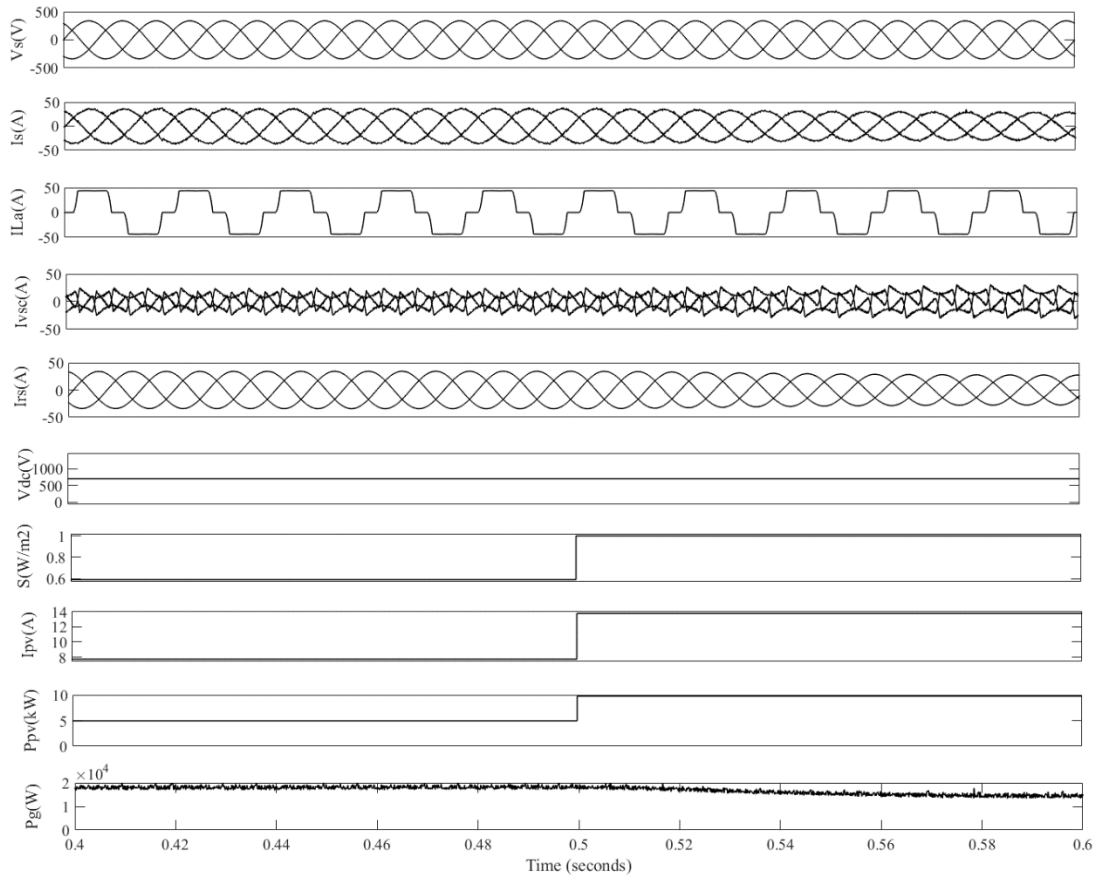


Fig. 6.29 Performance parameters under non-linear load conditions for variable solar irradiance

(v) Comparative study of developed algorithm with other conventional approaches

The proposed algorithm has been analyzed and found satisfactory for each of the case discussed in the result section. In this section the THD analysis of the proposed EKF GNN based controller is presented in Table 6.4 and compared with the GNN approach. The developed EKF GNN based control approach is found better than other ANN conventional approaches such as ADALINE and MLPN. A comparative analysis is made and presented in Table 6.5 under dynamic nonlinear load conditions. As the less number of unknown weights required and a single layer enhance the performance of the controller.

Table 6.4 Performance parameters of the proposed system for EKF GNN

Operating Mode	Parameters	GNN based control algorithm	EKF GNN based control algorithm
ZVR	Grid voltage(V), %THD at PCC	333.02 V, 1.89 %	338.3 V, 1.07 %
	Grid current (A), %THD at PCC	23.17 A, 2.54 %	25.73 A, 1.04 %
	Load current (A), %THD at PCC	40.58 A, 40.62 %	41.34 A, 39.78%

The proposed system is developed and tested using MATLAB simulation environment and performance of EKF GNN based VSC control approach is validated under linear and nonlinear load for static and dynamic scenarios.

Table 6.5 Comparative analysis with other existing algorithms

Performance parameters	ADALINE	PNN	GNN
Training	Least Mean Square	Back Propagation	EKF
Learning	Gradient decent (GD)	GD/GDM	GDM
Layers	Two	Three	One
Training pattern	Online Training	Offline stochastic training	Online training
Estimation nature	Linear	Nonlinear	Both types
Transfer function	Linear	Sigmoidal	All
Weight update Time	15.7 μ s	82 μ s	6 μ s
Settling period of dc link	1 cycle	2 ½ cycle	1 cycle
Max change in dc link voltage	4.5 V	10 V	3.7 V

The proposed EKF GNN approach has successfully improve the function of the developed SPV system. The developed system has also been subjected to load unbalancing and varying solar irradiance, output shows satisfactory performance of the developed system. Also it continues to operate in UPF mode of operation with providing reactive power compensation, load balancing, MPP extraction and harmonics compensation. The developed system functions very well with EKF GNN based approach and gives very fast response. The developed system obtain acceptable limits of harmonics in utility currents and voltage fluctuations according to the IEEE-519 and IEEE-1547 standards. Moreover, single stage topology is able to reduce the losses in semiconductor devices and increase the overall efficiency. The proposed control approach performs with more flexibly in training the network under dynamic conditions.

The experimental performance of the proposed system in PFC mode under linear load is given in Fig 6.30. It shows VSC current (I_{vsc}), load current (I_{La}), grid current (I_g) and dc link voltage (V_{dc}). Fig. 6.31 shows grid current and grid voltage of phase ‘a’ and depicts the performance of controller for PFC mode.

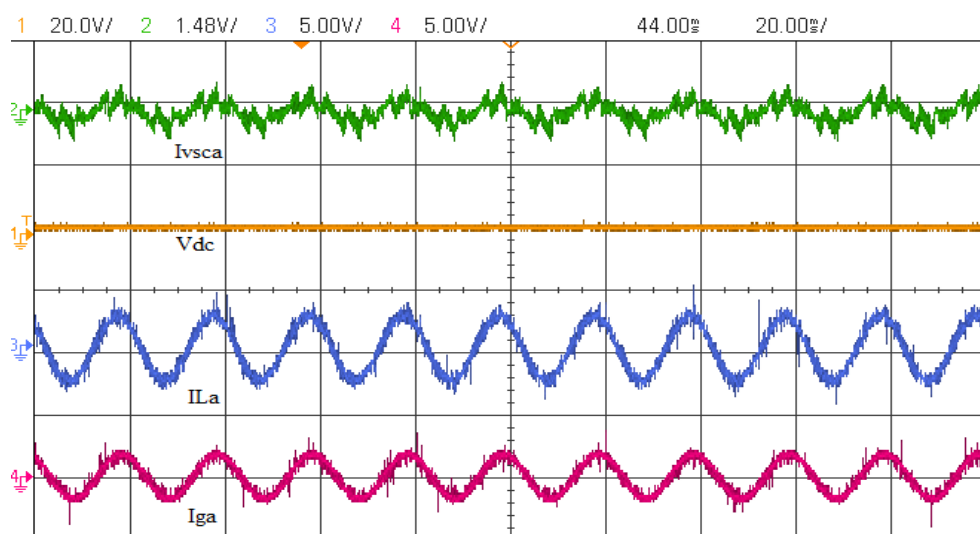


Fig. 6.30 Performance parameters under linear load for EKF GNN

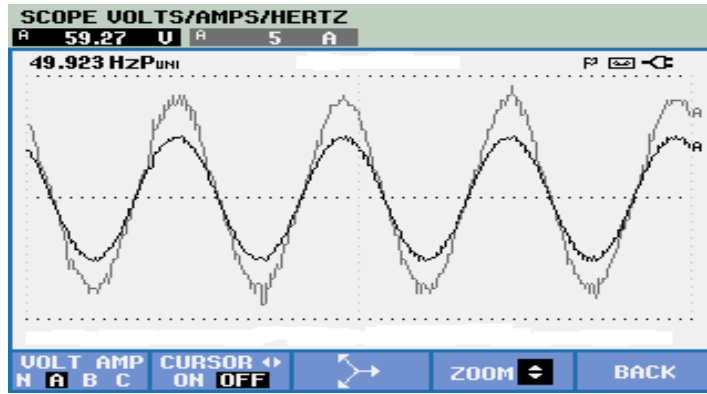


Fig. 6.31 Grid voltage and current of phase 'a' for PFC mode

The performance of the proposed system under nonlinear load is given in Fig. 6.32. Fig 6.33 shows nonlinear load current and (b) shows the source current and voltage for phase 'a'. THD in load current which is 26.5 % which is improved to 2.9% for the given algorithm and shown in Fig. 6.34.

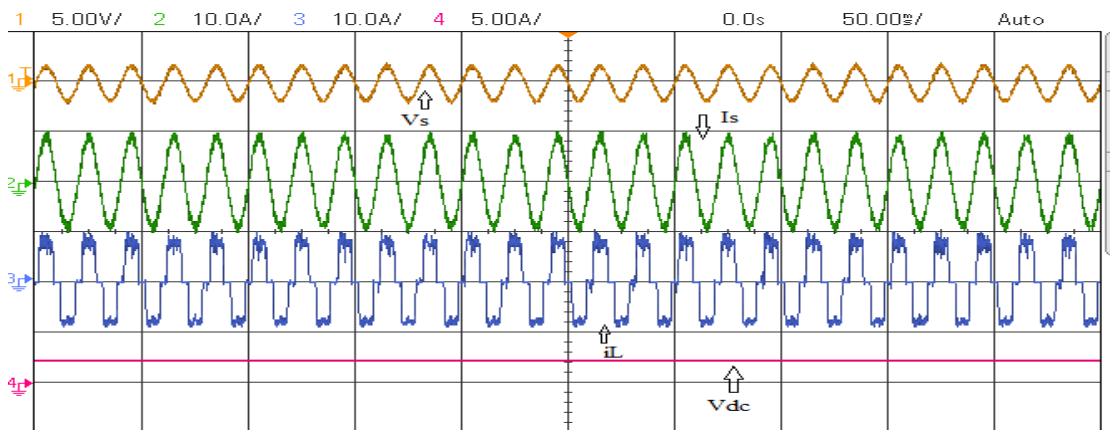
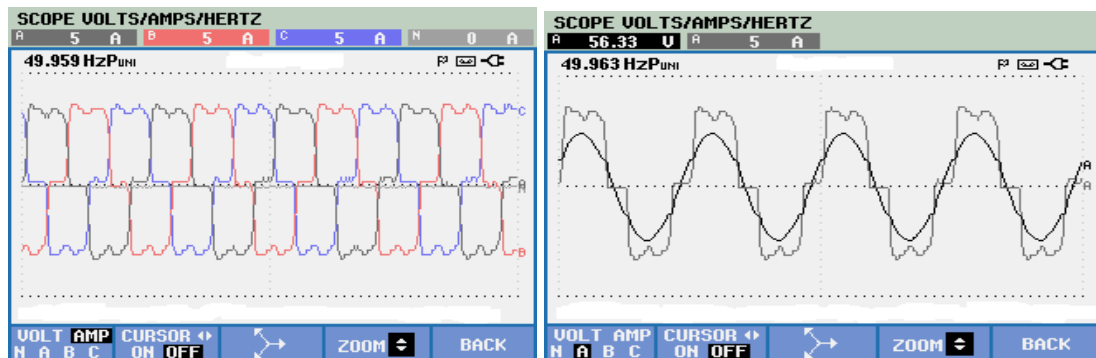


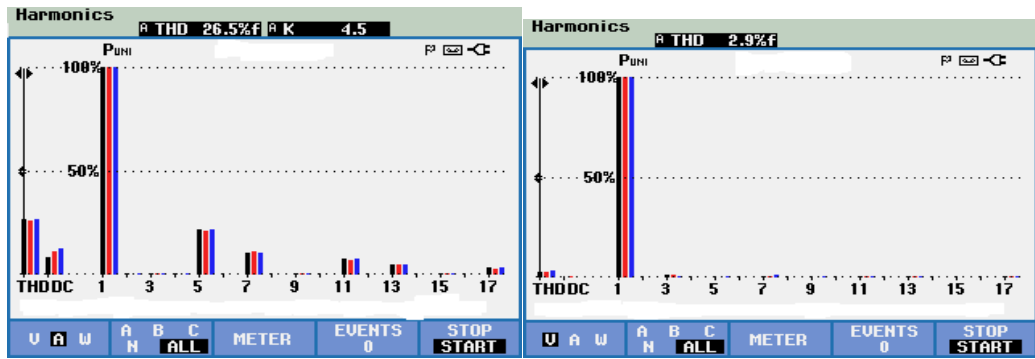
Fig. 6.32 Performance parameters under non-linear load conditions for EKF GNN



(a)

(b)

Fig. 6.33 (a) Non-linear current, (b) Current and voltage of Phase 'a'



(a)

(b)

Fig. 6.34 (a) THD spectrum of Non-Linear Load (b) Improved THD for grid current under non-linear load

The performance of the proposed controller under nonlinear dynamic load is shown in Fig 6.35, when load of phase ‘b’ is removed the grid current is reduced. Further, performance of intermediate signals for different weights is also shown in Fig. 6.36. Fig. 6.37 and Fig. 6.38 shows the controller performance under variable solar irradiance.

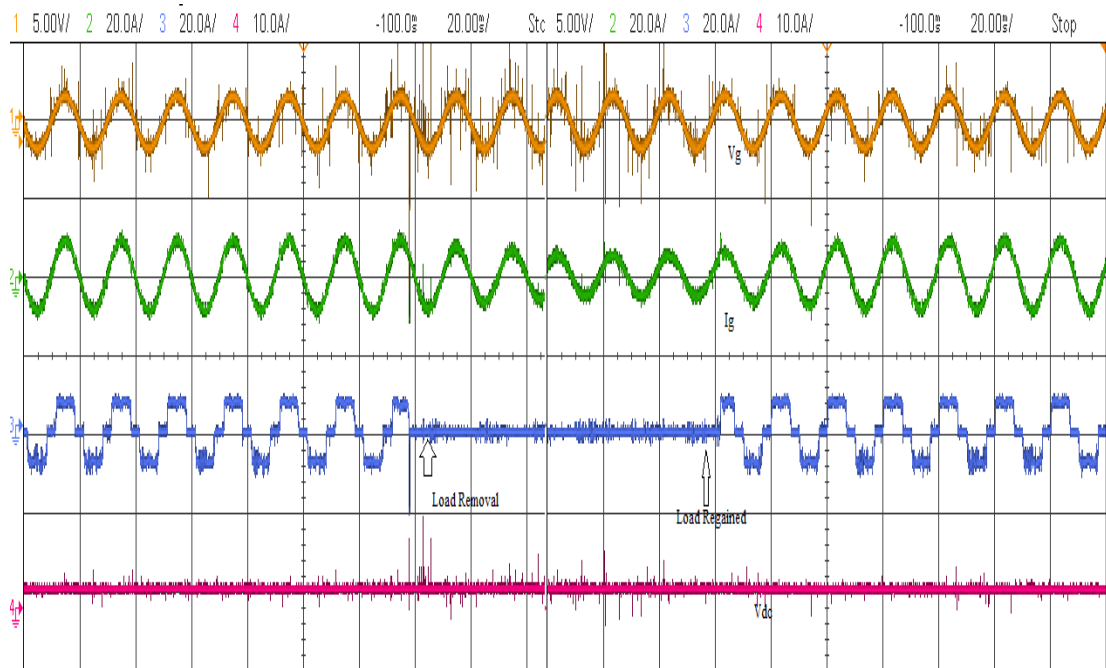


Fig. 6.35 Performance parameters under dynamic non-linear load for GNN EKF

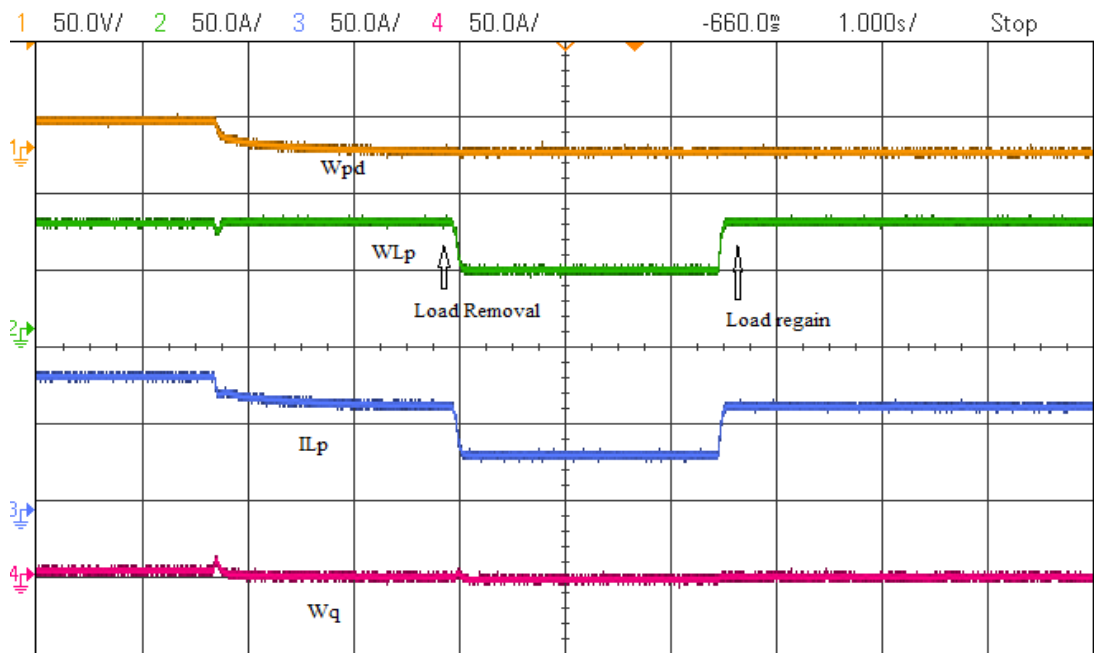


Fig. 6.36 Performance of intermediate weight signals under dynamic non-linear load for GNN EKF

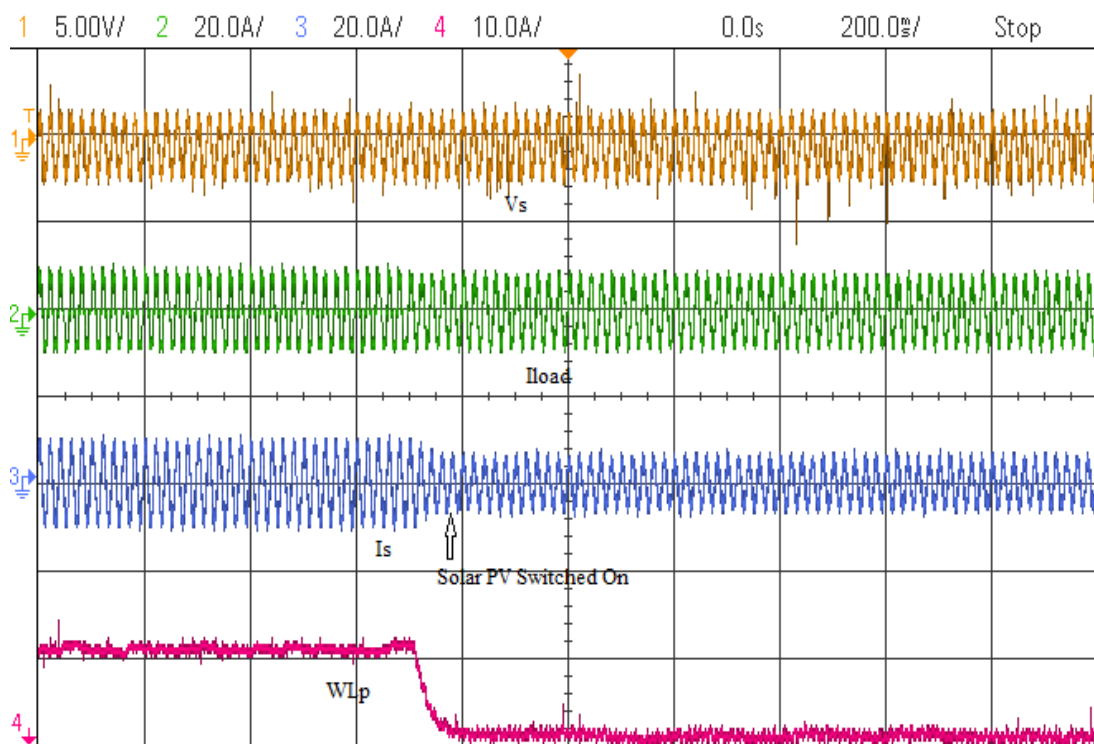


Fig. 6.37 Performance parameters under non-linear load with solar PV ON for GNN EKF

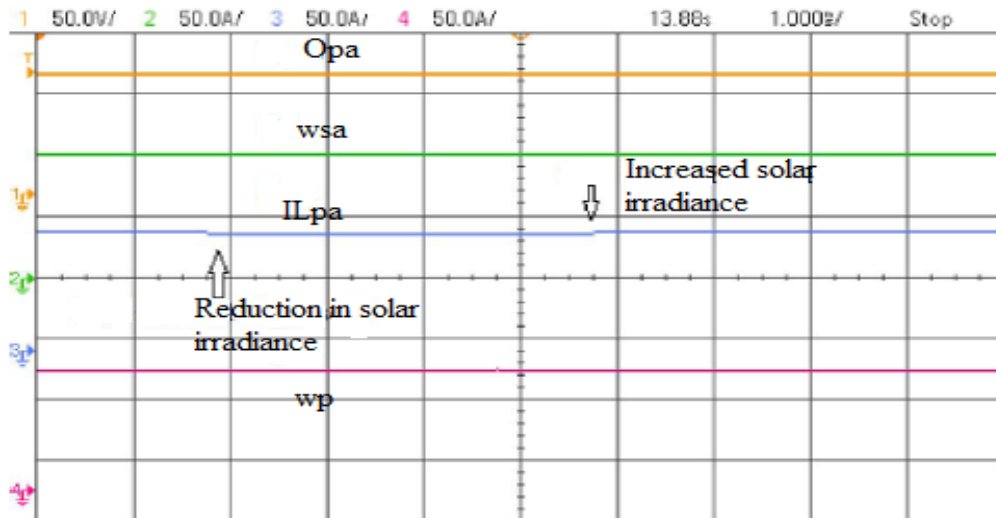


Fig. 6.38 Performance parameters under variable solar irradiance for GNN EKF

6.7 NLMS & PLMS BASED CONTROL

The knowledge of phase angle and frequency of grid side voltage is necessary to for inverter control. The reference sinusoidal source currents for generating inverter gate pulses obtained by using present control algorithm. The implemented control algorithm combines normalized least mean square (NLMS) algorithm with proportionate normalized least mean square (PNLMS) algorithm and a PI controller to regulate the DC link voltage. This results in a more stability with high convergence rate.

6.7.1 Control algorithm

(a) *Calculation of amplitude of terminal voltage and unit templates:*

In-phase and quadrature unit templates can be calculate in similar manner as equation (6.33) – equation (6.36).

(b) *Reference grid currents generation:*

Voltage at dc link (V_{dc}) is measured and compared with the reference dc link voltage (V_{dc}^*) to calculate the active loss component.

$$E_{dc}(k) = V_{dc}^*(k) - V_{dc}(k) \quad (6.102)$$

PI controller is used to minimal this difference (E_{dc}) which is further being used to get active current component (w_{pdc}). The controller's output at $(k + 1)^{th}$ instant:

$$w_{pd}(k + 1) = w_{pd}(k) + k_{pd}\{V_{dce}(k + 1) - V_{dce}(k)\} + k_{id} E_{dc}(k + 1) \quad (6.103)$$

Error V_{te} (difference between sensed and reference terminal voltage V_t and V_t^* respectively) at point of common coupling passed through a PI controller to compute reactive loss component which needed to maintain the constant terminal voltage.

$$E_{te}(k) = V_t^*(k) - V_t(k) \quad (6.104)$$

The controller output at $(k + 1)^{th}$ is:

$$w_{qt}(k + 1) = w_{qt}(k) + k_{pt}\{V_{te}(k + 1) - V_{te}(k)\} + k_{it}E_{te}(k + 1) \quad (6.105)$$

Where, k_{pt} and k_{it} are proportional and integral gains respectively. Fast dynamic response can be achieved with a feed forward weight which is a function of solar power (P_{PV}) and V_t .

$$w_{PV}(k) = \frac{2P_{PV}(k)}{3V_t} \quad (6.106)$$

Fundamental active and reactive components of load current extraction done by taking load currents (i_{La}, i_{Lb}, i_{Lc}).

The error for the system is considered as:

$$e_{Aj}(k) = i_{Lj}(k) - u_{pj}(k) * w_{pj}(k) \quad (6.107)$$

In above equation n shows the phases a, b and c, w_{pj} depicts the fundamental active load current component of phase 'j'.

$$w_{pj}(k+1) = w_{pj}(k) + \mu * u_{pj}(k) * e_{Aj}(k) * [g_{Aj}(k) + h_{Aj}(k)] \quad (6.108)$$

Here μ is adaption constant and values lie between 0 and 2. NLMS algorithm contribute as $g_{Aj}(k)$:

$$g_{Aj}(k) = \frac{(1-\alpha)}{2 * u_{pj}(k) * u_{pj}^T(k) + \epsilon} \quad (6.109)$$

PNLMS algorithm contribute as $h_{Aj}(k)$

$$h_{Aj}(k) = \frac{(1+\alpha) * p_{Aj}(k-1)}{2 * u_{pj}(k) * p_{Aj}(k-1) * u_{pj}^T(k) + \epsilon} \quad (6.110)$$

Where, $0 < \alpha < 0.5$ and regulation constant $0.001 < \epsilon < 0.01$ for finite output. $p_{Aj}(k)$ [180] can be written as:

$$p_{Aj}(k) = \frac{|w_{pj}(k)|}{\sum_{i=0}^{M-1} |w_{pj}(k)| + \delta} + \gamma \quad (6.111)$$

Where, δ and γ are considered as positive small constant for finite $p_{Aj}(k)$.

Weighted values for fundamental active current components for all phases:

$$\left. \begin{aligned} w_{Pa}(k+1) &= w_{Pa}(k) + \mu * u_{pa}(k) * e_{Aa}(k) * [g_{Aa}(k) + h_{Aa}(k)] \\ w_{Pb}(k+1) &= w_{Pb}(k) + \mu * u_{pb}(k) * e_{Ab}(k) * [g_{Ab}(k) + h_{Ab}(k)] \\ w_{Pc}(k+1) &= w_{Pc}(k) + \mu * u_{pc}(k) * e_{Ac}(k) * [g_{Ac}(k) + h_{Ac}(k)] \end{aligned} \right\} \quad (6.112)$$

The arithmetic mean active component of load currents (w_{Lp}) is calculated as below:

$$w_{Lp} = \frac{(w_{Pa} + w_{Pb} + w_{Pc})}{3} \quad (6.113)$$

Similarly, weighted values for mean reactive component of load currents (w_{qj}) is obtained as:

$$w_{Lq} = \frac{(w_{qa} + w_{qb} + w_{qc})}{3}. \quad (6.114)$$

Net fundamental active load current component is given as:

$$I_{Lp} = w_{pd} + w_{Lp} - w_{PV} \quad (6.115)$$

Net fundamental reactive current component of load current:

$$I_{Lq} = w_{qt} + w_{Lq} \quad (6.116)$$

The reference grid currents for active and reactive components are given as:

$$i_{psa} = I_{Lp} * u_{pa}, i_{psb} = I_{Lp} * u_{pb}, i_{psc} = I_{Lp} * u_{pc} \quad (6.117)$$

$$i_{qsa} = I_{Lq} * u_{qa}, i_{qsb} = I_{Lq} * u_{qb}, i_{qsc} = I_{Lq} * u_{qc} \quad (6.118)$$

Net reference grid currents (i_{sa}^* , i_{sb}^* , i_{sc}^*) is given as:

$$i_{sa}^* = i_{psa} + i_{qsa}, i_{sb}^* = i_{psb} + i_{qsb}, i_{sc}^* = i_{psc} + i_{qsc} \quad (6.119)$$

Gate pulses for inverter switches are generated by comparing reference (i_{sa}^* , i_{sb}^* , i_{sc}^*) and actual (i_{sa} , i_{sb} , i_{sc}) grid currents.

6.7.2 Results and discussions

The performance of developed system has been tested for various cases such as STC conditions, various irradiance levels with different kind of loads such as linear, nonlinear, balanced and unbalanced. Proposed model has been validated through analysis of various parameters such as grid voltage (V_s), DC bus voltage (V_{dc}), AC grid currents, (I_s), load currents, (I_L) the real power from and to the grid (P_g), the reactive

power (Q_g), SPV current (I_{pv}), SPV voltage (V_{pv}), SPV power (P_{pv}), inverter current (I_{inv}) and AC terminal voltage (V_t). Fig. 6.39 shows results of the system for dynamic linear load scenario.

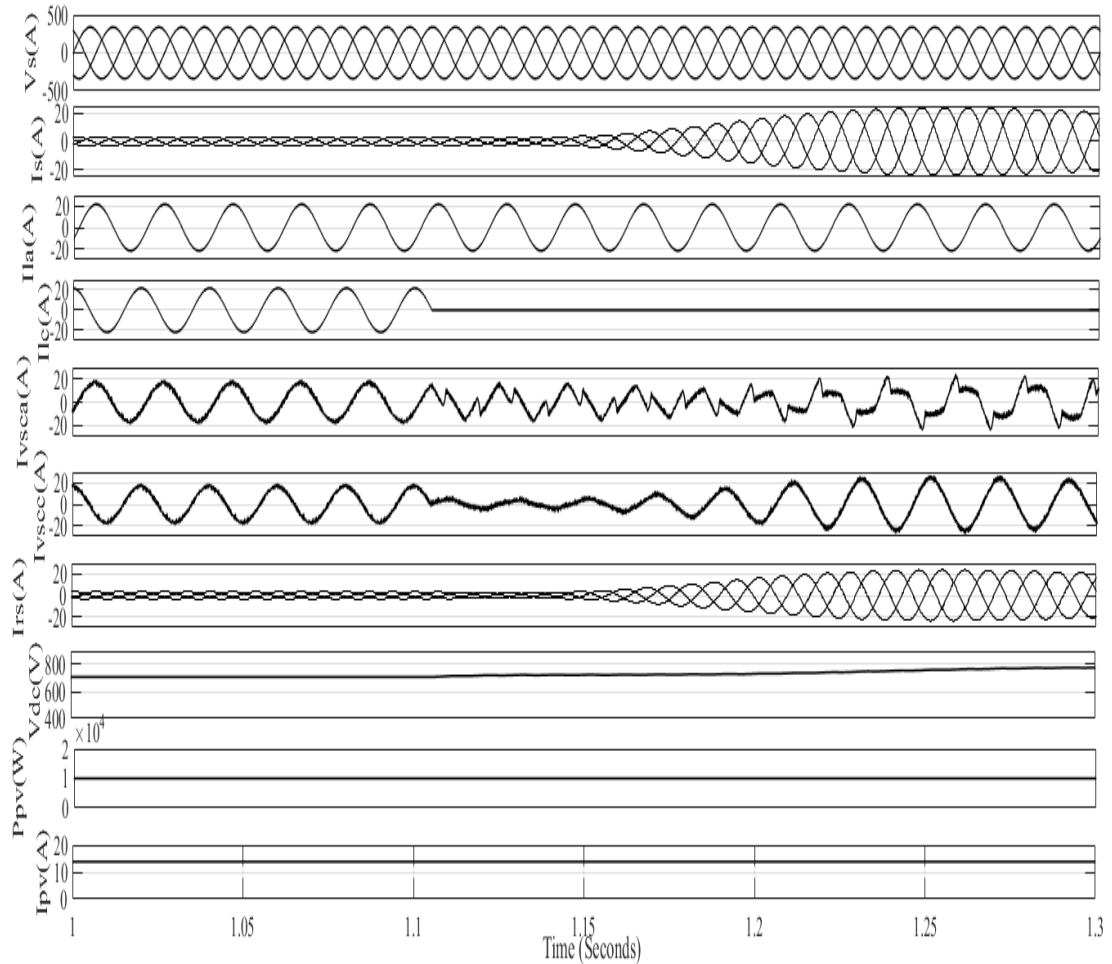


Fig. 6.39 Performance under linear dynamic load for PNLMS

Fig. 6.40 presents dynamic operation of the system under unbalanced nonlinear loads for zero voltage regulation (ZVR) mode. At 1.1 s phase ‘c’ of load is removed from supply, even under this situation, source currents (i_s) maintained sinusoidal. The proposed control helps V_t and V_{dc} are maintained at 415 V and 700 V, respectively without fluctuations.

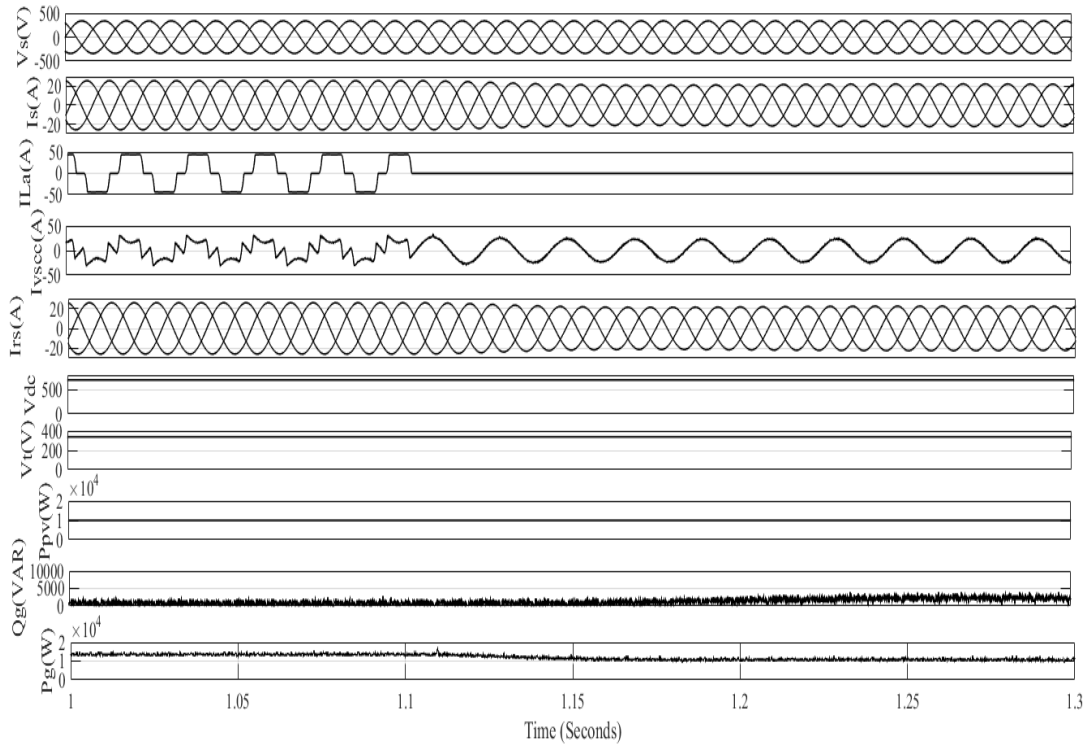


Fig. 6.40 Performance under non-linear dynamic load for PNLMS

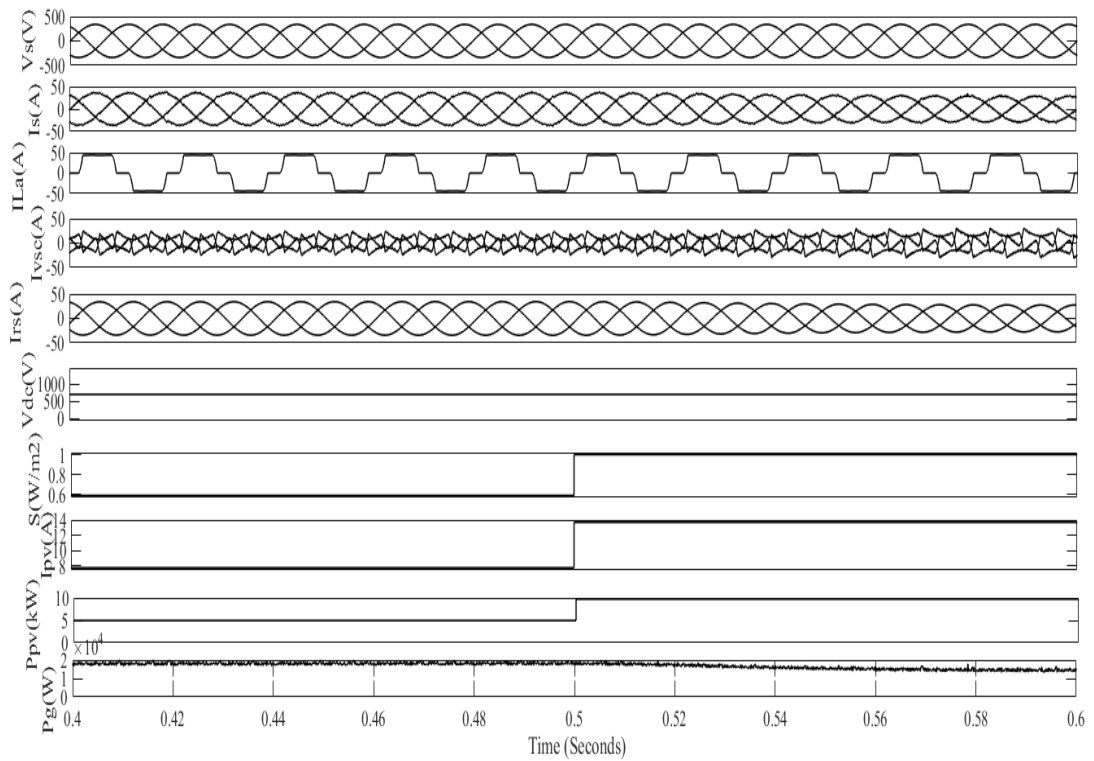


Fig. 6.41 Performance under variable solar irradiance for PNLMS

Performance of the given system under variable solar irradiance is shown in Fig. 6.41. Fig. 6.42 shows the THDs at PCC for load current phase ‘a’ and grid current respectively and it can be observe that THD within the limits according to IEEE-519 and IEEE-1547 standards.

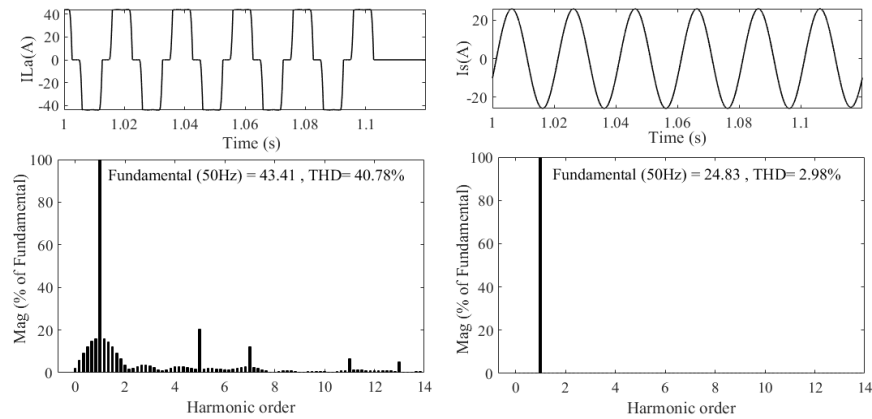


Fig. 6.42 THD spectrum for load current and grid current for PNLMS

The proposed system is developed in MATLAB/Simulink platform. Performance of the proposed control approach is analyzed for linear and nonlinear loads with steady state and dynamic states. Load unbalancing and solar irradiance variation to validate the results of the control algorithm and satisfactory performance has been achieved. System provides fast response and operates unity power factor (UPF) mode gives reactive power compensation, load balancing, maximum power extraction and harmonic reduction. Grid currents harmonics and voltage fluctuations are within limits as per IEEE-519 and IEEE-1547 standards.

The performance of the proposed system under nonlinear load is shown in Fig. 6.43. Fig. 6.44 (a) shows voltage and non-linear load current of phase ‘a’ and (b) shows THD in load current which is 25.2 %. Improved THD of grid current after VSC being switched on is given in Fig. 6.45 which is improved to 3.6% by using PNLMS algorithm.

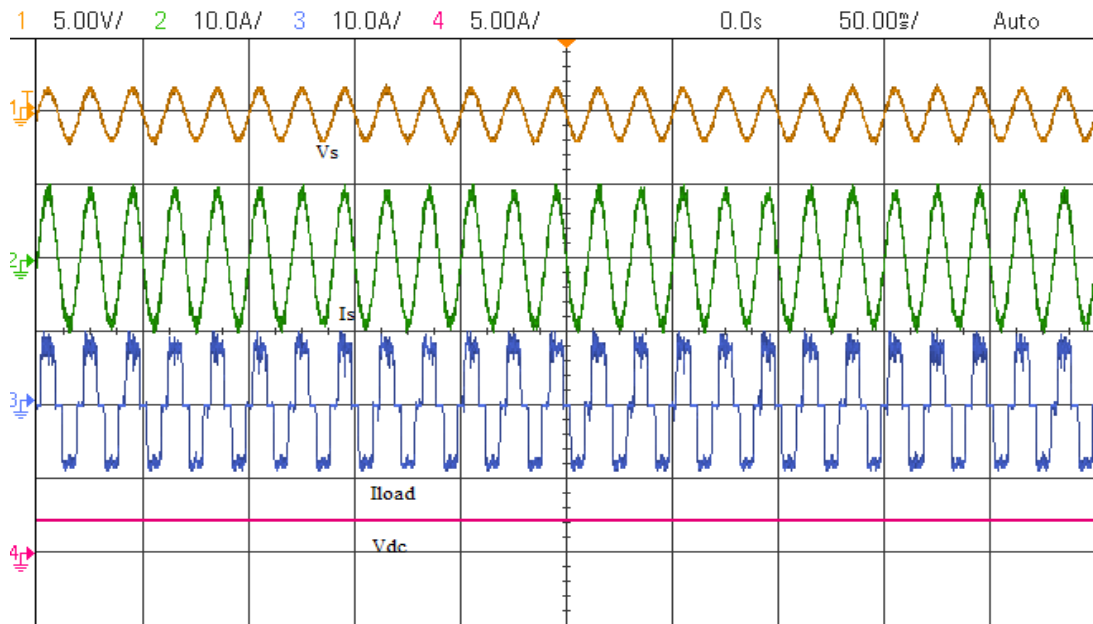
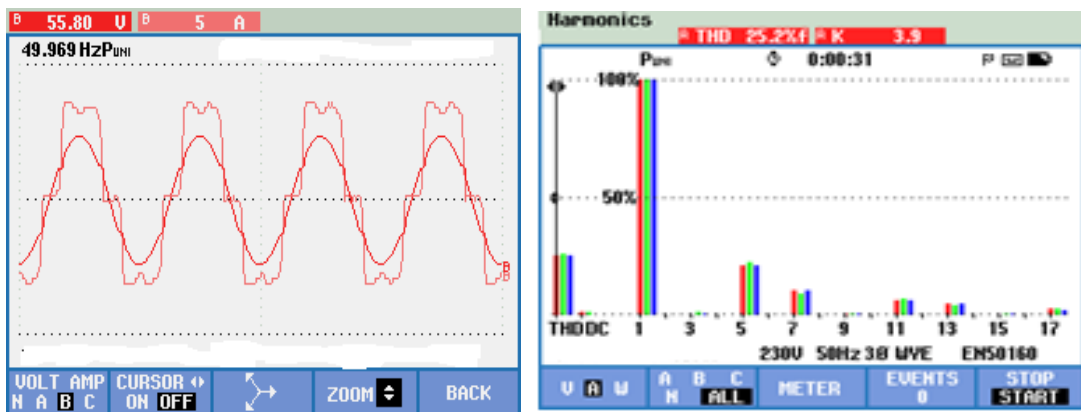


Fig. 6.43 Performance of developed controller under non-linear load conditions



(a)

(b)

Fig. 6.44 (a) Voltage and non-linear load current of Phase 'a', (b) THD of load current

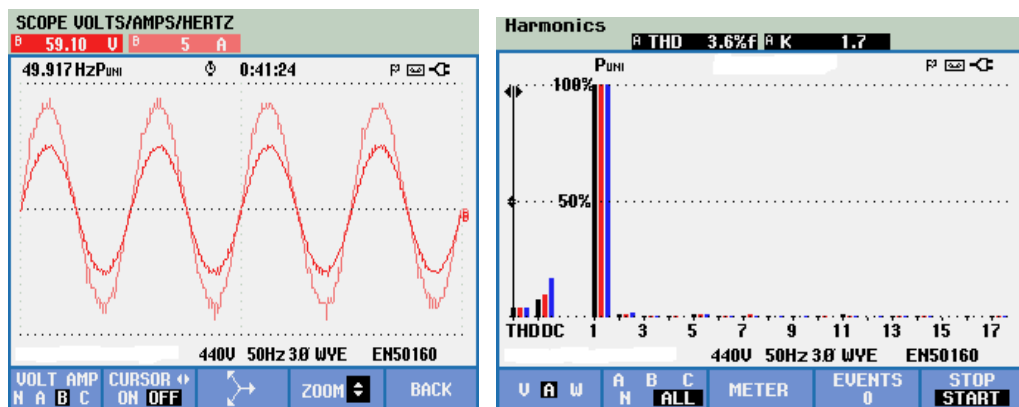


Fig. 6.45 Improved THD for grid current under non-linear load for PNLMs

The performance of the developed algorithm under nonlinear dynamic load is shown in Fig 6.46. Given results shows, that after sudden removal of load, the controller responds fast and system quickly achieves steady state. Intermediate weight signals are provided in Fig. 6.47 and 6.48.

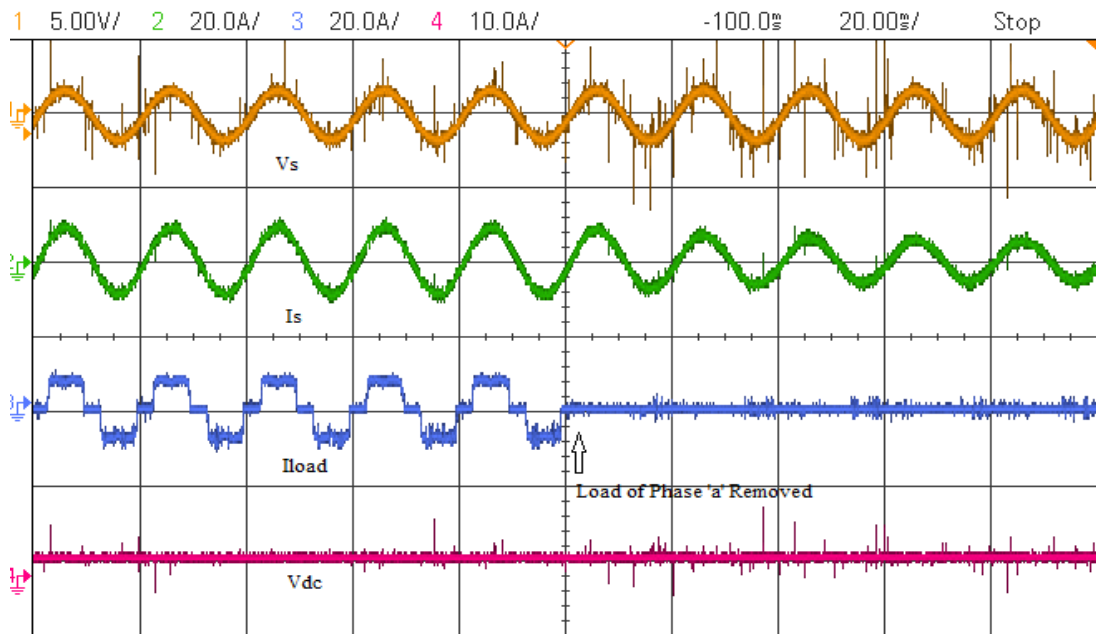


Fig. 6.46 Performance of developed controller under dynamic non-linear load for PNLMS

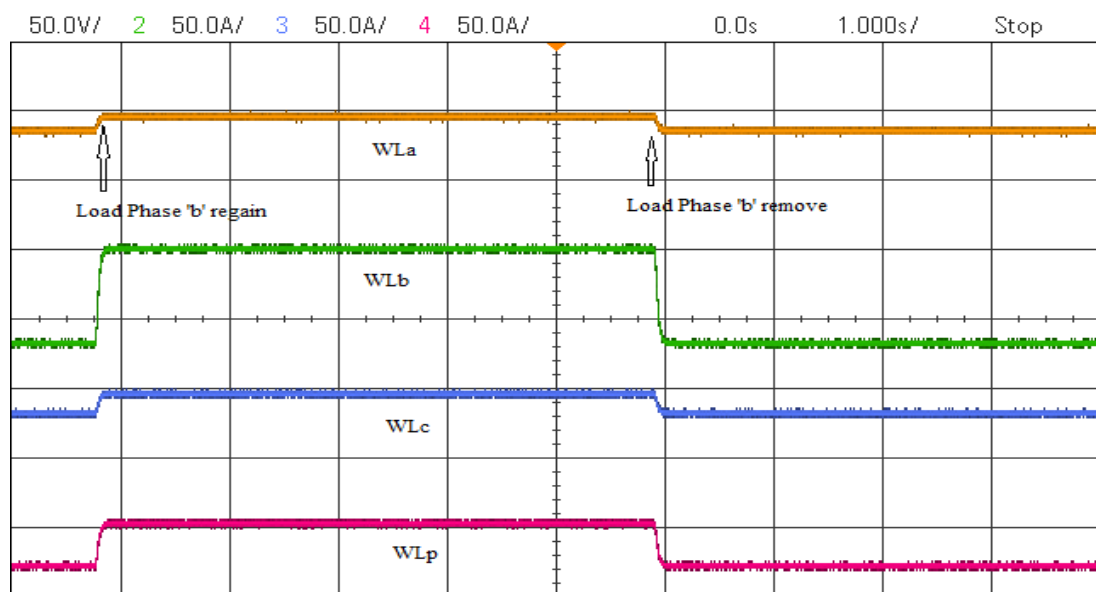


Fig. 6.47 Internal weight signals under dynamic non-linear load

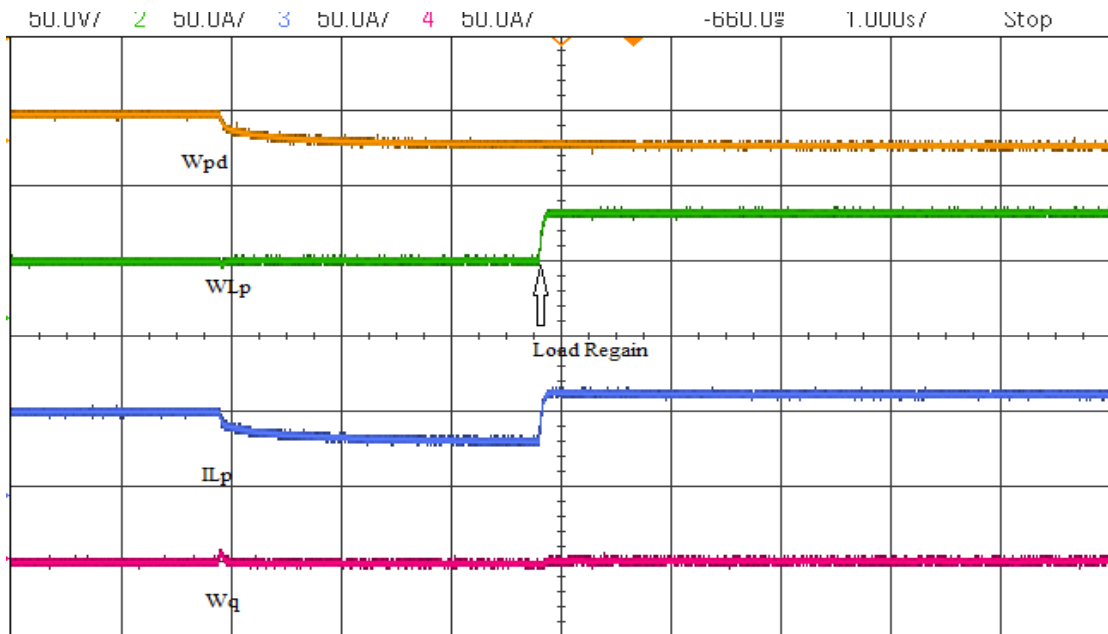


Fig. 6.48 Intermediate signals for dynamic non-linear load

6.8 PREDICTIVE CURRENT CONTROL APPROACH

6.8.1 Control algorithm

The control of VSI is required to make the output current same phase as the point of common coupling (PCC) voltages. The VSI output is synchronized with grid signal, for this purpose knowledge of PCC voltage magnitude and phase angle is needed. In the present work VSI reference currents are obtained by using synchronous reference frame (SRF) theory.

$$\begin{bmatrix} i_{\alpha} \\ i_{\beta} \\ i_0 \end{bmatrix} = \frac{2}{3} \begin{bmatrix} 1 & -\frac{1}{2} & -\frac{1}{2} \\ 0 & \frac{\sqrt{3}}{2} & -\frac{\sqrt{3}}{2} \\ \frac{1}{2} & \frac{1}{2} & \frac{1}{2} \end{bmatrix} \begin{bmatrix} i_{la} \\ i_{lb} \\ i_{lc} \end{bmatrix} \quad (6.120)$$

$$\begin{bmatrix} i_d \\ i_q \end{bmatrix} = \begin{bmatrix} \cos\theta & \sin\theta \\ -\sin\theta & \cos\theta \end{bmatrix} \begin{bmatrix} i_{\alpha} \\ i_{\beta} \end{bmatrix} \quad (6.121)$$

$$\begin{bmatrix} i_{inva}^* \\ i_{invb}^* \\ i_{invc}^* \end{bmatrix} = \frac{2}{3} \begin{bmatrix} 1 & 1 & 0 \\ 1 & -\frac{1}{2} & \frac{\sqrt{3}}{2} \\ 1 & -\frac{1}{2} & -\frac{\sqrt{3}}{2} \end{bmatrix} \begin{bmatrix} i_0 \\ i_\alpha^* \\ i_\beta^* \end{bmatrix} \quad (6.122)$$

i_{inva}^* , i_{invb}^* and i_{invc}^* depicts the extracted signals from the SRF theory control and being used as a reference signals for the switching pulses generation of VSC.

In the next step predictive current control algorithm is being used to control VSI. Reference current will be the input to the predictive current controller along with the actual current injected at PCC by the VSI. Predictive control need the model of the given system in order to predict the behavior. For this system current through interfacing inductor I_{inv} and capacitor voltage C_{se} of RC filter V_{se} are being taken as state variables. Dynamic of the proposed system can be expressed by using following differential equation:

$$\frac{dI_{inv}}{dt} = \frac{uV_{dc}}{L_f} - \frac{V_{se}}{L_f} - \frac{V_t}{L_f} - \frac{R_f I_{inv}}{L_f} \quad (6.123)$$

$$\frac{dV_{se}}{dt} = \frac{I_{inv}}{C_{se}} \quad (6.124)$$

Further equation (6.123) and (6.124) can be rewritten in matrix form as given:

$$\dot{x} = \begin{bmatrix} \frac{-R_f}{L_f} & \frac{-1}{L_f} \\ \frac{1}{C_{se}} & 0 \end{bmatrix} \begin{bmatrix} I_{inv} \\ V_{se} \end{bmatrix} + \begin{bmatrix} \frac{-1}{L_f} & \frac{V_{dc}}{L_f} \\ 0 & 0 \end{bmatrix} \begin{bmatrix} V_t \\ u \end{bmatrix} \quad (6.125)$$

The time domain solution of above mention equation can be written as:

$$x(t) = e^{C(t-t_0)}x(t_0) + \int_{t_0}^t e^{C(t-\tau)}DZ(\tau)d\tau \quad (6.126)$$

In the above equation discrete solution of the continuous state can be observed by putting $t_0=kT_d$ and $t = (kT_d + T_d)$.

$$x(k+1) = e^{C(t-t_0)}x(k) + \int_{kT_d}^{kT_d+T_d} e^{C(kT_d+T_d-\tau)}DZ(\tau)d\tau \quad (6.127)$$

Where, T_d and k represents kth sampling period and sample respectively. Equation (18) can be simplified as given below by changing the integration variables:

$$x(k+1) = e^{CT_d}x(k) + \int_0^{T_d} e^{C\alpha} D d\alpha z(k) \quad (6.128)$$

Further, the above equation can be written as:

$$x(k+1) = Rx(k) + Sz(k) \quad (6.129)$$

Matrices R and S can be obtained as:

$$R = \begin{bmatrix} R_{11} & R_{12} \\ R_{13} & R_{14} \end{bmatrix} = e^{CT_d} \approx I + CT_d + \frac{C^2 T_d^2}{2}$$

$$\approx \begin{bmatrix} 1 - \frac{R_f T_d}{L_f} - \frac{T_d^2}{2L_f} \left[\frac{1}{C_{se}} - \frac{R_f^2}{L_f} \right] & -\frac{T_d}{L_f} + \frac{T_d^2 R_f^2}{2L_f^2} \\ \frac{T_d}{C_{se}} - \frac{T_d^2 R_f}{2L_f C_{se}} & 1 - \frac{T_d^2}{2L_f C_{se}} \end{bmatrix} \quad (6.130)$$

$$S = \begin{bmatrix} S_{11} & S_{12} \\ S_{13} & S_{14} \end{bmatrix} = \int_0^{T_d} e^{C\alpha} D d\alpha \approx \int_0^{T_d} (I + C\alpha) D d\alpha$$

$$\approx \begin{bmatrix} -\frac{T_d}{L_f} + \frac{T_d^2 R_f^2}{2L_f^2} & \frac{V_{dc} T_d}{L_f} - \frac{V_{dc} T_d^2 R_f}{2L_f^2} \\ -\frac{T_d^2}{2L_f C_{se}} & \frac{T_d^2 V_{dc}}{2L_f C_{se}} \end{bmatrix} \quad (6.131)$$

State space domain dynamics of the proposed system can be described as:

$$I_{inv}(k+1) = R_{11}I_{inv}(k) + R_{12}V_{se}(k) + S_{11}V_t(k) + S_{12}u(k) \quad (6.132)$$

Inverter current primarily depends on the different VSI parameters like V_{dc} , C_{se} , L_f and k etc. The switching pattern of VSI require the future inverter current information, which is not known at the k th sampling period. Therefore, a cost function is taken and can be written as:

$$F = [I_{inv}^*(k+1) - I_{inv}(k+1)]^2 \quad (6.133)$$

In the above equation $I_{inv}^*(k+1)$ denotes the reference current of VSI at $(k+1)$ th sampling time. Reduction in error in between actual and predicted value and minimization of cost function can be done with the help of $u(k)$. Hence cost function is divided by $u(k)$, being equal to zero and cost function minimum value is given as

$$I_{inv}^*(k+1) = I_{inv}(k+1) \quad (6.134)$$

$$I_{inv}^*(k+1) = R_{11}I_{inv}(k) + R_{12}V_{se}(k) + S_{11}V_t(k) + S_{12}u(k) \quad (6.135)$$

$$u(k) = \frac{I_{inv}^*(k+1) - R_{11}I_{inv}(k) - R_{12}V_{se}(k) - S_{11}V_t(k)}{S_{12}} \quad (6.136)$$

Quadratic forecasting [183] for a step ahead of inverter current can be achieved by using second-order Lagrange extrapolation function given as:

$$I_{inv}^*(k+1) = I_{inv}^*(k) - 3I_{inv}^*(k-1) + I_{inv}^*(k-2) \quad (6.137)$$

The initial values of k_{th} , $(k-1)_{th}$ and $(k-2)_{th}$ samples in above equation are considered as zero. After predicted reference current, equation (6.137) is used to obtain the switching pattern of VSI. The switching strategy is necessary in order to obtain balanced and unity power factor (UPF) operation at point of common coupling. This given strategy provides in fast and accurate tracing of current which is known as reference.

6.8.2 Results and discussions

A simulation model of a grid tied solar PV system with the voltage source inverter has been developed and implemented in MATLAB/Simulink environment using variable step size P&O and predictive current control algorithm. The simulation studies of the proposed system has been performed under STC conditions and different solar irradiance levels with different kind of loads such as linear, nonlinear, balanced and unbalanced to test feasibility of the proposed control technique. Performance of the proposed system has been tested for various parameters such as grid voltage (V_s), DC bus voltage (V_{dc}), AC grid currents, (i_s), load currents, (I_L) the real power from and to the grid (P_g), the reactive power (Q_g), solar PV current (I_{pv}), solar PV voltage (V_{pv}), solar PV power (P_{pv}), inverter current (I_{inv}) and terminal voltage at PCC (V_t). Fig. 6.49 and 6.50 shows performance of the system for linear load for steady state PFC operation and transient operation respectively.

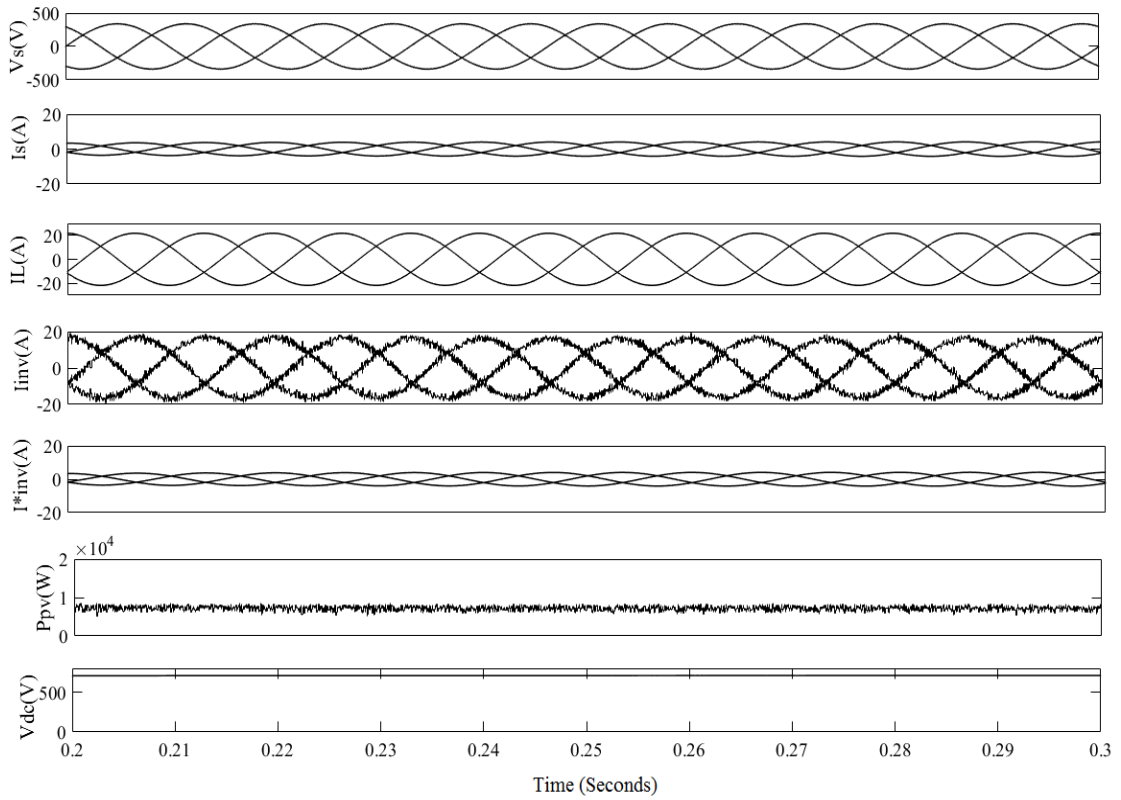


Fig. 6.49 Performance under steady state linear load conditions in PFC mode for predictive current control

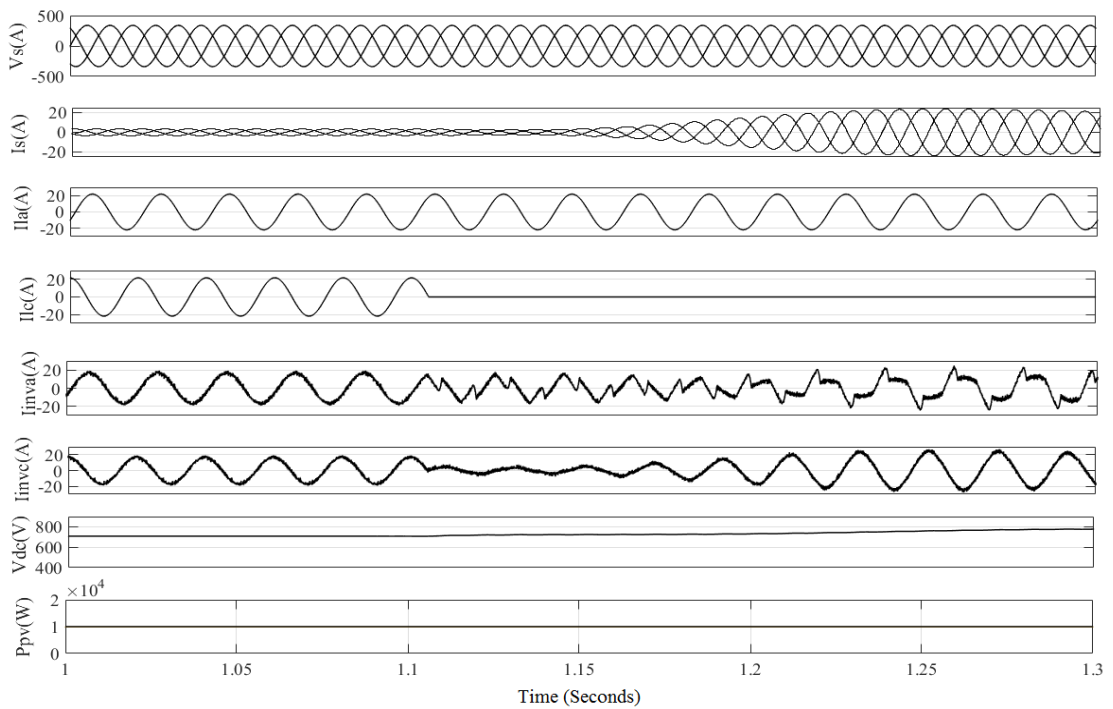


Fig. 6.50 Performance under dynamic linear load conditions for predictive current control

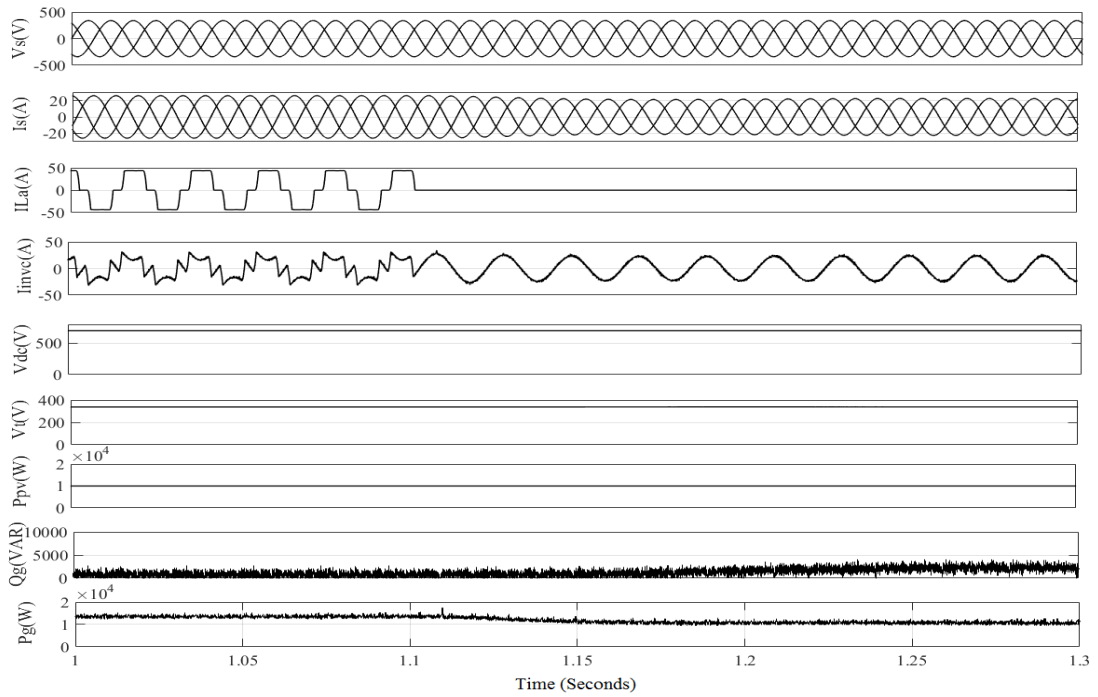


Fig. 6.51 Performance under dynamic non-linear load conditions in ZVR mode for predictive current control

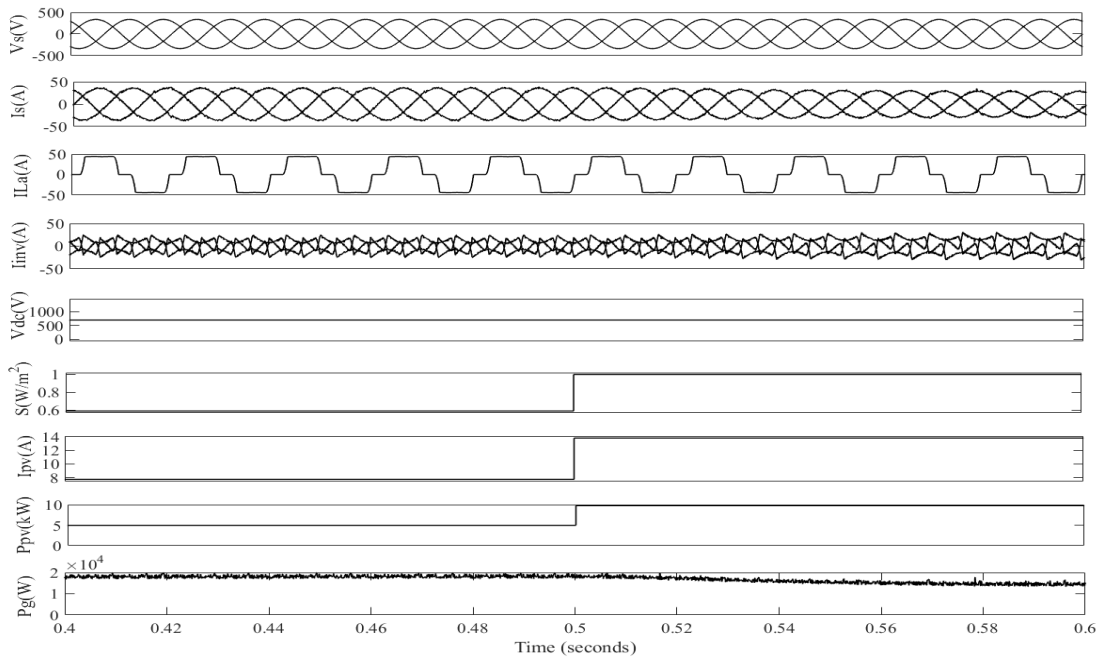


Fig. 6.52 Performance under variable solar irradiance for predictive current control

Fig. 6.51 shows dynamic behavior of developed system under unbalanced nonlinear load for zero voltage regulation (ZVR) operation. For removal of load phase

'c' at 1.1 s, grid currents (i_s) are maintained sinusoidal with the help of VSI. V_t and V_{dc} are maintained at 415 V and 700 V, respectively without any significant fluctuations.

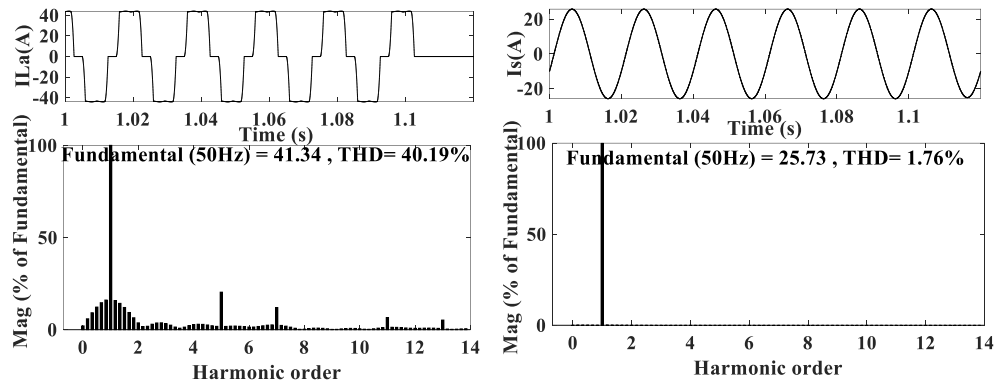


Fig. 6.53 THD spectrum of load and grid current predictive current control

Fig. 6.52 shows the performance of the system at variable solar irradiance (S) condition. Fig. 6.53 shows the THDs at PCC for load current phase 'a' and grid current respectively and obtained as 40.19% and 1.76% respectively. The proposed predictive current control of grid tied SPV VSI has successfully improved the performance of the developed system. Developed system subjected to unbalancing in load current and variation in irradiance, the given results shows satisfactory performance and continues to remain in unity power factor operation with reactive power compensation, load balancing, maximum power extraction and harmonics elimination.

6.9 ADAPTIVE NOTCH FILTER AND ANFIS BASED DC LINK VOLTAGE CONTROLLER FOR PV SYSTEM

6.9.1 Control algorithm

(a) Calculation of amplitude of terminal voltage and unit templates:

In-phase and quadrature unit templates can be calculate in similar manner as equation (6.33) – equation (6.36).

(b) Reference grid currents generation:

In this approach to estimate the fundamental active and reactive power components of load currents, we calculate the difference between actual load current and fundamental component of load current, this will be the error signal. Unit amplitude templates are in phase and quadrature component of source voltage, which are of unit magnitude. These templates are used by reference current at the later part of the algorithm. They are used to provide phase difference to different components of current so that they can be compared with actual current for generation of firing pulses.

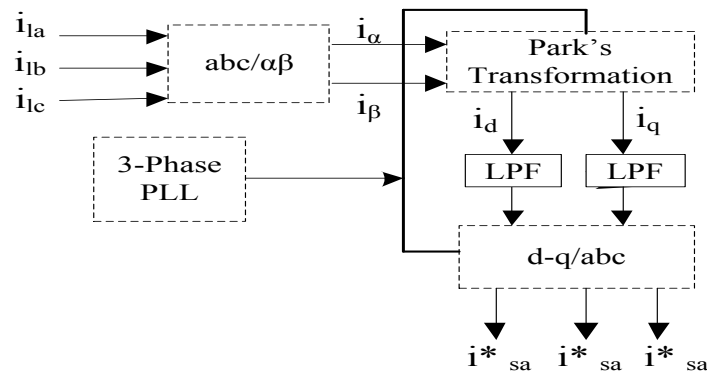


Fig. 6.54 Calculation of reference current

(c) ANFIS based DC link voltage Controller:

DC link voltage control strategy is given in Fig. 6.55 and depends on the energy balance at the input and output of VSC. The DC link voltage controller processes the error signal (difference between reference DC link voltage and actual DC link voltage) and produce a direct current component i_{DC} which goes to the reference current generation to counter the imbalances in energy. A simple first order PI controller is used in conventional DC link control approaches. In this work, the ANFIS based DC link voltage controller is being used to replace simple PI controller.

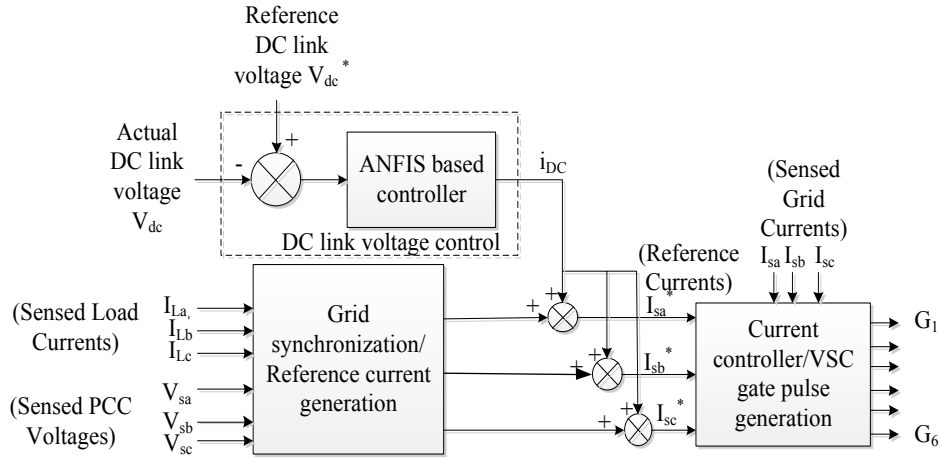


Fig. 6.55 Schematic of VSC control

ANFIS is the combination of neural network and the fuzzy inference system. The system use fixed membership functions chosen arbitrarily and rule base structure which is necessarily predetermined by the interpretation of user by using variable's characteristics of the system. Neural network precisely tune the rules of the initial fuzzy model to generate the final ANFIS model of the system. Considering $f(e, \Delta e)$, two rules of Sugeno FIS is formed and given as:

$$\text{Rule 1: if } e \text{ is } X_1 \text{ and } \Delta e \text{ is } Y_1 \text{ then } f_1 = a_1 e + b_1 \Delta e + c_1$$

$$\text{Rule 2: if } e \text{ is } X_2 \text{ and } \Delta e \text{ is } Y_2 \text{ then } f_2 = a_2 e + b_2 \Delta e + c_2$$

Individual layers of ANFIS structure are described below:

Layer 1: At this layer, every node denoted as i which is adaptive in nature:

$$O_i^1 = \mu_{X_i}(e) \quad (6.138)$$

Where, error (e) is the input to i^{th} node. μ_{X_i} is the membership function of X_i given as:

$$\mu_{X_i}(e) = \frac{1}{1 + \left[\left(\frac{e - r_i}{p_i} \right)^2 \right]^{q_i}} \quad (6.139)$$

Layer 2: Nodes of layer 2 act as a fixed node and determine the weight w_i for a rule.

Output of each node is calculated as product of all input signals and can be written as:

$$O_i^2 = w_i = \mu_{X_i}(e) * \mu_{Y_i}(\Delta e), \quad i = 1, 2 \quad (6.140)$$

Layer 3: At this layer each i^{th} node determines the ratio of i^{th} rule's firing strength to the sum of firing strengths of every rule. The output is written as:

$$O_i^3 = \bar{w}_i = \frac{w_i}{w_1+w_2}, \quad i = 1,2 \quad (6.141)$$

Layer 4: In this layer is an adaptive node with a node function given by

$$O_i^4 = \bar{w}_i f_i = \bar{w}_i (a_i x + b_i y + c_i), \quad i = 1,2 \quad (6.142)$$

Layer 5: This layer has a fixed node and calculates the final output as summation of all incoming signals which is written as:

$$O_i^5 = \sum_i \bar{w}_i f_i = \frac{\sum_i \bar{w}_i f_i}{\sum_i \bar{w}_i} \quad (6.143)$$

$$\begin{aligned} f &= \frac{w_1}{w_1+w_2} f_1 + \frac{w_2}{w_1+w_2} f_2 = \bar{w}_1 f_1 + \bar{w}_2 f_2 \\ &= (\bar{w}_1 e) a_1 + (\bar{w}_1 \Delta e) b_1 + (\bar{w}_1) c_1 + (\bar{w}_2 e) a_2 + (\bar{w}_2 \Delta e) a_2 + (\bar{w}_2) c_2 \end{aligned} \quad (6.144)$$

6.9.2 Results and discussions

The performance of proposed system in terms of PV output power, PV voltage, PV current, DC link voltage, grid voltage, grid current etc. found satisfactory. The solar irradiance (S) is raised to STC (1000 W/m²) from 600 W/m² at 0.5 s in Fig. 6.56 in grid connected configuration, the grid power (P_g) reduced after this when SPV power (P_{pv}) is increasing. Hence, SPV system is fulfilling the demand of the load and excess generation is being fed to the grid. THD analysis of the system which is less approx. 2.18 % and within limits as per the IEEE 519-2014 standards.

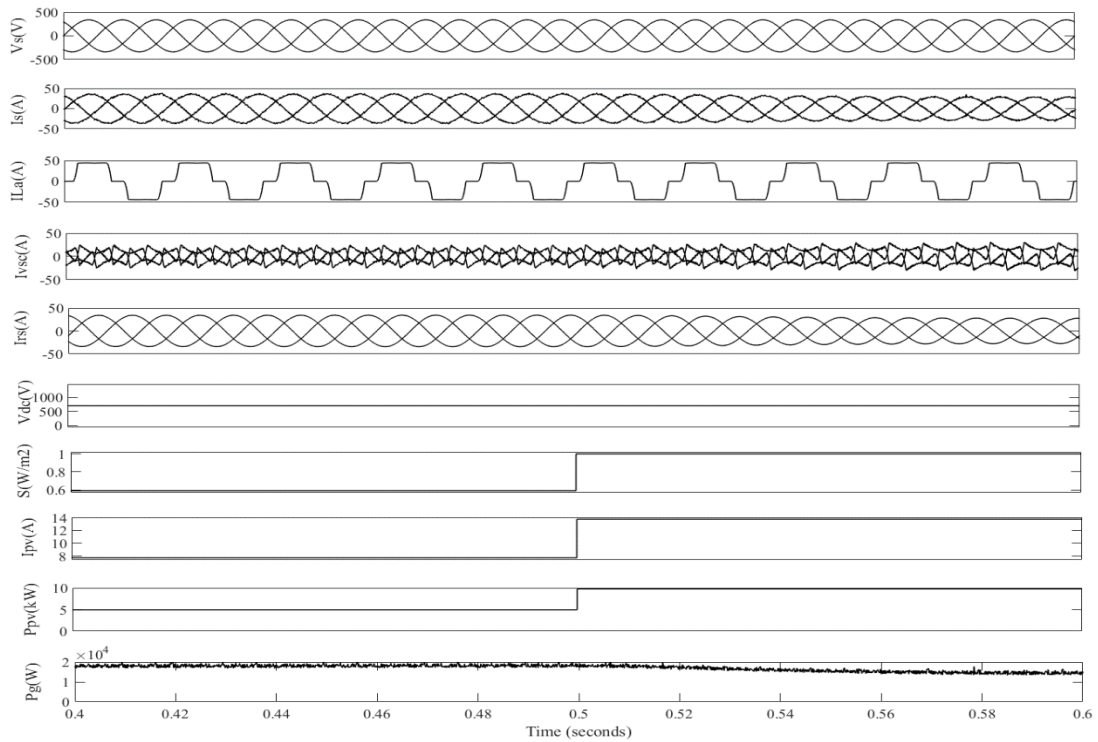


Fig. 6.56 Performance of proposed algorithm for Non-linear load with variable solar irradiance

6.10 CONCLUSION

The control algorithms have been designed and developed for the control of three phase grid connected solar PV system. These algorithms have been developed using intelligent control algorithms such as ANN, GNN. The performance analysis of these algorithms are discussed by considering various system parameters.

The developed system is subjected to load unbalancing and variable solar insolation to validate the performance of the proposed controllers and the results show satisfactory performance of the system with continuous operation under UPF mode with providing reactive power compensation, load balancing, maximum power extraction and grid harmonic reduction, gives very fast response.

The system has acceptable limits of harmonics in grid currents and voltage fluctuations according to the IEEE-519 and IEEE-1547 standards. The developed control strategies shall be advantageous for power system engineers to integrate more RES based generation systems with the utility grid.

CHAPTER 7

CONTROL AND STABILITY STUDIES OF GRID TIED SPV SYSTEM

7.1 INTRODUCTION

In previous chapter, intelligent control algorithms have been designed and developed for the control of three phase grid connected solar PV system. The performance analysis of these algorithms were discussed by considering various system parameters. In this chapter a robust controller is proposed for three phase grid connected PV system considering nonlinear and uncertain behavior. The proposed controller consists of a super twisting algorithm based second order sliding mode control. The controller is such designed to control DC link voltage and injected grid current in order to achieve maximum power from solar PV array. Uncertainties in solar PV system output is considered as the input conditions changes. The performance analysis of the proposed controller is demonstrated under different scenarios and meteoroidal conditions. The proposed system performs very well under transient conditions and gives very fast response.

Various nonlinear controller have been developed, such as robust controllers, feedback linearization, neural network based, sliding mode control and H_∞ controllers, etc. Sliding mode controllers (SMC) shows very robust performance considering system parameter variations and external disturbances. But standard first order sliding mode controller has the drawback of chattering phenomenon. This limitation can be improved significantly by designing high order sliding mode controllers. High order sliding mode control techniques have many applications in various nonlinear uncertain systems [181-186] but limited applications in grid connected solar PV systems. The

proposed controller consists of a super twisting algorithm based second order sliding mode control. Maximum power is extracted using INC method with variations in solar irradiations. The effectiveness of the proposed controller is tested under variable atmospheric conditions. The performance is also tested for different system conditions, such as single-line-to-ground fault and three phase faults. The stability analysis of the internal system dynamics is also discussed and control law is derived.

7.2 SYSTEM DESCRIPTION

The system consists of various components such as PV array; a three-phase voltage source converter, ripple filter and the transformer to integrate with the distribution grid at PCC. The three-phase solar PV system connected to distribution grid using single stage topology is considered. A Vikram Solar ELDORA 270 of 270.66 W_p solar PV module has been used in series-parallel combination to obtain a 100 kW_p solar PV array. The solar PV array is connected to the distribution system with the help of VSC and LCL filters. The proposed system considered in this study is shown in Fig. 7.1.

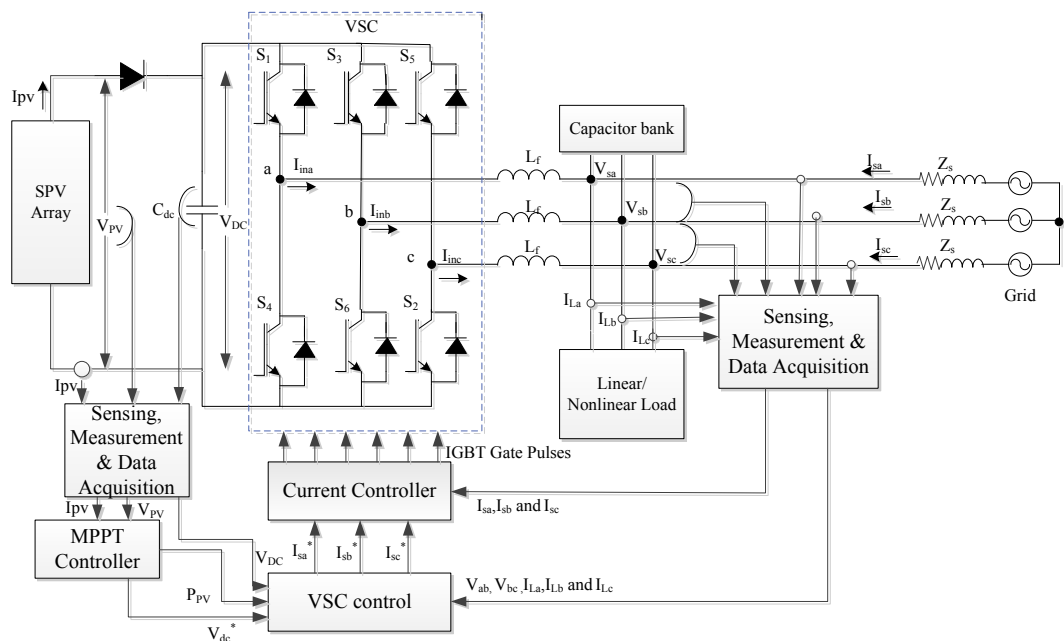


Fig. 7.1 Proposed system for stability studies

7.3 SPV SYSTEM MODELLING

The proposed system utilized a single stage circuit configuration and includes of a SPV array, voltage source converter (VSC), RC filter, hybrid loads and three phase AC grid. SPV array is formed by series – parallel connections of PV modules to achieve higher ratings. Further, solar cells are basic units for forming the SPV modules. At DC link the capacitor stores the output dc power of SPV array, which further converted into AC by using VSC. VSC deploys three arms and each arm made up of two semiconductor switches (IGBT) with antiparallel diodes. IGBT devices ratings decided according to the RMS load current and top and bottom switches of each arm switched in complementary manner. A low pass filter for each phase is used to add sufficient impedance on AC side inverter and eliminate the harmonics of VSC output. The SPV array output current equation can be written as:

$$I_{PV} = I_{sc}N_p - N_s I_o \left[\exp \left\{ \frac{q(V_{PV} + I_{PV}R_s)}{N_s A k T} \right\} - 1 \right] V_{PV} + \frac{I_{PV}R_s}{R_p} \quad (7.1)$$

Reverse saturation current I_{rs} is given as:

$$I_{rs} = I_{scref} + \left[\exp \left(\frac{qV_{oc}}{N_s k A T} \right) - 1 \right] \quad (7.2)$$

Saturation current (I_o) as a function of temperature given as:

$$I_o = I_{rs} \left[\frac{\left(\frac{T}{T_{ref}} \right)^3 e^{qCg}}{A k} * \left(\frac{1}{T_{ref}} - \frac{1}{T} \right) \right] \quad (7.3)$$

Where, k denotes the Boltzmann constant ($1.38 \times 10^{-23} \text{ J K}^{-1}$), q the electronic charge ($1.602 \times 10^{-19} \text{ C}$), T cell temperature (K); A diode ideality factor, R_s the series resistance (Ω) and R_p is the shunt resistance (Ω). N_s and N_p are number of cells connected in series and parallel respectively.

7.3.1 State space modelling

This section deals with state-space form analysis of a grid connected 3 phase-SPV system. Two loops can be obtained at the output side of the inverter. If i_a, i_b and i_c are the inverter's output currents for phase A, B and C respectively and voltage across ripple filter capacitors are considered as v_{fca}, v_{fcb} and v_{fcc} . Applying KVL at the loop before the LCL filter:

$$\begin{aligned} \dot{i}_a &= -\frac{R}{L_f} i_a - \frac{v_{fca}}{L_f} + \frac{v_{pv}}{3L_f} (2G_a - G_b - G_c) \\ \dot{i}_b &= -\frac{R}{L_f} i_b - \frac{v_{fcb}}{L_f} + \frac{v_{pv}}{3L_f} (-G_a - 2G_b - G_c) \\ \dot{i}_c &= -\frac{R}{L_f} i_c - \frac{v_{fcc}}{L_f} + \frac{v_{pv}}{3L_f} (-G_a - G_b - 2G_c) \end{aligned} \quad (7.4)$$

In above equations G_a, G_b and G_c are taken as input switching signals for phase A, B and C respectively. Further, by applying KCL at the loop after the filter:

$$\begin{aligned} v_{fca} &= \frac{1}{C_r} (i_a - i_a') \\ v_{fcb} &= \frac{1}{C_r} (i_b - i_b') \\ v_{fcc} &= \frac{1}{C_r} (i_c - i_c') \end{aligned} \quad (7.5)$$

Where, i_a', i_b' and i_c' are the output currents of LCL filter. The state space equations for grid side loop can be obtained as:

$$\begin{aligned} \dot{i}_a' &= \frac{1}{L_s} (v_{fca} - E_a) \\ \dot{i}_b' &= \frac{1}{L_s} (v_{fcb} - E_b) \\ \dot{i}_c' &= \frac{1}{L_s} (v_{fcc} - E_c) \end{aligned} \quad (7.6)$$

Further applying KCL at input node of the inverter:

$$v_{pv} \dot{=} \frac{1}{C} (i_{pv} - i_{dc}) \quad (7.7)$$

Inverter output current can be written as:

$$i_{dc} \dot{=} i_a G_a + i_b G_b + i_c G_c \quad (7.8)$$

Combining above two equations:

$$v_{pv} \dot{=} \frac{1}{C} i_{pv} - \frac{1}{C} i_a G_a + i_b G_b + i_c G_c \quad (7.9)$$

The above equations (7.4), (7.5), (7.6) and (7.9) explains the complete state space modelling of grid connected SPV system which is nonlinear and time variant in nature. To introduce simplicity in control the complete model is transformed in d-q frame for a grid angular frequency (ω).

$$\begin{aligned} \dot{I}_d &= -\frac{R}{L_f} I_d + \omega I_q - \frac{v_{fcd}}{L_f} + \frac{v_{pv}}{L_f} G_d \\ \dot{I}_q &= -\frac{R}{L_f} I_q - \omega I_d - \frac{v_{fcq}}{L_f} + \frac{v_{pv}}{L_f} G_q \\ v_{pv} \dot{=} &\frac{1}{C} i_{pv} - \frac{1}{C} I_q G_d + \frac{1}{C} I_q G_q \\ v_{fcd} \dot{=} &\omega v_{fcq} + \frac{1}{C_r} (I_d - I_d') \\ v_{fcq} \dot{=} &-\omega v_{fcd} + \frac{1}{C_r} (I_q - I_q') \\ \dot{I}_d' &= -\omega I_q' + \frac{1}{L_s} (v_{fcd} - E_d) \\ \dot{I}_q' &= -\omega I_d' + \frac{1}{L_s} (v_{fcq} - E_q) \end{aligned} \quad (7.10)$$

Above equations depict the complete mathematical modelling of 3 phase grid connected SPV system in state space form considering inverter, LCL filter and grid etc. It can be observed from the modelling equations that the model exhibit nonlinearity in nature due to SPV array output current and switching signals. Since rotating reference frame is considered synchronized with source, hence E_d component is equal to zero in

above equation. Where, G_d and G_q are defined as switching signals in d-q frame: $I_{dq} =$

$$M_{abc}^{dq} i_{abc}, E_{dq} = M_{abc}^{dq} E_{abc} \text{ and } G_{dq} = M_{abc}^{dq} G_{abc}.$$

$$M_{abc}^{dq} = \frac{2}{3} \begin{bmatrix} \cos\omega t & \cos(\omega t - 120) & \cos(\omega t + 120) \\ \sin\omega t & \sin(\omega t - 120) & \sin(\omega t + 120) \\ 1/2 & 1/2 & 1/2 \end{bmatrix} \quad (7.11)$$

Generally for practical implementation it is required to track instantaneous value of grid frequency. Enhanced phase locked loop (EPLL) based PLL is used for this work and shown in Fig 7.2.

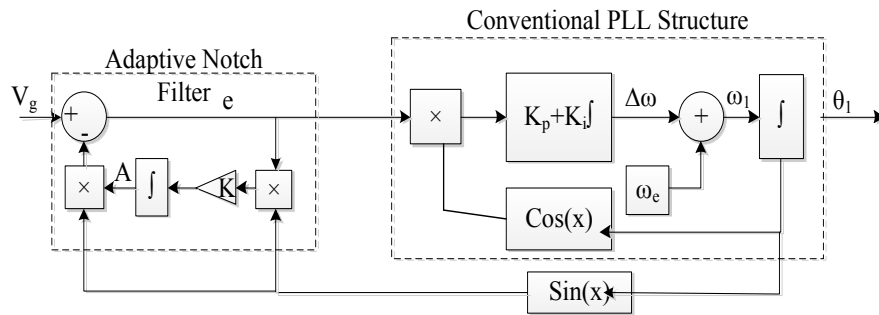


Fig. 7.2 Phase locked loop (PLL) for proposed controller

7.3.2 SPV system modelling considering uncertainties

The controller should be design to achieve maximum power output from solar PV array. This should control the DC link voltage and grid injected current. The dynamics of the VSC output current I_q have direct relationship with the IGBT switching signals. V_{DC} and I_q are the two control objectives for the proposed controller. The model of a three-phase grid-connected solar PV system can be represented by equation (7.12) with two control inputs G_d and G_q , can be further expressed as:

$$\dot{x} = f(x) + h_1(x) u_1 + h_2(x) u_2 \quad (7.12)$$

$$y_1 = g_1(x) \quad (7.13)$$

The model of a three-phase grid-connected solar PV system can be represented by equation (7.10) with two control inputs and can be further expressed as:

$$y_2 = g_2(x) \quad (7.14)$$

The controller model has two control objectives in terms of DC link voltage v_{dc} and quadrature axis current in d-q frame I_{1q} . From comparing equation (7.10) and equation (7.12),

$$x = [I_d \ I_q \ v_{pv} \ v_{fcd} \ v_{fcq} \ I_d' \ I_q']^T \quad (7.15)$$

$$f(x) = \begin{bmatrix} -\frac{R}{L_f} I_d + \omega I_q - \frac{v_{fcd}}{L_f} \\ -\frac{R}{L_f} I_q - \omega I_d - \frac{v_{fcq}}{L_f} \\ \frac{1}{C} i_{pv} \\ \omega v_{fcq} + \frac{1}{C_r} (I_d - I_d') \\ -\omega v_{fcd} + \frac{1}{C_r} (I_q - I_q') \\ -\omega I_q' + \frac{1}{L_s} (v_{fcd} - E_d) \\ \dot{I}_q' = -\omega I_d' + \frac{1}{L_s} (v_{fcq} - E_q) \end{bmatrix} \quad (7.16)$$

$$h(x) = \begin{bmatrix} \frac{v_{pv}}{L_f} & 0 \\ 0 & \frac{v_{pv}}{L_f} \\ -\frac{1}{C} I_d & -\frac{1}{C} I_q \\ 0 & 0 \\ 0 & 0 \\ 0 & 0 \end{bmatrix} \quad (7.17)$$

$$u = [G_d \ G_q]^T \quad (7.18)$$

$$y = [I_d \ I_q]^T \quad (7.19)$$

The output of solar PV array significantly depends on various meteorological parameters. However, the main parameter is solar irradiance which highly influenced the solar PV array output. The variations in solar irradiance cause changes in PV power output and need to be modelled as uncertainties. These uncertainties will be in form of solar PV array output current I_{PV} and ultimately effect the injected current into the grid. Here, parametric uncertainties also considered as unknown time varying parameters.

The model of a three-phase grid-connected solar PV system considering uncertainties further expressed as:

$$\dot{x} = [f(x) + \Delta f(x)] + [h_1(x) + \Delta h_1(x)] u_1 + [h_2(x) + \Delta h_2(x)] u_2 \quad (7.20)$$

$$y_1 = g_1(x) \quad (7.21)$$

$$y_2 = g_2(x) \quad (7.22)$$

$$\Delta f(x) = \begin{bmatrix} \Delta f_1(x) \\ \Delta f_2(x) \\ \Delta f_3(x) \\ \Delta f_4(x) \\ \Delta f_5(x) \\ \Delta f_6(x) \\ \Delta f_7(x) \end{bmatrix} \quad (7.23)$$

$$\Delta h(x) = \begin{bmatrix} \Delta h_{11}(x) & 0 \\ 0 & \Delta h_{22}(x) \\ \Delta h_{31}(x) & \Delta h_{32}(x) \\ 0 & 0 \\ 0 & 0 \\ 0 & 0 \\ 0 & 0 \end{bmatrix} \quad (7.24)$$

Maximum changes that are allowed in the system parameters are considered to 30% with the changes in irradiance and ambient temperature 80% of standard values.

Further, upper bound on uncertainties are calculated as:

$$\Delta f(x) = \begin{bmatrix} -0.025 \frac{R}{L_f} I_d + 0.6\omega I_q - 0.23 \frac{v_{fcd}}{L_f} \\ -0.36 \frac{R}{L_f} I_q - 0.042\omega I_d - 0.23 \frac{v_{fcq}}{L_f} \\ 0.16 \frac{1}{C} i_{pv} \\ 0.2\omega v_{fcq} + 0.72 \frac{1}{C_r} (I_d - I_d') \\ -0.12\omega v_{fcd} + 1.2 \frac{1}{C_r} (I_q - I_q') \\ -0.12\omega I_q' + \frac{2}{L_s} (0.12v_{fcd} - E_d) \\ -0.36\omega I_d' + \frac{2}{L_s} (0.2v_{fcq} - E_q) \end{bmatrix} \quad (7.25)$$

$$\Delta h(x) = \begin{bmatrix} 0.18 \frac{v_{pv}}{L_f} & 0 \\ 0 & 0.18 \frac{v_{pv}}{L_f} \\ -0.08 \frac{I_d}{C} & -0.14 \frac{I_q}{C} \\ 0 & 0 \\ 0 & 0 \\ 0 & 0 \\ 0 & 0 \end{bmatrix} \quad (7.26)$$

7.4 DEVELOPMENT OF CONTROL ALGORITHM

7.4.1 SPV system modelling considering uncertainties

Maximum power point tracking (MPPT) control is essential to track the maximum power point (MPP) of solar PV array under varying meteorological parameters. A large number of MPPT techniques are reported. Basically, MPPT techniques are based on the reference voltage or reference current signal of the solar PV array which is adjusted to extract maximum power from the system. In this work incremental conductance (INC) based MPPT technique is used. INC method is based on the fact that the slope of the PV module curve is zero at maximum power point. This slope will be positive for values of output power smaller than MPP and negative for output power greater than maximum power point.

$$\frac{dP}{dV} = I + v \frac{dI}{dV} = 0 \quad (7.27)$$

$$\frac{dI}{dV} \cong \frac{\Delta I}{\Delta V} = -\frac{I_{PV}}{V_{PV}} \quad (7.28)$$

$$\begin{aligned} \frac{dP}{dV} = 0 \quad \frac{\Delta I}{\Delta V} &= -\frac{I_{PV}}{V_{PV}} && \text{at MPP} \\ \frac{dP}{dV} > 0 \quad \frac{\Delta I}{\Delta V} &> -\frac{I_{PV}}{V_{PV}} && \text{left side of MPP} \\ \frac{dP}{dV} < 0 \quad \frac{\Delta I}{\Delta V} &< -\frac{I_{PV}}{V_{PV}} && \text{right side of MPP} \end{aligned}$$

At maximum power point (MPP) output power from solar PV array is the maximum power supplied from the solar PV array.

$$P_{PV} = P_{ref} = V_{PV}I_{PV} \quad (7.29)$$

$$P_{ref} = P = \frac{3}{2}E_q I_{qref} \quad (7.30)$$

From equation (7.29) and (7.30)

$$I_{qref} = \frac{2}{3} \frac{P_{ref}}{E_q} \quad (7.31)$$

$$V_{PVref} = \frac{P_{ref}}{I_{PV}}; V_{PVref} = V_{dcref} \quad (7.32)$$

These reference values will be the input to the second order SMC controller.

7.4.2 Controller design

The schematic diagram of the grid connected solar PV system with the proposed controller is shown in Fig. 7.3.

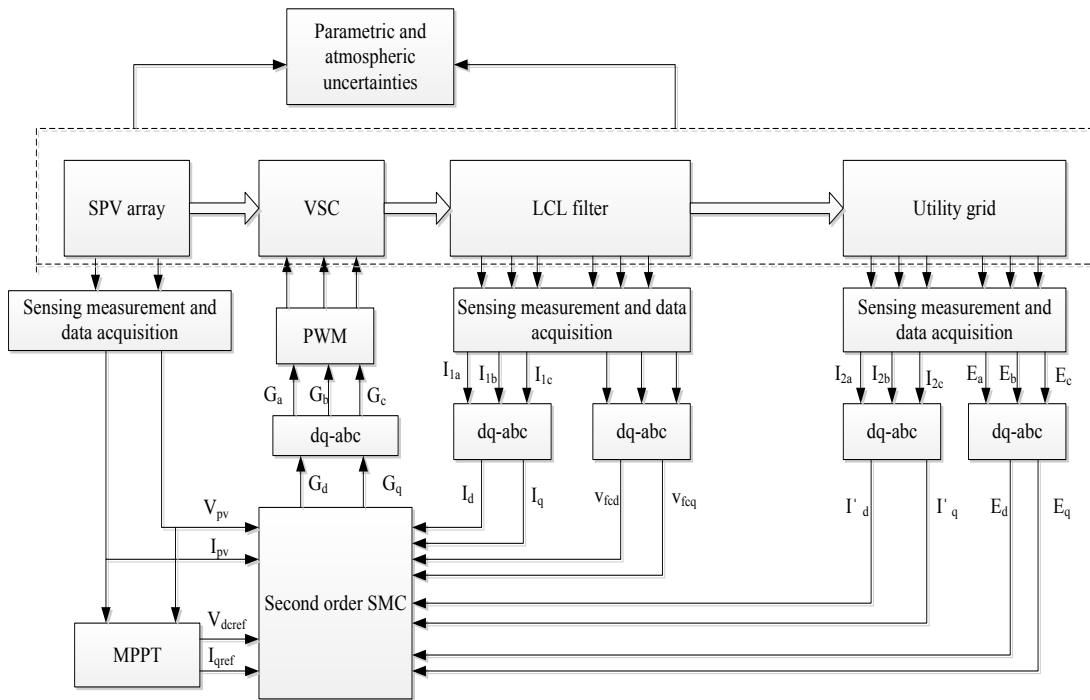


Fig. 7.3 Block diagram of proposed controller

Classical SMC suffers from the drawback known as chattering effect, while higher order SMC does not influence the first-order time derivative of sliding variable. It acts on higher order derivatives which results in reduction in chattering phenomenon.

The higher order SMC provide efficient sliding precision. DC link voltage V_{DC} and grid injected current I_q are the two control objectives for the proposed controller.

Control law design:

First a general SMC is designed, where the error between the actual DC link voltage V_{DC} and the reference DC link voltage V_{dcref} , is expressed as:

$$E_1 = V_{DC} - V_{dcref} \quad (7.33)$$

Further, the error between the I_q and I_{qref} , is given as:

$$E_2 = I_q - I_{qref} \quad (7.34)$$

Siding variables for above expression can be define as:

$$\sigma_1 = kE_1 + \frac{d}{dt}E_1 \quad (7.35)$$

$$= \dot{I}_q + kI_q - kI_{qref} - \dot{I}_{qref} \quad (7.36)$$

Where $k > 0$

$$\sigma_2 = E_2 = V_{DC} - V_{Dcref} \quad (7.37)$$

Further, state equations considering uncertainties becomes:

$$\dot{I}_d = -1.025 \frac{R}{L_f} I_d + 1.06\omega I_q - 1.023 \frac{v_{fcd}}{L_f} + 1.18 \frac{V_{DC}}{L_f} G_d$$

$$\dot{I}_q = -1.042 \frac{R}{L_f} I_q - 1.36\omega I_d - 1.23 \frac{v_{fcq}}{L_f} + 1.18 \frac{V_{DC}}{L_f} G_q$$

$$\dot{V}_{DC} = \frac{1.16}{c} i_{pv} - \frac{1.08}{c} I_d G_d - \frac{1.14}{c} I_q G_q$$

$$v_{fcd} = 1.2\omega v_{fcq} + \frac{1.72}{c_r} (I_d - I_d')$$

$$v_{fcq} = -1.12\omega v_{fcd} + \frac{2.21}{c_r} (I_q - I_q')$$

First order derivatives of defined sliding variables are:

$$\dot{\sigma}_1 = k\dot{E}_1 + \ddot{E}_1$$

$$= -1.042k \frac{R}{L_f} I_q - 1.36k\omega I_d - 1.23k \frac{v_{fcq}}{L_f} + 1.18k \frac{V_{DC}}{L_f} G_q + \dot{I}_q - kI_{qref} - I_{qref} \quad (7.38)$$

$$= G_1 + K_1 G_q$$

Where, G_1 contains parameter perturbation.

$$G_1 = -1.042k \frac{R}{L_f} I_q - 1.36k\omega I_d - 1.23k \frac{v_{fcq}}{L_f} + \dot{I}_q - kI_{qref} - I_{qref} \quad (7.39)$$

$$K_1 = 1.18k \frac{V_{DC}}{L_f} \quad (7.40)$$

$$\begin{aligned} \dot{\sigma}_2 = \dot{E}_2 &= V_{DC} - V_{DCref} \\ &= \frac{1.16}{c} i_{pv} - \frac{1.08}{c} I_d G_d - \frac{1.14}{c} I_q G_q - V_{DCref} \end{aligned} \quad (7.41)$$

$$= G_2 + K_2 G_d + K_3 G_q$$

Where, G_2 is contains parameter perturbation.

$$G_2 = \frac{1.16}{c} i_{pv} - V_{DCref}, K_2 = -\frac{1.08}{c} I_d, K_3 = -\frac{1.14}{c} I_q \quad (7.42)$$

As from equation (7.35) and (7.38), $\frac{\partial \sigma_1}{\partial G_q} = 0$ and $\frac{\partial \sigma_1}{\partial G_d} \neq 0$. Hence the relative

degree with respect to σ_1 is 1. For equation (7.37) and (7.41) the relative degree is also

1 with respect to σ_2 .

Approaching law method has been used and exponential approach law is selected:

$$\dot{\sigma} = -\varepsilon \cdot \text{sgn}(\sigma) - \delta \cdot \sigma \quad (7.43)$$

Where, ε and δ are the design parameters.

On combining equation (7.43), equation (7.38) and equation (7.41)

$$G_q = \frac{1}{K_1} (-\varepsilon_1 \cdot \text{sgn}(\sigma_1) - \delta_1 \cdot \sigma_1 - G_1) \quad (7.44)$$

$$G_d = \frac{1}{K_2} (-\varepsilon_2 \cdot \text{sgn}(\sigma_2) - \delta_2 \cdot \sigma_2 - G_2 - K_3 G_q) \quad (7.45)$$

Where, $\varepsilon_1, \delta_1, \varepsilon_2, \delta_2$ are control parameters which are not determined. The

switching term $\varepsilon \cdot sgn(\sigma)$ directly effects the working of controller. Because of this the control inputs G_q and G_d becomes discontinuous and chattering effect also occurs. This chattering phenomenon is avoided using super-twisting algorithm [188] and the control inputs G_q and G_d again formed as:

$$\left. \begin{aligned} G_q &= u_1 + u_2 \\ u_1 &= -\lambda_1 |\sigma_1|^{\frac{1}{2}} sgn(\sigma_1) \\ u_2 &= -\alpha_1 sgn(\sigma_1) \end{aligned} \right\} \quad (7.46)$$

$$\left. \begin{aligned} G_d &= u_3 + u_4 \\ u_3 &= -\lambda_2 |\sigma_2|^{\frac{1}{2}} sgn(\sigma_2) \\ u_4 &= -\alpha_2 sgn(\sigma_2) \end{aligned} \right\} \quad (7.47)$$

Where, $\lambda_1, \alpha_1, \lambda_2, \alpha_2$ are control parameters which are not determined. From above equations, it can be seen that the discontinuity of super-twisting theorem based second order SMC reflect only in derivative term. However, the control inputs G_d and G_q are continuous.

Stability of internal dynamics:

After developing the control law it is required to obtain the values of control parameters such that the system operates stable. Lyapunov method is used to determine the range of control parameters. To achieve a control over I_q , the ranges of λ_1 and α_1 are required. A state transformation is used as:

$$z = G_1 - \alpha_1 K_1 \int_0^t sgn(\sigma_1) d\tau \quad (7.48)$$

From equation (7.46) and (7.48):

$$\left. \begin{aligned} \dot{\sigma}_1 &= -K_1 \lambda_1 |\sigma_1|^{\frac{1}{2}} sgn(\sigma_1) + z \\ \dot{z} &= -\alpha_1 sgn(\sigma_1) + \dot{G}_1 \end{aligned} \right\} \quad (7.49)$$

Since, G_1 is differentiable with first order derivative uniformly bounded. This

satisfies:

$$|\dot{G}_1| \leq \Psi_1 \quad \forall t > 0 \quad (7.50)$$

Ψ is a positive constant.

On choosing the quadratic Lyapunov function:

$$V(\sigma, z) = \zeta^T P \zeta \quad (7.51)$$

Where, $\zeta = [\zeta_1 \quad \zeta_2]^T = [|\sigma_1|^{\frac{1}{2}} \text{sgn}(\sigma_1) \quad z]^T$

$$P = \begin{bmatrix} 2K_1\alpha_1 + \frac{1}{2}K_1^2\lambda_1^2 & -\frac{1}{2}K_1\lambda_1 \\ -\frac{1}{2}K_1\lambda_1 & 1 \end{bmatrix} \text{ is chosen as positive definite symmetric}$$

matrix.

Considering $\frac{d|x|}{dt} = \dot{x} \text{sgn}(x)$ and equation (7.49):

$$\dot{\zeta} = \frac{1}{|\zeta_1|} (A\zeta + B\widehat{G}_1) \quad (7.52)$$

In above equation:

$$A = \begin{bmatrix} -\frac{1}{2}K_1\lambda_1 & \frac{1}{2} \\ -K_1\alpha_1 & 0 \end{bmatrix} \quad B = [0 \quad 1]^T \quad \widehat{G}_1 = |\zeta_1| \dot{G}_1$$

Considering perturbed system, derivative of the Lyapunov function along with trajectories is:

$$\begin{aligned} \dot{V}(\sigma, z) &= 2\dot{\zeta}^T P \zeta \\ &= \frac{1}{|\zeta_1|} (2\zeta^T A^T + 2\widehat{G}_1 B^T) P \zeta \\ &\leq \frac{1}{|\zeta_1|} (2\zeta^T A^T P \zeta + 2\widehat{G}_1 B^T P \zeta + \Psi_1^2 |\zeta_1| - \widehat{G}_1^2) \\ &= \frac{1}{|\zeta_1|} \zeta^T (A^T P + PA + \Psi_1^2 C C^T + P B B^T P) \zeta \end{aligned} \quad (7.53)$$

Where, matrix $C = [1 \quad 0]$

Consider $M = (A^T P + PA + \Psi_1^2 C C^T + P B B^T P)$, than equation (7.53)

becomes:

$$\dot{V} \leq \frac{1}{|\zeta_1|} \zeta^T M \zeta \quad (7.54)$$

$$\dot{V} \leq \frac{1}{|\zeta_1|} \zeta^T M \zeta < 0, \text{ Satisfies Lyapunov theorem for } M \text{ to be a positive}$$

definite symmetric matrix. The system will converge in finite time to origin [189].

$$M = \begin{bmatrix} \frac{1}{2} K_1^2 \left(\frac{1}{2} K_1^2 \lambda_1^3 + \lambda_1 \alpha_1 - \frac{1}{4} \lambda_1^2 \right) - \Psi_1^2 & \frac{1}{2} K_1 (\lambda_1 - K_1^2 \lambda_1^2) \\ \frac{1}{2} K_1 (\lambda_1 - K_1^2 \lambda_1^2) & \frac{1}{2} K_1 \lambda_1 - 1 \end{bmatrix}$$

Range of α_1, λ_1 must satisfy:

$$\left. \begin{array}{l} \alpha_1 > \frac{\lambda_1^2 K_1}{4(K_1 \lambda_1 - 2)} + \frac{\Psi_1^2}{K_1 \lambda_1} \\ \lambda_1 > \frac{2}{K_1} \end{array} \right\} \quad (7.55)$$

Similarly, G_2 is also differentiable with first order derivative bound uniformly and satisfies:

$$|\dot{G}_2| \leq \Psi_2 \quad \forall t > 0$$

The ranges for α_2 and λ_2 can be obtained in similar manner:

$$\left. \begin{array}{l} \alpha_2 > \frac{\lambda_2^2 K_2}{4(K_2 \lambda_2 - 2)} + \frac{\Psi_2^2}{K_2 \lambda_2} \\ \lambda_2 > \frac{2}{K_2} \end{array} \right\} \quad (7.56)$$

The system is stable for the ranges for parameters fall into the limits.

7.5 RESULT AND DISCUSSION

This section deals with the performance analysis of the three-phase grid-connected solar PV system with the developed controller. The output voltage of the PV array is 700 V, PV output current is 14 A, with the maximum output power 10 kW. The dc-link capacitor is chosen as 10 mf, interfacing inductance is 2.6 mH with inverter switching frequency of 10 kHz. Performance analysis is carried out considering non-linear loads of real and reactive power demand 20 kW and 5 kVAR respectively as the

practical scenario. The performance is evaluated under various practical conditions and explained in further subsections

(a) Performance of developed controller under STC

In this section, the performance of developed controller is tested under standard conditions (STC). The main task for the controller is to inject maximum power into the grid. The proposed controller is ensuring the unity power factor (UPF) operation of the system considering uncertainties also and it can be seen from Fig. 7.4. Here, 30% variations are considered in the system parameters with 70% uncertainties in solar irradiation and cell temperature for the solar PV system modelling.

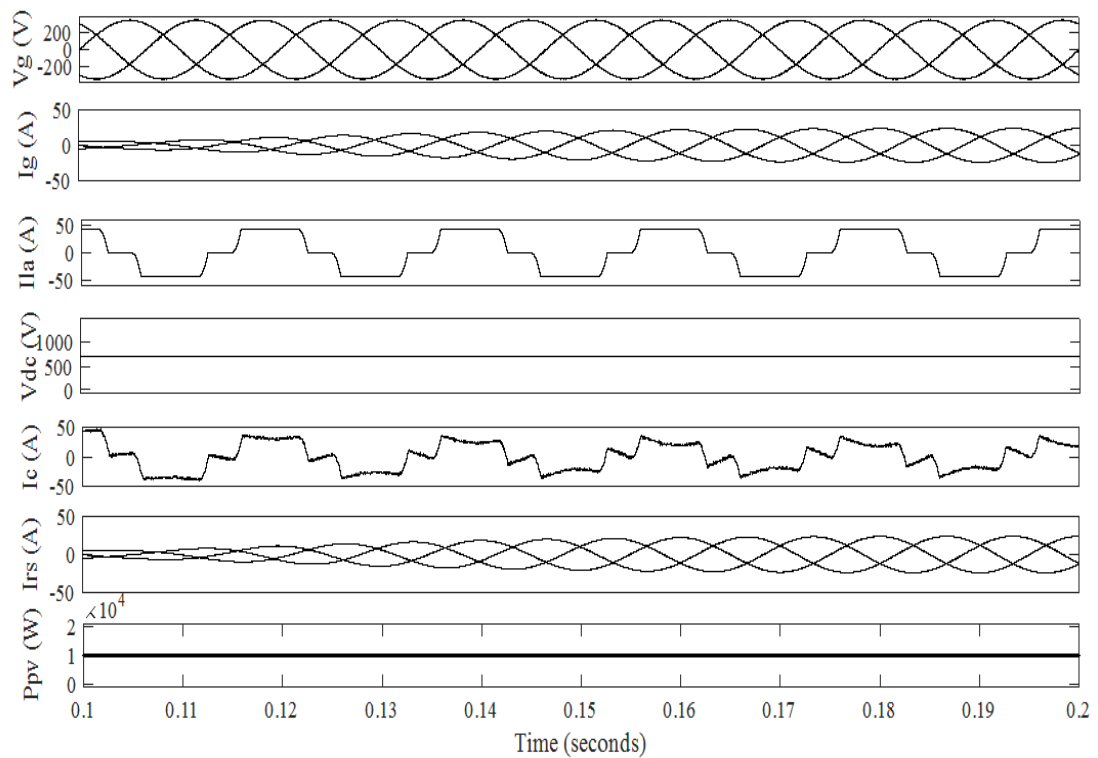


Fig. 7.4 Performance of 10 kW PV system under STC

(b) Performance of developed controller under varying meteorological parameters

The performance of the controller is also validated under varying irradiances considering DC link voltage (V_{dc}) and shown in Fig. 7.5. A small step change of 20 V

is applied in reference DC link voltage ($V_{dc\text{ref}}$). It can be clearly seen that with the help of proposed controller, DC link voltage is closely following the reference voltage irrespective of the change in solar irradiance (S). Fig. 7.6 shows the results of grid current (I_g) following the reference current (I_{rs}) for the proposed controller and a PI controller. For PI controller the grid current slightly lag behind the reference current but for the proposed controller is exactly follow the reference current even for variable irradiance. At 0.5 s the value of irradiance is changed to 800 W/m^2 , further it is changed to 1000 W/m^2 at 0.6 s. In this duration the value of grid current is increased due to decrease in PV output current because of reduction in irradiance.

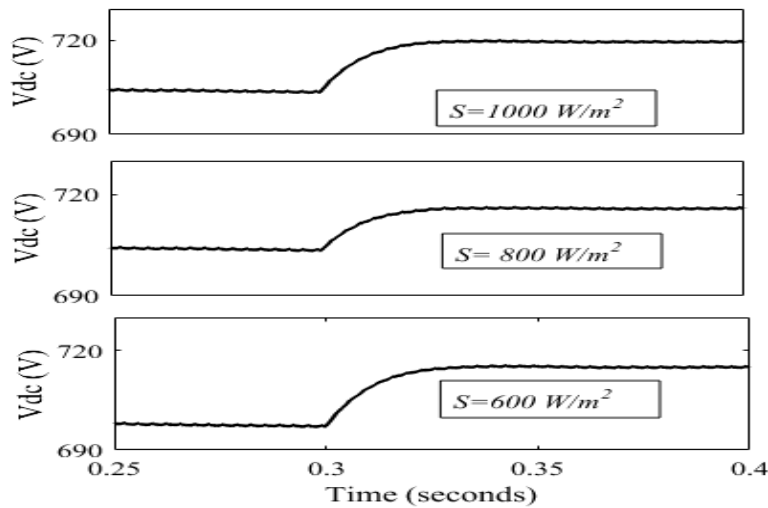


Fig. 7.5 V_{dc} (V) for various irradiances

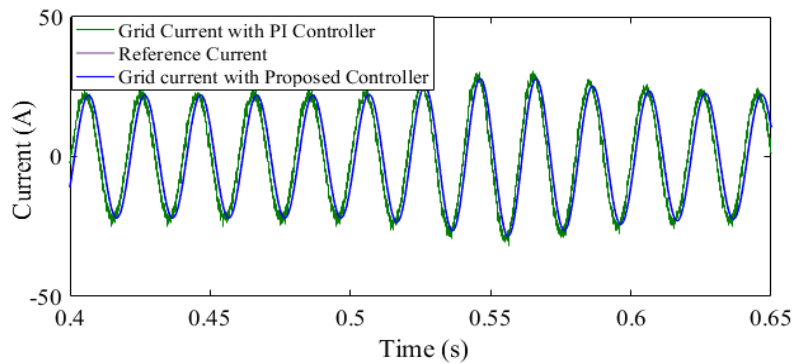


Fig. 7.6 Performance at changing atmospheric conditions in terms of Grid current compared with performance of PI controller

The response of the proposed system in terms of power is shown in Fig. 7.7. The solar irradiance is reduced to 500 W/m^2 at 0.5 s and increased back to 1000 W/m^2 at 0.58 s . It can be observed that the PV power is reduced at 0.5 s , hence grid power is increased. The reactive power (Q_g) is constant irrespective change in the solar irradiance.

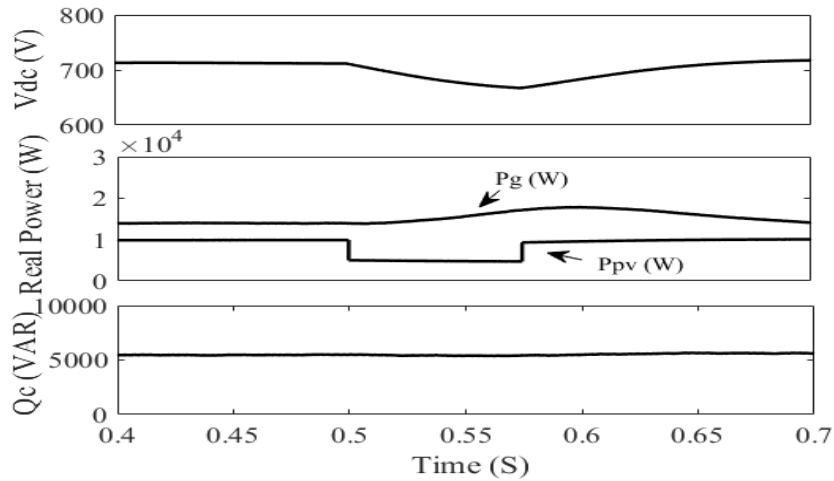


Fig. 7.7 PV array voltage for MPPT, PV array (P_{PV}) and grid power (P_g), reactive power supplied by inverter (Q_g)

(c) Performance of developed controller for LG fault

To evaluate the robustness of the proposed controller against fault condition, a single line-to-ground (LG) fault is applied to phase a on for a duration of 0.1 s from $t = 0.3$ to 0.4 s , shown in Fig. 7.8.

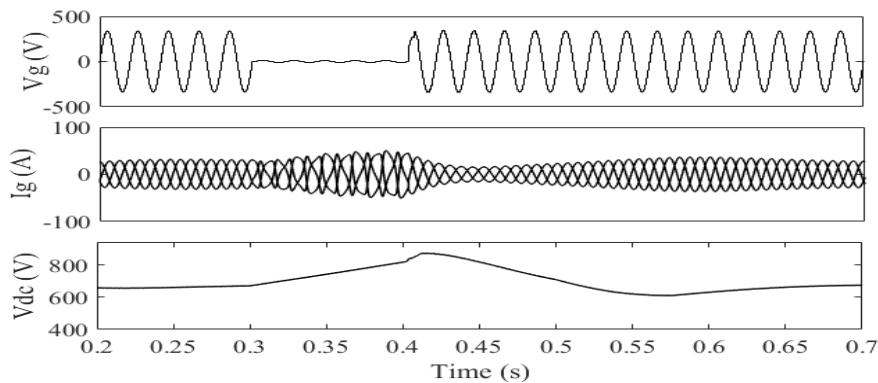


Fig. 7.8 Performance under LG fault

Due to unbalance in PCC voltage the grid current is also unbalance but once fault is cleared, it becomes stable. The positive-sequence active and reactive current are given in Fig. 7.9.

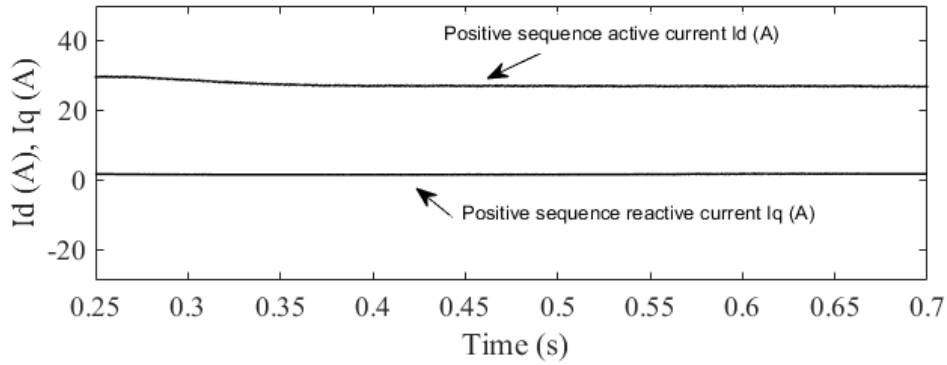


Fig. 7.9 Corresponding positive sequence active and reactive currents

(d) Performance of developed controller for three phase short circuit fault

A three phase fault is created at 0.3 s to test the performance of developed controller. Fig. 7.10 shows that the grid voltage is become zero for this duration and grid current follow the reference current. In this case solar PV system is not able to produce active power because three-phase voltage collapse. After fault clearance, the controller acts quickly and system restored.

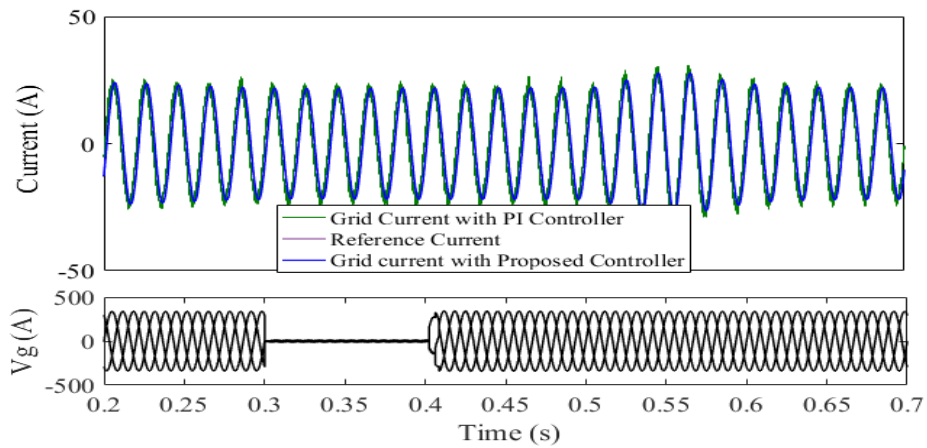


Fig. 7.10 Performance analysis for three phase short circuit fault

7.6 CONCLUSION

A robust controller based on second order sliding mode controller is developed by considering model uncertainties of a three-phase grid-connected PV system. The proposed controller ensure the operation of solar PV system at unity power factor irrespective to the changes in the atmospheric parameters. The resulting robust controller enhances the overall stability of a three-phase grid-connected PV system considering admissible network uncertainties. When the developed system is subjected to uncertainties and variable solar insolation, results shows satisfactory performance of the system and continues to operate in unity power factor mode of operation with providing reactive power compensation, and maximum power extraction.

CHAPTER 8

CONCLUSION AND FUTURE SCOPE

8.1 CONCLUSIONS OF THE CURRENT RESEARCH

The integration of solar photovoltaic (SPV) with grid as distributed generation (DG) are able to solve the demand and generation mismatch issues especially in developing countries. Challenges of integration of SPV based distributed power generation to the main grid are analysed and some of the method to mitigate these issues are presented in this thesis.

Further, the output of solar PV system highly depends on meteorological parameters. The variability and uncertainty associated with the solar energy becomes significant challenges for successful and economically efficient integration of solar power generating plants into utility grid. Hence, the forecasting of solar energy will play a significant role for sustainable power generation. The mathematical and regression models of solar energy forecasting were found satisfactory for clear sky weather condition. Due to high uncertainty in weather conditions, fuzzy logic, neural network and other intelligent approaches based models are proposed by researchers to estimate the solar irradiance at a particular location using different meteorological parameters. Short term solar energy forecasting models such as hourly, weekly are available in literature but 15 minutes ahead solar energy forecasting models are rarely available in the literature. In this work, an intelligent model based on wavelet transform and generalized neural network (GNN) is developed and proposed for the very short term solar energy forecasting. Using GNN some of the drawbacks of ANN can be overcome such as difficulty in deciding the structure of ANN, neuron type selection,

needs large training time etc. The results obtained from the proposed model are evaluated on the basis of statistical indicators like root mean square error (RMSE) and mean absolute error (MAE). From the obtained results, it is observed that the performance of the proposed model is found better as compared to the other existing models. Further, the obtained data have been used to forecast the PV power output of a PV plant.

However, the developed hybrid model has the advantage of fast convergence and stronger training and learning ability. Wavelet transform plays significant role in error points removing and enhancing the data stability. The proposed work would be useful for power engineers in proper operation and control of power plants.

Further, in this thesis, a very short term solar energy forecasting model is developed and pumped hydro storage have been selected to feed the power to the grid whenever required. A pumped hydro storage (PHS) is used to meet the grid requirements. In order to obtain more accurate and practical results, demand response (DR) program has been also integrated in the proposed system. An adequacy analysis is also carried out under various consumer flexibility scenarios. The proposed energy management system model is developed in MATLAB/Simulink platform, and validated on 5 kW PV system installed at the rooftop of laboratory.

The thesis also presents intelligent control approaches for grid connected solar PV system. Various control algorithms have been developed using intelligent approaches such as Artificial Neural Network (ANN), Generalized Neural Network (GNN), etc. These algorithms provides reactive power, harmonic compensation and help system to transmit active power to the grid and loads effectively. In this work Gradient Descent Back Propagation (GDBP) NN based $I \cos\phi$, Quasi Newton Back

Propagation (QNBP) NN based $I \cos\phi$, Extended Kalman Filter (EKF) based GNN, etc. algorithms are proposed for three phase grid connected PV system. The proposed algorithms have been developed in MATLAB/Simulink platform and also implemented on hardware prototype in laboratory. The performance analysis of these algorithms are discussed by considering various system parameters in this thesis. The system is subjected to unbalancing in load and variation in solar insolation to validate the performance. It can be observed from the results that the proposed controller gives efficient performance and provide UPF operation with reactive power compensation, load balancing, maximum power extraction and grid harmonic reduction. The developed controller acts very fast under transient conditions. The grid voltage and current harmonics are also reduced and which are within acceptable limits according to the IEEE-519 and IEEE-1547 standards. The developed control algorithms overcomes the drawbacks associated with conventional approaches for VSC grid synchronization such as not accurate for nonlinearities associated with RES based, large overshoots and long settling time in response.

A robust controller is developed for three phase grid connected PV system considering nonlinear and uncertain behavior. The proposed controller consists of a super twisting algorithm based second order sliding mode control. Maximum power is extracted using INC method with variations in solar irradiations. The effectiveness of the proposed controller is tested under variable atmospheric conditions. The performance is also tested for different system conditions, such as single-line-to-ground fault and three phase faults. The stability studies of the internal system dynamics is also discussed and control law is derived.

8.2 RECOMMENDATIONS FOR FUTURE WORK

In the current research, all efforts have been made to present the problem related to grid integrated solar PV system. Presented hybrid model consisting of wavelet GNN may be improved by using genetic algorithms for optimal weight updation of GNN.

The energy management system has been developed using pumped hydro storage. In future, other energy storage devices may be considered and comparative analysis can be made for superiority. Further, hardware prototype can be fabricated for the proposed system.

References

- [1] Renewables Global status report. REN21; 2016.
- [2] IEEE standard for interconnecting distributed resources with electric power system. IEEE standard 1547-2003, 2003: 1-6.
- [3] R. Hudson and G. Heilscher, "PV grid integration system management issues and utility concerns," *Energy Procedia*, vol. 25, pp. 82-91, 2012.
- [4] S. Shivashankar, S. Mekhilef, H. Mokhliz and M. Karimi, "Mitigating methods of power fluctuations of photovoltaic (PV) sources-A review," *Renewable and Sustainable Energy Reviews*, vol. 59, pp. 1170-1184, 2016.
- [5] M. M. Haque and P. Wolfs, "A review of high PV penetrations in LV distribution networks: Present status, impacts and mitigation measures," *Renewable and Sustainable Energy Reviews*, vol. 62, pp. 582-585, 2016.
- [6] N. Mahmud and A. Zahedi, "Review of control strategies for voltage regulation of the smart distribution network with high penetration of renewable distributed generation," *Renewable and Sustainable Energy Reviews*, vol. 64, pp. 1170-1184, 2016.
- [7] R. Singh, Y. R. Sood and N. P. Padhy, "Development of Renewable Energy Sources for Indian Power Sector Moving Towards Competitive Electricity Market," *IEEE Power & Energy Society General Meeting*, pp 1 – 6, 2009.
- [8] Ministry of New and Renewable Energy Source (MNRE), <http://www.mnre.gov.in/achievements.htm>.
- [9] Ministry of Power, India, <http://www.mnre.gov.in/achievements.htm>.
- [10] Government of India. National Electricity Policy 2005. Available: <http://www.powermin.nic.in> [online].
- [11] Government of India. Annual Report 2009-10, New Delhi: Ministry of New and Renewable Energy, Government of India; 2010 [online].
- [12] The Electricity Act, 2003 by Ministry of Law and Justice, Government of India, published in *The Gazette of India Extraordinary Part II Section I*, at New Delhi on 2nd June, 2003.

- [13] The Electricity (Amendment) Act, 2003 by Ministry of Law and Justice, Government of India, published in The Gazette of India Extraordinary Part II Section I, at New Delhi on 2nd May, 2007.
- [14] Government of India, “Tariff policy”, 6th January, 2006 [Online]. Available: <http://www.powermin.nic.in>
- [15] Government of India “National Electricity policy and plan” [Online]. Available: www.powermin.nic.in
- [16] Electricity, Electricity Feed Laws, Feed-in Tariffs, and Advanced Renewable Tariffs, [Online]. Available: <http://www.wind-works.org>
- [17] Ministry of New and Renewable Energy source (MNRES) “Policy Support for Grid Interactive Renewable Power” [Online]. Available: <http://mnres.nic.in>.
- [18] Government of India National Knowledge Commission Science and Environment, “Policies for renewable energies/biomass in India”
- [19] MNRE, “Jawaharlal Nehru National Solar Mission,” Towards Building SOLAR INDIA, (2010).
- [20] S. Chowdhury and T. Matlokotsi, “Role of grid integration of distributed generation in power quality enhancement: A review,” 2016 IEEE PES PowerAfrica, Livingstone, 2016, pp. 164-168.
- [21] G. G. Matei and M. Gavrilas, “Voltage regulation in distribution networks with distributed generation - A review,” 2016 International Conference and Exposition on Electrical and Power Engineering (EPE), Iasi, 2016, pp. 728-732.
- [22] A. Naresh, M. Pukar and N. Mithulananthan, “An Analytical Approach for DG Allocation in Primary Distribution Network,” International Journal of Electrical Power & Energy Systems, vol. 28, no. 10, pp. 669-678, 2006.
- [23] P. Kailasapathi and D. Sivakumar, “Methods to analyze power quality disturbances,” European Journal of Scientific Research, vol. 47, no. 1, pp. 6–16, 2010.
- [24] O. Ozgonenel, T. Yalcin, I. Guney and U. Kurt, “A new classification for power quality events in distribution systems,” Electric Power Systems Research, vol. 95, pp. 192– 199, 2013.

- [25] B. Singh, K. Al-Haddad and A. Chandra, "A review of active filters for power quality improvement," *IEEE Transactions on Industrial Electronics*, vol. 46, no. 5, pp. 960-971, October 1999.
- [26] Yuvaraj and S. N. Deepa, "Improving Grid Power Quality With FACTS Device on Integration of Wind Energy System," *Student Pulse Academic Journal*, vol. 3, no. 4, pp 1-8, April 2011.
- [27] H. L. Tsai, C. S. Tu and Y. J. Su, "Development of Generalized Photovoltaic Model Using MATLAB/SIMULINK," *Proceedings of the World Congress on Engineering and Computer Science WCECS*, San Francisco, USA, 2008.
- [28] J. A. Gow and C. D. Manning, "Development of a photovoltaic array model for use in power-electronics simulation studies," *IEE Proceedings on Electric Power Applications*, vol. 146, no. 2, pp. 193–200, 1999.
- [29] N. Pandiarajan, R. Ramaprabha and M. Ranganath, "Application of circuit model for photovoltaic energy conversion system," *International Journal of Advanced Engineering Technology*, vol. 2, no. 4, pp. 118-127, 2011.
- [30] S. Said, A Massoud, M Benammar and S Ahmed, "A MATLAB/Simulink based photovoltaic array model employing Simpower system toolbox," *Journal of Energy and Power Engineering*, vol. 6, pp. 1965-1975, 2012.
- [31] K. Ishaque, Z. Salam and H. Tahri, "Accurate MATLAB Simulink PV systems simulator based on a two-diode model," *Journal of power electronics*, vol. 11, no. 2, pp. 179-187, 2011.
- [32] H. A. El Khateb, N. A. Rahim, and J. Selvaraj, "Cuk – buck converter for standalone photovoltaic systems," *Journal of Clean Energy Technologies*, vol. 1, no. 1, pp. 69-74, 2013.
- [33] D. Amudhavalli, M. Meyyappan, S. Imaya and V. Preetha Kumari, "Interleaved soft switching boost converter with MPPT for photovoltaic power generation system," *Proceedings of 2013 International Conference on Information Communication and Embedded Systems (ICICES)*, Chennai, 2013, pp. 1214-1219.
- [34] Y. Jang and M. M. Jovanovic, "New two inductor boost converter with auxiliary transformer," *IEEE transactions on power electronics*, vol. 19, no. 1, pp. 169-175, 2004.

- [35] B. Samaiah, V. Agarwal, SR. Choudhury, S. P. Dutttagupta and K. Govindan, "Analysis and comparative study of pulsating current of fuel cells by inverter load with different power converter topologies," *International Journal Hydrogen Energy*, vol. 36, no. 22, pp. 15018-15028, 2011.
- [36] M. Jang, M. Ciobotaru and V. G. Agelidis, "A single-phase grid connected fuel cell system based on a boost inverter," *IEEE Transaction on Power Electronics*, vol. 28, no. 1, pp. 279-288, 2013.
- [37] S. Bensmail, D. Reioua and H. Azzi, "Study of hybrid photovoltaic/fuel cell system for standalone applications," *International Journal Hydrogen Energy*, vol. 40, no. 19, pp. 13820-13826, 2015.
- [38] B. Akin and M.H. Sarul, "Soft switched SVPWM controlled PRDCL inverter," *International Journal Hydrogen Energy*, vol. 42, no. 28, pp. 17886-17894, 2017,
- [39] R. Seyezhai and B. L. Mathur, "Modelling and control of a PEM fuel cell based hybrid multilevel inverter," *International Journal Hydrogen Energy*, vol. 36, no. 22, pp. 15029-15043, 2011.
- [40] S. Ekoh, I. Unsal and A. Maheri, "Optimal sizing of wind-PV-pumped hydro energy storage systems," 2016 4th International Symposium on Environmental Friendly Energies and Applications (EFEA), Belgrade, 2016, pp. 1-6.
- [41] T. Ma, H. Young, L. Lu and J. Pang, "Technical feasibility study on a standalone hybrid solarwind system with pumped hydro storage for a remote island in Hong Kong," *Renewable Energy*, vol. 69, pp. 7-15, 2014.
- [42] S. Rehman, L. M. Al-Hadhrami and M. M. Alam, "Pumped hydro energy storage system: A technological review," *Renewable and Sustainable Energy Reviews*, vol. 44, pp. 586-598, 2015.
- [43] Y. S. Jeong, K. H. Lee, K.H. Hang, D. Ryu and Y. Jung, "Design of Short Term Forecasting Model of Distributed Power for Solar Power Generation," *International Journal of Science and Technology*, vol. 8, no. 1, pp. 261-270, 2015.
- [44] S. Pelland, J. Remund, J. Kleissl, T. Oozeki and K. D. Brabandere, "Photovoltaic and Solar Forecasting: State of the Art," International Energy Agency, October 2013.

- [45] M. G. D. Giorgi, P. M. Congedo and M. Malvoni, "Photovoltaic power forecasting using statistical methods: impact of weather data," *IET Science, Measurement & Technology*, vol. 8, no. 3, pp. 90-97, 2014.
- [46] S. N. Kaplanis, "New methodologies to estimate the hourly global solar radiation; comparison with existing models," *Renewable Energy*, vol. 31, no. 6, pp. 781-790, 2006.
- [47] A. Mellita and S. A. Kalogirou, "Artificial intelligence techniques for photovoltaic applications: A review," *Progress in Energy and Combustion Sciences*, vol. 34, no. 5, pp. 574-632, 2008.
- [48] N. Sharma, P. Sharma, D. Irwin and P. Shenoy, "Predicting solar generation from weather forecasts using machine learning," *Proceedings of IEEE Conference on Smart Grid Communications (Smart Grid Comm)*, 2011, pp. 528-533.
- [49] A. Chaouachi, R. M. Kamel, R. Ichikawa, H. Hayashi and K. Nagasaka, "Neural network ensemble-based solar power generation short-term forecasting," *World Academy of Science, Engineering and Technology*, vol. 3, no. 6, 2009.
- [50] R. Huang, T. Huang, R. Gadh and N. Li, "Solar generation prediction using the ARMA model in a laboratory-level micro-grid," *Proceedings of IEEE Conference on Smart Grid Communications (SmartGridComm)*, 2012, pp. 528-533.
- [51] A. U. Haque, M. H. Nehrir and O. Mandal, "Solar PV power generation forecast using hybrid intelligent approach," *Proceedings of Power and Energy Society General Meeting (PES)*, 2013.
- [52] H. T. Yang, C. M. Huang, Y. C. Huang and Y. S. Pai, "A weather-based hybrid method for 1-day ahead hourly forecasting of PV power output," *IEEE Transactions on Sustainable Energy*, vol. 5, no. 3, pp. 917-926, 2014.
- [53] C. Chen, S. Duan, T. Cai and B. Liu, "Online 24-h solar power forecasting based on weather type classification using artificial neural network," *Solar Energy*, vol. 85, no. 11, pp.574-632, 2011.
- [54] J. Kou, J. Liu, Q. Li, W. Fang, Z. Chen, L. Liu and T. Guan, "Photovoltaic power forecasting based on artificial neural network and meteorological data," *Proceedings of IEEE International Conference of IEEE Region 10 (TENCON 2013)*, Xi'an, 2013, pp. 1-4.

- [55] C. Yang and L. Xie, "A novel ARX-based multi-scale spatio-temporal solar power forecast model," Proceedings of North American Power Symposium (NAPS), Champaign, IL, 2012, pp. 1-6.
- [56] S. K. H. Chow, E. V. M. Lee and D. H. W. Li, "Short-term prediction of photovoltaic energy generation by intelligent approach," Energy and Buildings, vol. 55, pp. 660-667, 2012.
- [57] M. Rizwan, M. Jamil and D. P. Kothari, "Solar energy estimation using REST model for PV-ECS based distributed power generating system," Solar Energy Materials and Solar Cells, vol. 94, no. 8, pp. 1324-1328, 2010.
- [58] A. Khotanzad, R. Afkhami-Rohani, T. L. Lu, A. Abaye, M. Davis and D. J. Maratukulam, "ANNSTLF-A neural-network-based electric load forecasting system. IEEE Transaction on Neural Network, vol. 8, no. 4, pp. 835-846, 1997.
- [59] M. A. Ahmed, F. Ahmed and M. W. Akhter, "Estimation of global and diffuse solar radiation for Hyderabad, Pakistan," Journal of Basic and Applied Sciences, vol. 5, no. 2, pp. 73-77, 2009.
- [60] M. Rizwan, M. Jamil and D. P. Kothari, "Estimation of global solar irradiance using regression model for Jodhpur, India," Proceedings of International Symposium on Photovoltaic Science & Technology, Kanpur, vol. 43, 2010.
- [61] D. K. Chaturvedi, A. P. Sinha and A. Chandiok, "Short-term load forecasting using soft computing techniques," International journal Communications, Network and System Sciences, vol. 3, pp. 273-279, 2010.
- [62] K. J. Hwan and G. W. Kim, "A short-term load forecasting expert system," Proceedings of the fifth Russian–Korean international symposium on science and technology, 2001, pp. 112-116.
- [63] Manmohan, D. K. Chaturvedi, P. S. Satsangi and P. K. Kalra, "Neuro fuzzy approach for development of new neuron model," Soft Computing, vol. 8, no.7, pp. 19-27, 2003.
- [64] D. K. Chaturvedi, P. K. Satsangi and P. K. Kalra, "Load frequency control: A generalized neural network approach," International Journal Electrical Power Energy Systems, vol. 21, no. 6, pp. 405-415, 1999.

- [65] D. K. Chaturvedi, R. Chauhan and P. K. Kalra, "Applications of generalized neural networks in for aircraft landing control system," *Soft Computing*, vol. 6, no. 6, pp. 441-448, 2002.
- [66] H. S. Hippert, C. E. Poedreira and R. C. Souza, "Neural network for short-term load forecasting: A review and evaluation," *IEEE Transaction on Power Systems*, vol. 16, no. 1, pp. 44-45, 2001.
- [67] S. A. Kalogirous, "Artificial neural networks in renewable energy systems applications: A review," *Renewable Sustainable Energy Review*, vol. 5, no. 4, pp. 373-401, 2001.
- [68] D. K. Chaturvedi, *Soft Computing Techniques and Its Applications in Electrical Engineering*, Berlin, Heidelberg, Germany: Springer Verlag, 2008.
- [69] S. Rahman and O. Hazim, "A generalized knowledge based short-term load forecasting technique," *IEEE Transactions on Power Systems*, vol. 8, no 2, pp. 508-514, 1993.
- [70] J. Liu, W. Fang, X. Zhang and C. Yang, "An improved photovoltaic power forecasting model with the assistance of aerosol index data," *IEEE Transactions on Sustainable Energy*, vol. 6, no. 2, pp. 434-442, 2015.
- [71] H. T. Yang, C. M. Huang, Y. C. Huang and Y. S. Pai, "A Weather-based hybrid method for 1-day ahead hourly forecasting of PV power output," *IEEE Transactions on Sustainable Energy*, vol. 5, no. 3, pp. 917-926, 2014.
- [72] B. k. Chauhanl and M. Hanmandlu, "Load forecasting using wavelet fuzzy neural network," *International Journal of Knowledge-based and Intelligent Engineering Systems*, IOS Press, vol. 14, no. 2, pp. 57-71, 2010.
- [73] X. Li, "Electrical load forecasting based on fuzzy wavelet neural networks," *Conference on Future Biomedical information Engineering*, 2008, pp. 122-125.
- [74] P. Mandal, S. T. S. Madhira, A. Uhaque, J. Mehng and R. L. Pineda, "Forecasting power output of solar photovoltaic system using wavelet transform and atrtificial intelligence techniques," *Procedia Computer Science*, vol. 12, pp. 332-337, 2012.
- [75] D. K. Chaturvedi, A. P. Sinha and O. P. Malik, "Short term load forecast using fuzzy logic and wavelet transform integrated generalized neural network," *Electrical Power and Energy Systems*, vol. 67, pp. 230-237, 2015.

- [76] M. Rizwan, M. Jamil and D. P. Kothari, "Generalized neural network approach for global solar energy estimation in India," *IEEE Transactions on Sustainable Energy*, vol. 3, no. 3, pp. 576-584, 2012.
- [77] S. Shivashankar, S. Mekhilef, H. Mokhliz and M. Karimi, "Mitigating methods of power fluctuations of photovoltaic (PV) sources-A review," *Renewable and Sustainable Energy Reviews*, vol. 59, pp. 1170-1184, 2016.
- [78] M. H. Mejboul and P. Wolfs, "A review of high PV penetrations in LV distribution networks: Present status, impacts and mitigation measures," *Renewable and Sustainable Energy Reviews*, vol. 62, pp. 582-585, 2016.
- [79] M. J. E. Alam, K. M. Muttaqi and D. Sutanto, "A comprehensive assessment tool for solar PV impacts on low voltage three phase distribution networks," "Proceedings of 2nd International Conference on the Developments in Renewable Energy Technology (ICDRET), Dhaka; 2014, pp. 1-5.
- [80] M. E. Baran, H. Hooshyar, Z. Shen and A. Huang, "Accommodating high PV penetration on distribution feeders," *IEEE Transaction on Smart Grid*, vol. 3, no. 2, pp. 1039-1046, 2012.
- [81] E. Demirok, D. Ser, R. Teodorescu, P. Rodriguez and U. Borup, "Clustered PV inverters in LV network: An overview of impacts and comparison of voltage control strategies," *Proceedings of IEEE Electrical Power & Energy Conference (EPEC)*, Montreal, QC; 2009, pp. 1-6.
- [82] P. C. Chen, R. Salcedo, Q. Zhu and F. D. Leon, "Analysis of voltage profile problems due to the penetration of distributed generation in low voltage secondary distribution network," *IEEE Transaction on Power Delivery*, vol. 27, no. 4, pp. 2020-2028, 2012.
- [83] M. Zillmann, R. Yan and T. K. Saha, "Regulation of distribution network voltage using dispersed battery storage system: A case study of a rural network," *Proceedings of IEEE PES General Meeting*, 2011, pp. 1-8.
- [84] Y. Yang, H. Li, A. Aichhorn, J. Zheng and M. Greenleaf, "Sizing strategy of distributed battery storage system with high penetration of photovoltaic for voltage regulation and peak load shaving," *IEEE Transaction on Smart Grid*, vol. 5, no. 2, pp. 982-991, 2014.

- [85] F. Marra, T. Y. Tanek and B. Blazi, "Energy storage options for voltage support in low voltage grids with high penetration of photovoltaic," Proceedings of IEEE PES Innovation Smart Grid Technologies (ISGT), 2012.
- [86] S. Ghosh, S. Rahman and M. Pipattanasomporn, "Local distribution voltage control by reactive power injection from PV inverters enhanced with active power curtailment," Proceedings of IEEE PES General Meeting Conference & Exposition, 2014, pp. 1-5.
- [87] G. Mokhtari, A. Ghosh, G. Nourbakhsh and G. Ledwich, "Smart robust resource control in LV networks to deal with voltage rise issues," IEEE Transaction on Sustainable Energy, vol. 4, no. 4, pp. 1043-1050, 2013.
- [88] H. T. Yang, Y. T. Chen, J. T. Liao and C. T. Yang, "Overvoltage mitigation control strategies for distribution system with high PV penetration," 18th International Conference on Intelligent System Application to Power Systems (ISAP), 2015, pp. 1-6.
- [89] T. T. Ku, C. H. Lin, C. S. Chen, C. T. Hsu, W. L. Hsieh and S. C. Hsieh, "Coordination of PV inverters to mitigate voltage violation for load transfer between distribution feeder with high penetration of PV installation," IEEE Transaction on Industry Applications, vol. 52, no. 2, pp. 1167-1174, 2016.
- [90] S. Ghosh, S. Rahman and M. Pipattanasomporn, "Distribution voltage regulation through active power curtailment with PV inverters and solar generation forecast," IEEE PES Transaction on Sustainable Energy, vol. 8, no. 1, pp. 13-22, 2017.
- [91] S. J. Lewis, "Analysis and management of the impacts of a high penetration of photovoltaic system in an electricity distribution network," In Proceedings IEEE PES Innovative Smart Grid Technology Asia (ISGT), 2011, pp. 1-7.
- [92] T. Stetz, M. Kraiczy, M. Braun and S. Schmidt, "Technical and economical assessment of voltage control strategies in distribution grids," Progress in Photovoltaics: research and applications, vol. 21, no. 6, pp. 1292-1307, 2013.
- [93] S. Hashemi, J. Østergaard and G. Yang, "Effect on reactive power management of PV inverters on need for energy storage," IEEE 39th Photovoltaic Specialists Conference (PVSC), 2013, pp. 2304-2308.

- [94] R. Yan and T. K. Saha, "Investigation of voltage stability for residential customers due to high photovoltaic penetrations," *IEEE Transactions on Power Systems*, vol. 27, no. 2, pp. 651-662, 2012.
- [95] H. Math and J. Bollen, *Understanding power quality problems: voltage sags and interruptions*, in New York, IEEE Press, 1999.
- [96] G. Wang, M. Ciobotaru and V. G. Agelidis, "Power management for improved dispatch of utility-scale PV plants," *IEEE Transaction on Power Systems*, vol. 31, no. 3, pp. 2297-2306, 2016.
- [97] C. Wan, J. Zhao, Y. Song, Z. Xu, J. Lin and Z. Hu, "Photovoltaic and solar power forecasting for smart grid energy management system," *CSEE Journal of Power and Energy Systems*, vol. 1, no. 4, pp. 38-46, 2015.
- [98] B. Doucoure, K. Agbossou and A. Cardenas, "Time series prediction using artificial wavelet neural network and multi-resolution analysis: Application to wind speed data," *Renewable Energy*, vol. 92, pp. 202-211, 2016.
- [99] O. Hyungseon, "Optimal planning to include storage devices in power systems," *IEEE Transaction on Power System*, vol. 26, no. 3, pp. 1118-1128, 2011.
- [100] X. Wang, A. Palazoglu and H. N. El-Fana, "Operation of residential hybrid renewable energy systems: Integrating forecasting, optimization and demand response," *Proceedings of American Control Conference (ACC)*, Portland, Oregon, USA 2014, pp. 5043-5048.
- [101] P. Tian, X. I. Xiao, K. Wang and R. Ding, "A hierarchical energy management system Based on hierarchical optimization for microgrid community economic operation," *IEEE Transactions on Smart Grid*, vol. 7, no. 5, pp. 2230-2241, 2016.
- [102] S. Kotra and M. K. Mishra, "A supervisory power management system for a hybrid microgrid with HESS," *IEEE Transactions on Industrial Electronics*, vol. 64, no. 5, pp. 3640-3649, 2017.
- [103] M. Rouholamini and M. Mohammadian, "Heuristic-based power management of a grid-connected hybrid energy system combined with hydrogen storage," *Renewable Energy*, vol. 96, pp. 354-365, 2016.
- [104] M. Rouholamini and M. Mohammadian, "Energy management of a grid-tied residential-scale hybrid renewable generation system incorporating fuel cell and electrolyzer," *Journal of Energy and Buildings*, vol. 102, pp. 406-416, 2015.

- [105] N. Korada and M. K. Mishra, "Grid adaptive power management strategy for an integrated microgrid with hybrid energy storage," *IEEE Transactions on Industrial Electronics*, vol. 64, no. 4, pp. 2884-2892, 2017.
- [106] H. Geramifan, M. Shahabi and T. Barforosh, "Coordination of energy storage systems and DR resources for optional scheduling of microgrid under uncertainties," *IET Renewable Power Generation*, vol. 11, no. 2, pp. 378-388, 2017.
- [107] G. K. Venayagamoorthy, R. K. Sharma, P. K. Gautam and A. Ahmadi, "Dynamic energy management system for a smart microgrid," *IEEE Transactions on Neural Networks and Learning Systems*, vol.27, no. 8, pp. 1643-1656, 2016.
- [108] M. Rouholamini, M. Mohammadian, C. Wang and AA. Gharaveisi, "Optimal fuzzy-based power management for real time application in a hybrid generation system," *IET Renewable Power Generation*, vol. 11, no. 10, pp. 1325-1334, 2017.
- [109] A. Merabet, K. Taufique, H. Ibrahim, R. Beguenane and A. M. Y. M. Ghias, "Energy management system and control system for laboratory scale microgrid based wind-PV-battery," *IEEE Transactions on Sustainable Energy*, vol.8, no. 1, pp. 145-154, 2017.
- [110] L. Guo, W. Liu, X. Li, Y. Liu, B. Jio, W. Wang, C. Wang and F. Li, "Energy management system for standalone wind powered desalination microgrid," *IEEE Transactions on Smart Grid*, vol. 7, no. 2, pp. 1079-1087, 2016.
- [111] D. Stimoniari, D. Tsiamitros and E. Dialynas, "Improved energy storage management and PV-active power control infrastructure and strategies for microgrids," *IEEE Transactions on Power Systems*, vol. 31, no. 1, pp. 813-820, 2016.
- [112] M. Khalid, A. Abdollah, A. V. Saukin and V. G. Agelidis, "Minimizing energy cost for microgrid integrated with renewable energy resources and conventional generation using controlled battery energy storage," *Renewable Energy*, vol. 97, pp. 646-655, 2016.
- [113] A. J. Roscoe and G. Ault, "Supporting high penetration of renewable generation via implementation of real-time electricity pricing and demand response," *IET Renewable Power Generation*, vol. 4, no. 4, pp. 369-382, 2010.

- [114] Y. Zhang, R. Wang, J. Zhang and B. Guo, "Model predictive Control Based Operation Management for a Residential Microgrid with Considering Forecast Uncertainties and Demand Response Strategies," *IET Generation, Transmission and Distribution*, vol. 10, no. 10, pp. 2367-2378, 2016.
- [115] C. Yang, J. Yao, W. Lou and S. Xie, "On demand response management performance optimization for microgrids under imperfect communication constraints," *IEEE Internet of Things Journal*, vol.4, no. 4, pp. 881-893, 2017.
- [116] N. I. Nwulu and X. Xia, "Optimal dispatch for a microgrid incorporating renewables and demand response," *Renewable Energy*, vol. 101, pp. 16-28, 2017.
- [117] F. Valencia, J. Collado, D. Saez and L. G. Marin, "Robust energy management mystem for a Mcrogrid based on a fuzzy prediction interval model," *IEEE Transactions on Smart Grid*, vol. 7, no. 3, pp. 1486-1494, 2016.
- [118] B. V. Solanki, A. Raghurajan, K. Bhattacharya and C. A. Canizares, "Including smart loads for optimal demand response in integrated energy management systems for isolated microgrids," *IEEE Transactions on Smart Grid*, vol. 8, no. 4, pp. 1739-1784, 2017.
- [119] M. Jin, W. Jang, P. Liu, C. Marnay and C. Spanes, "MOD-DR: microgrid optimal dispatch with demand response," *Applied Energy*, vol. 187, pp. 758-776, 2017.
- [120] J. He and Y. W. Li, "Hybrid voltage and current control approach for dg-grid interfacing converters with LCL filters. *IEEE Trans*," *Industrial Electronics*, vol. 60, no. 5, pp. 1797-1809, 2013.
- [121] R. K. Agarwal, I. Hussain and B. Singh, "Implementation of LLMF control algorithm for three-phase grid tied PV-DSTATCOM system," *IEEE Transactions on Industrial Electronics*, vol. 64, no. 9, pp. 7414-7424, 2017.
- [122] R. K. Agarwal, I. Hussain and B. Singh, "Three-phase single-stage grid tied solar PV ECS using PLL-less fast CTF control technique," *IET Power Electronics*, vol. 10, no. 2, pp. 178-188, 2017.
- [123] B. Singh, C. Jain, S. Goel, A. Chandra and K. Al-Haddad, "A Multifunctional grid-tied solar energy conversion system with ANF-based control approach," *IEEE Transactions on Industry Applications*, vol. 52, no. 5, pp. 3663-3672, 2016.

- [124] C. Jain and B. Singh, "An adjustable DC link voltage based control of multifunctional grid interfaced solar PV system," *IEEE Journal of Emerging and Selected Topics in Power Electronics*, vol. 5, no. 2, pp. 651-660, 2017.
- [125] L. Campanhol, S. Silva, A. Oliveira and V. Bacon, "Single-stage three-phase grid-tied PV system with universal filtering capability applied to DG systems and AC microgrids," *IEEE Transactions on Power Electronics*, vol. 32, no. 12, pp. 9131-9142, 2017.
- [126] Q. N. Trinh and H. H. Lee, "An enhanced grid current compensator for grid-connected distributed generation under nonlinear loads and grid voltage distortions," *IEEE Trans. Industrial Electronics*, vol. 61, no. 12, pp. 6528-6537, 2014.
- [127] R. K. Varma, S. A. Rahman and T. Vanderheide, "New control of PV solar farm as STATCOM (PV-STATCOM) for increasing grid power transmission limits during night and day," *IEEE Transacation on Power Delivery*, vol. 30, no. 2, pp. 755-763, 2015.
- [128] M. I. Hamid, A. Jusoh and M. Anwari, "Photovoltaic plant with reduced output current harmonics using generation-side active power conditioner," *IET Renewable Power Generation*, vol. 8, no. 7, pp. 817-826. 2014.
- [129] V. K. Kannan, N. Rengarajan, "Investigating the performance of photovoltaic based DSTATCOM using $I \cos \Phi$ algorithm," *International Journal of Electrical Power and Energy Systems*, vol. 54, pp. 376-386, 2014.
- [130] S. R. Arya, B. Singh, A. Chandra and K. Al-Haddad, "Learning-based anti-hebbian algorithm for control of distribution static compensator," *IEEE Transaction on Industrial Electronics*, vol. 61, no. 11, pp. 6004-6012, 2014.
- [131] Mishra A. Rajput, N. Beniwal, S. Pradhan, B. Singh and S. Mishra, "Single-phase grid interactive solar PV system having active shunt capabilities," 2017 7th International Conference on Power Systems (ICPS), Pune, India, 2017, pp. 194-199.
- [132] B. Sing, C. Jain and S. Goel, "ILST control algorithm of single-stage dual purpose grid connected solar PV system," *IEEE Transactions on Power Electronics*, vol. 29, no. 10, pp. 5347-5357, 2014.

- [133] C. Jain and B. Singh, "An adjustable DC link voltage based control of multifunctional grid interfaced solar PV system," *IEEE Journal of Emerging and Selected Topics in Power Electronics*, vol. 5, no. 2, pp. 651-660, 2017.
- [134] J. Mazumdar and R. G. Harley, "Recurrent neural networks trained with back propagation through time algorithm to estimate nonlinear load harmonic currents," *IEEE Transaction on Industrial Electronics*, vol. 55, no. 9, pp. 3484–3491, 2008.
- [135] S. R. Arya and B. Singh, "Neural network based conductance estimation control algorithm for shunt compensation," *IEEE Transaction on Industrial Informatics*, vol. 10, no. 1, pp. 569-577, 2014.
- [136] B. Singh and S. R. Arya, "Back-Propagation control algorithm for power quality improvement using DSTATCOM," *IEEE Transaction on Industrial Electronics*, vol. 61, no. 3, pp. 1204-1212, 2014.
- [137] B. Singh, P. Jayaprakash, S. Kumar and D. P. Kothari, "Implementation of neural network controlled three leg VSC and a transformer as three phase four wire DSTATCOM," *IEEE Transaction on Industrial Applications*, vol. 47, no. 4, pp. 1892- 1901, 2011.
- [138] J. Jayachandran and R. Sachithanandam, "Neural network based control algorithm for DSTATCOM under nonideal source voltage and varying load conditions," *Canadian Journal of Electrical and Computer Engineering*, vol. 38, no. 4, pp. 307- 317, 2015.
- [139] M. Singh and A. Chandra, "Real-time implementation of ANFIS control for renewable interfacing inverter in 3P4W distribution network," *IEEE Transactions on Industrial Electronics*, vol. 60, no. 1, pp. 121-128, 2013.
- [140] S. Janpong, K. L. Areerak and K. N. Areerak, "A literature survey of neural network applications for shunt active power filters," *World Academy of Science, Engineering and Technology*, vol. 5, no. 12, pp. 392-398, 2011.
- [141] B. Singh, D. T. Shahani and A. K. Verma, "Neural Network Controlled Grid Interfaced Solar Photovoltaic Power Generation," *IET Power Electronics*, vol. 7, no. 3, pp. 614-626, 2013.

- [142] A. P. Kumar and M. Mangaraj, "DSTATCOM employing hybrid neural network control technique for power quality improvement," *IET Power Electronics*, vol. 10, no. 4, pp. 480-489, 2013.
- [143] D. K. Chaturvedi, O. P. Malik and P. K. Kalra, "Generalised neuron-based adaptive power system stabilizer," *IEEE Generation Transmission Distribution*, vol. 151, no. 2, 2004.
- [144] D. K. Chaturvedi and O. P. Malik, "Generalized neuron-based PSS and adaptive PSS," *Control Engineering Practice*, vol. 13, no. 12, pp. 1507-1514, 2005.
- [145] D. K. Chaturvedi, O. P. Malik and P. K. Kalra, "Experimental studies with a generalized neuron based power system stabilizer," *IEEE Transaction on Power System*, vol. 19, no. 3, pp. 1445-1453, 2004.
- [146] D. K. Chaturvedi, "Soft computing techniques and its applications in electrical engineering," Springer-Berlin Heidelberg, 2008.
- [147] M. Rizwan, M. Jamil and D. P. Kothari, "Generalized neural network approach for global solar energy estimation in India," *IEEE Transaction on Sustainable Energy*, vol. 3, no. 3, pp. 576-583, 2012.
- [148] R. V. Kulkarni and G. K. Venayagamoorthy, "Generalized neuron: Feedforward and recurrent architecture," *Elsevier Neural Network*, vol. 22, no 7, pp. 1011-1017, 2009.
- [149] J. Sum, C. Leung, G. H. Young and W. Kan, "On the Kalman Filtering Method in neural-network training and pruning," *IEEE Transactions on Neural Network*, vol. 10, no. 1, pp. 161-166, 1999.
- [150] R. J. Williams, "Training recurrent networks using the extended Kalman filter," *IJCNN'92*, Baltimore, pp. 241-246, 1992.
- [151] M. A. D. Oliveira, "An application of neural networks trained with Kalman Filter Variants (EKF and UKF) to heteroscedastic time Series forecasting," *Applied Mathematical Sciences*, vol. 6, no. 74, pp. 3675 – 3686, 2012.
- [152] G. Welch and G. Bishop, "An introduction to the kalman filter," 1995.
- [153] A. R. Reisi, M. H. Moradi and S Jamsab, "Classification and comparison of maximum power point tracking techniques for photovoltaic system: A review," *Renewable and Sustainable Energy Reviews*, vol. 19, pp. 433-443, 2013.

- [154] R. Faranda, S. Leva and V. Maugeri, "MPPT techniques for PV systems: energetic and cost comparison," Proceedings of IEEE PES GM 2008, July 2008.
- [155] H. N. Zainudin and S. Mekhilef, "Comparison study of maximum power point tracker techniques for PV systems," Proceedings of the 14th International Middle East Power Systems Conference (MEPCON'10), Cairo University, Egypt, December 2010.
- [156] C. P. Ragasudha, H. Algazar, A. L. Monier, H. A. El-halim and M. E. K. Salem, "Maximum power point tracking using fuzzy logic control," International Journal of Electrical Power and Energy Systems, vol. 39, no. 1, pp. 21-28, 2012.
- [157] M. Abdulkadir, A. S. Samosir, Member and A. H. M. Yatim, "Modeling and simulation of maximum power point tracking of photovoltaic system in Simulink model," IEEE International Conference on Power and Energy (PECon), Kota Kinabalu Sabah, Malaysia, 2012.
- [158] M. Mosal, H. A. Rubl, E. Mahrous, Ahmed and J. Rodriguez, "Modified MPPT with using model predictive control for multilevel boost converter," IECON 2012 - 38th Annual Conference on IEEE Industrial Electronics Society, Montreal, QC, 2012, pp. 5080-5085.
- [159] A. Kusko and T. M. Thomson, Power Quality in Electrical Systems, McGraw-Hill Press, New York, 2007.
- [160] R. S. Vedam and S. M. Sarma, Power Quality: VAR Compensation in Power Systems, CRC Press, Taylor & Francis Group, 2009.
- [161] N. G. Hingorani and L. Gyugyi, Understanding FACTS: Concept and Technology of Flexible AC Transmission Systems, IEEE Press, New York, 2000.
- [162] B. Singh, A. Chandra and K. Al-Haddad, Power Quality: Problems and Mitigation Techniques, John Wiley and Sons, U.K., 2015.
- [163] M. Moreno, Power Quality: Mitigation Technologies in a Distributed Environment, Springer-Verlag, New York, 2007.
- [164] A. Ghosh and G. Ledwich, Power Quality Enhancement Using Custom Power Devices, Springer international Edition, New Delhi, India, 2009.
- [165] S. K. Khadem, M. Basu and M. F. Conlon, "Power quality in grid connected renewable energy systems: Role of custom power devices," International

conference on renewable energies and power quality (ICREPQ'10) Granada (Spain), March 2010.

- [166] M. Farhoodnea, A. Mohamed, H. Shareef and H. Zayandehroodi, "Power quality analysis of grid connected photovoltaic system in distribution networks," 2012 IEEE Student Conference on Research and Development (SCOREd), Pulau Pinang, 2012, pp. 1-6.
- [167] P. S. Addison. The illustrated wavelet transform handbook: Introductory theory and applications in science, engineering medicine and finance, IOP Publishing LTD 2002.
- [168] Z. Bashir and El-Hawary, "Short term load forecasting by using wavelet neural networks," 2000 Canadian Conference on Electrical and Computer Engineering. Conference Proceedings. Navigating to a New Era (Cat. No.00TH8492), Halifax, NS, 2000, pp. 163-166.
- [169] I. Daubechies I, "Where do wavelets come from? A personal point of view," IEEE Proceedings, vol. 84, no. 4, pp. 510-513, 1996.
- [170] J. Liu, W. Fang, X. Zhang and C. Yang, "An improved photovoltaic power forecasting model with the assistance of aerosol index data," IEEE Transactions on Sustainable Energy, vol. 6, no. 2, pp. 434-442, 2015.
- [171] H. T. Yang, C. M. Huang, Y. C. Huang and Y. S. Pai, "A Weather-Based Hybrid Method for 1-Day Ahead Hourly Forecasting of PV Power Output," IEEE Transactions on Sustainable Energy, vol. 5, no. 3, pp. 917-926, 2014.
- [172] J. A. Duffie and W. A. Beckman. Solar Engineering of Thermal Processes, Second edition, John Wiley & Sons Inc., Jun 1980.
- [173] K. Pearson, "Notes on regression and inheritance in case of two parents," In Proceedings Royal Social London, vol. 58 pp. 240-242, 1895.
- [174] Z. Zhao, W. C. Lee, Y. Shin and K. B. Song, "An optimal power scheduling method for demand response in home energy management system," IEEE Transactions on Smart Grids, vol. 4, no. 3, pp. 1391-1400, 2013.
- [175] M. H. Albadi and E. El-Saadany E, "A summary of demand response in electricity markets," Electric Power Systems Research, vol. 78, no. 11, pp. 1989-1996, 2008.

- [176] A. S. Leger, E. Sobiesk, A. Farmer and B. Rulison B, "Demand response with photovoltaic energy source and time-of-use pricing," IEEE PES T&D conference and Exposition 2014, Chicago, IL, USA, 2014, pp. 1-5.
- [177] S. O. Pawaskar and S. S. More, "Time of Day Tariff Structure," IE (I) 23rd National Convention of Electrical Engineers, 2016, pp. 119-123.
- [178] Y. Zhou, P. Mancarella and J. Mutale, "Modelling and assessment of the contribution of demand response and electrical energy storage to adequacy of supply," Sustainable Energy, Grids and Networks, vol. 3, pp. 12–23, 2015.
- [179] C. R. Chen and M. J. Lan, "Optimal demand response of smart home with PV generators," International Journal of Photoenergy, vol. 2, pp. 1-9, 2014.
- [180] A. Maleki and K. Nayebi, "A new efficient PNLMS based algorithm for adaptive line echo cancellation", Seventh International Symposium on Signal Processing and Its Applications, vol. 2, 2003, pp. 555-558.
- [181] C. Kumar and M K. Mishra, "Predictive voltage control of transformerless dynamic voltage restorer," IEEE Transaction on Industrial Electronics, vol. 62, no. 5, pp. 2639–2697, 2015
- [182] D. Meza, D. Biel, D. Jeltsema and J.M.A. Scherpen, "Lyapunov-based control scheme for single-phase grid-connected PV central inverters," IEEE Transaction on Control System Technology, vol. 20, no. 2, pp. 520–529, 2012.
- [183] M. A. Mahmud, M. J. Hossain, H. R. Pota and N. K. Roy, "Robust Nonlinear Controller Design for Three-Phase Grid-Connected Photovoltaic Systems under Structured Uncertainties," IEEE Transaction on Power Deliver, vol. 29, no. 3, pp. 1221-1230, 2014.
- [184] Y. T. Weng and Y. Y Hsu, "Sliding mode regulator for maximum power tracking and copper loss minimisation of a doubly fed induction generator," IET Renewable Power Generation, vol. 9, no. 4, pp. 297–305, 2015.
- [185] B. Beltran, T. Ahmed-Ali and M. E. H. Benbouzid, Sliding mode power control of variable-speed wind energy conversion systems. IEEE Transction Energy Conversion, vol. 23, no. 2, pp. 551–558, 2008.
- [186] M. A. Mahmud, H. R. Pota and M. J. Hossain, "Nonlinear Current Control Scheme for a Single-Phase Grid-Connected Photovoltaic System," IEEE Transaction on Sustainable Energy, vol. 5, no.1, pp. 218-227, 2014.

- [187] MA Mahmud, H. R. Pota and M. J. Hossain, “Dynamic Stability of Three-Phase Grid-Connected Photovoltaic System Using Zero Dynamic Design Approach,” IEEE Journal of Photovoltaics, vol. 2, no. 4, pp. 564-571, 2012.
- [188] A. Levant, “Sliding order and sliding accuracy in sliding mode control,” International Journal Control, vol. 58, no. 6, pp. 1247–1263, 1993.
- [189] J. A. Moreno and M. Osorio, “Strict Lyapunov functions for the super-twisting algorithm,” IEEE Transaction on Automation Control, vol. 57, no. 4, pp. 1035–1040, 2012.

Appendix – A

Table A.1 The developed system design specifications.

Serial No.	Components of the test system model	Specifications
1.	AC Grid specifications	3 ϕ , 415 V, 50 Hz,
2.	SPV array voltage (V_{MPP})	700V
3.	SPV array current (I_{MPP})	14 A
4.	SPV array power (P_{MPP})	10kW
5.	Interfacing inductor ($L_{fa}= L_{fb}= L_{fc}$)	2.6 mH
6.	DC bus capacitor (C_{DC})	10mf
7.	DC bus voltage (V_{DC})	700V
8.	Ripple Filter (R_f) and(C_f)	5 Ω , 10 μF
9.	Gains for DC link controller K_{pd} and K_{id}	0.25 and 0.28
10.	Gains for AC bus controller K_{pt} and K_{it}	0.75 and 0.67

Appendix – B



Fig. B.1 5 kW_p PV system installed at roof top of EEU laboratory, DTU



Fig. B.2 5 kW_p PV system output and grid connection



Fig. B.3 Grid connected inverter in laboratory

List of Research Publications

□ List of papers (s) published in Peer Reviewed Referred International Journals:

1. **Priyanka Chaudhary** and M. Rizwan, “Energy management supporting high penetration of solar photovoltaic generation for smart grid using solar forecasts and pumped hydro storage system,” **Renewable Energy**, An International Journal (Elsevier), vol. 118, pp. 928-946, 2018. ISSN: 0960-1481, **Impact Factor: 4.357**.
2. **Priyanka Chaudhary** and M. Rizwan, “Hybrid control approach for PV/FC fed voltage source converter tied to grid,” **International Journal of Hydrogen Energy** (Elsevier), vol. 43, no. 14, pp. 6851-6866, 2018. ISSN: 0360-3199, **Impact Factor: 3.582**.
3. **Priyanka Chaudhary** and M. Rizwan, “Voltage regulation mitigation techniques in distribution system with high PV penetration: a review,” **Renewable and Sustainable Energy Reviews** (Elsevier), vol. 82, no. 3, pp. 3279-3287, 2018. ISSN: 1364-0321, **Impact Factor: 8.05**.
4. **Priyanka Chaudhary**, M. Rizwan and Tausif Ahmad, “Performance Analysis of Maximum Power Point Tracking Techniques for Photovoltaic Systems,” **Advanced Science Letters**, vol. 20, July 2014, pp. 1231-1247. ISSN: 1936-6612 (Print): EISSN: 1936-7317 (Online), **Impact Factor: 1.253**.
5. **Priyanka Chaudhary** and M. Rizwan, “Short term solar energy forecasting using GNN integrated wavelet based approach,” Accepted in **International Journal of Renewable Energy Technology**, Inderscience. ISSN No. 1757-3971.

□ List of papers (s) communicated in Peer Reviewed Referred International Journals:

1. **Priyanka Chaudhary** and M. Rizwan, “Grid tied solar PV system control using extended Kalman filter based generalized neural network approach,” **IETE, Journal of Research**, ISSN No. 0377-2063. (Manuscript Id: TIJR-2017-1884)
2. **Priyanka Chaudhary** and M. Rizwan, “Solar PV system Control Using Improved I Cos ϕ based NN Algorithm Integrated with LV/MV Grid ,” **IET Renewable Power Generation**. (Manuscript Id: RPG-2018-5577)

3. Priyanka Chaudhary and M. Rizwan, “Nonlinear control and stability analysis of grid tied SPV system considering uncertainties,” **IET Generation, Transmission & Distribution**. (Manuscript Id: GTD-2018-6585)

□ **List of Paper(s) Published in Peer Reviewed International/National Conference Proceedings/Presented in the Conference:**

1. **Priyanka Chaudhary** and M. Rizwan, “A Predictive current control for solar PV fed VSI in distribution system,” Proceedings of 17th IEEE International Conference on Environment and Electrical Engineering (IEEE EEEIC17), June 6-9, 2017, Milan, Italy.
2. **Priyanka Chaudhary** and M. Rizwan, “Grid integration control algorithm for SPV based power system,” Proceedings of 2018 International Electrical Engineering Congress (IEECON 2018), March 7-9, 2018, Krabi, Thailand.
3. **Priyanka Chaudhary** and M. Rizwan, “Hybrid control approach using NLMS and PLMS algorithms for grid connected SPV system” Proceedings of World Congress on Engineering 2018 (WCE 2018) 4-6 July 2018, London, UK.
4. **Priyanka Chaudhary** and M. Rizwan, “A three phase grid connected SPV power generating system using EPLL based control technique,” Proceedings of IEEE Second International Conference on Electrical, Computer and Communication Technologies (ICECCT 2017), February 22-24, 2017 Coimbatore, Tamil Nadu, India.
5. **Priyanka Chaudhary** and M. Rizwan, “Design and development of controller for solar PV and storage based micro grid” Proceedings of IEEE 41st National Systems Conference (NSC) 2017 on Super-Intelligent Machines and Man, December 1-3, 2017, Agra.
6. **Priyanka Chaudhary** and M. Rizwan, “Short term PV power forecasting using generalized neural network and weather type classification” Proceedings of International Conference on Advancement in Energy, Drive & Control (ICAEDC-2017) April 7-8, 2017, Greater Noida, India.